LBL--26612-Vol.1

DE90 003119

The Ahuachapán Geothermal Field, El Salvador
— Reservoir Analysis —

Volume I: Text and Main Figures

by

Z. Aunzo,[*] *G. S. Bodvarsson,*[*] *C. Laky,*[*] *M. J. Lippmann,*[*] *B. Steingrimsson,*[†] *A. H. Truesdell,*[‡] *and P. A. Witherspoon*[*]

[*]Earth Sciences Division
Lawrence Berkeley Laboratory
1 Cyclotron Road
Berkeley, California 94720

[†]Icelandic National Energy Authority
Grensasvegi 9
108 Reykjavik, Iceland

[‡]U.S. Geological Survey
345 Middlefield Road
Menlo Park, California 94025

Principal Investigators

Gudmundur S. Bodvarsson and Marcelo J. Lippmann

prepared for

Earth and Space Science Division
Los Alamos National Laboratory
Los Alamos, New Mexico 87545

August 1989

This work was supported by USAID through a subcontract from LANL and through US Department of Energy Contract No. DE-AC03-76SF00098.

DISCLAIMER

Executive Summary

The Earth Sciences Division of Lawrence Berkeley Laboratory (LBL) is conducting a reservoir evaluation study of the Ahuachapán geothermal field in El Salvador. This work is being performed in cooperation with the Comisíon Ejecutiva Hidroeléctrica del Río Lempa (CEL) and the Los Alamos National Laboratory (LANL). This report describes the work done during the first year of the study (FY 1988-89), and includes the (1) development of geological and conceptual models of the field, (2) evaluation of the initial thermodynamic and chemical conditions and their changes during exploitation, (3) evaluation of interference test data and the observed reservoir pressure decline and, (4) the development of a natural state model for the field.

The geological model of the field indicates that there are seven (7) major and five (5) minor faults that control the fluid movement in the Ahuachapán area. Some of the faults act as a barrier to flow as indicated by large temperature declines towards the north and west. Other faults act as preferential pathways to flow. The Ahuachapán Andesites provide good horizontal permeability to flow and provide most of the fluids to the wells. The underlying Older Agglomerates also contribute to well production, but considerably less than the Andesites.

The geothermal reservoir is underpressured with respect to the overlying Shallow Aquifer and the Regional Saturated Aquifer. This gives rise to a potential downflow of cooler fluids from the Regional Saturated Aquifer into the geothermal reservoir. Prior to exploitation the pressure in the geothermal reservoir was near-uniform (about 36 bar-g); higher pressures were found in the cooler peripheral wells, which are in poor hydrologic communication with the hot reservoir. Geochemical data shows higher chloride concentrations in the western part of the reservoir (about 8000 ppm) than in the eastern part (about 7000 ppm). Similarly the Na-K-Ca geothermometer shows higher temperatures in the western part (≈ 260 °C) than the eastern one (≈ 240 °C). These data suggest dilution with cooler fluids in the eastern part of the reservoir. The geothermometer temperatures are about 10-15 °C higher than the measured temperatures of the wells, for reasons which are not clear at present.

The conceptual model of the field indicates that hot fluids recharge the Ahuachapán field from the southeast; possibly the upflow zone resides beneath the Laguna Verde Volcanic Complex. The hot fluids feed the wellfield area through major faults and also flow horizontally in the permeable Ahuachapán Andesites. The Younger Agglomerates act as

caprock to the system. Some of the geothermal fluids discharge through surface manifestations in the Ahuachapán/Chipilapa area; the majority of the hot fluids are discharged at El Salitre springs some 7 km north of Ahuachapán. It is estimated that prior to exploitation 1300 L/s of fluids (mixture of geothermal water and Regional Saturated Aquifer water) were discharged at El Salitre. The variations in chloride concentrations and geothermometer temperatures in the wellfield are believed to be due to dilution with cooler fluids in the eastern part of the wellfield, through cold water downflow from the Regional Saturated Aquifer and/or by cold water recharge from the north. All evidence support hypothesis that the Ahuachapán and Chipilapa fields are a part of the same geothermal system.

Some exploitation started at Ahuachapán in the early 1970's. Since then, large changes in the thermodynamic conditions of the reservoir have been observed. Pressure drawdown of up to 15 bars has developed in the production field and temperatures have declined by 10-15 °C. This pressure drawdown has caused the initial localized two-phase zone to expand areally over most of the wellfield; less vertical expansion of the two-phase zone has been observed (about 50 m) because of cooling in the liquid zone associated with the exploitation. The pressure drawdown data have been analyzed using a coarse model and results indicate reservoir transmissivity and storativity of 30 Dm and 3.5×10^{-6} m/Pa, respectively. These values agree well with the results of the interference test analysis (25 Dm and 2.5×10^{-6} m/Pa). These storativity values are intermediate between those expected for single-phase liquid and vapor systems, reflecting the presence of the two-phase zone in the reservoir.

The reservoir cooling is caused by several processes, including (i) boiling, (ii) cold water recharge and (iii) reinjection effects. In the two-phase zone, boiling is the primary cause of the cooling. In the underlying liquid zone significant cooling has also occurred, and is attributed to recharge of boiling fluids into the wellfield, followed by vertical segregation of the phases. Some cooling due to reinjection and lateral cold water recharge has been observed, but in general these cooling processes are secondary in importance. Geochemical data suggest dilution in a north-south trending zone in the wellfield. This zone coincides with several major faults in the wellfield, suggesting downflow of cooler fluids from the overlying Regional Saturated Aquifer.

A natural-state model of Ahuachapán has been developed and matches the observed initial thermodynamic conditions of the system. The model extends from the inferred upflow zone close to Laguna Verde in the south to the El Salitre springs in the north. The model covers both Ahuachapán and Chipilapa and all the observed surface manifestations in the area. The model indicates that about 225 kg/s of 255 °C water recharge the

area through the upflow zone, which is equivalent to a thermal throughflow of about 250 MW_t. Most of these fluids discharge at El Salitre springs (170 kg/s of geothermal fluids), but significant energy is also lost through surface manifestations in the Ahuachapán/Chipilapa area (≈ 60 MW_t) and through conduction to the surface (≈ 20 MW_t). Based upon the model, the horizontal permeability of the Ahuachapán Andesites is estimated to be about 80 md, yielding a transmissivity of about 30 Dm. This transmissivity value is consistent with the results of the interference tests analysis and the analysis of the pressure drawdown history. The horizontal permeability of the Older Agglomerates is estimated to be 20 md. For both units the model indicates that the vertical permeability is about five (5) times lower than the horizontal one (anisotropic medium).

Resumen Ejecutivo

La División Ciencias de la Tierra del Laboratorio Lawrence Berkeley (LBL) está realizando un estudio de evaluación de yacimiento del campo geotérmico de Ahuachapán en El Salvador. Este trabajo se está efectuando en cooperación con la Comisión Ejecutiva Hidroeléctrica del Río Lempa (CEL) y el Laboratorio Nacional de Los Alamos (LANL). Este informe describe las actividades realizadas durante el primer año de estudios (Año Fiscal 1988-89) e incluye: (1) el desarrollo de los modelos geológicos y conceptuales del campo, (2) la evaluación de las condiciones termodinámicas y químicas iniciales y de los cambios debido a la explotación del campo, (3) la interpretación de los datos de pruebas de interferencia y de la caída de presión observada en el yacimiento, y (4) el desarrollo del modelo del estado natural del campo.

El modelo geológico del campo indica que existen siete (7) fallas principales y cinco (5) fallas secundarias que controlan el movimiento de fluidos en el área de Ahuachapán. Algunas de estas fallas constituyen barreras al flujo de fluidos, indicado por las grandes caídas de temperatura en las zonas norte y oeste del campo. Otras de las fallas actúan como conductos preferenciales para el movimiento de fluidos. Las Andesitas de Ahuachapán presentan buena permeabilidad horizontal y proveen la mayor parte de los fluidos producidos por los pozos. Los Aglomerados Antiguos que están debajo de las Andesitas, también contribuyen fluidos a los pozos pero en cantidades considerablemente menores.

El yacimiento geotérmico está subpresionizado con respecto a los suprayacentes Acuíferos Somero y Regional Saturado. Esto resulta en un posible flujo descendente de aguas más frías desde el Acuífero Regional Saturado al yacimiento geotérmico. Antes de comenzar la explotación del campo, la presión en el yacimiento era casi uniforme (alrededor de 36 baras manom.). Mayores presiones se encontraron en pozos periféricos más fríos, los que presentan una pobre comunicación hidrológica con el yacimiento geotérmico. Los datos geoquímicos indican una concentración mayor de cloruros en la zona occidental del campo (alrededor de 8000 ppm) que en la zona oriental (alrededor de 7000 ppm). Del mismo modo, el geotermómetro de Na-Ca-K indica temperaturas mayores en la parte occidental (≈ 260 °C) que en la oriental (≈ 240 °C). Estos datos sugieren dilución con aguas más frías en la zona oriental del campo. Debido a causas aún no determinadas las temperaturas basadas en geotermómetros son aproximadamente 10 a 15 °C superiores a las medidas en los pozos.

El modelo conceptual del campo indica que en Ahuachapán la recarga de fluidos calientes proviene del sudeste; posiblemente relacionada con una zona de flujo

ascendente localizada debajo del Complejo Volcánico de Laguna Verde. Los fluidos calientes alimentan al área productora fluyendo por las fallas principales y horizontalmente por las Andesitas de Ahuachapán. Los Aglomerados Jóvenes actúan como la capa sello del sistema. Parte de los fluidos geotérmicos descargan a la superficie en la zona de manifestaciones del área Ahuachapán/Chipilapa. La mayoría de los fluidos calientes son descargados en los manantiales de El Salitre, a unos 7 km al norte de Ahuachapán. Se estima que antes de comenzar la explotación del campo la descarga de fluidos en El Salitre (mezcla de agua geotérmica y agua del Acuífero Regional Saturado) era de 1300 L/s. Se considera que los cambios en concentraciones de cloruros y temperaturas basadas en geotermómetros observados en el campo, están relacionados con la dilución con aguas más frías que ocurre en la parte oriental de la zona de pozos. Esto es debido a flujo descendente de aguas frías del Acuífero Regional Saturado y/o a la recarga de aguas frías provenientes del norte. Todas las evidencias respaldan la hipótesis que los campos de Ahuachapán y Chipilapa son parte de un mismo sistema geotérmico.

A comienzos de la década de los setenta se inició la explotación de Ahuachapán y desde entonces se han observado grandes cambios en las condiciones termodinámicas del yacimiento. En la zona de producción la caída de presión llega a alcanzar 15 baras, mientras que la temperatura ha disminuído 10 a 15 °C. Esta caída de presión ha causado la expansión de la inicialmente localizada zona bifásica hasta cubrir horizontalmente la mayor parte del área de pozos. Se ha observado una menor expansión vertical de dicha zona bifásica (unos 50 m) debido al enfriamiento de la zona líquida asociado con la explotación. Los datos de caída de presión han sido analizados utilizando un modelo poco detallado. Los resultados indican una transmisividad de 30 Darcy-metros (Dm) y un coeficiente de almacenamiento ("storativity") de 3.5×10^{-6} m/Pa para el yacimiento. Estos valores coinciden bastante bien con los obtenidos del análisis de datos de pruebas de interferencia (25 Dm y 2.5×10^{-6} m/Pa). Los coeficientes de almacenamiento son valores intermedios entre los correspondientes a sistemas monofásicos de líquido y de vapor, lo que indica la presencia de una zona bifásica en el yacimiento.

El enfriamiento del yacimiento se debe a varias razones, las que incluyen: (i) ebullición, (ii) recarga de agua fría y (iii) efectos de reinyección. En la zona bifásica ebullición es la causa principal del enfriamiento. En la zona líquida infrayacente también ha ocurrido un importante enfriamiento, el que se atribuye a la recarga de la zona de pozos por fluidos en ebullición, seguida por la segregación de las dos fases. También ha sido observado cierto enfriamiento debido a reinyección y a recarga lateral de aguas frías, pero en general estos procesos de enfriamiento tienen una importancia secundaria. Los datos geoquímicos sugieren dilución en el área de pozos a lo largo de

una zona de rumbo norte-sur. Esta zona coincide con varias fallas principales, lo que sugiere un flujo descendente de aguas frías proveniente del Acuífero Regional Saturado localizado sobre el yacimiento geotérmico.

Se ha desarrollado un modelo del estado natural de Ahuachapán que presenta condiciones termodinámicas similares a las observadas inicialmente en el sistema. El modelo se extiende al sur desde la inferida zona de flujo ascendente cercana a Laguna Verde, y al norte hasta los manantiales de El Salitre. El modelo comprende tanto Ahuachapán como Chipilapa y todas las zonas de manifesticiones superficiales observadas en el área. El modelo indica una recarga de aproximadamente 225 kg/s de agua a 255 °C proveniente de la zona de flujo ascendente, equivalente a una circulación térmica de aproximamente 250 MW_t. La mayor parte de estos fluidos son descargados en los manantiales de El Salitre (170 kg/s de fluidos geotérmicos). Sin embargo, una parte importante de la energía también se pierde en las manifesticiones superficiales del área Ahuachapán/Chipilapa (≈ 60 MW_t) y por conducción a la superficie (≈ 20 MW_t). En base a este modelo, se estima que la permeabilidad horizontal de las Andesitas de Ahuachapán es de alrededor de 80 md, lo que resulta en una transmisividad de aproximadamente 30 Dm. Este valor de transmisividad está de acuerdo con los resultados de los análisis de pruebas de interferencia y de la evolución de la caída de presión en el yacimiento. La permeabilidad de los Aglomerados Jóvenes se estima en unos 20 md. El modelo indica que las permeabilidades verticales de ambas unidades son unas cinco (5) veces menores que las horizontales (i.e., constituyen un medio anisótropo).

Table of Contents

Volume I

1.0 INTRODUCTION

The Ahuachapán geothermal field in El Salvador has been producing electrical power since 1975. The power plant consists of three units, two 30 MW_e units and a 35 MW_e unit with a total rated capacity of 95 MW_e. However, mainly because of declining reservoir pressures and limited drilling of make-up wells, the power plant has not operated at capacity; currently, about 45 MW_e are being produced at Ahuachapán.

Since 1985, Los Alamos National Laboratory (LANL), with financial support from the United States Agency for International Development (USAID), has conducted various geothermal studies in Central American countries, including El Salvador, Costa Rica, Guatemala and Panama (Hanold et al., 1986). This work has involved geological, geochemical and geophysical studies and well logging. As the need for increasing the electrical output at Ahuachapán became evident, it was recognized that a properly designed reinjection scheme and further drilling in appropriate locations, would help increase the productivity of the Ahuachapán reservoir. As the first step in achieving this objective, the USAID evaluation team recommended the involvement of LBL, stating, "As soon as possible, a team experienced in geothermal reservoir simulation should be brought in to speed up the reservoir simulation of Ahuachapán. The evaluation team strongly recommends the Lawrence Berkeley Laboratory reservoir engineering group for that task, because of its considerable experience in predictive geothermal reservoir modeling."

The present report describes the work done at LBL during the first year of the Ahuachapán project (FY 1987-1988). The work has focused on understanding the available data and the development of a conceptual model of the Ahuachapán reservoir. This has involved the development of a geological model of the field, analysis of geochemical data, interpretation of pressure and temperature logs, and evaluation of well data and pressure drawdown data. In addition, a natural state model of the field has been developed that matches the observed thermodynamic conditions of the field. The model has yielded important insight into the mass and heat flow

within the Ahuachapán system, and provide the necessary initial conditions for future exploitation simulation studies.

It should be noted that our work was conducted in close cooperation with colleagues from the Comisíon Ejecutiva Hidroeléctrica del Río Lempa (CEL) and LANL, and their input and expertise is reflected throughout the report.

This report is in three volumes. Volume 1 contains the text and primary data and figures of the report; Volumes II and III contain plots of most of the available data on Ahuachapán organized in different Appendices.

2.0 FIELD DEVELOPMENT

In 1953 the Comisión Ejecutiva Hidroeléctrica del Río Lempa (CEL) began evaluation of the geothermal resources of El Salvador. The project included geologic, geochemical and geophysical studies and the drilling of small-diameter exploration and gradient wells. From 1968 to 1971, CEL and the United Nations Development Program (UNDP) carried out further exploration to characterize the resources, including the drilling of deep exploration wells in Ahuachapán. By 1970, four commercially productive wells had been drilled in the area, and by 1971, several successful reinjection tests had been completed.

Based on promising test results, CEL contracted the consulting firm Kingston, Reynolds, Thom and Allardice (KRTA) to assess the feasibility of electrical generation using fluids from the Ahuachapán geothermal fields. Their assessment was positive, and in 1973, CEL placed an order for two 30 MW_e single-flash turbo-generators (inlet pressure: 81.1 psi).

After 1972, CEL continued to explore and characterize the Ahuachapán field with the assistance of the consulting firm Electroconsult (ELC). A major development drilling effort began at that time to supply steam to the two planned power plants, which came on-line in June 1975 and June 1976.

Based on the experience gained from the operation of the first two power plants, CEL ordered an additional 35 MW_e unit in 1978 with a dual-pressure turbine (inlet pressures: 81.1 and 21.8 psi). This third unit started commercial operation in November 1980, bringing the total installed capacity at Ahuachapán to 95 MW_e.

By 1979, 27 deep wells had been completed, 12 of them producers and 4 injectors. After that, the drilling program continued at a slower pace. A total of 32 deep wells have now been drilled in the Ahuachapán area.

Originally, waste brine at Ahuachapán was injected into the reservoir or discharged to a nearby river, Rio Paz. Injected water could be piped directly from the wellhead separators to the

injectors because the separator pressure was sufficiently high to transport the liquid, and the temperature was high enough (about 155 °C) to make chemical treatment of the brine unnecessary. In late 1980, the third unit came on-line, requiring lower pressure steam. This required water from the separators to be flashed a second time, which lowered the temperature of the brine to about 110 °C, and greatly increased the potential for mineral precipitation in the injection wells and the surrounding formation. A temperature decline was observed in several production wells during these years, a possible result of reinjection into nearby wells.

In the light of these developments, CEL decided to stop all reinjection in late 1982. Since then, a 75-km long, covered, concrete channel, has transported all the waste brine, including condensate from the plant to the Pacific Ocean.

The history of electrical power generation at Ahuachapán is shown in Figure 2.1. From 1975 to 1982 there was a general increase in the power output as the new units came on-line. Since then, the power generation has gradually declined due to increasing reservoir drawdowns, and consequently, decreasing well productivities, partly due to the suspension of the injection operations.

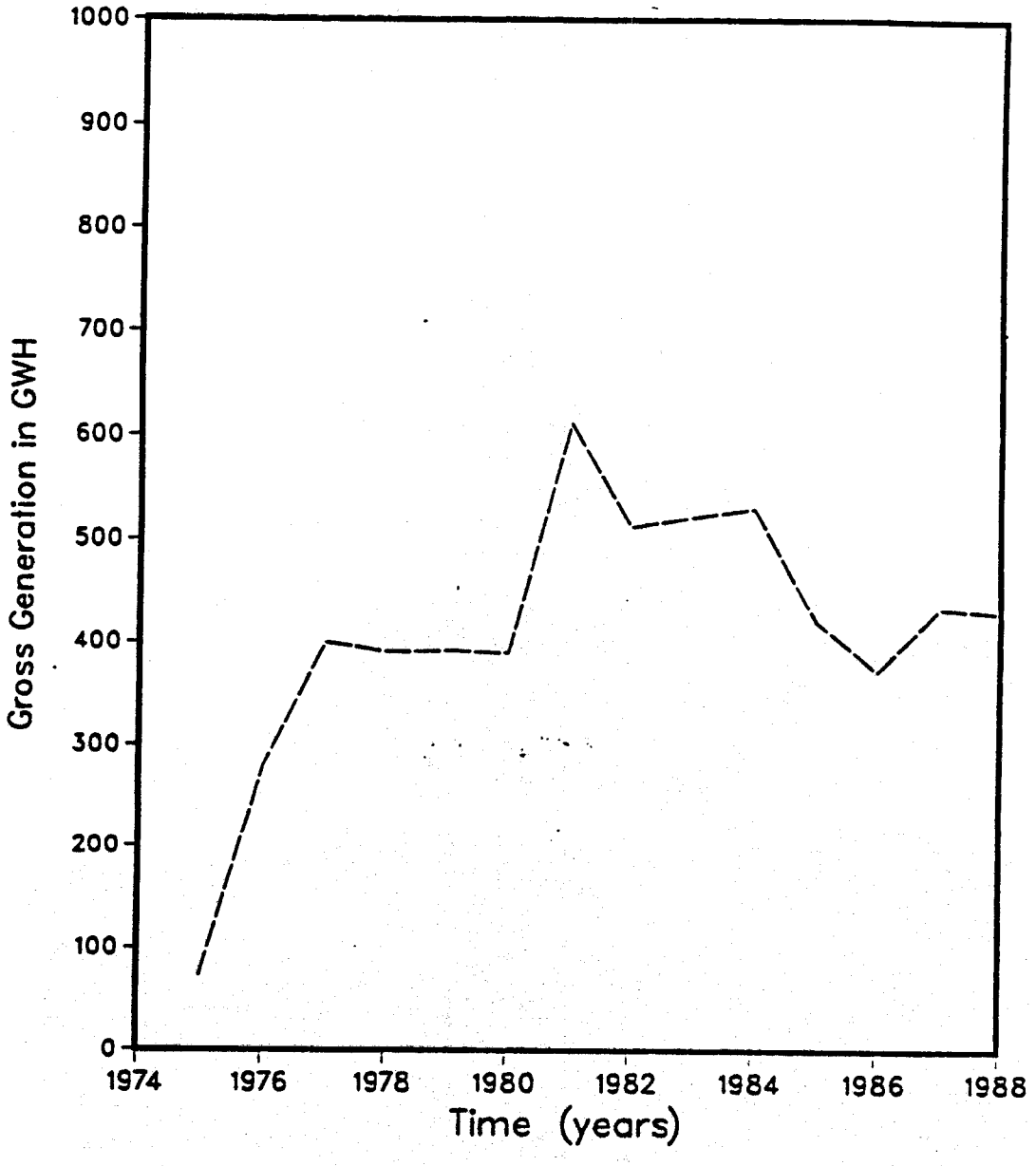

Figure 2.1. History of Electrical Power Generation at Ahuachapán.

3.0 WORKSCOPE

The main goal of this project is to develop a detailed numerical model of the Ahuachapán field that can be used to guide the reservoir management program. This model will be consistent with the observed thermodynamic conditions of the field, the history of production, enthalpy changes, the pressure decline, and the past reinjection history and its effects on pressures, flow rates and enthalpies of all wells. The model and other reservoir engineering techniques will be used to determine appropriate reinjection locations and define new exploitation strategies aimed at increasing the power output of the plant.

In the first year emphasis will be placed upon understanding the available data from Ahuachapán, especially in terms of the fractured nature of the field. A natural state model will be developed that reproduces all relevant features of the field observed before exploitation started. This will provide the necessary framework for the exploitation studies to be performed in subsequent years. Below we briefly describe the list of tasks carried out during the first year of the project.

Task A: Collection and review of all relevant data from Ahuachapán

These will include:

1. Surface Geology
    a. Fault map.
    b. Geologic map.
    c. Shallow water levels - ground water flow directions.
    d. Locations of thermal springs - estimates of discharge.
2. Geophysics
    a. Summary reports of geophysical measurements taken and results.

b. Resistivity maps at various depths.

c. Resistivity from well logs.

3. Subsurface Geology

a. Geologic cross sections involving all wells.

b. Hydrothermal alteration data.

c. Flow characteristics - fractures, intrusions, etc.

d. Porosity/permeabilities from well logs.

4. Well Data

a. Casing diagrams for all wells.

b. Temperature and pressure profiles in wells (static).

c. Temperature and pressure profiles in wells (flowing).

d. Temperature and pressure contour maps for various depths.

e. Locations of feed zones (fractures) in all wells.

5. Geochemistry

a. Concentrations of dissolved solids and noncondensible gases in produced fluids of individual wells - changes with time and flow rate.

b. Contour maps showing concentrations of dissolved solids, gases, various gas ratios, etc.

c. Map showing flow directions based upon geochemical data.

6. Well Testing

a. Raw data for all pressure transient tests conducted, including drawdown, buildup, injection and interference tests.

b. Reports describing analysis of data.

c. Maps showing the permeability-thickness distribution.

7. Production History

   a. Data on flow rates, enthalpies, and wellhead pressure for all wells from start of production to present time.

   b. Pressure decline in observation wells.

   c. Injection rates and temperatures of injection wells.

   d. Data on observed thermal interference.

   e. Summary reports on scaling and corrosion problems.

8. Reservoir Engineering Reports

   a. All available reports on Ahuachapán that have been prepared by CEL, ELC and other consultants.

Task B: Interpretation of existing well test data

All existing well test data will be interpreted using state-of-the-art methods. When necessary the interpretation will take into account two-phase effects, fracture effects and non-isothermal effects. Recommendations will be given for future testing of existing wells.

Recent research has shown that the analysis of pressure transient data in two-phase reservoirs is greatly complicated by counterflow of liquid and vapor (Bodvarsson and Cox, 1986). The observed pressure drawdown depends strongly on the depth of the feed zones, with little or no pressure decline in shallow feeds and much larger drawdowns in deeper areas. This phenomena in addition to the heterogeneous fractured nature of the Ahuachapán reservoir suggests that careful analysis of the pressure transient data is needed if reliable results are to be obtained.

Task C: Development of a conceptual model

In developing a conceptual model of a geothermal field all of the available data must be integrated into a reliable model, that considers all important processes that

are occurring in the system. In contrast to oil and gas reservoirs, geothermal systems are very dynamic in their natural state. There is continuous transport of fluid, heat, and chemical species. Important processes in geothermal systems include mass transport, convective and conductive heat transfer, phase change (boiling and condensation), dissolution and precipitation of minerals, and stress changes caused by pore-pressure changes. Most of these processes are strongly coupled; for example, a phase change disturbs chemical equilibria, often resulting in precipitation/dissolution of minerals that in time can alter porosities and permeabilities of the subsurface rocks. This in turn can affect the mass transport in the system. In collaboration with scientists from CEL, and LANL, LBL will develop a conceptual model for the Ahuachapán field.

Task D: Development of a natural state model

Geothermal reservoirs evolve over geologic time. The rates at which thermodynamic conditions change in the natural state are generally small in comparison to the changes induced by exploitation. Therefore, for most practical purposes, undeveloped geothermal reservoirs can be considered to be in a quasi-steady state. Efforts at quantitatively modeling this natural state can provide very useful information for evaluating a geothermal resource and for planning its development.

Quantitative modeling of the natural state must be based on a (perhaps preliminary) conceptual model that in turn is developed from diverse pieces of information (i.e., geological, geophysical, geochemical, and reservoir engineering data). By quantification of its various aspects, a conceptual model can be tested and refined. A successful natural-state model will match quantitatively or qualitatively a wide range of observations and, in doing so, will provide insight into important reservoir parameters, such as formation permeability, boundary conditions for fluid and heat flow at depth, and thermodynamic state of fluids throughout the system. Even if an unambiguous quantification of these parameters cannot be achieved, it may be

possible to obtain constraints that are useful for modeling reservoir response to exploitation.

LBL will develop a natural state model of Ahuachapán, that is consistent with the observed thermodynamic conditions of the field. This will allow for the determination of the recharge rate through the upflow zone(s), the coarse permeability structure of the system and natural flow of heat and mass within it.

Task E: Investigation of fault and fracture effects on fluid and heat flow

Faults and fractures play an important role in the mass and heat transfer at Ahuachapán. The thermal anomaly is controlled by major faults, and information about their additional characteristics will be obtained through the natural state modeling study. Fractures and faults also govern the productivities of wells, enthalpy transients and pressure declines. Furthermore, cold water recharge from reservoir boundaries and injection wells will primarily occur through the fracture system, with conductive heat transfer from the rock providing energy input for heating of these fluids. It is therefore extremely important to investigate the location and nature of major faults and fractures as these will control the behavior of the field during exploitation. LBL will review all available data and develop a fracture model for the Ahuachapán system. This model will be very useful in further studies, including exploitation modeling and the development of a reinjection plan for the field.

4.0 GEOLOGIC MODEL OF AHUACHAPAN

4.1 Regional Geology

The line of young volcanoes that extends across El Salvador, approximately 40 km north of, and more or less parallel to, the Pacific coast is closely associated with the geothermal fields in the country (Figures 4.1 and 4.2). Although Ahuachapán is the only area currently being exploited, exploration is being carried out at the Berlín, Chinameca, Chipilapa, and San Vicente fields (Vides-Ramos, 1983).

The geologic structure of the Ahuachapán area is strongly influenced by the regional tectonics of Central America, where approximately five lithospheric plates interact with one another (Weyl, 1980). El Salvador is located on the Caribbean Plate which is underthrust by the Cocos Plate (Figure 4.3). This subduction is responsible for the fracture tectonics and chain of active volcanos extending between Guatemala and Costa Rica (Figure 4.4). Segmentation of the subduction zone is evident by the shifting of individual rows of volcanoes and by transverse discontinuities. In El Salvador and Nicaragua a chain of extinct (Pliocene?) volcanoes north of the active volcanoes, suggests an older zone of magma formation several tens of kilometers further north than it is today.

El Salvador, covering an area of approximately 21,000 km^2, is located in the region of the Tertiary and Quaternary volcanic formations; the exception to this is the extreme northern part of the country. The country can be divided into four morphological-geological units: the Coastal Plains, in the west and central part of the country with alluvial deposits, spits and mangrove swamps; the Coastal Ranges, including the Tacuba, Bálsamo and Jucurán Ranges, with beds and peneplains dipping gently towards the coast; the Great Interior Valley (or Central Graben), a heterogeneous basin of low mountain topography with more or less eroded extinct volcanoes, and the Northern Mountain Ranges, uplifted blocks of predominantly Tertiary volcanics (Figure

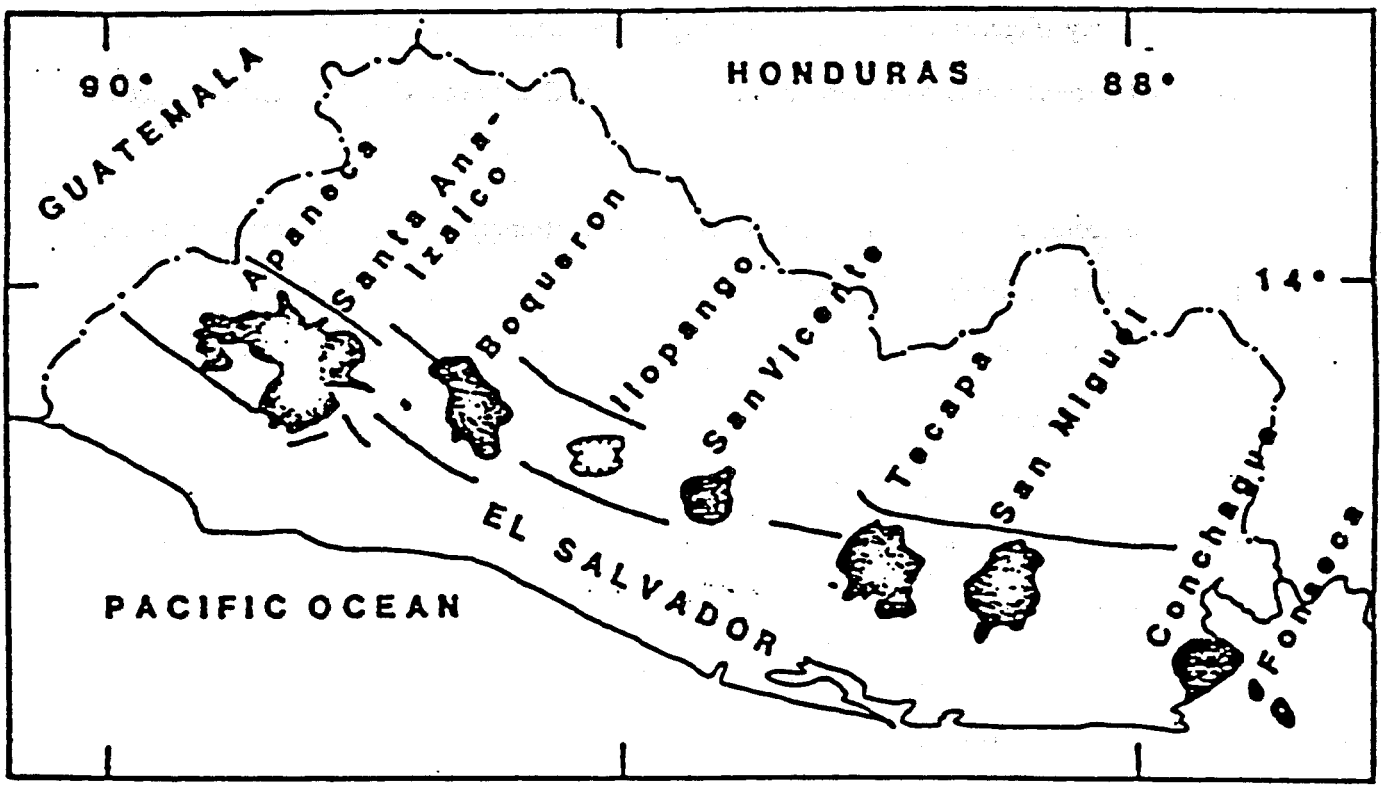

Figure 4.1. Location map of Salvadoran volcanic centers. Solid lines are boundary faults of the Great Interior Valley (from Carr, et al., 1981).

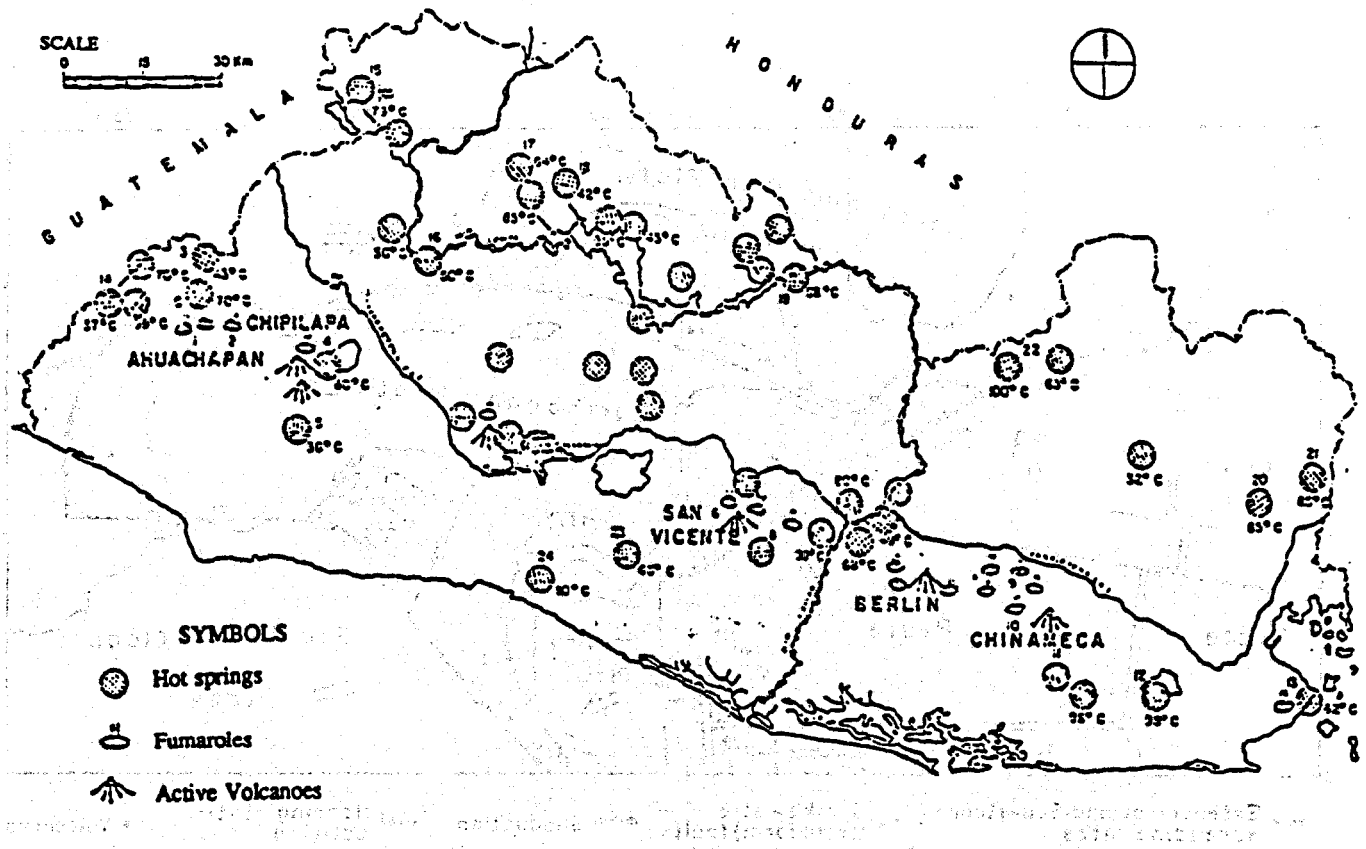

Figure 4.2. Location of geothermal areas in El Salvador (from Vides-Ramos, 1983).

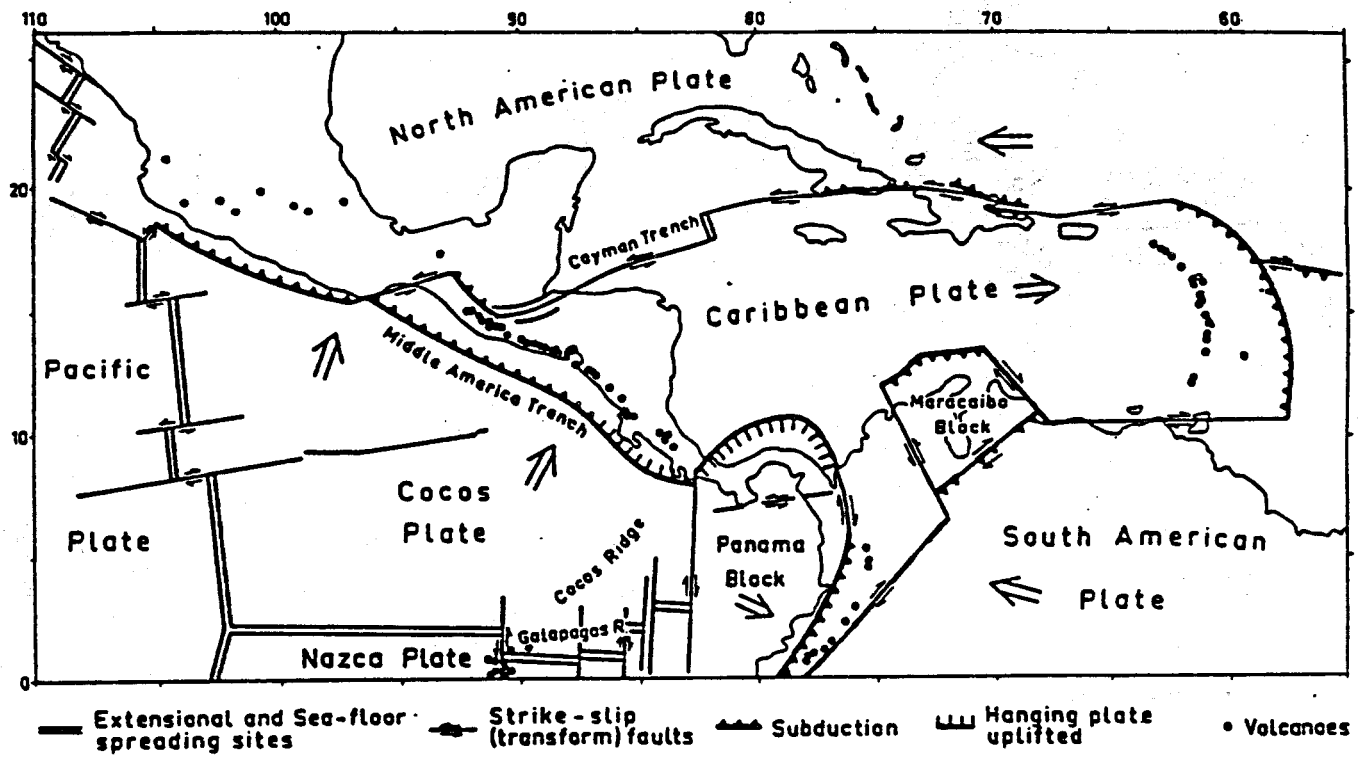

Figure 4.3. Inferred present plates and plate boundaries in the Central America-Caribbean Region (from Weyl, 1980).

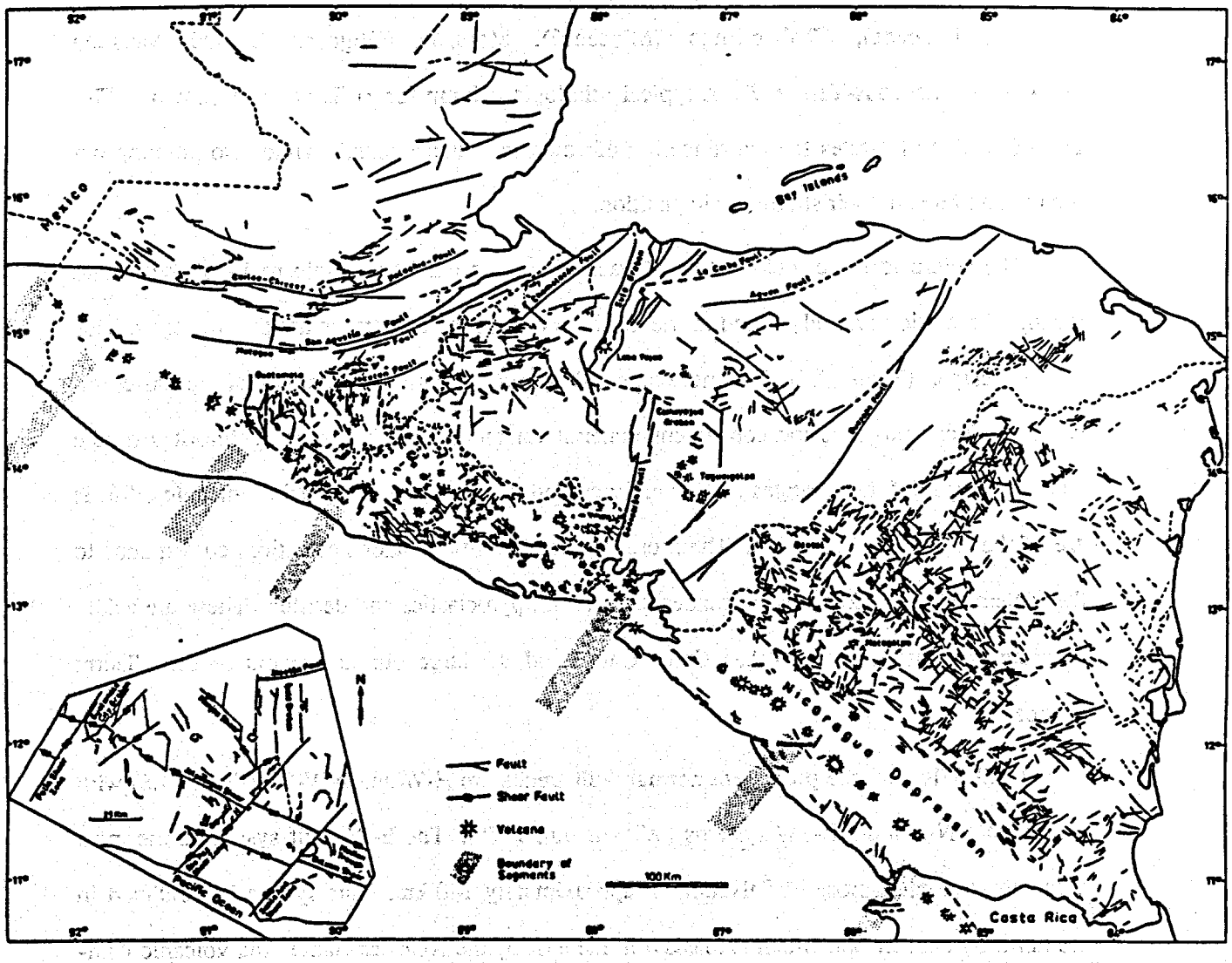

Figure 4.4. Fault pattern in Northern Central America (from Weyl, 1980).

4.5).

Stratigraphically, El Salvador is almost entirely underlain by Tertiary to Holocene volcanic rocks and debris. These have been classified into acidic, intermediate, and basic, and into effusive and pyroclastic rocks and epiclastic volcanic rocks (Weisemann, 1975). The formations include: San Salvador (Pleistocene?-Holocene), Cuscatlán (Pliocene-Pleistocene), Bálsamo (Miocene?-Pliocene), Chalatenango (Miocene?), Morazán (Oligocene?), and Metapán (Jurassic?-Cretaceous-Tertiary?). A typical lithologic column for El Salvador is shown in Figure 4.6, which illustrates the interfingering of volcanic "successions," while also pointing out the uncertainties in their stratigraphic position.

The acidic to basic rocks of the Morazan Formation and the acidic rocks of the Chalatenango Formation are only found in the northern part of the country as are the Mesozoic beds of the Metapan (Figure 4.7). The more recent Balsamo Formation of intermediate to basic volcanic products, provides the constituent material for the Coastal Ranges. Ignimbrites on the southern slopes of these ranges and severely eroded ruins of (acidic to basic) volcanic edifices are of the Cuscatlan Formation. The most recent, the San Salvador Formation, corresponds to the Pleistocene and Holocene volcanoes, their lavas, pyroclastics and detritus. These are acidic to basic and include the "Tobas Color Cafe" and the large pumice covers of the "Tierra Blanca"

In El Salvador, the prominent normal fault trends are E-W and NW-SE (Figure 4.8) with subordinate N-S and NE-SW systems (Wiesemann, 1975). The E-W fault system is the most dominant and cuts across El Salvador for approximately 180 km. This system is paralleled in the north by another one which is masked in the east by the Apaneca-Santa Ana volcanic complexes. The subordinate N-S system is particularly apparent in the Ahuachapán area.

The NW-SE striking faults commonly determine the location of volcanoes and mark the boundaries in the echelon SSE-NNW-oriented Plio-Pleistocene basins that form the great Interior Valley of El Salvador and are the extension of the Nicaraguan Depression. Because of the large number of transverse and diagonal faults, this valley does not stand out clearly on the

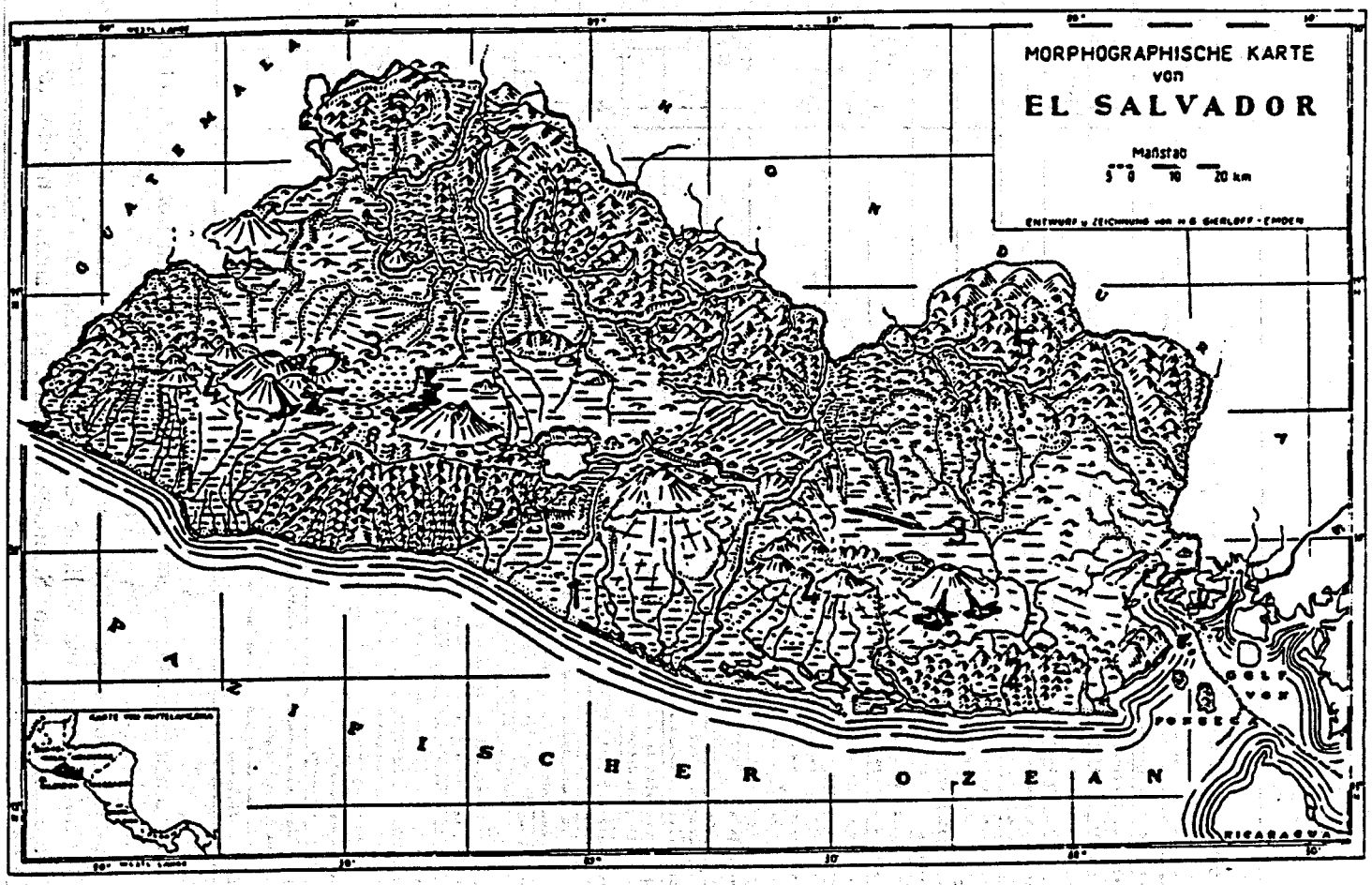

Figure 4.5. Morphological map of El Salvador. 1: Coastal Plains, 2: Coastal Ranges, 3:

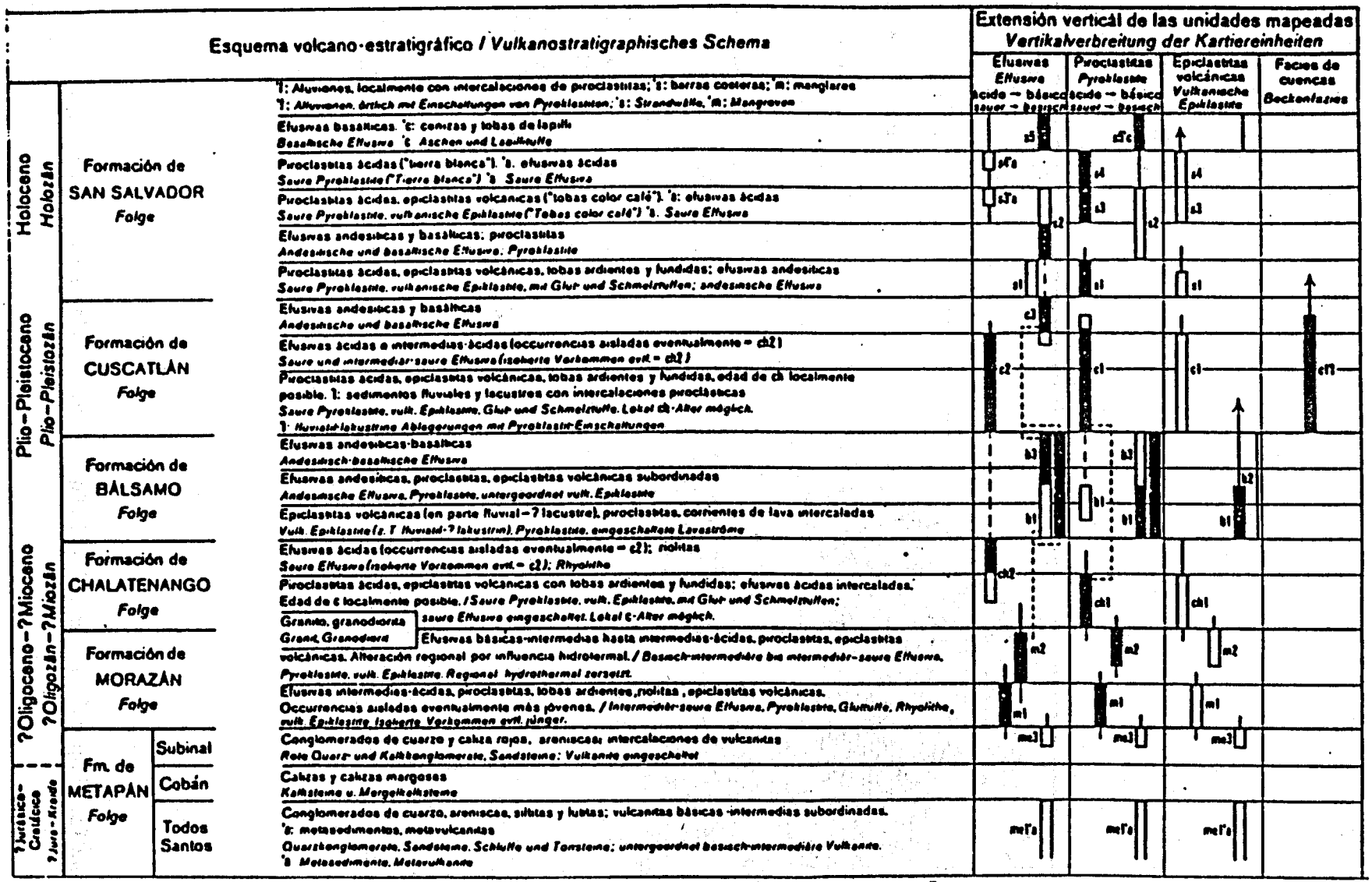

Figure 4.6. Volcanostratigraphic scheme of El Salvador. (Adapted from "Geologische Ubersichtskarte der Republik El Salvador 1:500,000", Hanover 1974. Revised nomenclature: For Formacion de Metapan read Estratos de Metapan, for Subinal-Serie read Valle de Angeles Formation, for Coban-Serie read Yojoa Group, for Todos Santos-Serie read Todos Santos Formation (see Wiesemann, 1975)

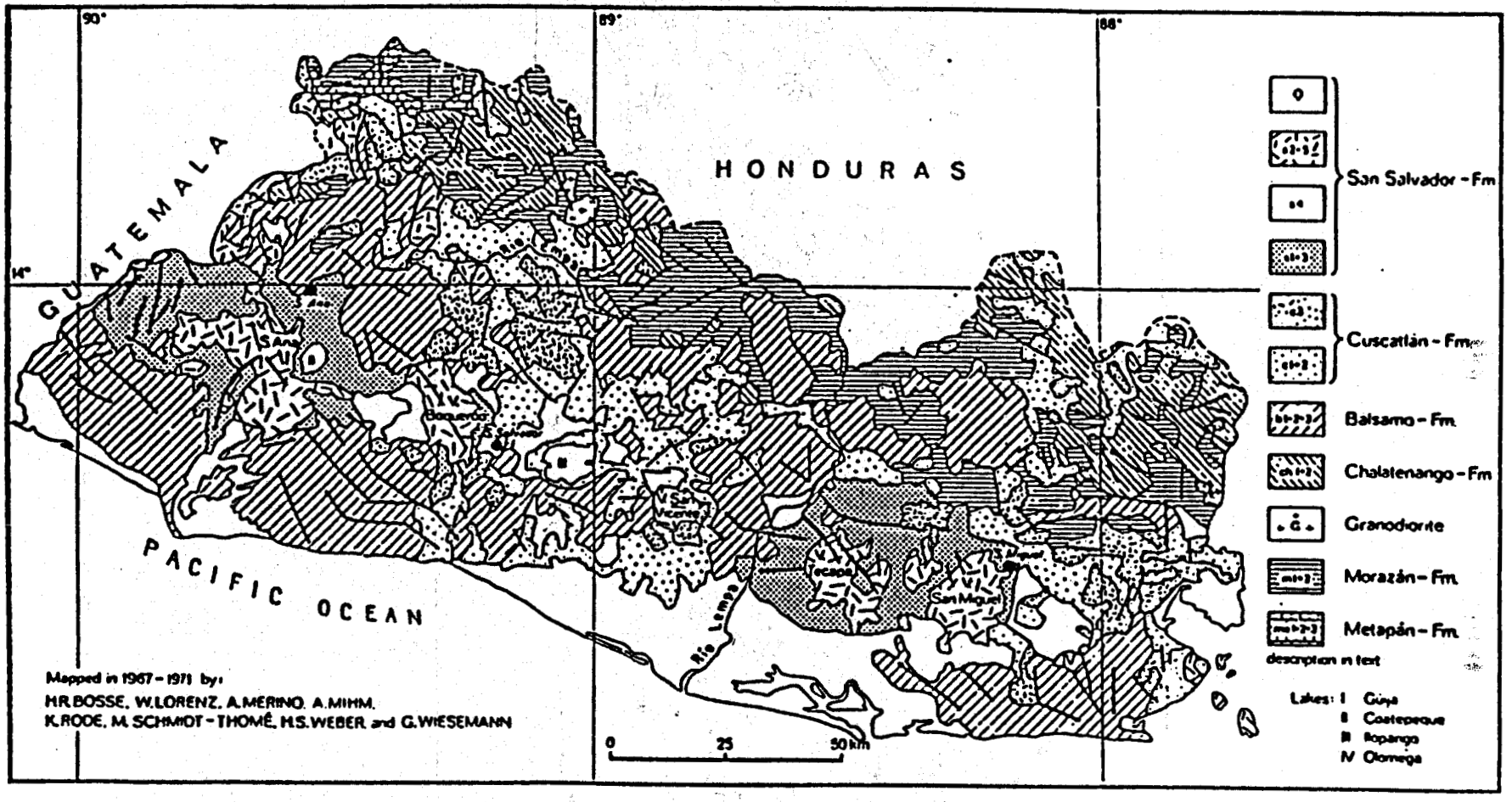

Figure 4.7. Geological map of El Salvador (from Wiesemann, 1975).

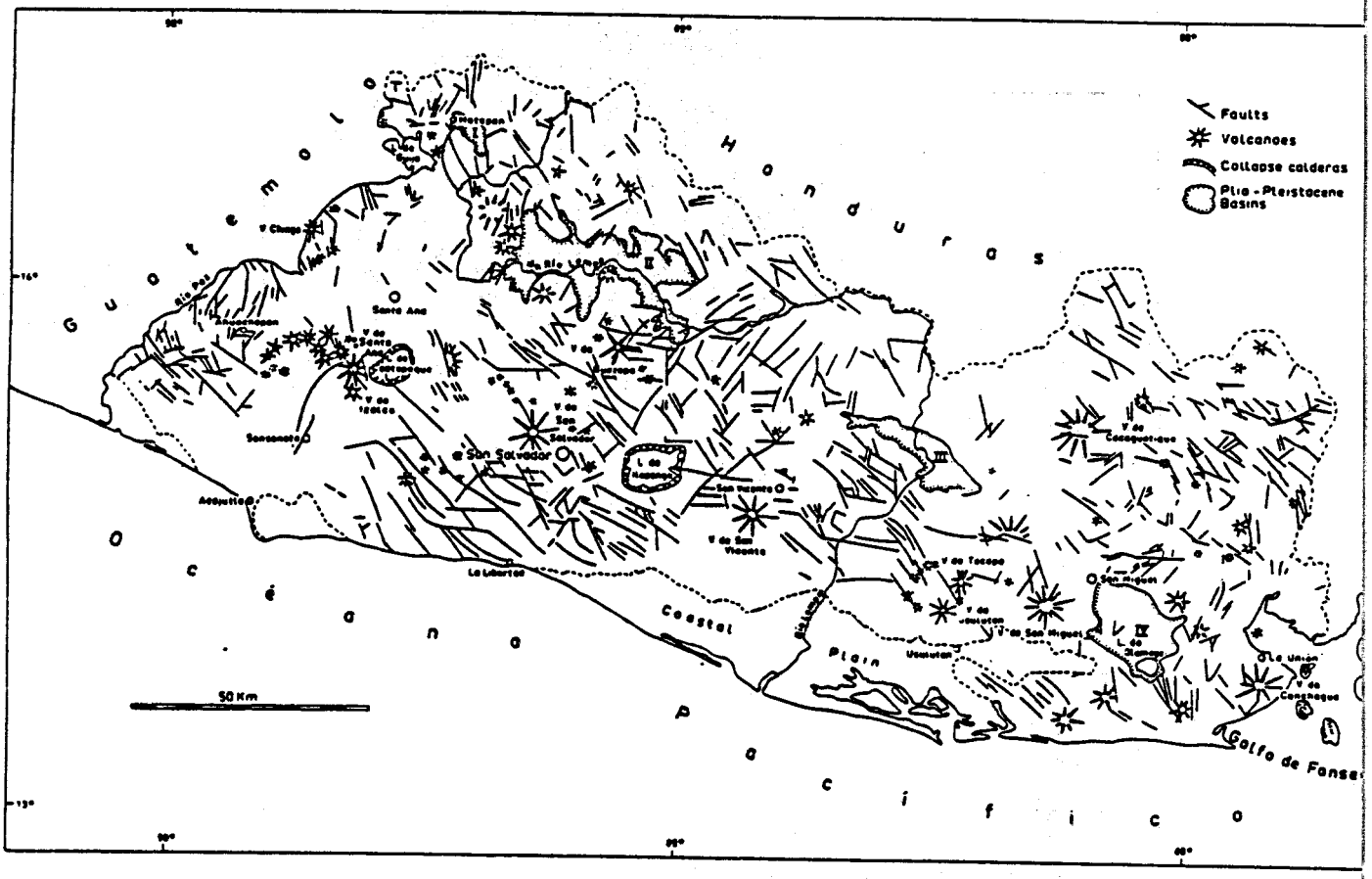

Figure 4.8. Structural map of El Salvador (from Weyl, 1980).

structural map (Figure 4.8), it is, however, the area in which the most frequent and most violent shallow-focus earthquakes occur.

Because El Salvador is in one of the world's most intense seismic areas, there are different views and interpretations on the geologic structure of the country. Wiesemann (1975) lists seven tectonic interpretations with major fault trends listed as: WNW-ESE, NW-SE, NE-SW, NNE-SSW, N-S, E-W, and NNW-SSE. Most faults are considered normal but those listed with horizontal displacements are said to be right lateral on the W-E and E-NE(?) fault zones. The NNE- to NE-trending transverse fault system is considered an important zone of left-lateral strike-slip faulting. Studies of the 1968 San Salvador earthquake suggest that right lateral slip occurred along a fault sub-parallel to the Central American volcanic chain, i.e., WNW, and left-lateral slip on the fault perpendicular to the chain (White et. al., 1987). A conjugate fault system in the border region between Guatemala and El Salvador displaces individual parallelogram-shaped segments eastward and northward on W-NW trending, right-lateral, strike-slip faults, and NE-trending, left-lateral, strike-slip faults (Burkart and Self, 1985).

4.2 Geology of Ahuachapán

The Ahuachapán field is located in the northwestern sector of the Laguna Verde volcanic group on the southern flank of the central Salvadoran graben. The field is two km northwest of the Laguna Verde volcano (13° 54'N, 89° 47'W), an extinct, andesitic, stratovolcano approximately 1900 m in height (Figure 4.9).

4.2.1 Lithologic Units

Lithologically, the Ahuachapán reservoir lies mostly within the San Salvador Formation (Figure 4.6) with only the basement rock from the Balsamo. The stratigraphic column was divided by Jonsson (1970) into the following units: upper brown tuff, gray ignimbrite, pink ignimbrite, lower brown tuff, gray agglomerate, blue ignimbrite, old andesitic lavas, and ancient agglomerate. On the basis of CEL lithologic logs from the 32 wells drilled in field (Figure

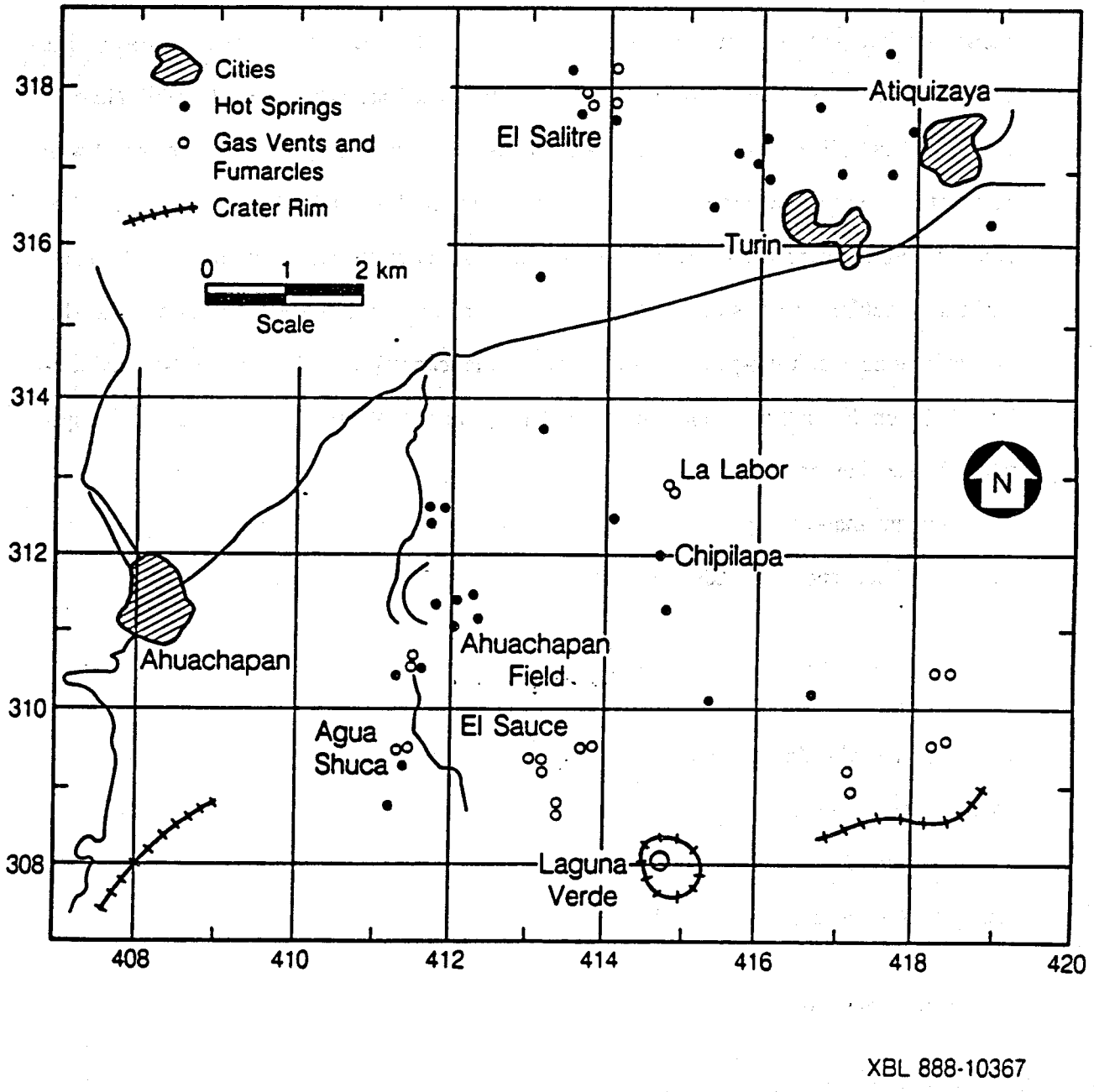

Figure 4.9. Ahuachapán/Chipilapa area, El Salvador (from DiPippo, 1986).

4.10a-d), we have defined four major units that are similar to those of Aumento et al. (1982). These are, Surficial Materials (SM), Young Agglomerates (YA), Ahuachapán Andesites (AA), and Older Agglomerates (OA), (Table 4.1).

The CEL lithologic logs used to designate the units were supplemented by temperature and pressure logs, data on loss of circulation zones, inferred aquifer locations (Appendix C), and core data (Figure 4.10a-d). Jonsson (1970) includes very detailed well logs in his report, but for only six wells. We were unable to obtain a copy of his geologic map of the area.

Table 4.1
Geologic descriptions of Ahuachapán rocks

Formation	Rock Type	Designation	Aquifer
San Salvador (Quaternary)	Colluvium, altered pyroclastics and lavas (Holocene)	Surficial Materials	Shallow Aquifer
	pyroclastics, andesites (Pleistocene)	Young Agglomerates	Regional Saturated Aquifer
	andesites (Plio-Pleistocene)	Ahuachapán Andesites	Saline Aquifer (reservoir)
Bálsamo (Pliocene)	breccias, andesites	Older Agglomerates	

The Surficial Materials (SM), in the top 100-150 m, are composed of a series of pyroclastics and lavas that contain the groundwater zone so-called "Shallow Aquifer" (Cuellar et al., 1979; Romagnoli et al., 1976). Beneath this unit, reside the Young Agglomerates (YA), a sequence of young pyroclastics and andesites ranging in thickness from 300 to 800 m. Circulation losses in this unit are attributed to the so-called "Regional Saturated Aquifer".

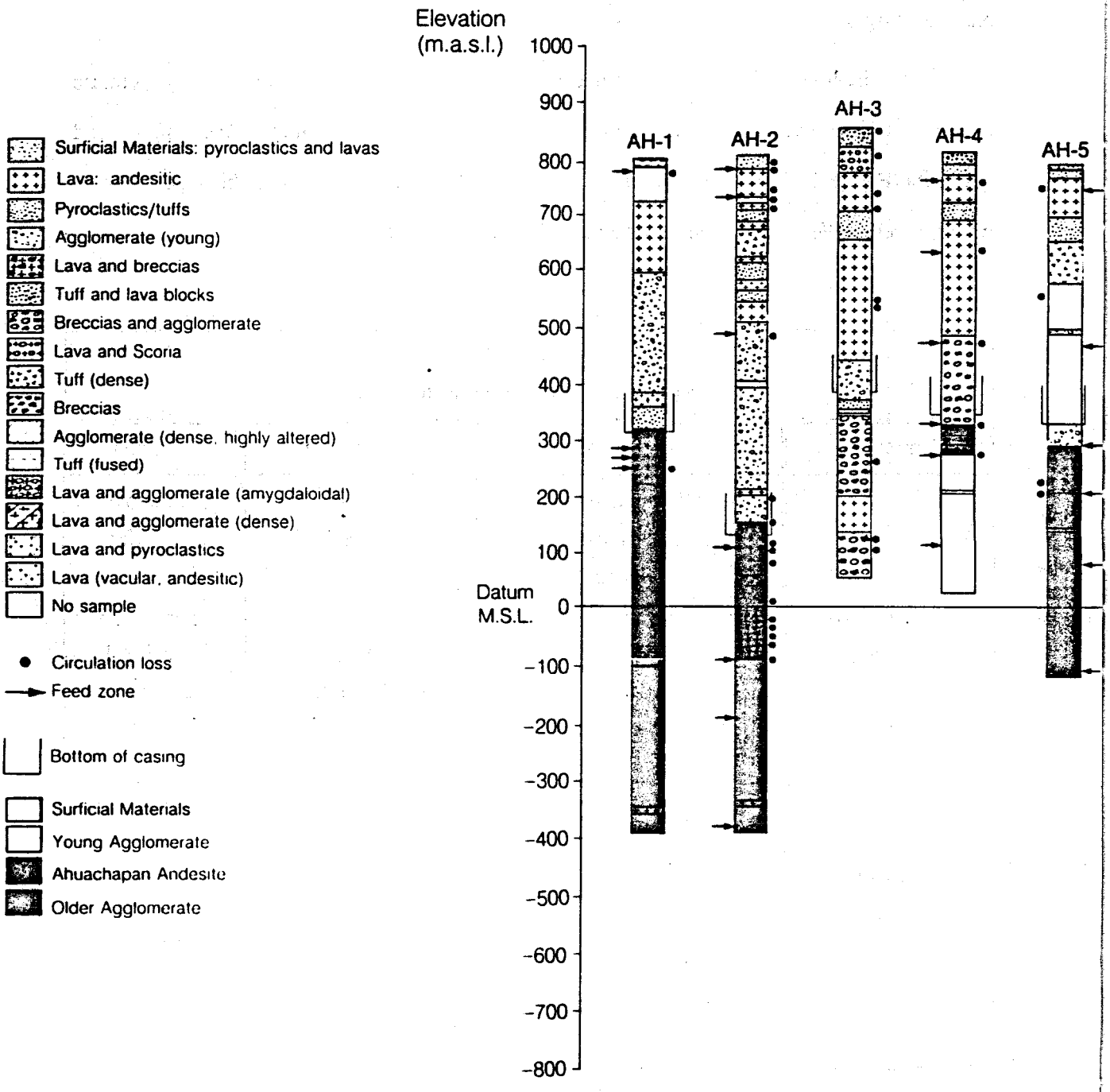

Figure 4.10a Ahuachapan well lithology

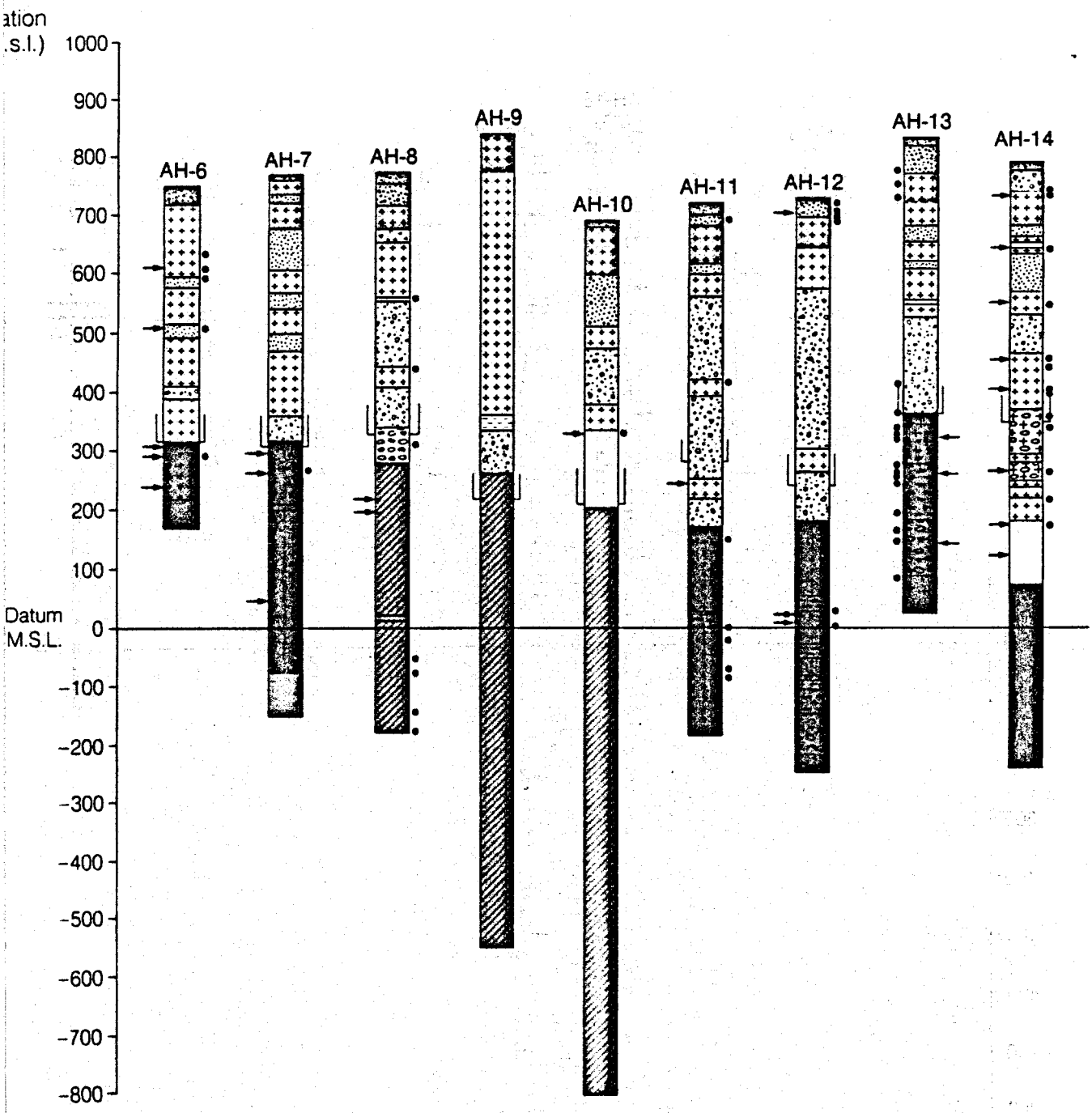

Figure 4.10b Ahuachapan well lithology

XBL 887-10326

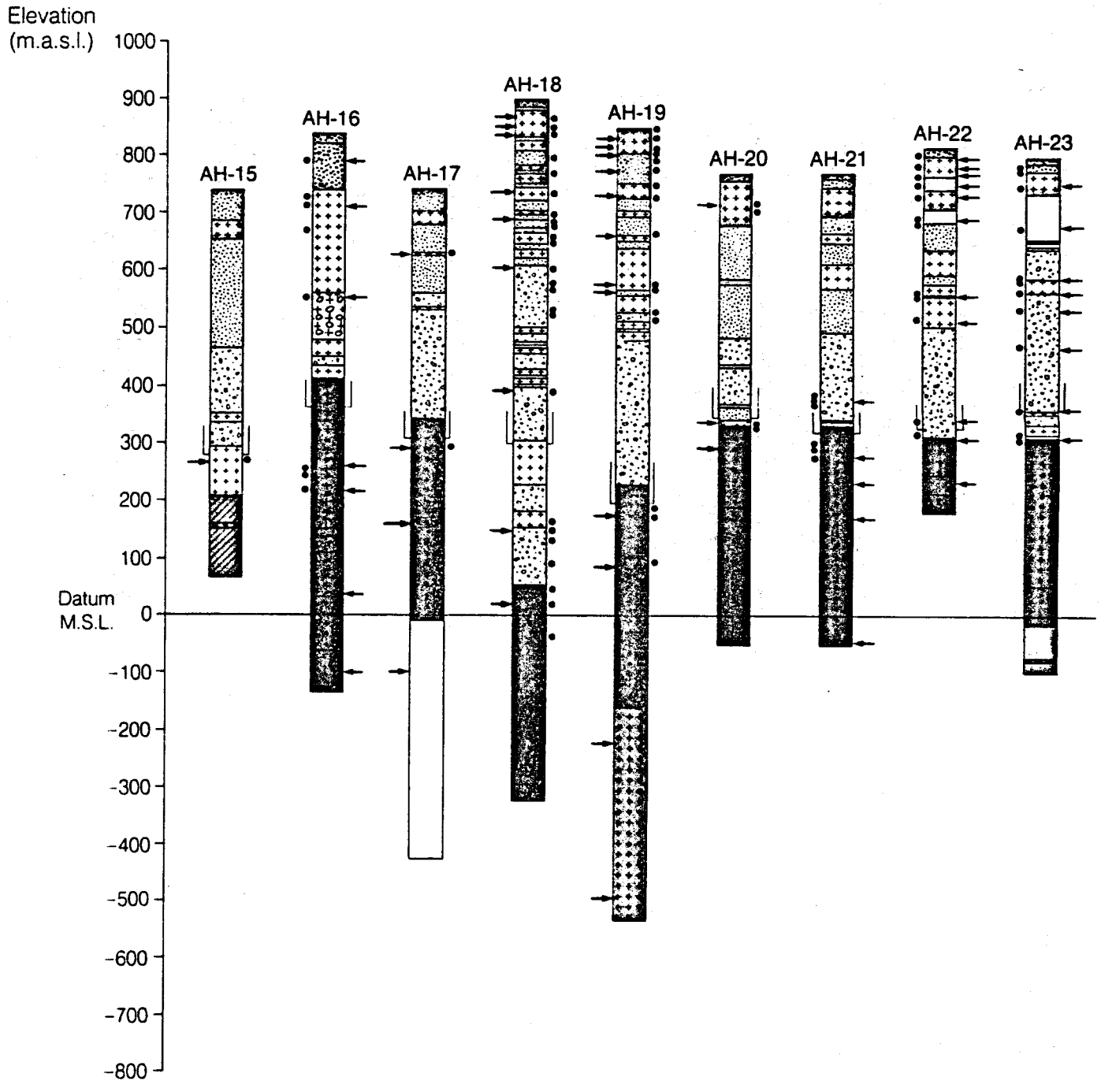

Figure 4.10c Ahuachapan well lithology

XBL 887 10327

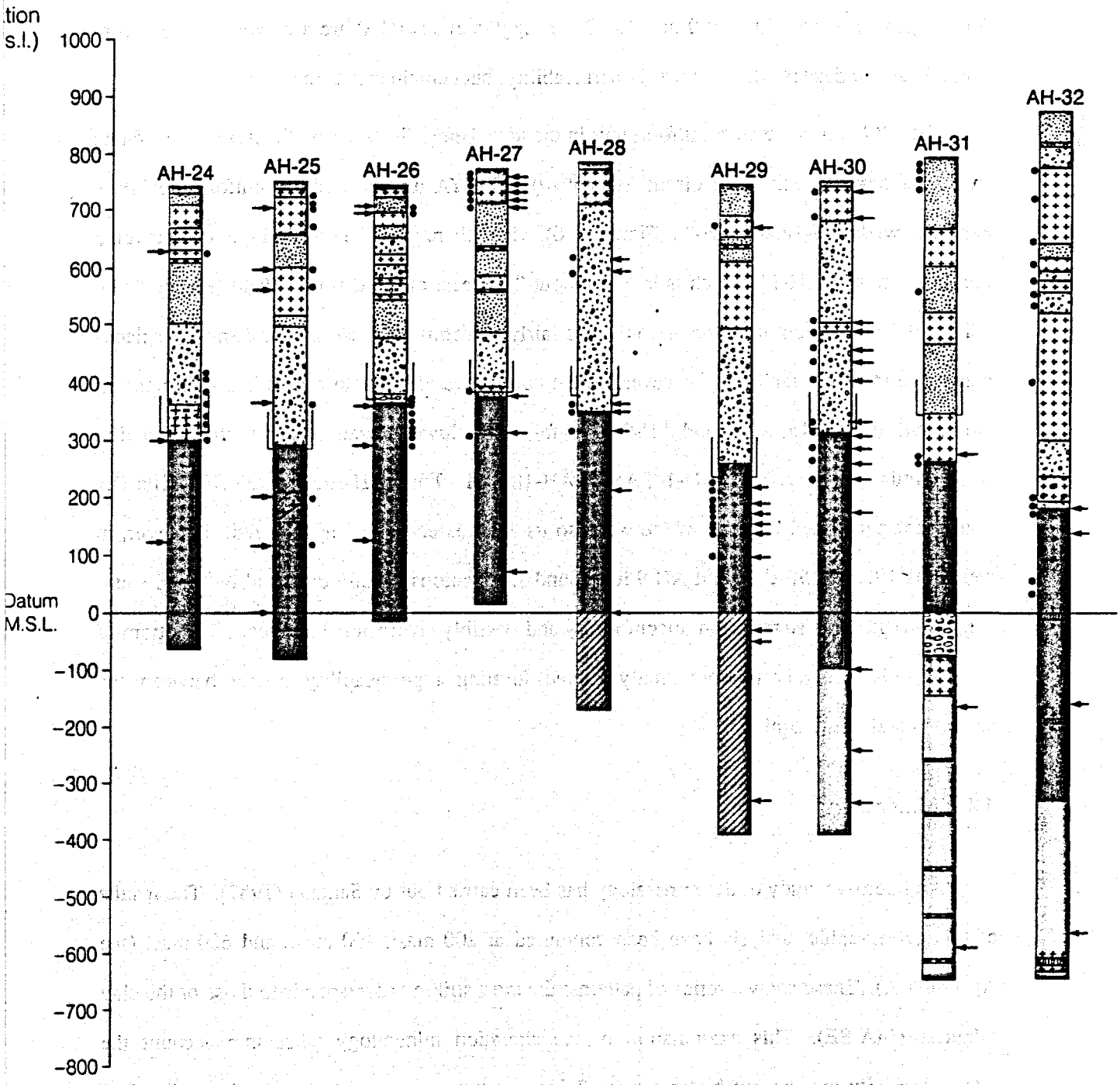

Figure 4.10d Ahuachapan well lithology

XBL 887-10328

Below the YA are the Ahuachapán Andesites (AA), a highly fractured andesite unit that presents the most permeable reservoir zone. Secondary permeability in this unit is related to columnar jointing and to contact surfaces between different layers. The thickness of the AA unit ranges between 200 to 600 m. The Older Agglomerates (OA) are a combination of dense breccias and andesites with low matrix permeability, but contain some fractures.

The SM unit is the most uniform unit in the area, being displaced by the most recent faults in only a few locations (see discussion below). The YA unit is of fairly uniform thickness except in wells AH-18 and AH-32 (Figure 4.10), where there is evidence of a high-angle reverse fault, and in well AH-14, which is located about 2 km east of the main wellfield (Figure 4.11). Within the production area, the AA unit has fairly uniform thickness showing small displacements due to recent faulting. However, on the boundaries of the field this unit is either absent (wells AH-10, AH-15, AH-8 and AH-9) or is found at a lower elevation than in the production wells (wells AH-11, AH-12, AH-14, AH-2, AH-18, AH-19 and AH-32; Figure 4.10). The OA unit is not penetrated by most of the wells so its areal extent is largely inferred. However, in wells AH-10, AH-15, AH-8 and AH-9 it is found at elevations usually occupied by the AA unit (Figure 4.10). This suggests an unconformity and possibly an erosional surface. The bottom of the YA unit is highly hydrothermally altered forming a permeability barrier between the saturated and saline aquifers.

4.2.2 Mineralogy

An intensive study of the mineralogy has been carried out by Santana (1987). The results of this petrographic analysis have been contoured at 200 masl, 400 masl, and 600 masl (see Appendix A). These show a series of patterns; the most striking corresponds to those of the clay minerals (MA-SE). This examination of the alteration mineralogy takes into account the interaction between the hot hydrothermal fluids and the country rock that result in chemical exchanges between the two media. This exchange first alters the fluid chemistry, then the existing primary mineralogy, and ultimately the texture of the rocks. By studying these changes in a

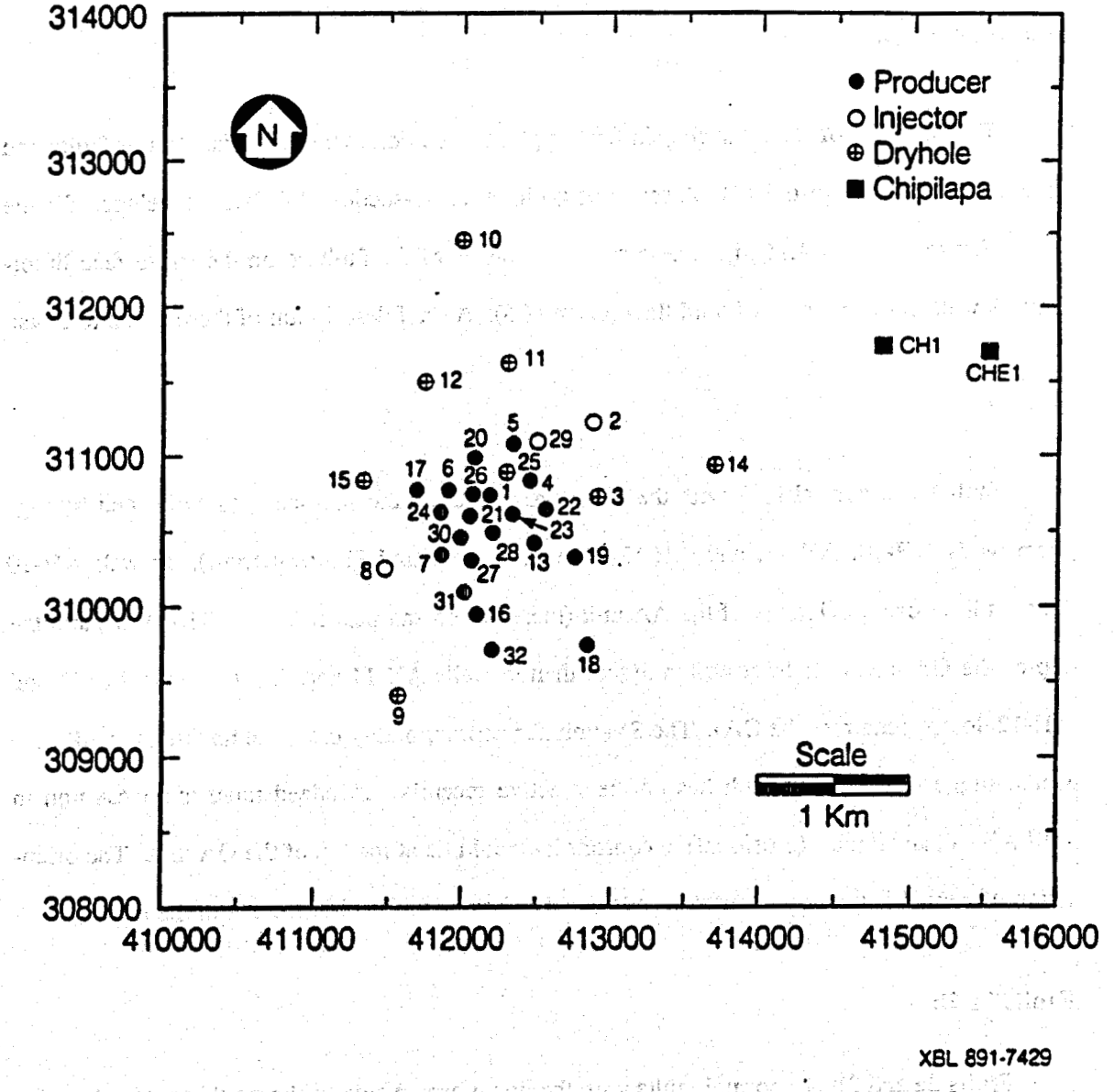

Figure 4.11. Location map of Ahuachapán wells (distance in meters).

series of wells, one can obtain three-dimensional data not only on the steady-state temperature conditions but also the locations and relative mass flows of the different fluid circulation zones (Aumento et al., 1982). See Figure 4.12 for the temperature ranges corresponding to the secondary minerals found in the field.

4.3 Main Faults

The structure of the Ahuachapán field appears to be dominated by seven major faults and five minor faults (Figure 4.13). A series of geologic cross-sections has been developed for the field (Figure 4.14 and 4.15a-i). These show the effects of the faulting on the subsurface lithology, as well as the patterns of fluid flow (Chapter 6). A brief description of these faults follows:

Fault 1

Fault 1 is a normal fault with the downthrown side to the southeast, as evidenced by logs from wells AH-10, AH-11, and AH-12 (Figure. 4.10a-d and Figure 4.15a-i). In well AH-10 there is little or no evidence of the AA unit (there are no samples from 200-350 masl), and the top of the OA unit is at least 400 m higher than in wells AH-11 and AH-12 (wells AH-11 and AH-12 do not penetrate the OA). The SM unit has approximately the same thickness in all three wells, suggesting that the fault has not been active recently. If indeed there is no AA unit in well AH-10, an angular (erosional) unconformity would lie at the top of the OA unit. The orientation of Fault 1 is unknown, but it is considered to be one of the oldest faults in the field.

Faults 2a-2b

Faults 2a and 2b are normal faults with the downthrown side to the northeast (see logs for wells AH-15, AH-17, AH-8, AH-7, AH-9, and AH-32; Figure 4.10a-d and Figure 4.15a-i). In wells AH-15, AH-8, and AH-9 there is little or no AA unit present, and the top of the OA unit is at least 400 m higher than in wells AH-17, AH-7, and AH-32 (it is not known at what depth wells AH-17 and AH-7 penetrate the OA unit, but it is assumed to be below mean sea level).

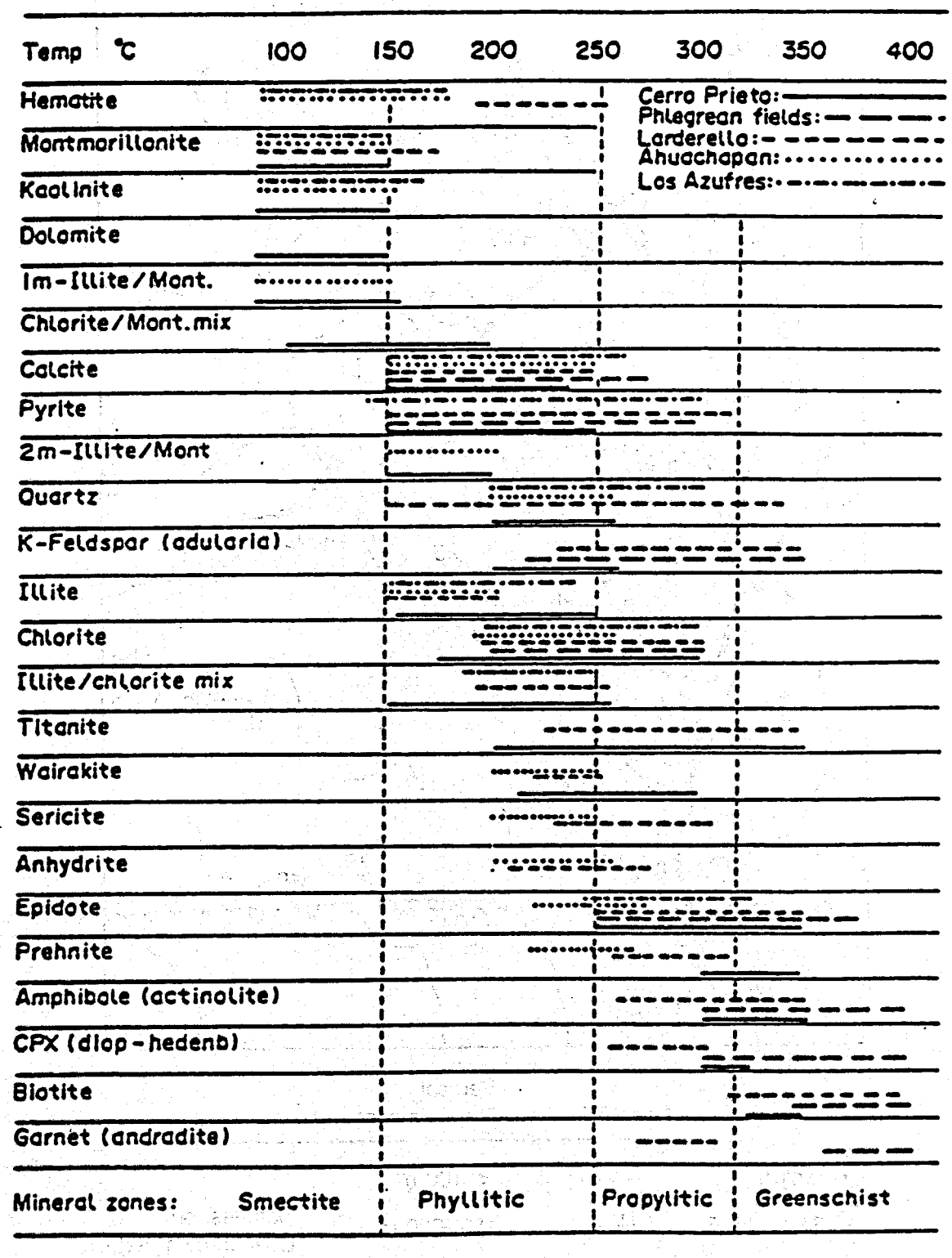

Figure 4.12. Temperature of occurence of secondary minerals in Ahuachapán geothermal field (from Aumento et al., 1982).

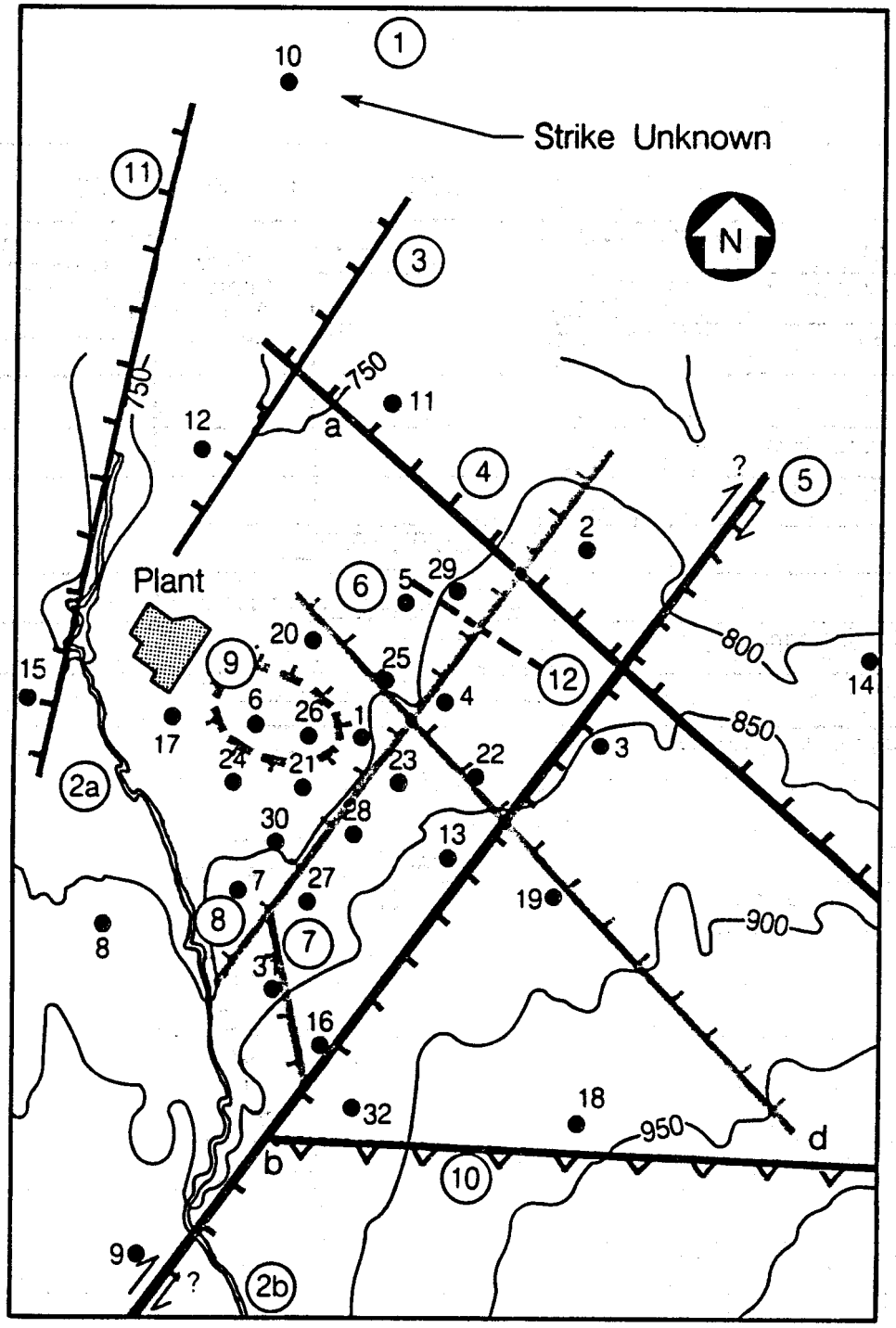

Normal Faults	Vertical Displacement	
	< 100 m	Hatches on Downthrown Side
	100–200 m	
	> 200 m	
	High Angle Reverse Fault	Sawteeth on Upthrown Block
	Right Lateral Strike-slip	

5 ● Well 5

(5) Fault No. 5

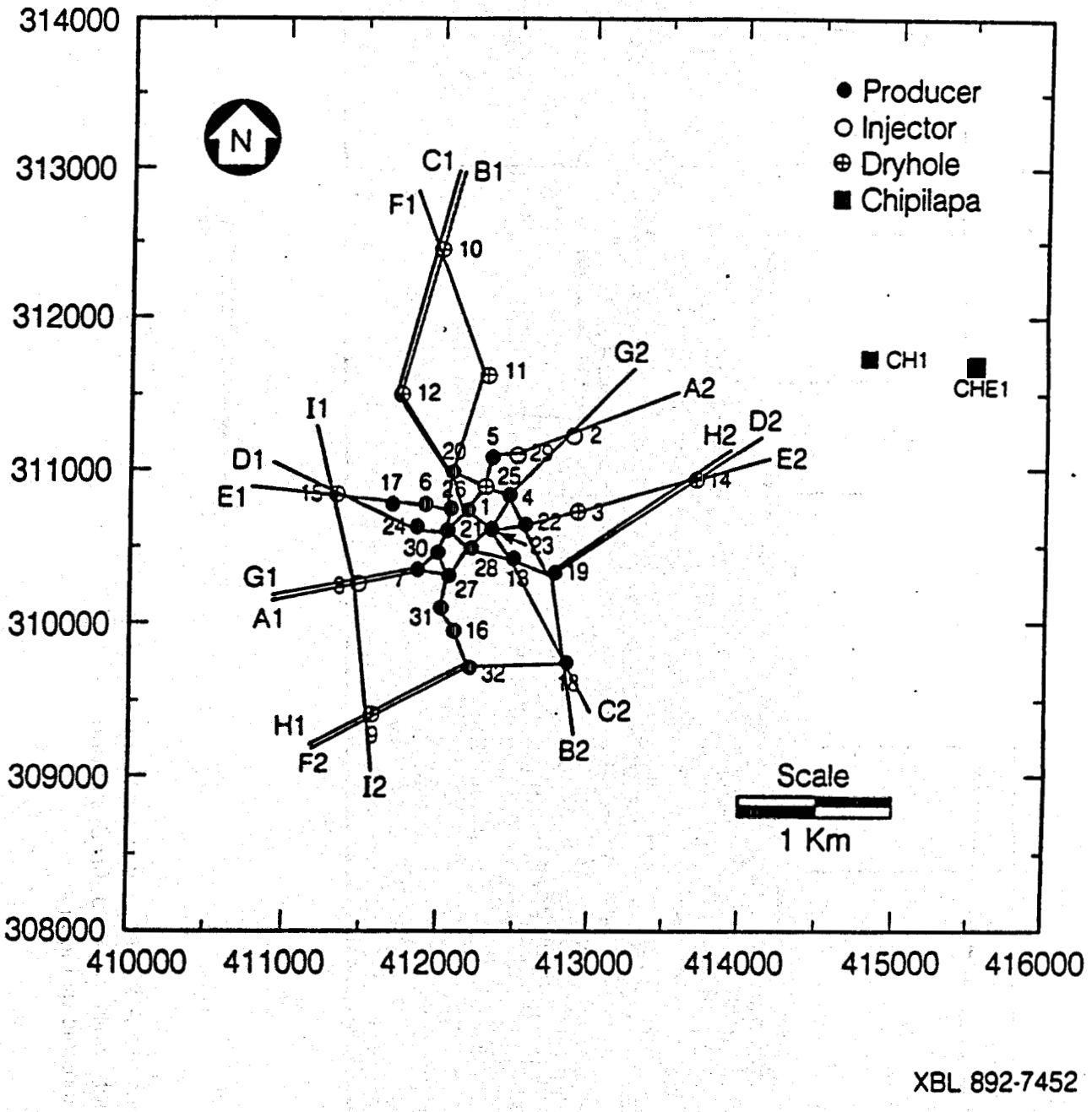

Figure 4.14. Locations of cross-sections developed for the Ahuachapán area.

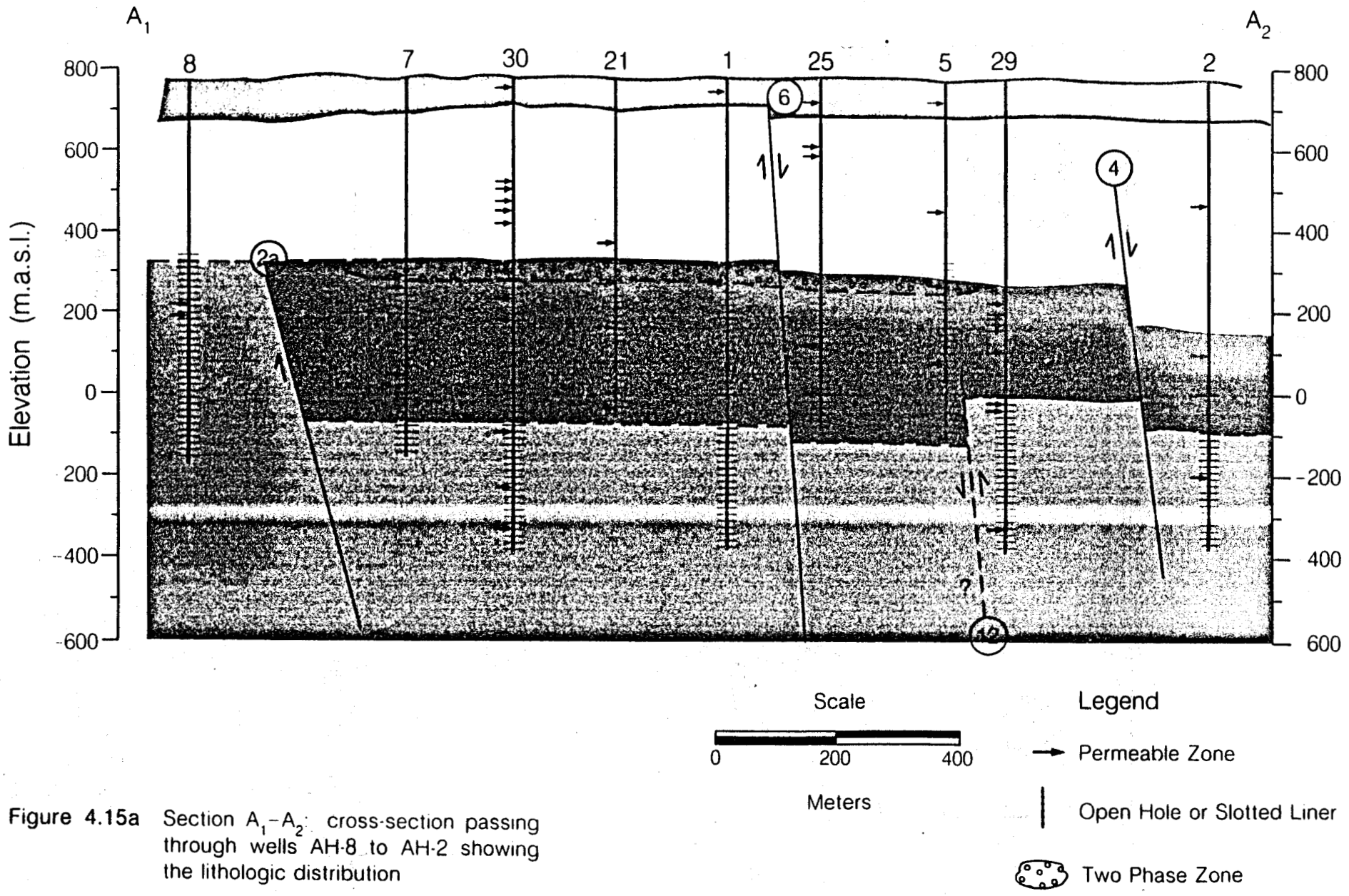

Figure 4.15a Section A_1–A_2: cross-section passing through wells AH-8 to AH-2 showing the lithologic distribution

XBL 887-10318

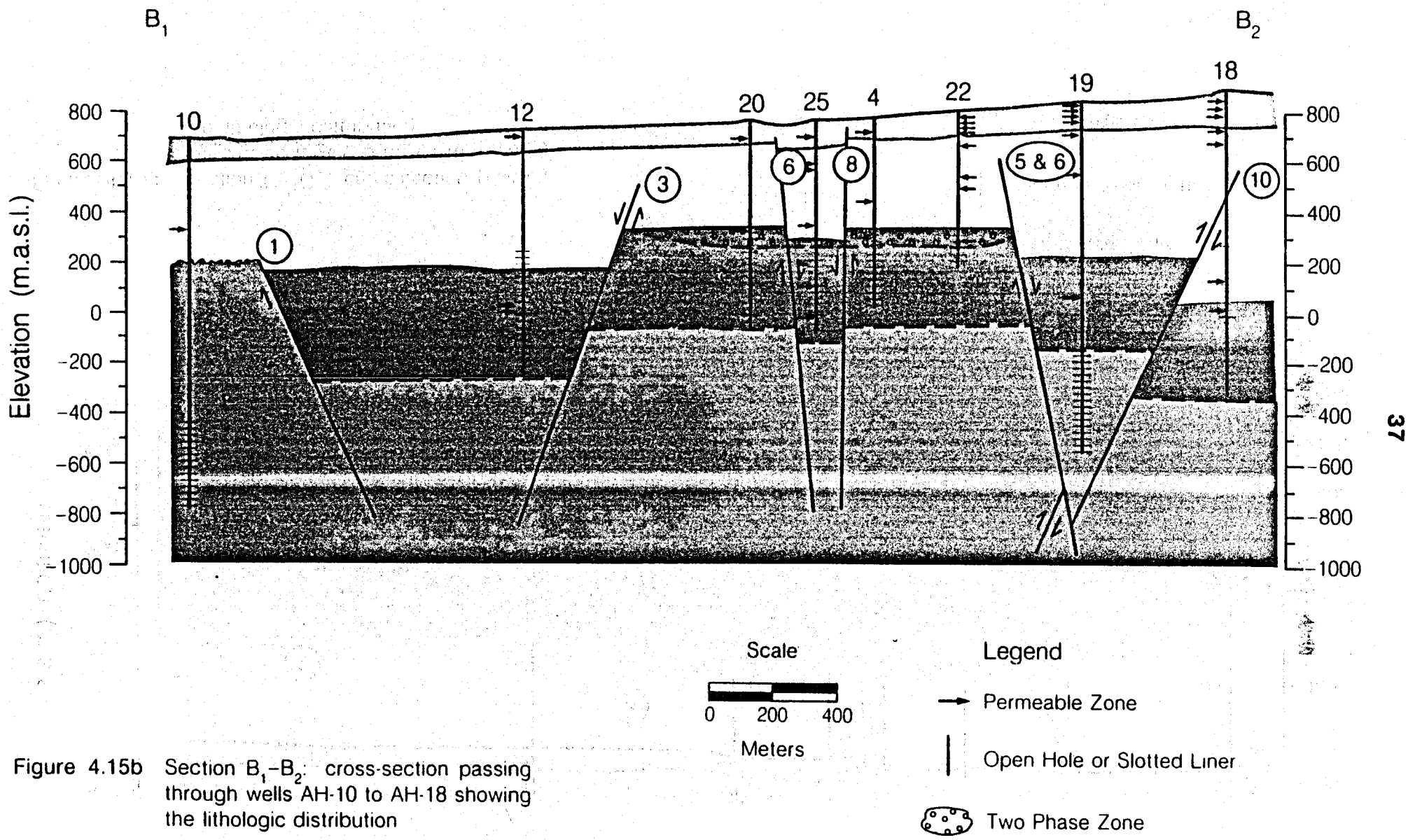

Figure 4.15b Section B_1–B_2: cross-section passing through wells AH-10 to AH-18 showing the lithologic distribution

XBL 887-10319

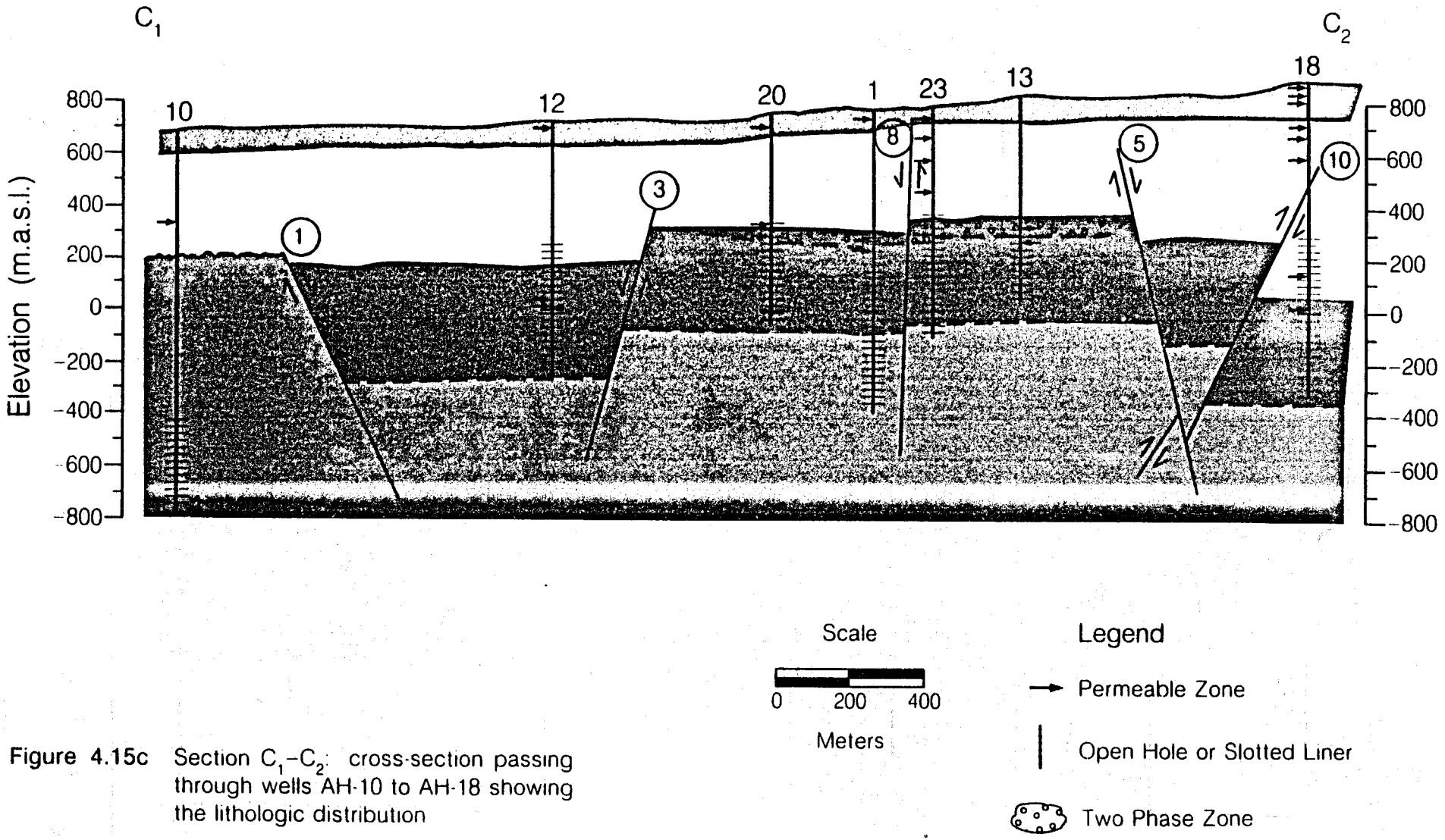

Figure 4.15c Section C_1–C_2: cross-section passing through wells AH-10 to AH-18 showing the lithologic distribution

XBL 887-10320

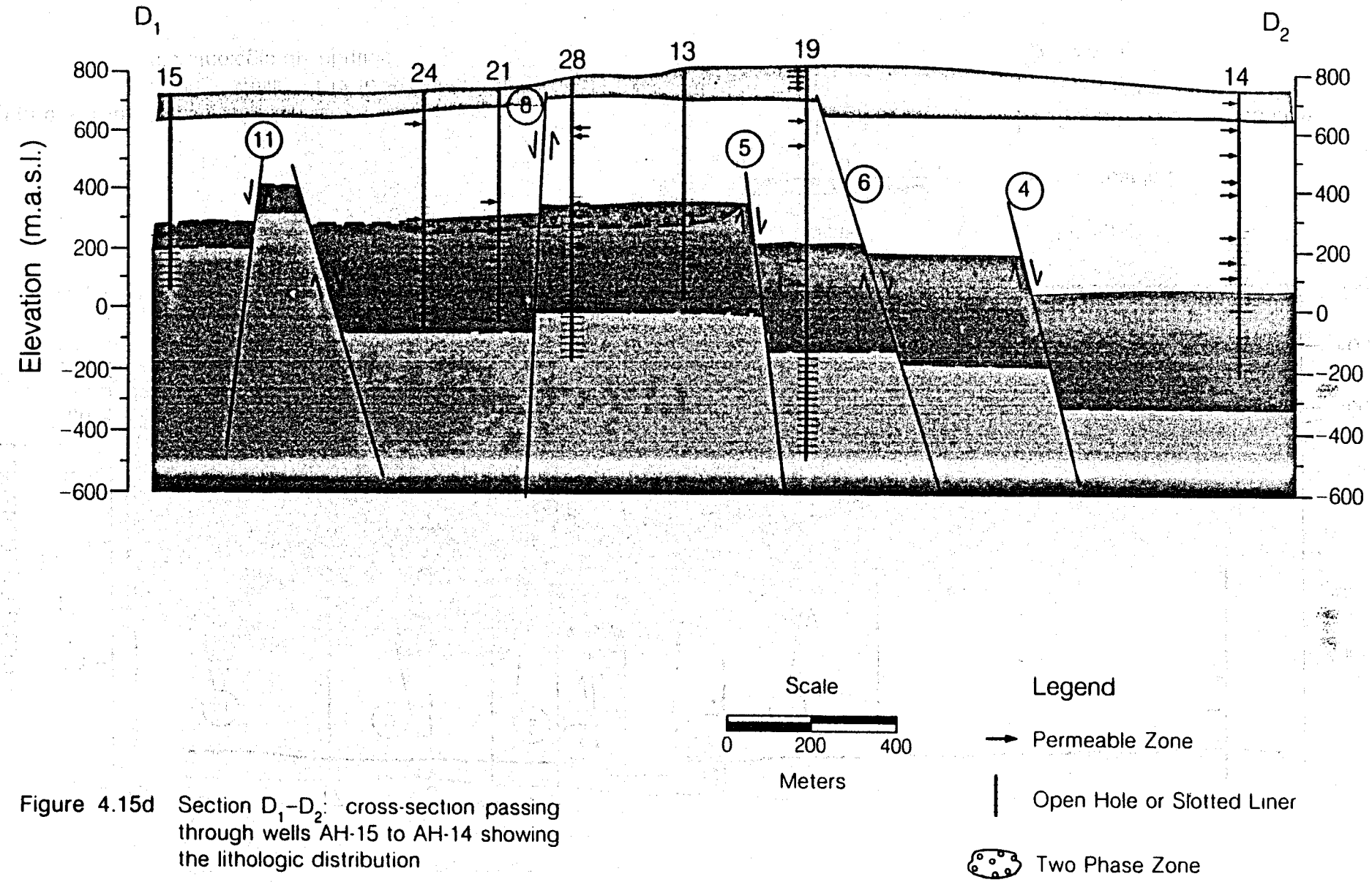

Figure 4.15d Section D_1–D_2: cross-section passing through wells AH-15 to AH-14 showing the lithologic distribution

XBL 887-10321

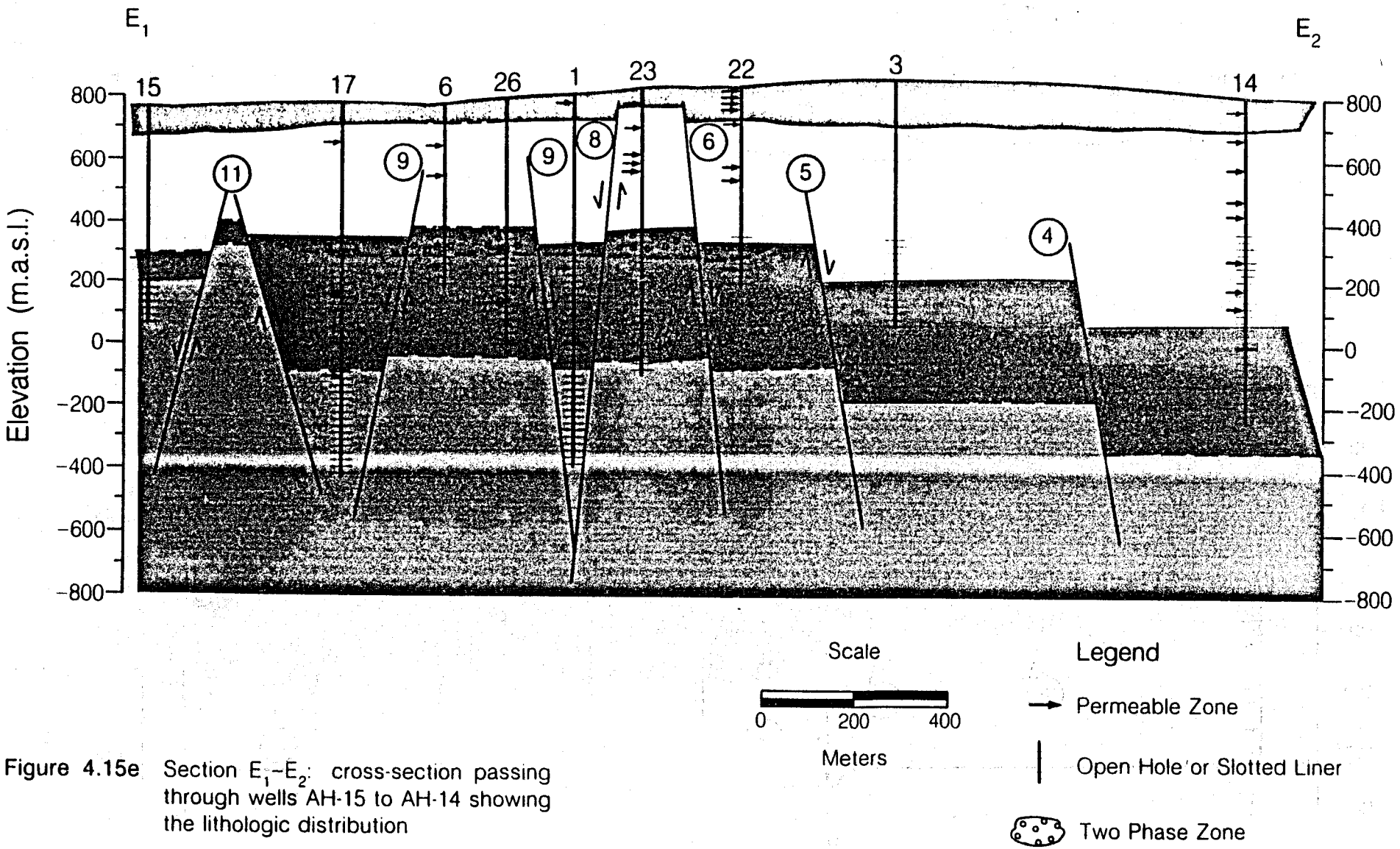

Figure 4.15e Section E_1–E_2: cross-section passing through wells AH-15 to AH-14 showing the lithologic distribution

XBL 887-10322

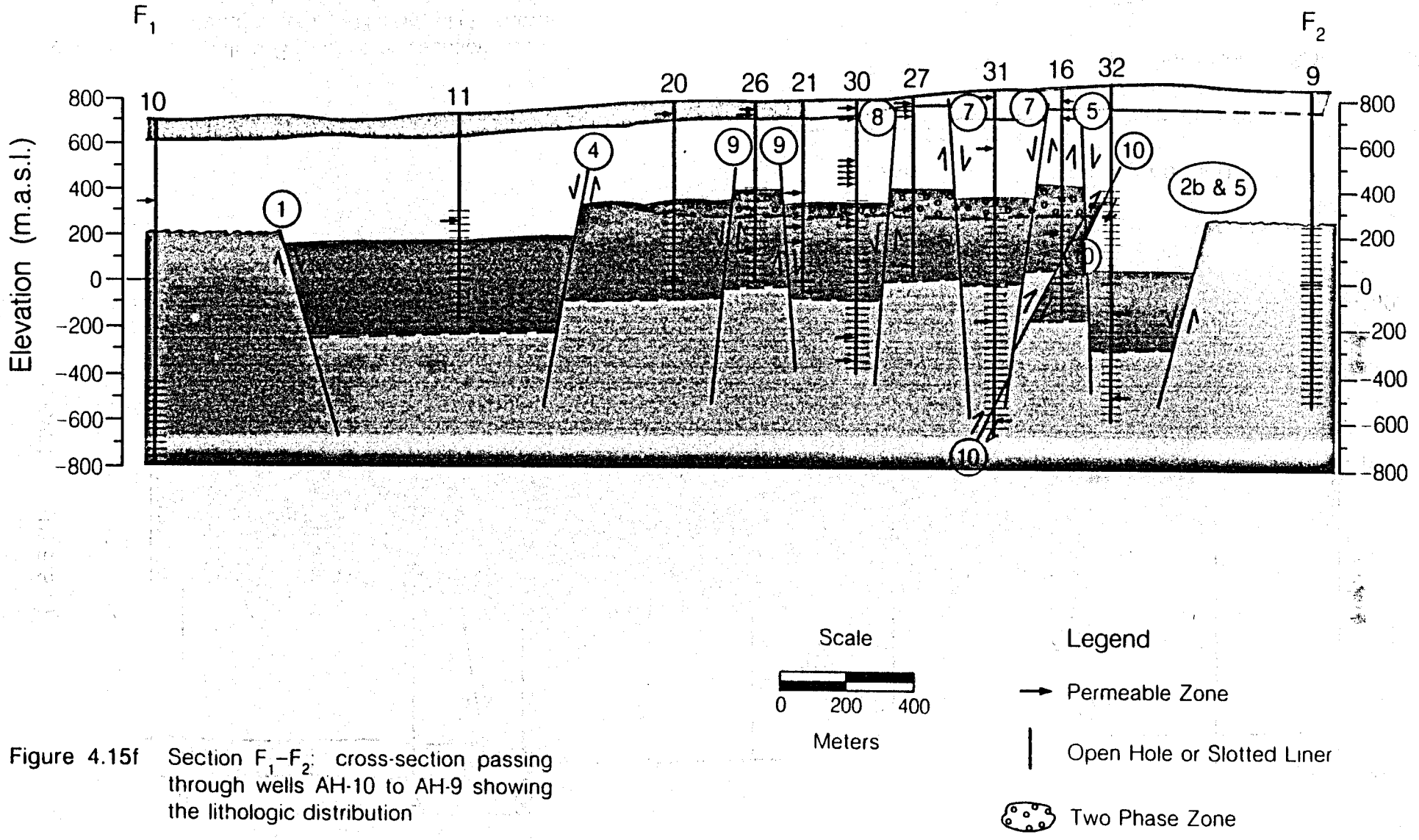

Figure 4.15f Section F_1–F_2: cross-section passing through wells AH-10 to AH-9 showing the lithologic distribution

XBL 887-10323

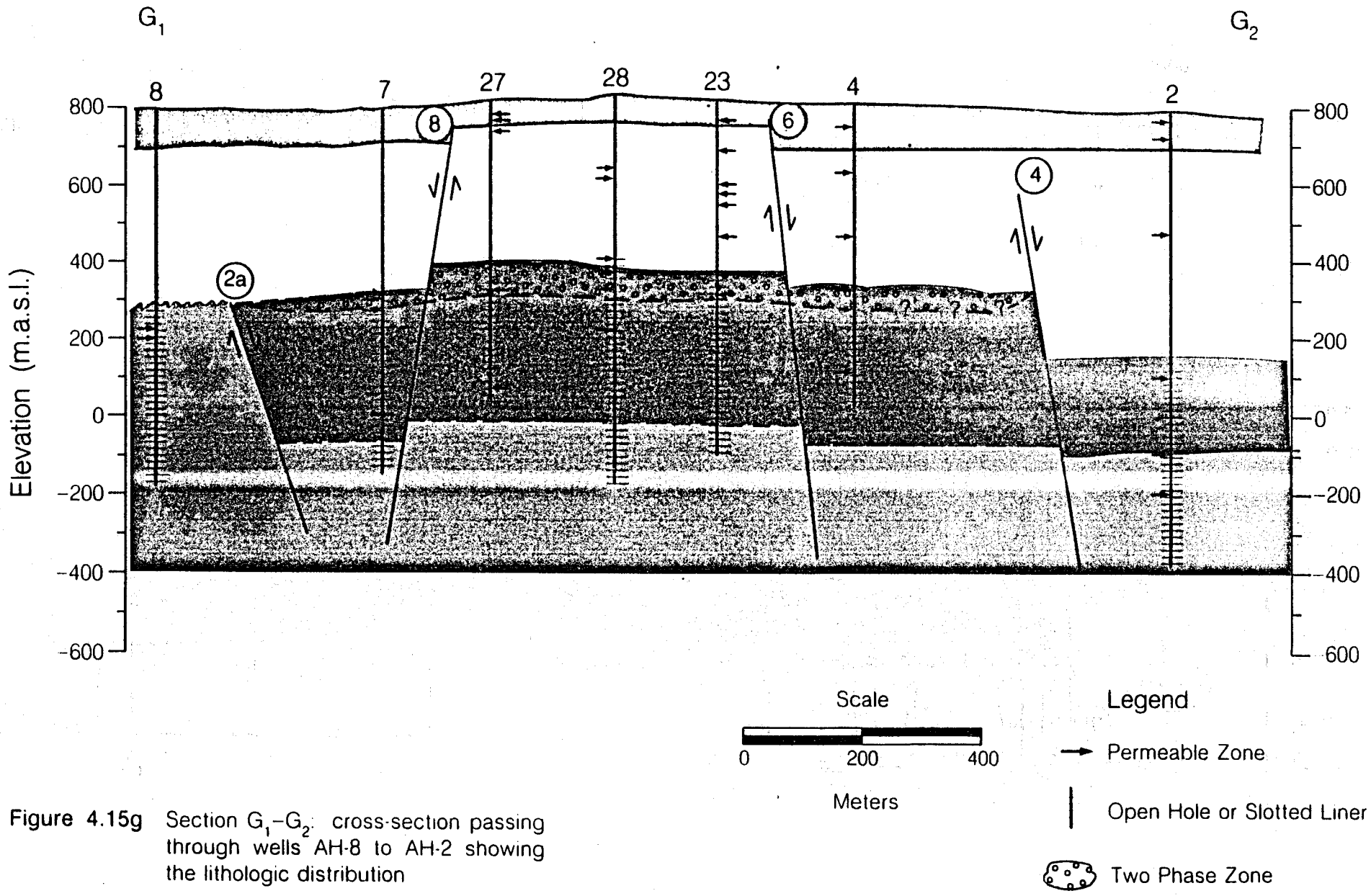

Figure 4.15g Section G_1–G_2: cross-section passing through wells AH-8 to AH-2 showing the lithologic distribution

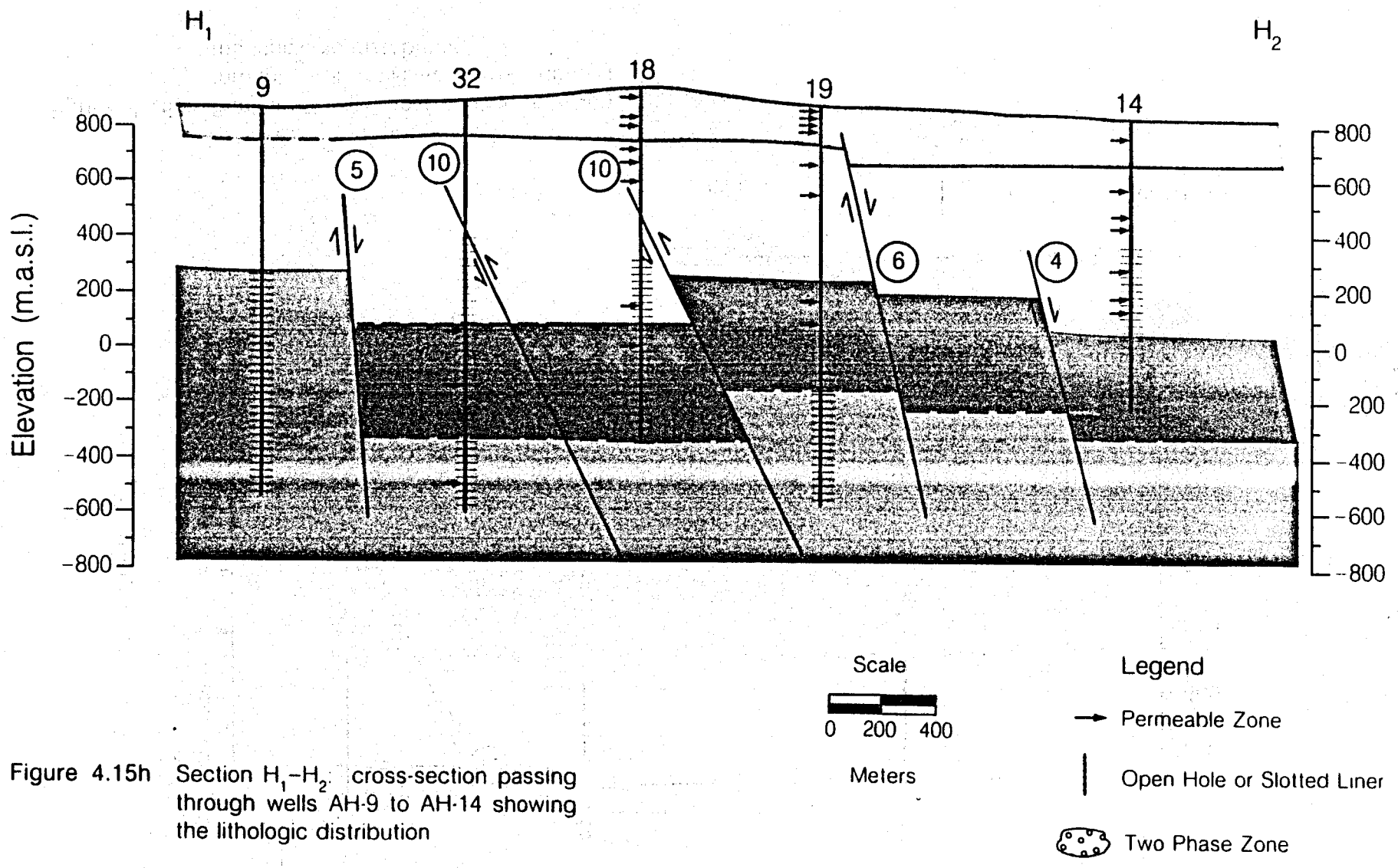

Figure 4.15h Section H_1–H_2 cross-section passing through wells AH-9 to AH-14 showing the lithologic distribution

XBL 888-10366

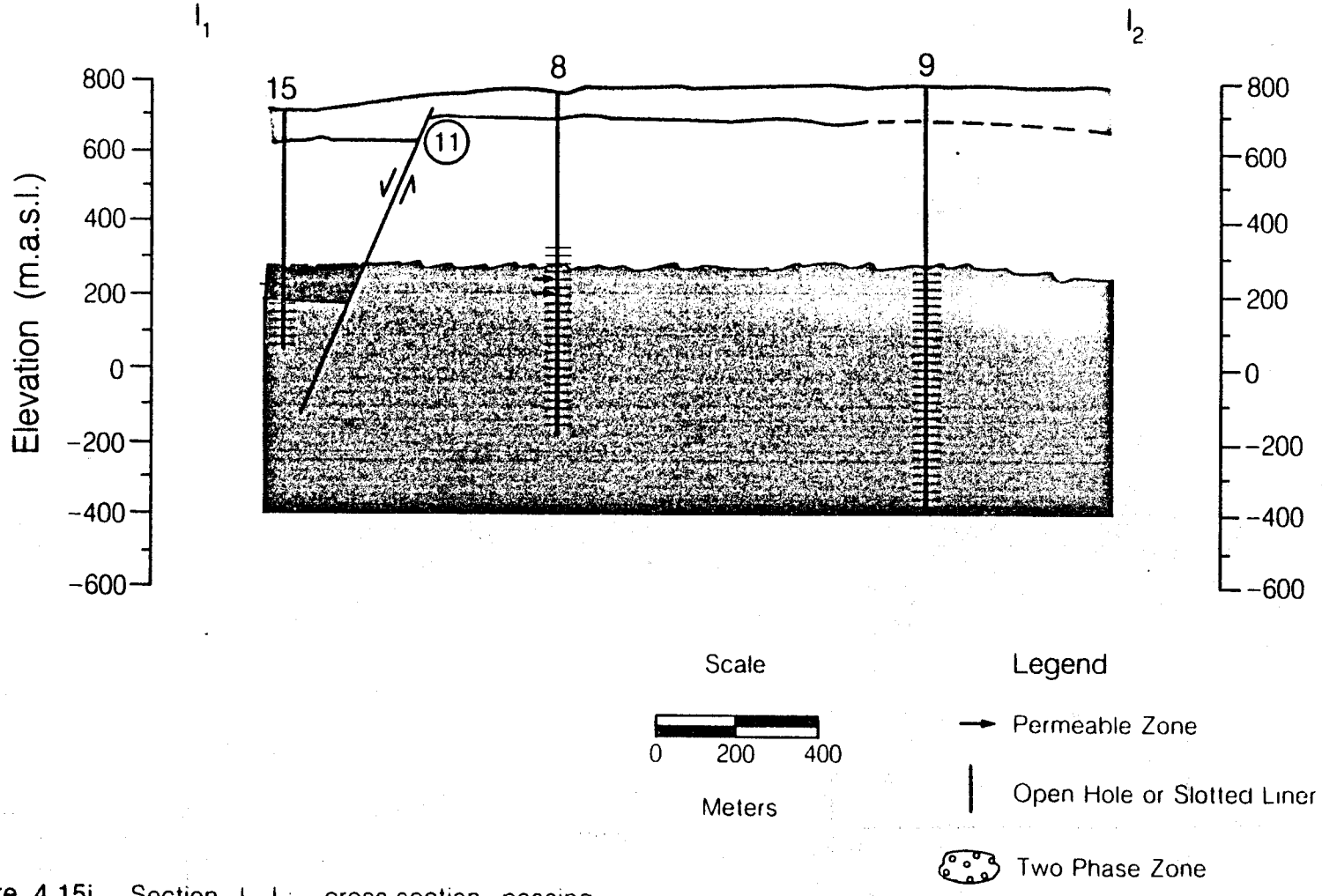

Figure 4.15i Section I_1–I_2 cross-section passing through wells AH-9 to AH-14 showing the lithologic distribution

XBL 892-7461

Jonsson (1970) supports this interpretation, and suggests the presence of a major geologic structure between these two groups of wells. The SM unit has approximately the same thickness in neighboring wells, suggesting that Faults 2a and 2b have not recently been active. If the AA unit is not found in wells AH-15, AH-8, and AH-9, an unconformity could be present at the top of the OA unit, indicating an erosional surface. These faults are believed to strike along the bed of the Río Los Ausoles, which appears to be offset by Fault 5 (see below). This suggests that the original Fault 2 has been offset (300-400 m) segmenting it into Faults 2a and 2b. Fault 2 is also considered to be among the oldest in the field.

Fault 3

Fault 3 is a normal fault with the downthrown side to the northwest (see logs for wells AH-20 and AH-12; Figure 4.10a-d and Figure 4.15a-i). The top of the AA unit is approximately 150 m higher in well AH-20 than in well AH-12. This interpretation is supported by Romagnoli et al. (1976), who suggest that the geothermal field is limited to the north by another E-NE/W-SW fault which lowers the block in which wells AH-11 and AH-12 are located. The SM unit has approximately the same thickness in both wells, suggesting that the fault has not recently been active. The orientation of Fault 3 is along a lineation (fault scarp?) that is clearly seen on aerial photos, although the topography suggests a downthrow toward the southeast (perhaps due to erosional effects).

Fault 4

Fault 4 is a normal fault with its downthrown block to the northeast (see logs for wells AH-2, AH-5, AH-11, and AH-29; Figure 4.10a-d and Figure 4.15a-i). The top of the AA unit is approximately 120 m higher in wells AH-5 and AH-29 than in wells AH-11 and AH-2. This is the fault that lowers the block surrounding well AH-11 as discussed by Romagnoli et. al. (1976). The SM unit has approximately the same thickness in all four wells, suggesting that Fault 4 has not been recently active. A recent tracer injection test into AH-2 using tritium showed no tracer

returns in the nearby wells (Alejandro Quintanilla, verbal communication, 1988). This is a further indication of the existence of Fault 4 and its role as at least a partial barrier to flow. The orientation of this fault is also inferred from lineations appearing on aerial photos. These include a cleft in the ridge north of wells AH-11 and AH-12, a rise on which well AH-2 is situated, and the orientation of a stream bed northeast of well AH-3. Fault 4 is thought to be younger than Fault 5 since it is not displaced by it.

Fault 5

Fault 5 is a normal fault with the downthrown side to the southeast. It is also possible that it has a right lateral strike-slip component as supported by the inferred offset of Fault 2. This would make the transform movement of this fault older than all but Fault 2, creating a plane of weakness for the subsequent normal faulting along its strike. There are also indications of this displacement in the aerial photos but clear evidence has been obscured by more recent flows and sedimentation.

A quandry is the fact that Fault 5 shows right-lateral offset in an orientation that has previously been mapped in El Salvador as showing only left-lateral displacement (Section 4.1). The normal displacement is evident in logs of wells AH-13, AH-16, AH-19, and AH-32 (Figure 4.10a-d and Figure 4.15a-i). Between wells AH-13 and AH-19, there is a 150 m offset of the top of the AA unit. This offset is 350 m between wells AH-16 and AH-32, but 200 m of it can be attributed to Fault 10 (see below). The SM unit has approximately the same thickness in all four wells, suggesting that Fault 5 has not been recently active. The orientation of this fault is suggested by the lineations (i.e., riverbeds) observed in the aerial photos and by the mineralogy contours plotted for three different elevations (Appendix A). These contours, especially those for the clay minerals (MA-SE) show a distinct orientation that agrees with the fault's strike. In addition, the logs for both wells AH-13 and AH-16 indicate a large brecciated sequence, although it is not known whether it is related to a fault or volcanic breccia. The surface manifestation Agua Shuca (Figure 4.9), south of well AH-9, may also be associated with Fault 5.

Fault 6

Fault 6 is a normal fault with its downthrown block to the northeast (see logs for wells AH-20, AH-25, AH-1, AH-4, AH-23, AH-22, AH-19, and AH-14; Figure 4.10a-d and Figure 4.15a-i). It is a minor fault with a displacement of approximately 50 m that is apparent in both the AA and SM units, indicating that this is a relatively recent fault. The orientation of Fault 6 is suggested by a lineation observed on the aerial photos; this lineation follows the stream bed to the northeast of well AH-19 and continues across the field. Further support is given by the mineralogy contours showing trends in this direction (i.e., MA-SE at 200 m, Q at 400 m, MA-SE at 600 m, HE-OX at 600 m, and Q at 600 m; Appendix A).

Fault 7

Fault 7 is a normal fault with the downthrown side to the west-southwest (see logs for wells AH-27, AH-31, and AH-16; Figure 4.10a-d and Figure 4.15a-i). The fault displaces both the AA and SM units by about 40 m suggesting recent movement. Virtually all of the mineralogy contours (Appendix A) confirm the existence of this fault and its orientation.

Fault 8

Fault 8 is a normal fault with the downthrown side to the northwest (see logs for wells AH-7, AH-31, AH-27, AH-30, AH-21, AH-28, AH-23, and AH-1; Figure 4.10a-d and Figure 4.15a-i). Both the AA and SM units are displaced, indicating recent movement along this fault. The mineralogy contours that support the presence of Fault 8 in the field are MA-SE at 200 and 600 m, HE-OX at 200 and 400 m, CL-PE at 400 m, and Q at 400 and 600 m (Appendix A).

Fault 9

The apparent Fault 9 may actually be a dome structure, although the displacement is only 50 m and does not appear in the SM unit The evidence for this structure lies in the logs for wells AH-17, AH-6, AH-26, AH-20, AH-1, AH-21, and AH-24 (Figures 4.10a-d and 4.15a-i and

Appendix C). This interpretation is supported by Cuellar et al. (1979), who point out that wells AH-6 and AH-26, with higher steam percentages correspond exactly to the structural high of the reservoir. The aerial photos also suggest a structural high in this area. The mineralogy contours that support this structure are MA-SE at 600 m, HE-OX at 600 m, CA at 600 m, CL-PE at 400 m, and Q at 400 m (Appendix A).

Fault 10

Fault 10 is interpreted as being a high-angle reverse fault with its overriding block oriented north-northwest. The evidence for this fault is found in the logs for wells AH-18, AH-19, AH-32, and AH-16 (Figures 4.10a-e and Figure 4.15a-i and Appendix C). There is evidence of a repeated sequence of the YA unit in well 18 (Figure 4.16). The YA unit is extremely thick in this well, but when the repeated sequence is removed, the thickness of the unit is similar to that observed in well AH-19 (Figure 4.17). The 180 m elevation difference between the bottom of the YA unit in the wells AH-18 and AH-19 supports the interpretation that Fault 10 is a high angle reverse fault. There was also a large loss of circulation while drilling throughout this unit, which suggests a fault zone.

In well AH-32 there is also a possibility of a repeated YA sequence, although a different lithologic classification was used by CEL for this well. However, it is evident that in well AH-32 the bottom of the YA unit is 330 m lower than in well AH-16. This displacement corresponds to the sum of the downthrows of Fault 5 (150 m) and Fault 10 (180 m). In AH-16, the AA is extremely thick and brecciated, suggesting the reverse fault intersection and AH-31 could be displaced in the OA (see cross-section $F_1 - F_2$).

It is possible that Fault 10 extends to the west of Fault 5. AH-8 is a shallow well and the reverse fault dips steeply so their intersection is highly improbable. There is however a 100 m difference in the lower level of the YA in AH-8 and AH-9 that could be attributed to Fault 10.

Although Ahuachapán is in an area of extentional tectonics, it is believed that this compressional feature could be caused by rupture deformation (Figure 4.18). The lifting of the

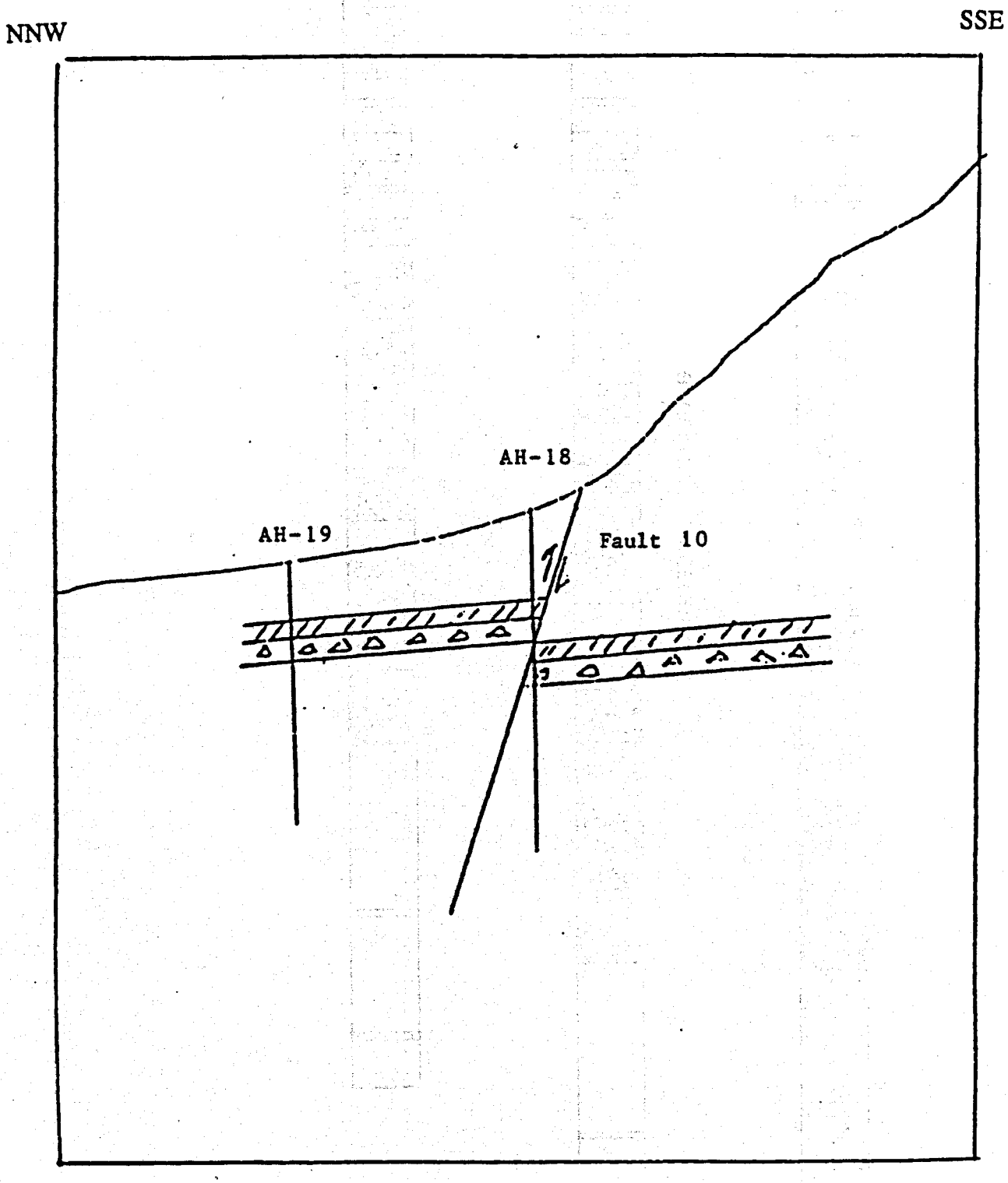

Figure 4.16. High angle reverse fault with repeated sequence.

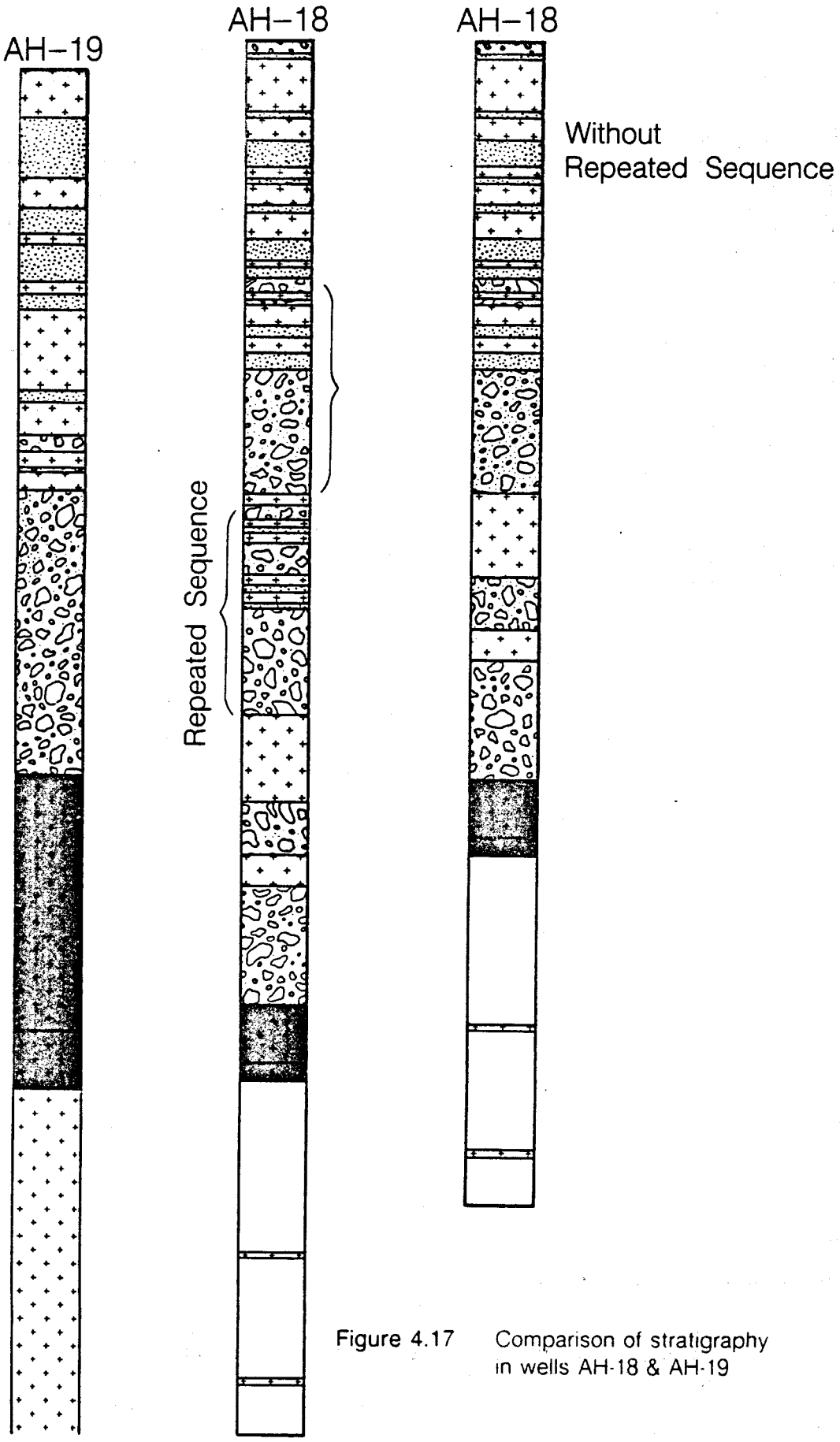

Figure 4.17 Comparison of stratigraphy in wells AH-18 & AH-19

XBL 887-10316

roof rocks by an underlying magma body would cause the formation of a dome similar to that shown in Figure 4.19. Note that approximately halfway through the overburden there is a surface, defined as the neutral plane, that shows neither extension nor compression during folding. Above the neutral plane the rocks undergo extension and beneath, the rocks are subjected to compression (Nielson and Hulen, 1984). Since the Ahuachapán field is on a flank of a volcano it is not unreasonable to hypothesize that such a deformation may have taken place.

The existence of Fault 10, although suggested by the data, is not certain; other interpretations are possible as suggested by CEL. One may consider that existence of Fault 10 as a working hypothesis that will have to be tested during the modeling of the behavior of the field and/or by new wells that may be drilled in that part of Ahuachapán.

Fault 11

Fault 11 is a normal fault with a downthrow of 100 m to the northwest. The evidence for this fault is found in the logs for AH-15, AH-17, AH-8 and AH-7 (Figs. 4.10a-d and 4.15a-i). Where there is a 400 m difference in the top of the OA between wells AH-8 and AH-7 due to Fault 2, there is only a 300 m difference between AH-15 and AH-17. This can be accounted for by a later displacement due to Fault 11. This also is evident when comparing the top of the OA in AH-15 and AH-8. The observed pressure drawdown in wells AH-9 and AH-8 as a result of the exploitation but not in AH-15 suggests that this fault acts as a barrier to flow. Also, the AA in AH-15 is not host to the reservoir fluids (see cross-sections $D_1 - D_2$ and $E_1 - E_2$). Since the SM have not been displaced, there has been no recent movement along this fault. The orientation of Fault 11 is along the bed of the Río Los Ausoles causing the bend in the river at its intersection with Fault 2.

Fault 12

Fault 12 is possibly a normal fault with a downthrow of 100 m to the southwest. There is little evidence for this fault except in the logs for AH-5 and AH-29 (Figs. 4.10a-d and 4.15a-i).

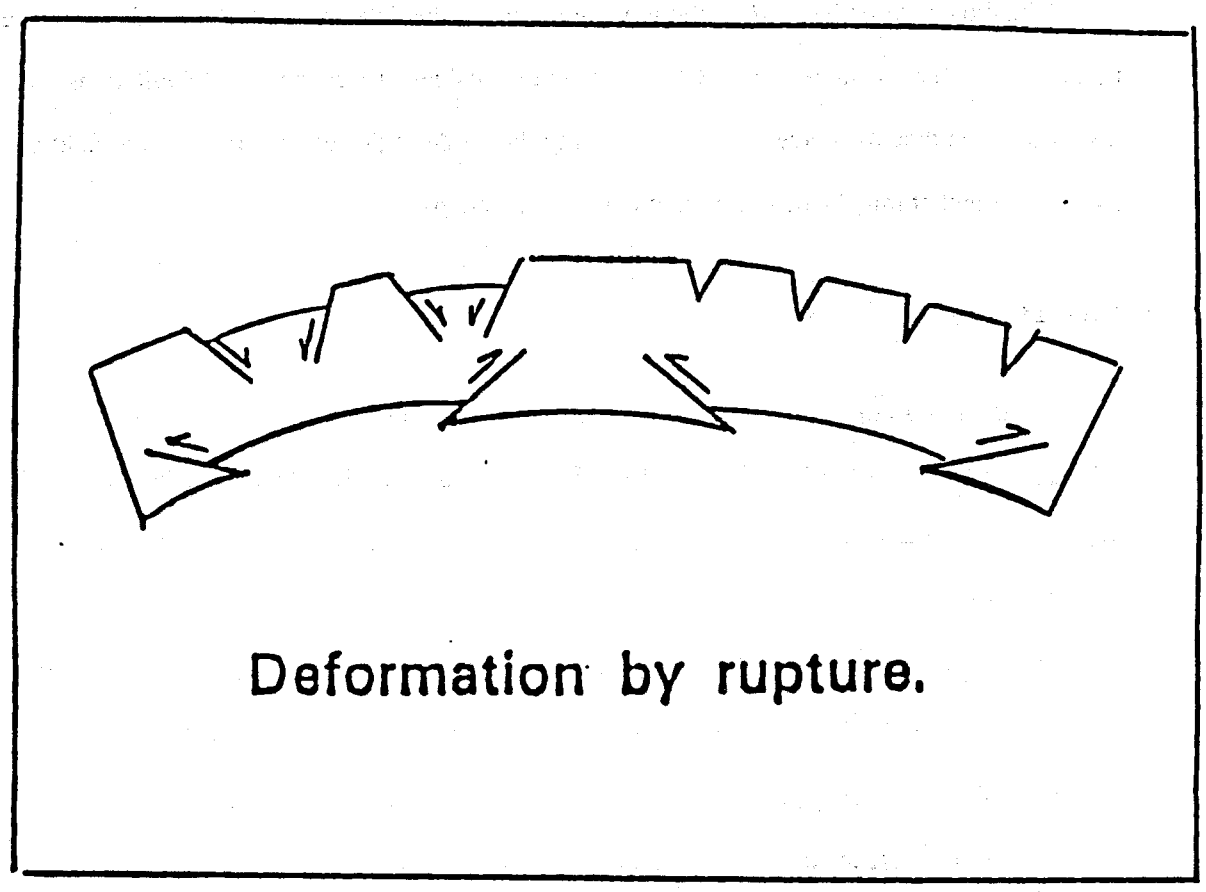

Figure 4.18. Deformation by rupture (after Billings, 1972).

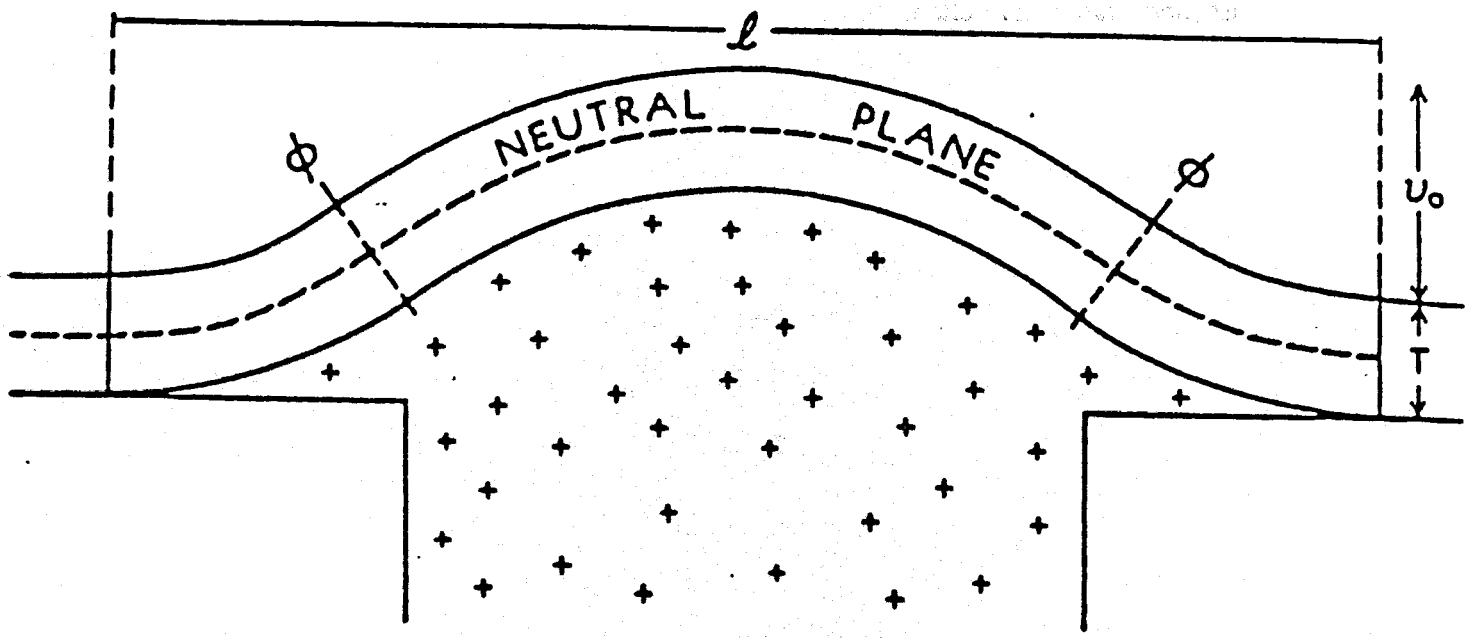

Figure 4.19. Idealized model of dome development (from Nielson and Hulen, 1984).

Although the logs for AH-29 show the top of the OA at msl, there are numerous permeable zones between msl and -100 m msl. These are unusual and suggest that this unit is AA. The movement along this fault would be fairly old since the top of the AA is not affected. The orientation has been shown parallel to Faults 4 and 6.

There is little information to suggest the dips of the above faults, however, a microearthquake survey by Ward and Jacob in 1971 clearly indicated an active fault-like structure through the Ahuachapán thermal area striking approximately N 10° E and dipping about 80° toward the east (Bodvarsson and Bolton, 1971).

5.0 GEOCHEMICAL STUDIES

Chemical studies of produced fluids from geothermal wells provide information on the temperature, salinity, physical state and subsurface flow of fluids in the reservoir. Extrapolation to the time of first production provides estimates of initial conditions, and changes in fluid composition indicate reservoir processes, including boiling, entry of different (usually cooler and less saline) fluids, and conductive heat transfer. The study of Ahuachapán well discharges was concentrated on the calculation of chemical geothermometer temperatures and aquifer chlorinity as a function of time. The resulting time-series diagrams have been used to indicate a range of reservoir processes at Ahuachapán.

5.1 Geothermometry of Fluids

Fluid geothermometers depend on temperature-sensitive reactions of fluids and rock minerals or fluid components. In a producing field, downhole temperatures may be conveniently estimated through the use of geothermometers applied to analyses of produced fluids, provided the geothermometer reaction is in equilibrium at downhole conditions. Geothermometer reactions differ in how quickly they reach equilibration. If fluid temperatures change by boiling, passage through hotter or cooler rocks, or mixture with hotter or cooler fluids, or if fluids have enthalpy contents higher than those expected for liquid at the expected temperature, then comparison of geothermometer temperatures may indicate reservoir processes. A particularly useful set of temperature indicators for this purpose is the Na-K-Ca cation geothermometer, the quartz-saturation geothermometer and the calculated "enthalpy temperature," (i.e., the temperature of liquid water corresponding to the enthalpy of the total fluid discharge). These indicators have been successfully applied at Cerro Prieto, Mexico, where extensive chemical data similar to that from Ahuachapán that have been collected on well discharges.

5.2 Interpretation of Temperature-Time Plots

The temperature-time plots presented in Appendix I consist of calculated values of the Na-K-Ca, quartz-adiabatic and enthalpy temperatures plotted together against time. The differences between these temperatures are interpreted to indicate reservoir processes in the following manner.

The Na-K-Ca temperatures are assumed to represent the temperatures of the fluid at distance from the well not affected by near-well mixing and boiling. The relatively distant fluid is assumed to have remained at its indicated temperature long enough to be fully equilibrated. This results from the slow re-equilibration of the geothermometer, which occurs through ion exchange on surfaces of feldspar and other aluminosilicates. These surfaces may not be available for reaction because of mantling with precipitated quartz.

Silica (quartz-saturation) temperatures are assumed to represent near-well temperatures and are usually fully equilibrated. At reservoir temperatures, the silica geothermometer equilibrates relatively rapidly (in days at 220 °C, in hours at 280 °C) through precipitation (decreasing temperatures) or solution of quartz. No other precipitation occurs to mantle quartz, which is universally present in reservoir rocks. The equilibration of quartz with solution is much more rapid than that of cations unless the solution is dilute. For Cerro Prieto, calculated well-bottom temperatures have been shown to agree reasonably well with quartz-saturation geothermometer temperatures.

Finally, enthalpy temperatures indicate either the actual temperature of the liquid if no vapor is present in the well feed or indicates the relative amount of excess steam (or excess enthalpy). In the second case, the indicated temperatures do not correspond to any real reservoir temperature.

Some explanation is required in the use of "enthalpy temperature." As described earlier, this is the temperature of liquid water with the enthalpy of the total fluid. If the fluid that enters the well is entirely liquid with no vapor and the enthalpy is correctly measured, then the

enthalpy temperature will be the same as the actual inflow temperature. If there is excess steam, the enthalpy temperature will be higher than the actual inflow temperature. The comparison of geothermometer and enthalpy temperatures can indicate excess steam or near-well addition of cooler water. Enthalpy temperature is calculated from steam tables, using data for temperature and enthalpy of vapor-saturated liquid. For this calculation, both liquid and vapor phases must be present, so there is some inaccuracy for compressed liquid conditions. This error is small because the enthalpy of water is a weak function of pressure. A more serious limitation is that enthalpies exceeding that of water at the critical point (2100 kJ/kg at 374°C) cannot be represented by enthalpy temperatures since vapor-saturated liquid cannot exist with these enthalpies.

5.3 Observed Reservoir Processes

The well may have an all-liquid feed of fully equilibrated water without temperature change due to near-well processes. Alternately, during passage to the well, the temperature may change due to one of the following reasons:

1) Boiling, in which the temperature is reduced as pressure drops and the fluid temperature and pressure corresponds to the two-phase liquid-vapor curve,

2) mixing with other water (almost always cooler) drawn into the reservoir due to the pressure decline resulting in cooling of the reservoir water,

3) passage of cooler water (from outside the reservoir) through hotter reservoir rock with an increase in fluid temperature,

4) mixing with steam from another (usually higher) feed zone that enters the well separately from the deeper liquid,

5) mixing in the well of (usually) cooler water from a separate feed zone with no re-equilibration of geothermometers (due to the short time and the lack of mineral surfaces) but with a decrease in calculated silica temperatures effects caused by dilution, and

6) conductive cooling through wellbore heat loss.

The effects (or lack) of these processes on the chosen geothermometers (abbreviated as T_{NKC}, T_{SIL}, T_E) can be divided into the following cases:

1. No boiling, no mixing

$T_{NKC} = T_{SIL} = T_E$ because all temperatures refer to the same unchanged fluid with no excess enthalpy and all geothermometers fully equilibrated.

2. Boiling with heat transfer from rock

The usual order is $T_E > T_{NKC} > T_{SIL}$ because the near well fluid is cooled by boiling, and as a result, heat is transferred to the fluid from the reservoir rock. This is common at Cerro Prieto and Ahuachapán. The mechanism probably differs in these fields because Cerro Prieto produces from matrix permeability and Ahuachapán from fractures. The "leaky" cap at Cerro Prieto connecting the reservoir to cooler fluids acts as a constant pressure boundary and causes a characteristic exponential decline of enthalpy until rock and water temperatures equilibrate. At Ahuachapán, this condition probably results from flashing flow in fractures that on a large scale may behave like a uniform matrix but may allow segregation of liquid and vapor.

3. Boiling without heat transfer

After boiling zones stabilize and rocks cool to fluid temperatures, no heat is transferred and no excess steam is produced. The order becomes $T_E = T_{NKC} > T_{SIL}$. T_{SIL} is still lower than the other temperatures because the fluid is still boiling near the well.

4. Mixing near the well

The order will be $T_{NKC} > T_{SIL} = T_E$ if mixing occurs far enough from the well so that fluids are cooled and have equilibrated with silica but have not remained at the lower temperature long enough to lower T_{NKC}.

5. Separate steam entry

If the well has two feed zones, one with equilibrated liquid water and the other (usually shallower) with steam, then we expect $T_E > T_{NKC} = T_{SIL}$. Both case (5) and case (2) show excess enthalpy, with case (2) showing lower T_{SIL} due to boiling.

6. Separate cool water entry

When cool water enters the well and mixes with reservoir fluid, it lowers the enthalpy and T_{SIL} with little change to T_{NKC}. This case is indicated by $T_{NKC} > T_{SIL} > T_E$.

Cooling by mixing with cooler water in the wellbore does not cause re-equilibration but does produce lower silica temperatures because of dilution (Figure 5.1). In the example, mixing in the wellbore produces silica concentration and water enthalpy shown by the point MIX. The silica temperature for this mixture is $T_{SIL(MIX)}$, intermediate between the actual temperature (T_E) and the Na-K-Ca temperature ($T_{NKC} > T_{SIL} > T_E$). If mixing occurred in the reservoir with enough time for silica equilibration, then the silica content would drop to $T_{SIL(EQ)}$ which is equal to T_E ($T_{NKC} > T_{SIL} = T_E$). Mixing in the wellbore appears to be common at Ahuachapán, possibly due to casing problems or lowering of the cold water-hot water interface as pressures have decreased.

7. Water heated by rock

Since near-well temperatures are higher than those at a distance from the well, we expect $T_{SIL} > T_{NKC}$. If near-well boiling occurs, T_E may be higher than T_{SIL}. Near-well mixing would lower T_{SIL} and T_E, so the pattern would be ambiguous.

8. Conductive cooling in the well

If T_{NKC} is very similar to T_{SIL} and T_E is much lower, then the water has probably been cooled in the wellbore by conductive heat loss. Temperatures cannot have been lowered by mixing because T_{SIL} would have been affected by dilution. Conductive cooling is likely when the flow rate is low.

Other cases can occur by combination of these processes; for example, boiling in the reservoir could be combined with cool water entry into the well. Some of these combinations

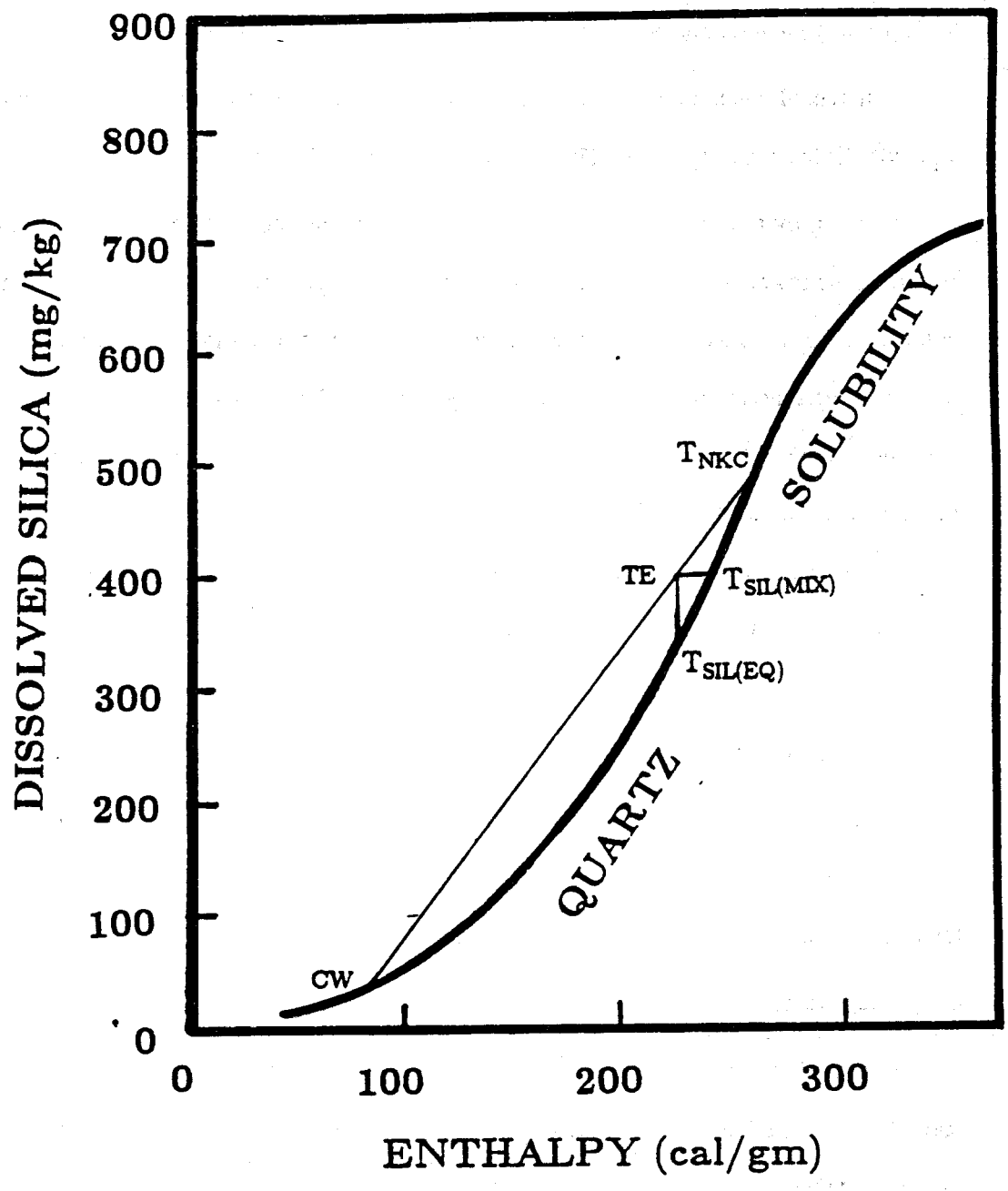

Figure 5.1. Quartz solubility diagram.

produce ambiguous indications. Consideration of changes in aquifer chloride is of value in sorting out these processes.

5.4 Calculation and Interpretation of Aquifer Chloride

Water from geothermal wells is usually sampled from the weirbox of the silencer or cooled (conductively) from the water exit of the separator. In both cases the composition of the sample differs from the composition of the aquifer liquid because steam (containing H_2O but essentially no salts) has separated during boiling. If the enthalpy of the aquifer liquid (before boiling) is known, then the fraction of steam separating and the change in solute concentrations can be calculated. This involves the use of enthalpy and chemical balances and results in the equations (e.g., for chloride) for samples collected from the separators,

$$Cl_{aquifer} = Cl_{separator} \times WF_{sep} \tag{5.1}$$

$$WF_{sep} = \frac{h_{steam,\,sep} - h_{water,\,aqu}}{h_{steam,\,sep} - h_{water,\,sep}} \tag{5.2}$$

For weirbox samples,

$$Cl_{separator} = Cl_{weirbox} \times WF_{silencer} \tag{5.3}$$

$$WF_{silencer} = \frac{h_{steam,\,sil} - h_{water,\,sep}}{h_{steam,\,sil} - h_{water,\,sil}} \tag{5.4}$$

in which WF is the water fraction, and the enthalpies of steam and water at separator and silencer pressures are obtained from steam tables. For wells with no excess steam, the measured enthalpy is assumed equal to the aquifer liquid enthalpy for calculating aquifer chloride.

For excess-steam wells, the measured total enthalpy is not equal to the enthalpy of the reservoir liquid, so another method is used. Because the liquid enthalpy of most interest to us is that at a distance from the well unaffected by near-well boiling, liquid enthalpy calculated from the Na-K-Ca temperature is used. This method has been used for calculations of aquifer chloride presented in this report. An advantage of this procedure is that excess enthalpy produced by near-well boiling without re-equilibration of Na-K-Ca temperatures does not affect calculation of aquifer chloride concentration away from the well. A possible disadvantage is

that the chloride values do not help to distinguish between sources of excess enthalpy.

The aquifer chloride is complementary to geothermometer temperatures for indication of reservoir processes involving concentration or dilution of reservoir fluids. Concentration processes include boiling with heat transfer from rock (case 2) and mixing with more concentrated waters (case 4). Mixing with more concentrated waters is rare because geothermal reservoir fluids are usually the most concentrated waters in the system but might occur if seawater enters a freshwater geothermal system. Mixing with more dilute waters is very common (cases 4, 6 and 7).

If boiling occurs near the well with or without excess enthalpy (case 2 or 3), then the concentration of solutes will increase in the aquifer close to the well. If the enthalpy of aquifer liquid used in the calculation is that at the well bottom, then the calculated aquifer chloride will show this concentration. This could result from the use of T_{SIL} in the calculations. If, however, the liquid enthalpy refers to conditions away from the well not affected by near-well boiling, then the calculated aquifer chloride is not affected by the boiling which becomes, in the calculation, part of the total boiling due to production. If the boiling is widespread and occurs far enough from the well to cause re-equilibration of the T_{NKC}, then the resulting increase in chloride will appear in the results. Mixing with steam produced far from the well (case 5) does not change aquifer chloride significantly.

The entry of cooler, more dilute water into the reservoir (case 4 and 7) produces a "cold sweep" in which the water is heated by the rock and may enable a more complete extraction of the total heat in the system. Because the water is heated by the rock (until rock temperatures along the flow path are cooled to original water temperatures), the "thermal front" indicated by a drop in temperature lags behind the "hydraulic" or "chemical" front, indicated by a change in chemistry. The time lag between these fronts is a function of the heat capacities of rock and water, the porosity and the amount of thermal and chemical dispersion along the flow path. Since the chemical front precedes the drop in fluid temperature, changes in production strategy can be made to delay or prevent the entry of lower enthalpy fluid into producing wells.

The relations between calculated aquifer chloride values are shown in Figure 5.2. This figure shows the major "boiling" line connecting the chlorinity and enthalpy of water sampled at the weirbox (WB) and that of steam (S). On this line lie the values for the aquifer (AQ) chloride and enthalpy calculated from geothermometer temperatures (T_{NKC} and T_{SIL}) and measured liquid enthalpy (T_E) as well as excess enthalpy from boiling and heat transfer or steam addition (EE). Boiling, heat transfer and steam addition increase or decrease enthalpy without changing the chloride, so compositions remain on the WB-S boiling line. If mixture with cold water (CW) occurs, then compositions move off the boiling line along a dilution line (AQ-CW) to a point (E, MIX) depending on the amount of mixing. A second boiling line (WB, MIX-S) describes processes that occur after mixing. Coupled processes such as mixing in the reservoir and conductive heating of fluids produce more complicated relations. In the discussion of individual wells, T_{NKC} has been assumed to be the aquifer temperature.

5.5 Chemical Histories of Ahuachapán Fluids

The methods described earlier have been applied to the analyses of Ahuachapán production fluids provided by the Gerencia de Recursos Geotérmicos of the Comisión Ejecutiva Hydroeléctrica del Río Lempa (GEO-CEL). These analyses were accompanied by physical data, including enthalpy measurements and separator pressures. The analyses are in general very complete, although in the present study only silica, chloride and alkali earth metals were used.

For each well, geothermometer temperatures based on silica, Na-K-Ca and measured enthalpy were plotted together against time. The analyzed chloride concentrations and calculated aquifer chloride are plotted separately. All of these plots are given in Appendix I. Aquifer chloride concentrations, calculated using Na-K-Ca temperature as an indicator of reservoir liquid enthalpy, have been plotted for all wells. For wells with all-liquid feed (without excess steam), true aquifer chloride (after mixing) calculated from measured enthalpy, and for excess enthalpy wells, concentrations based on silica temperatures indicating well-bottom

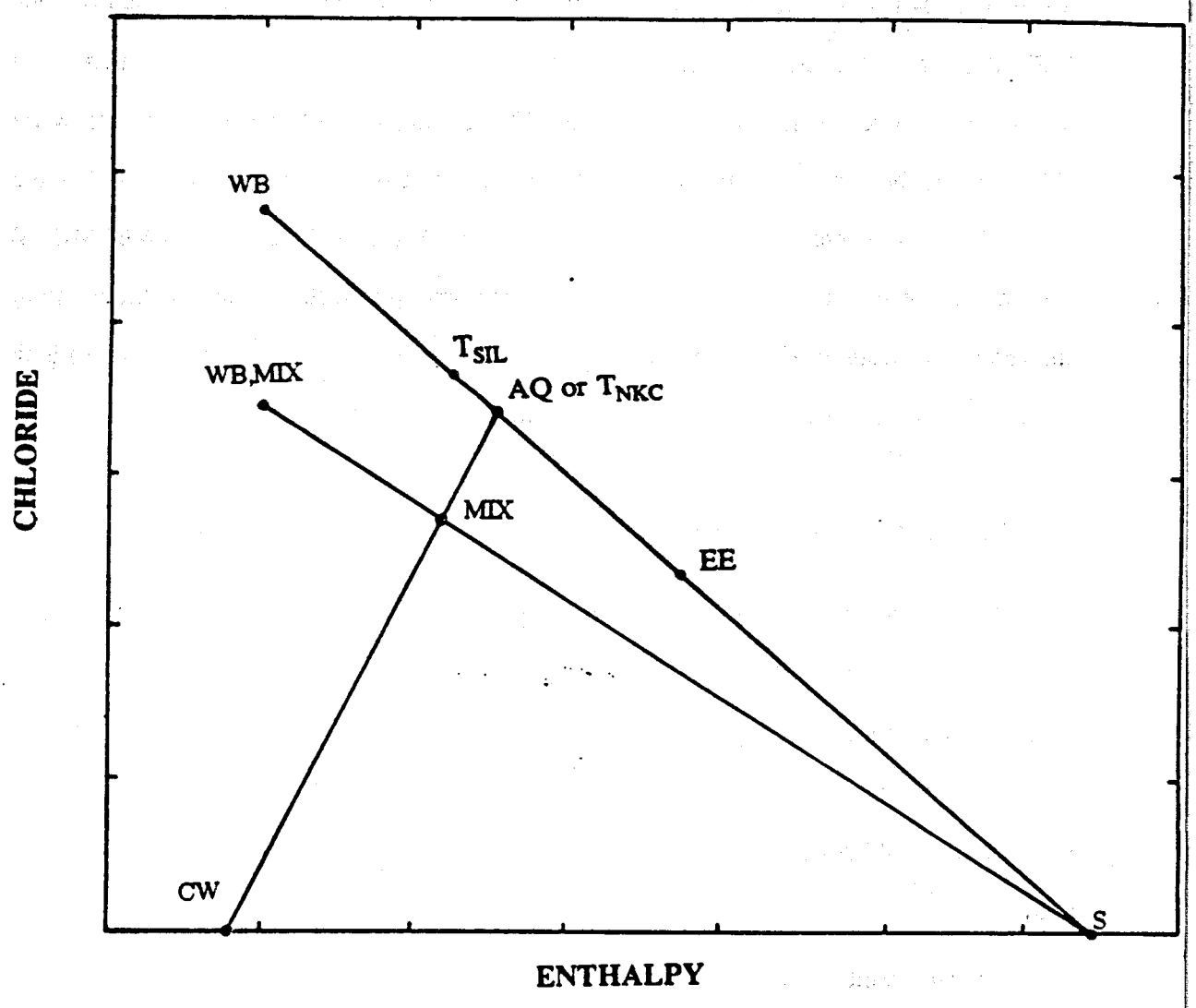

Figure 5.2. Chloride vs. enthalpy mixing diagram.

concentrations are also shown.

One objective of this study is to indicate the initial conditions of temperature and chlorinity in the reservoir adjacent to each well. These are indicated by the earliest data; if these are influenced by drilling water or start-up problems, later data are extrapolated to initial times. The later changes in well chemistry are evaluated as indicators of reservoir processes and the overall behavior of the well is summarized (Appendix C).

5.6 Fieldwide Variations

Data on initial conditions and reservoir processes in individual wells have been combined into maps of the field showing initial temperature and initial chloride (Figures 5.3 and 5.4). These maps show information not available through drilling or wellhead physical measurements and complement downhole temperature logs.

The initial temperature map (Figure 5.3) is based largely on indications and estimates of the initial Na-K-Ca temperature. The map shows increasing temperatures from 233°C in the eastern part of the field to 262°C in the west, with fairly regular temperature contours. As the measured downhole temperatures do not exceed 245 °C and indicate little temperature variation within the wellfield, the Na-K-Ca temperatures probably indicate a natural gradient produced by mixing. The Na-K-Ca temperatures possibly reflect deeper, higher temperatues below drilled depths..

The chloride map (Figure 5.4) shows similar zoning with high-chloride waters in the west (to 8600 ppm) and lower chloride waters in the east (6100 ppm). The trends of these chloride concentrations and temperature suggest that they both result from the same mixing process. This is shown in an enthalpy-chloride plot (Figure 5.5).

The lower chloride concentrations and lower Na-K-Ca temperatures in the eastern part of the wellfield are due to inflow of cooler, low salinity fluids from the north and/or downward flow from the overlying saturated aquifer. This is consistent with chloride changes during exploita-

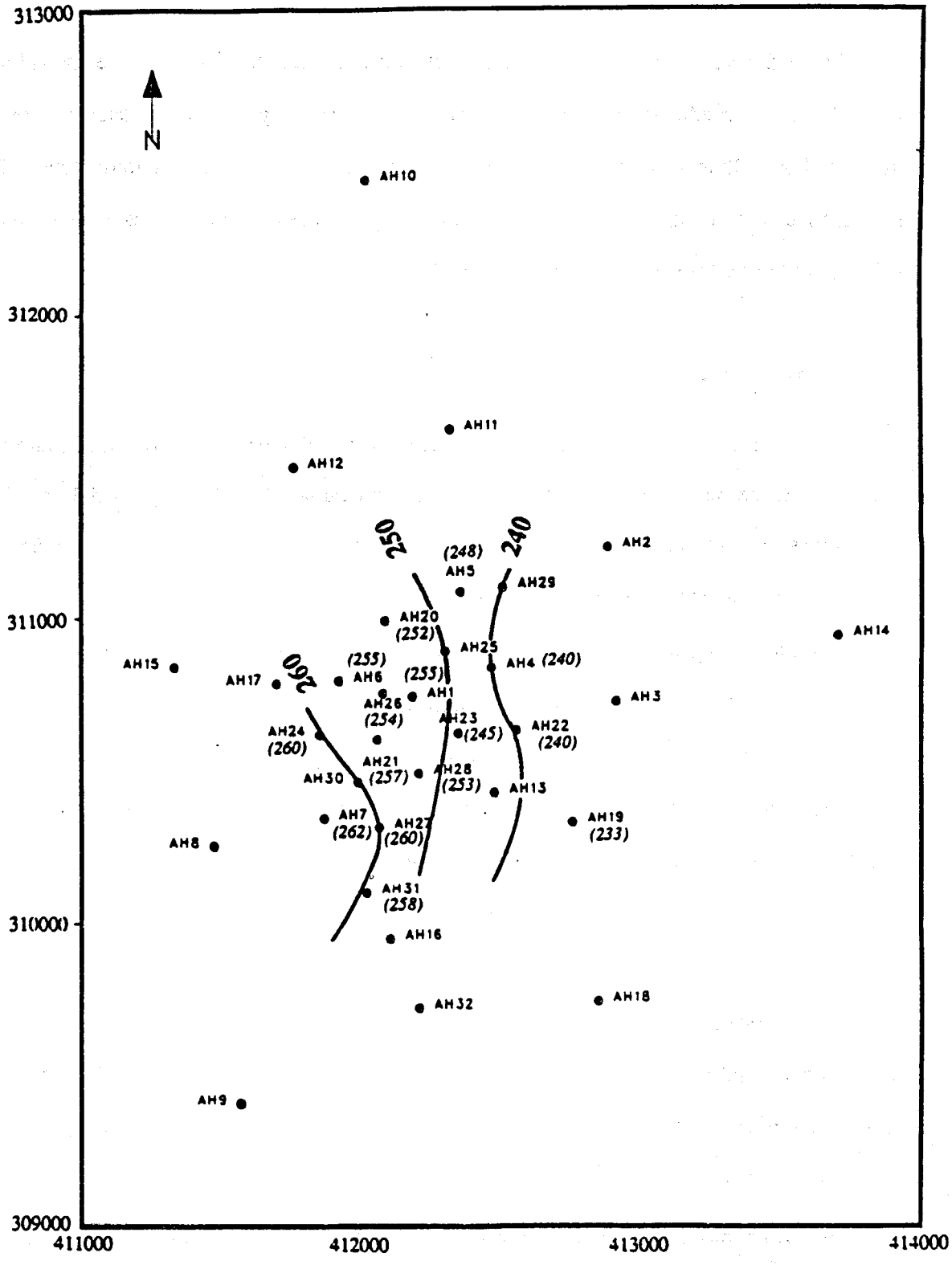

Figure 5.3. Initial aquifer temperature in °C.

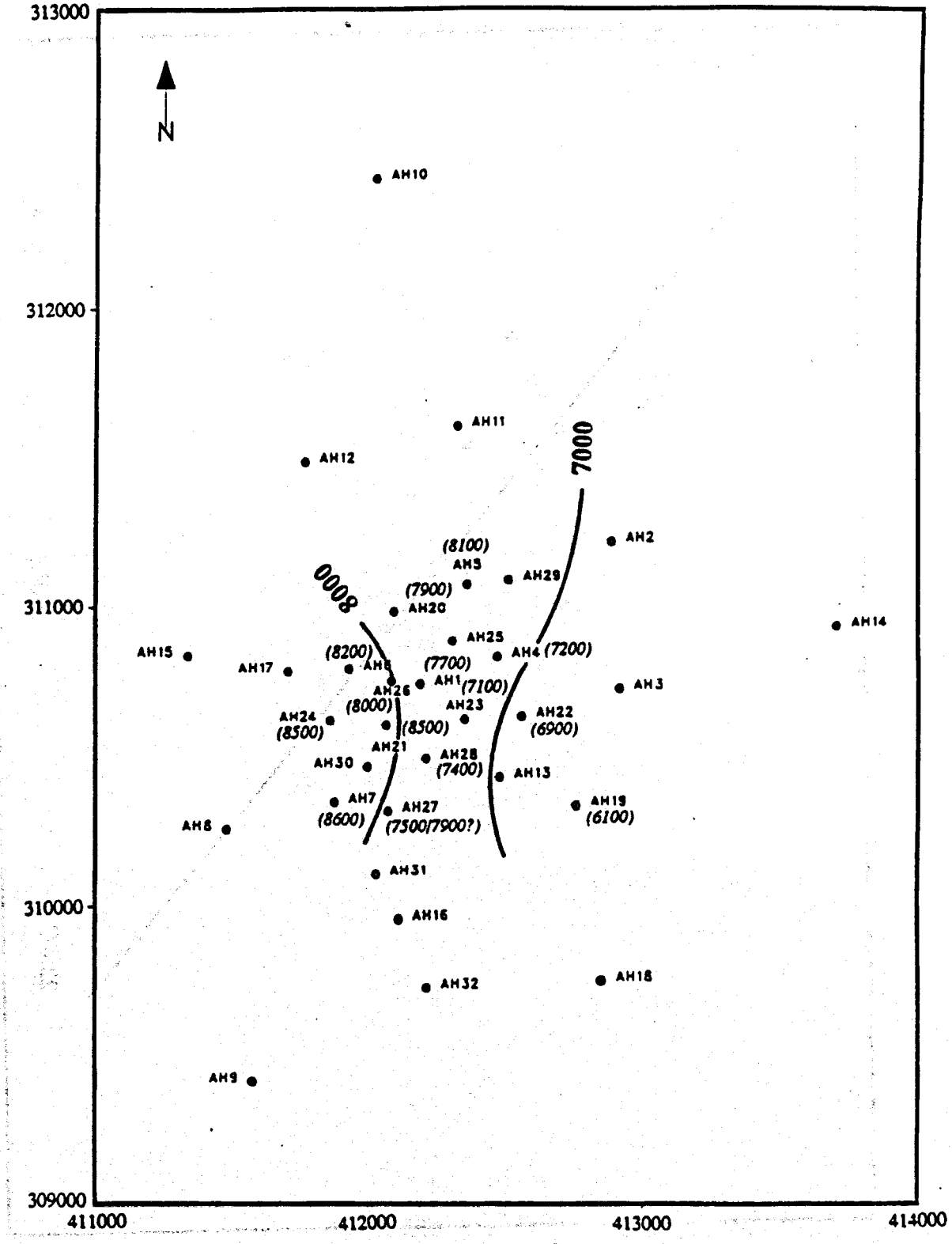

Figure 5.4. Initial aquifer chloride in ppm.

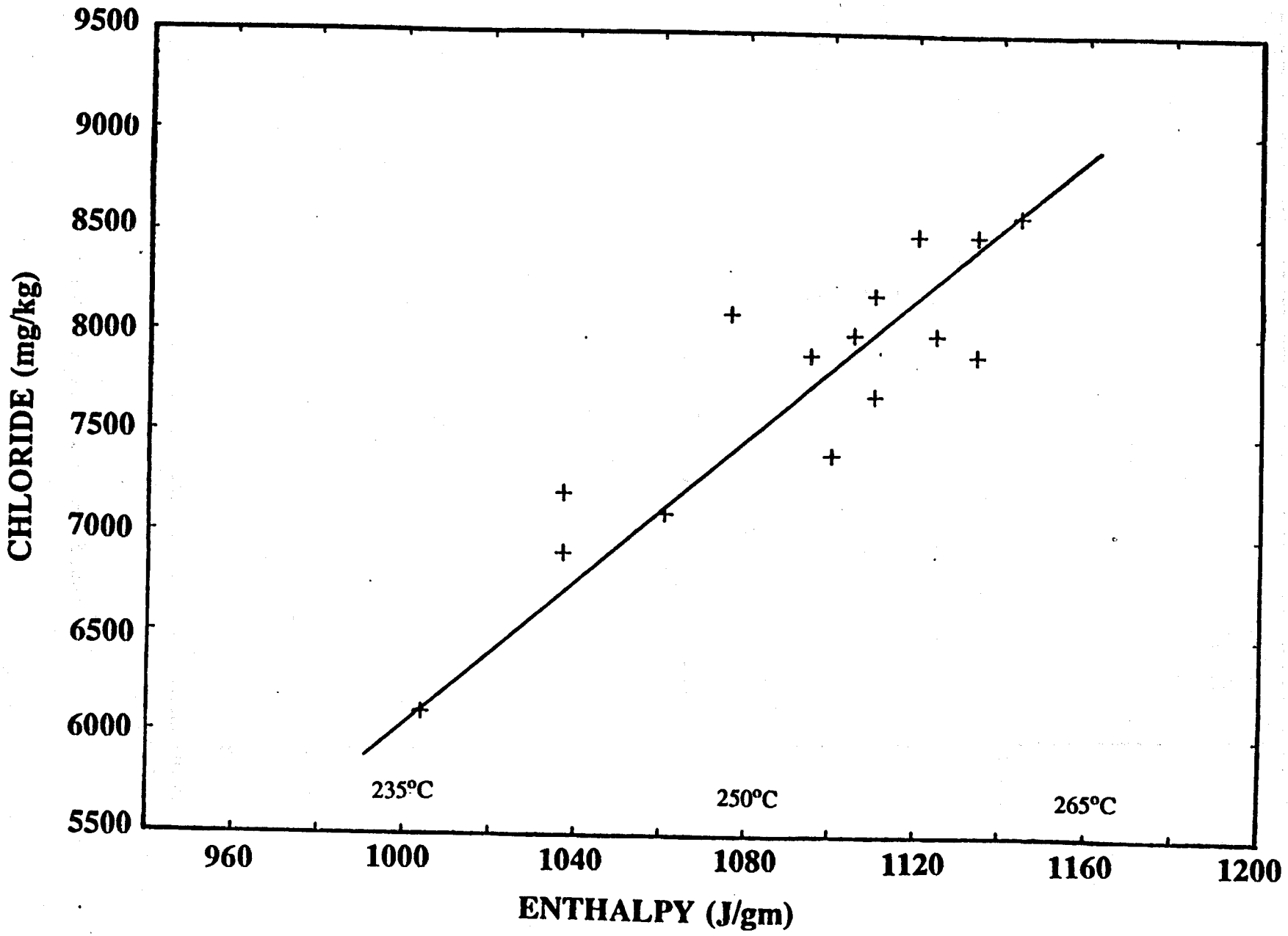
9500
9000
8500
8000
7500
7000
6500
6000
5500
CHLORIDE (mg/kg)
960
1000
1040
1080
1120
1160
1200
ENTHALPY (J/gm)
235°C
250°C
265°C

tion as some wells near the center of the field (well AH-1 and AH-23) have decreased in chloride concentration from about 8000 ppm to near 6000 ppm. This is probably due to enhanced cold water recharge because of the reservoir pressure decline.

6.0 AQUIFERS AND FEED ZONES

Three different aquifer systems have been identified at Ahuachapán and are referred to as the shallow, saturated and saline aquifers (Romagnoli et al., 1975; Cuellar et al., 1979). This classification was originally based on the differences in water chemistry and their different pressure response to seasonal variations in precipitation. The aquifers also have vastly different temperature and pressure distributions, as discussed in Chapter 7.

6.1 Characteristics of the Three Aquifers

The shallow aquifer contains calcium-carbonate waters locally mixed with sulphatic water. The total dissolved solids (TDS) of this aquifer are less than 500 ppm. It is an unconfined aquifer showing a rapid water level response to variations in rainfall. It is said to be of local interest only in the uphill slopes of the geothermal field (Cuellar et al., 1979).

The saturated aquifer contains carbonate waters (calcium and sodium) with TDS up to 400 ppm. It responds much slower to variations in precipitation than the shallow aquifer, but still shows a significant response.

The saline aquifer corresponds to the Ahuachapán geothermal reservoir. In the wellfield this zone is found up to an elevation of 300-350 masl. Steam from this aquifer channels upwards and feeds the shallower aquifers and the surface manifestations in the area. The geothermal fluid is of sodium chloride type with a TDS of up to 22,000 ppm.

6.2 Feed Zones

The locations of feed zones in the Ahuachapán wells are given in the well summaries in Appendix C. These locations were determined by circulation losses during drilling and measurements done after drilling (temperature and spinner logs). To assign the feed zones to aquifers according to the classification given above, some simplified assumptions had to be made. For

example, there is no information available on fluid chemistry of the zones sealed behind casings. It was decided to use the elevation of the feeds to decide to which aquifer they correspond. All circulation losses above 700 masl were assigned to the shallow aquifer, and losses between 350 and 700 masl to the saturated aquifer. Deeper feeds are in the open hole intervals of the wells and their geochemical characteristics are known. These zones are generally connected to the saline aquifer (the main geothermal reservoir) except in the northern and western part of the wellfield where the saturated aquifer extends to the bottom of the wells.

The three aquifers appear to coincide with the lithologic units discussed in Chapter 4. The shallow aquifer is found in the SM unit, the saturated zone in the YA unit, and the saline zone (reservoir) in the AA and OA units, (Table 4.1, Chapter 4). Specific feed zones are thought to indicate fractures and contact surfaces between different layers and to be controlled by the offsets of the various faults (Figure 6.1a-i).

In the shallow aquifer, the horizontal flow is seldom affected by faults since few displacements have been recent enough to affect the SM unit. A map of the wells showing circulation losses above 700 masl indicates a virtually uniform flow through the SM unit (Figure 6.2), suggesting extensive permeability in these less consolidated materials. On the other hand, in the saturated aquifer, there is evidence of structural control (Figure 6.3).

The saline aquifer is also affected by faults, most notably to the north and west, where they act as flow barriers and confine the reservoir. The presence of these boundaries is reflected by the temperature distributions in the field (Figure 6.1a-i).

6.3 Flowing T-P Surveys

Flowing temperature and pressure surveys have been performed in several of the production wells in Ahuachapán (Campos, 1980; Escobar, 1985; Bob Hendron, personal communications, 1987, 1988; Escobar, personal communication, 1988).

The data from these surveys have been analyzed to locate the different feed zones in the wells. Flow rates and the enthalpies of individual feeds have been estimated using a multi-

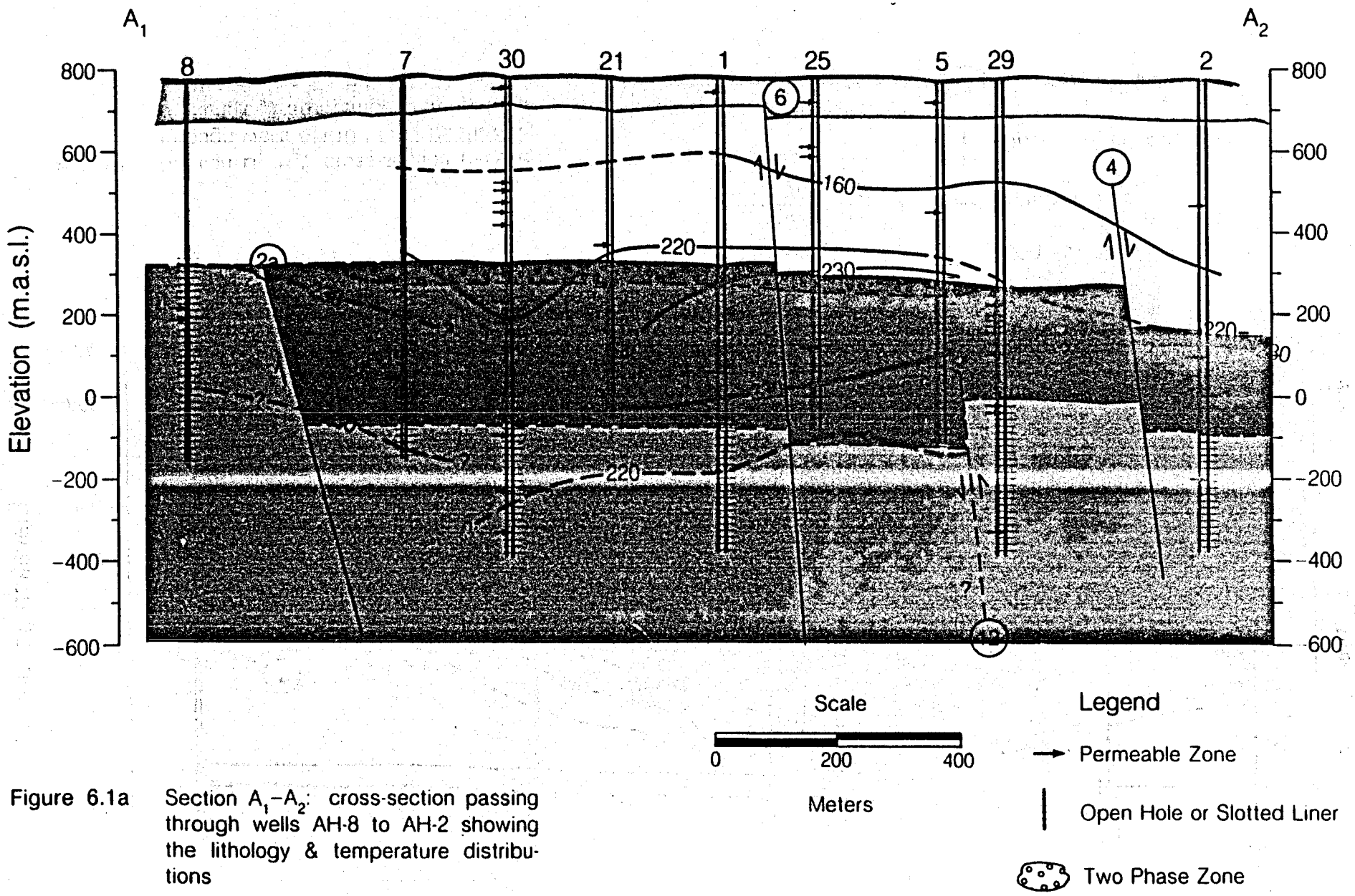

Figure 6.1a Section A_1–A_2: cross-section passing through wells AH-8 to AH-2 showing the lithology & temperature distributions

XBL 887-10318

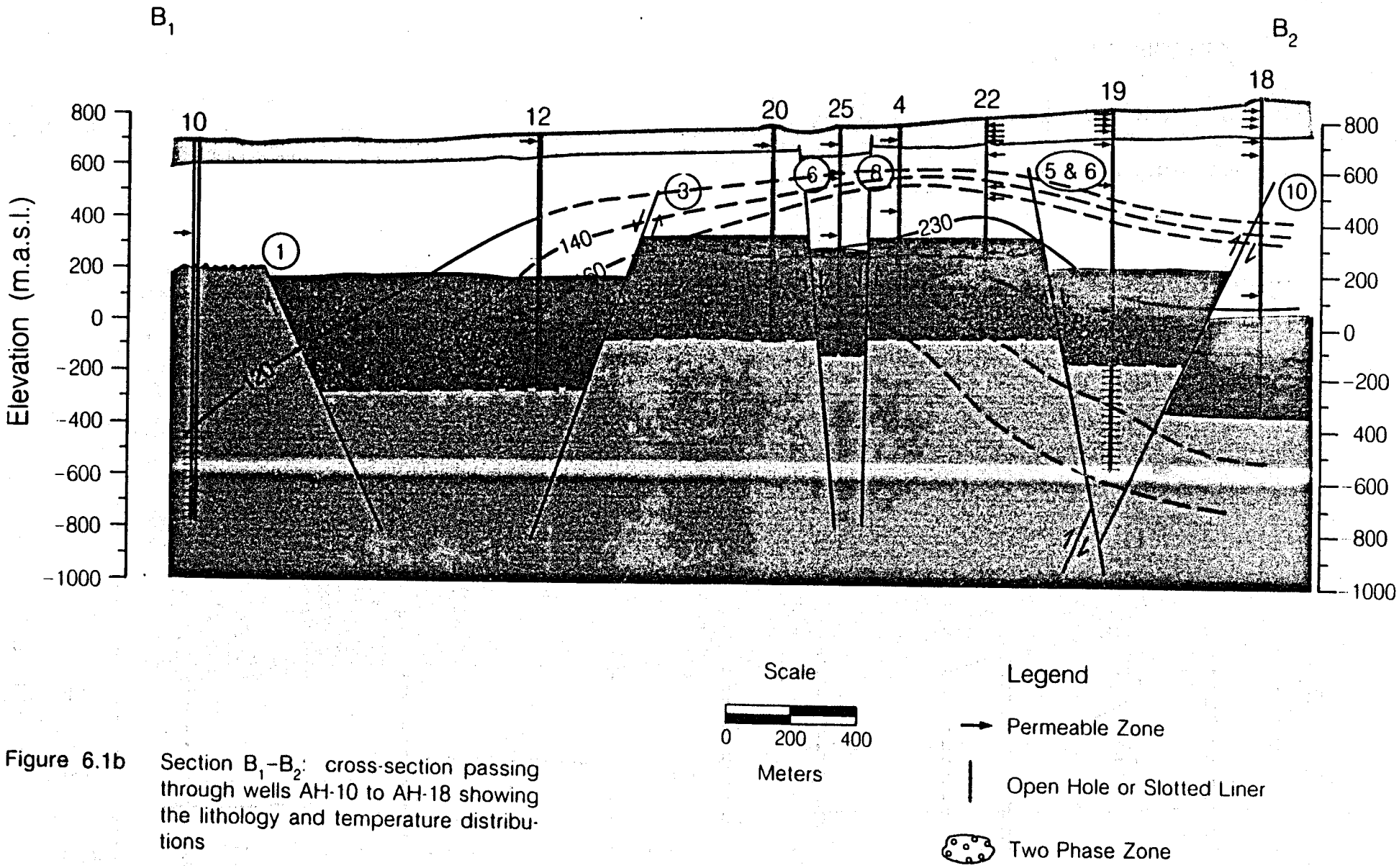

Figure 6.1b Section B_1–B_2: cross-section passing through wells AH-10 to AH-18 showing the lithology and temperature distributions

XBL 887-10319

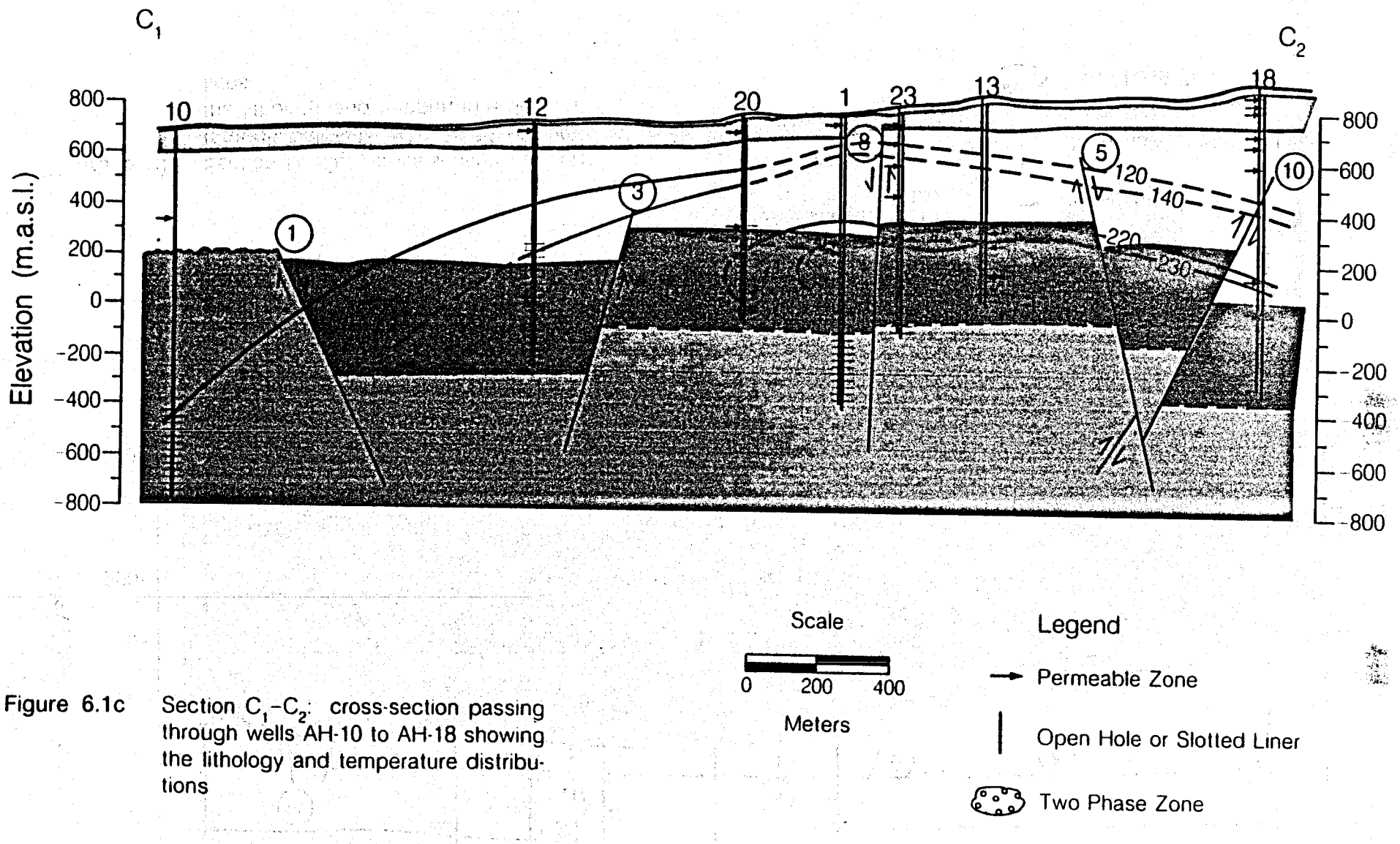

Figure 6.1c Section C_1–C_2: cross-section passing through wells AH-10 to AH-18 showing the lithology and temperature distributions

XBL 887-10320

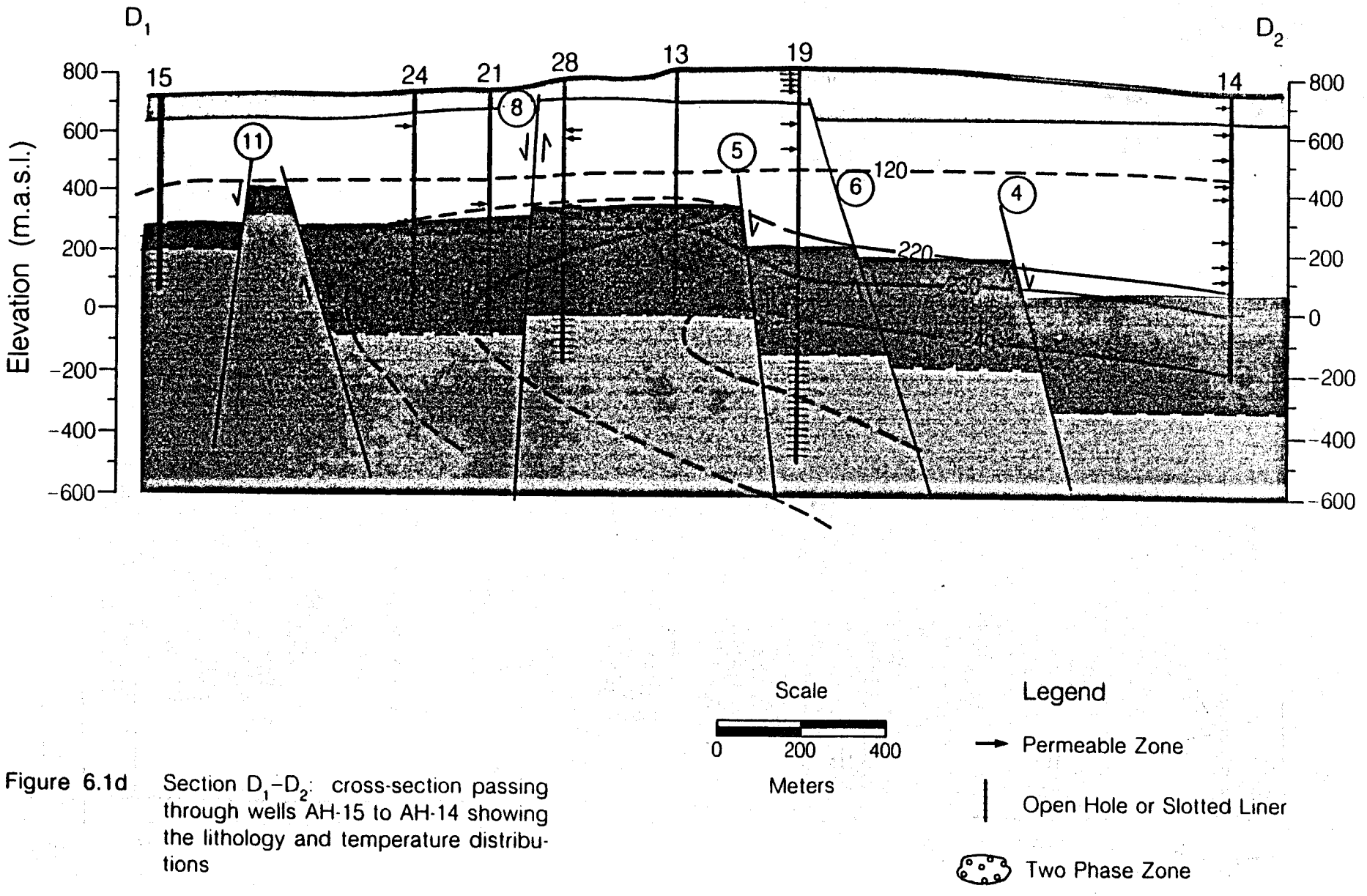

Figure 6.1d Section D_1–D_2: cross-section passing through wells AH-15 to AH-14 showing the lithology and temperature distributions

XBL 887-10321

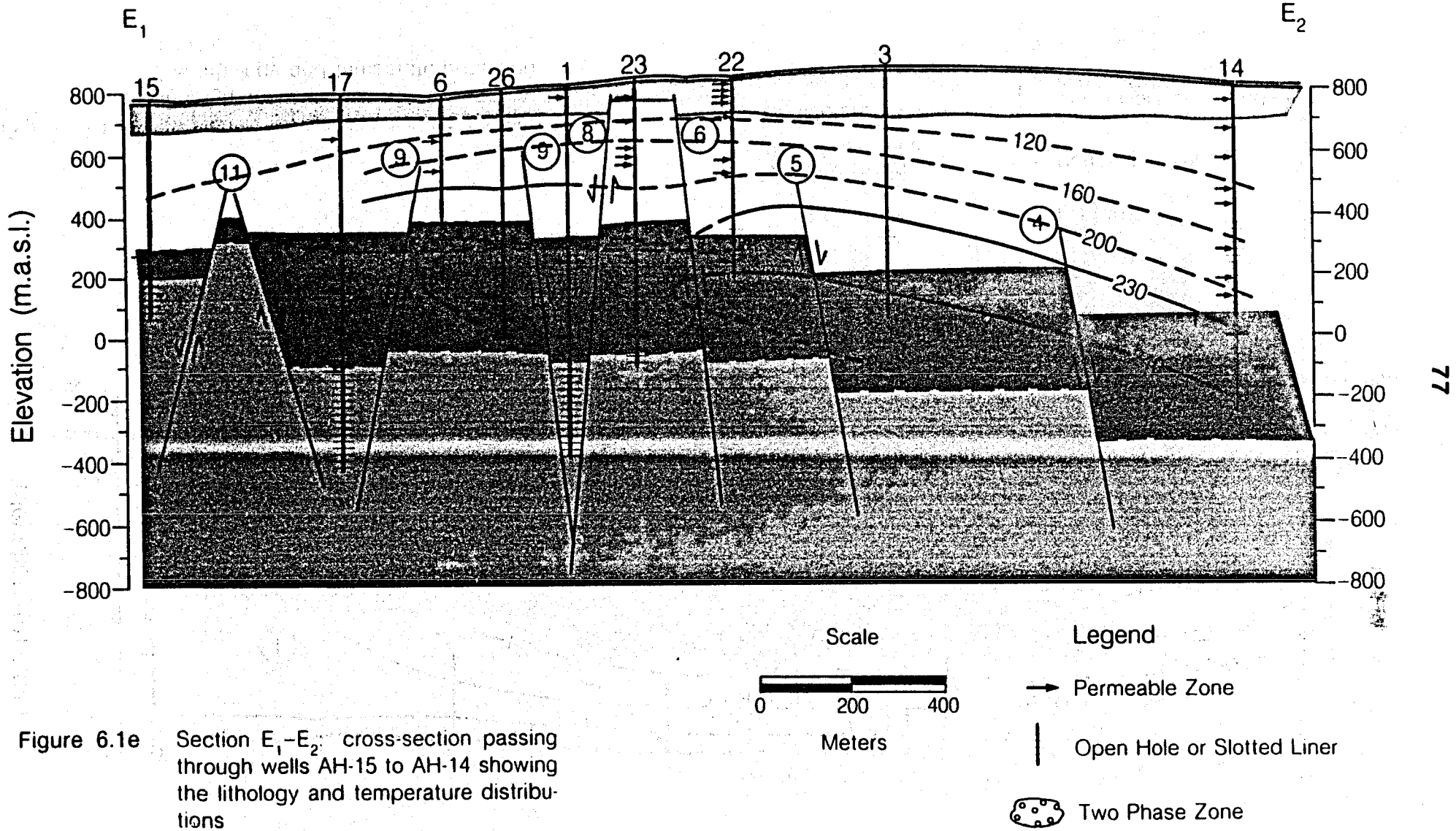

Figure 6.1e Section E_1–E_2: cross-section passing through wells AH-15 to AH-14 showing the lithology and temperature distributions

XBL 887-10322

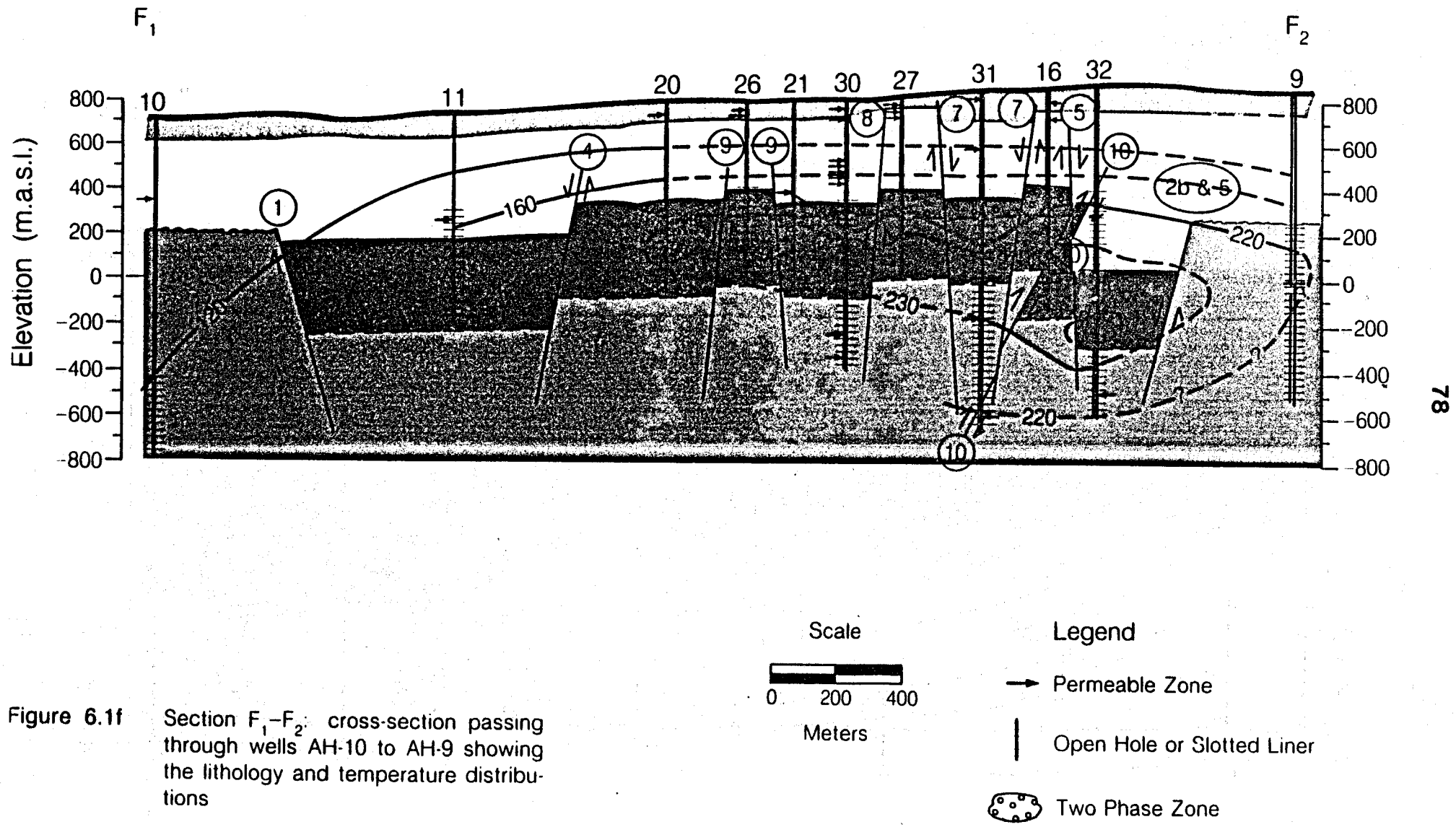

Figure 6.1f Section F_1–F_2: cross-section passing through wells AH-10 to AH-9 showing the lithology and temperature distributions

XBL 887-10323

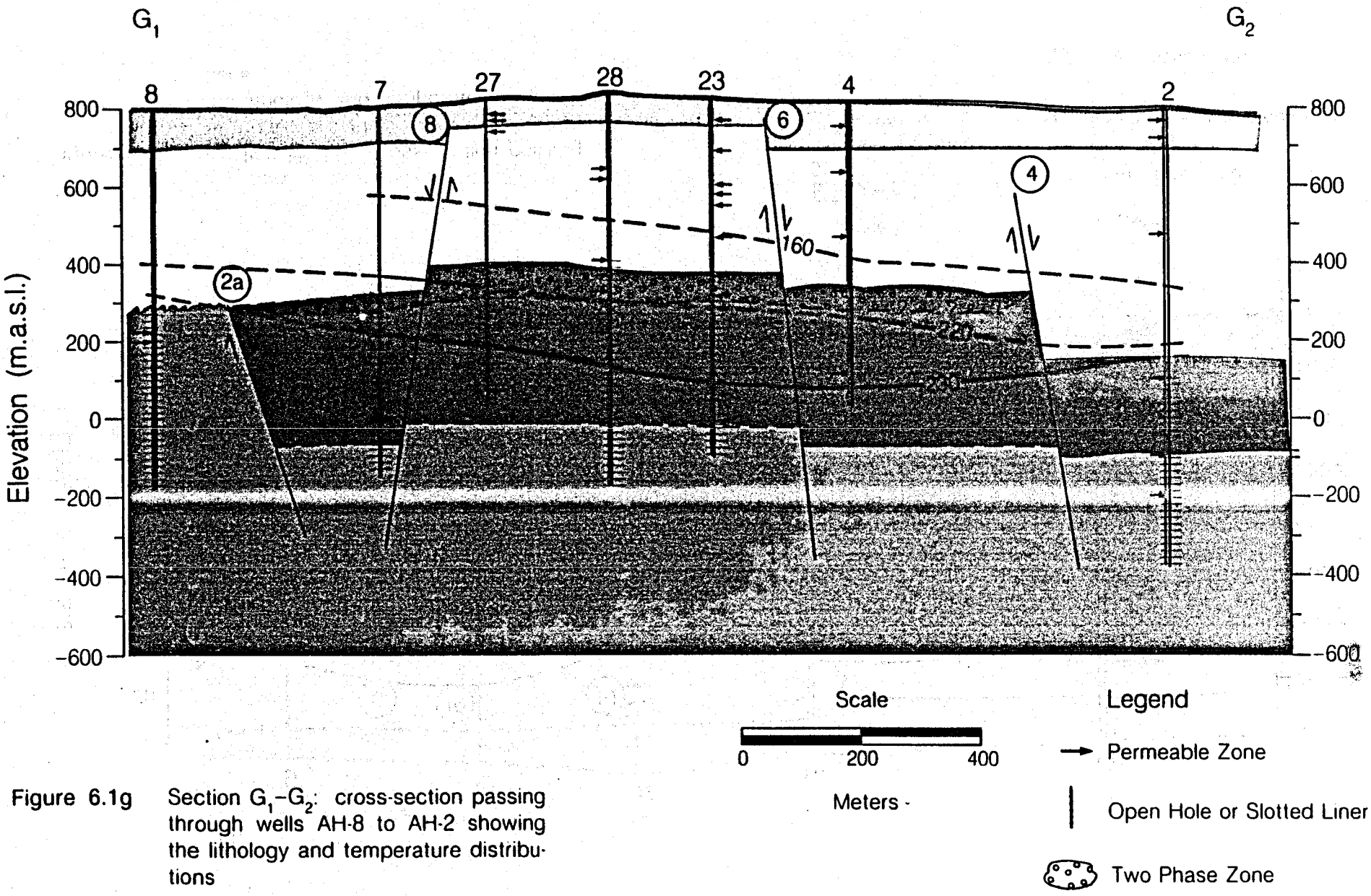

Figure 6.1g Section G_1–G_2: cross-section passing through wells AH-8 to AH-2 showing the lithology and temperature distributions

XBL 887-10324

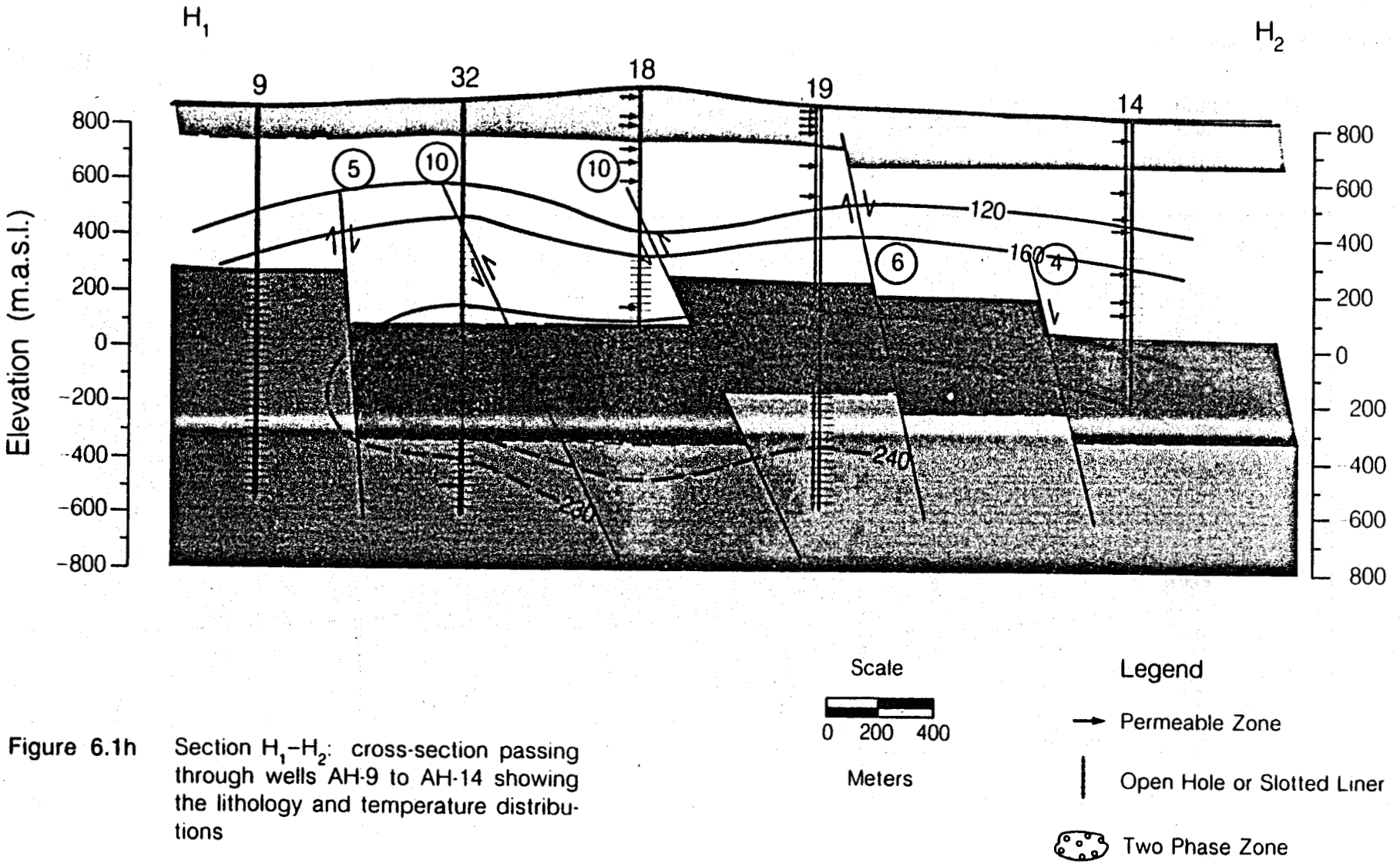

Figure 6.1h Section H_1–H_2: cross-section passing through wells AH-9 to AH-14 showing the lithology and temperature distributions

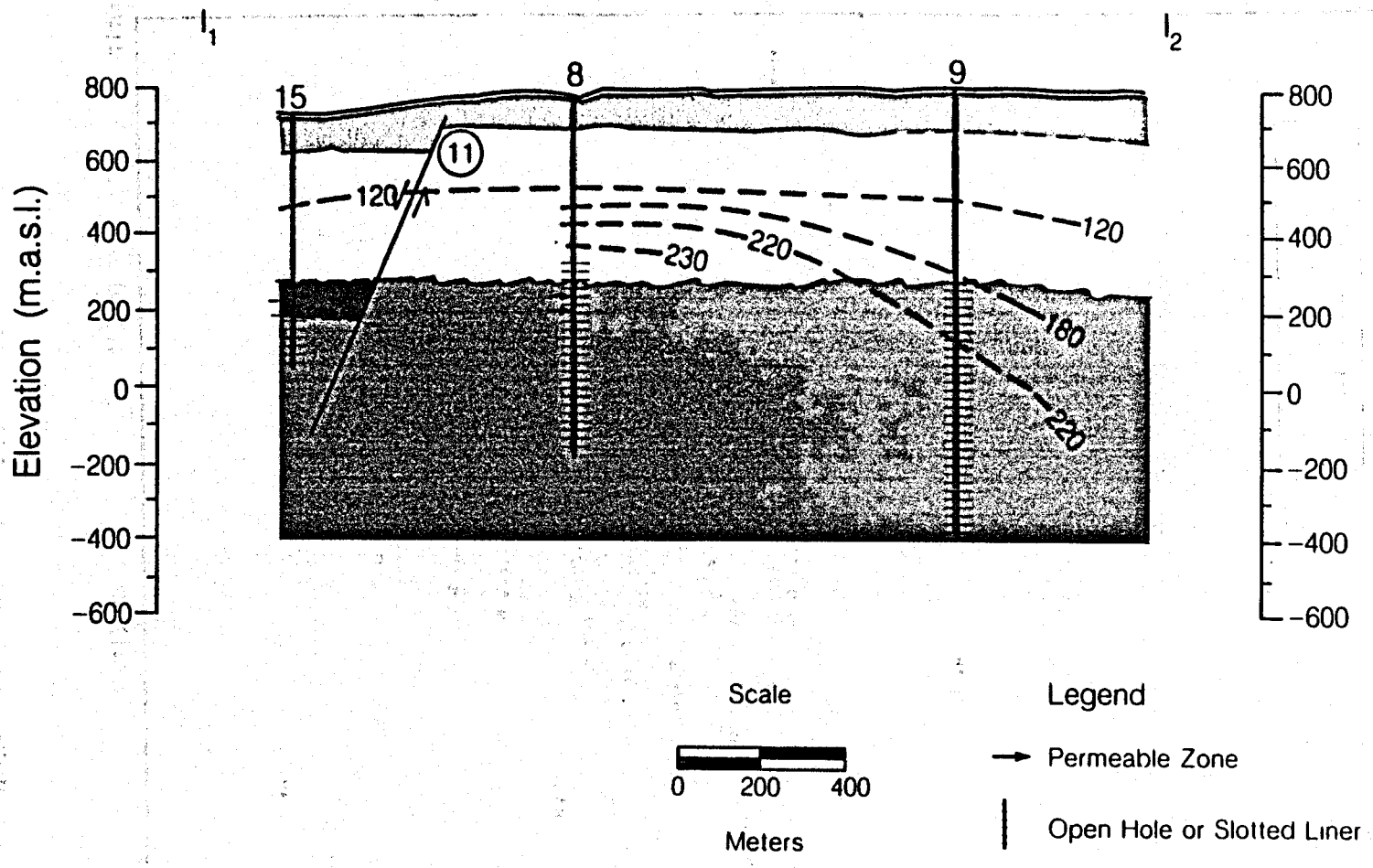

Figure 6.1i Section I_1–I_2: cross-section passing through wells AH-15 to AH-9 showing the lithology and temperature distributions

XBL 892-7461

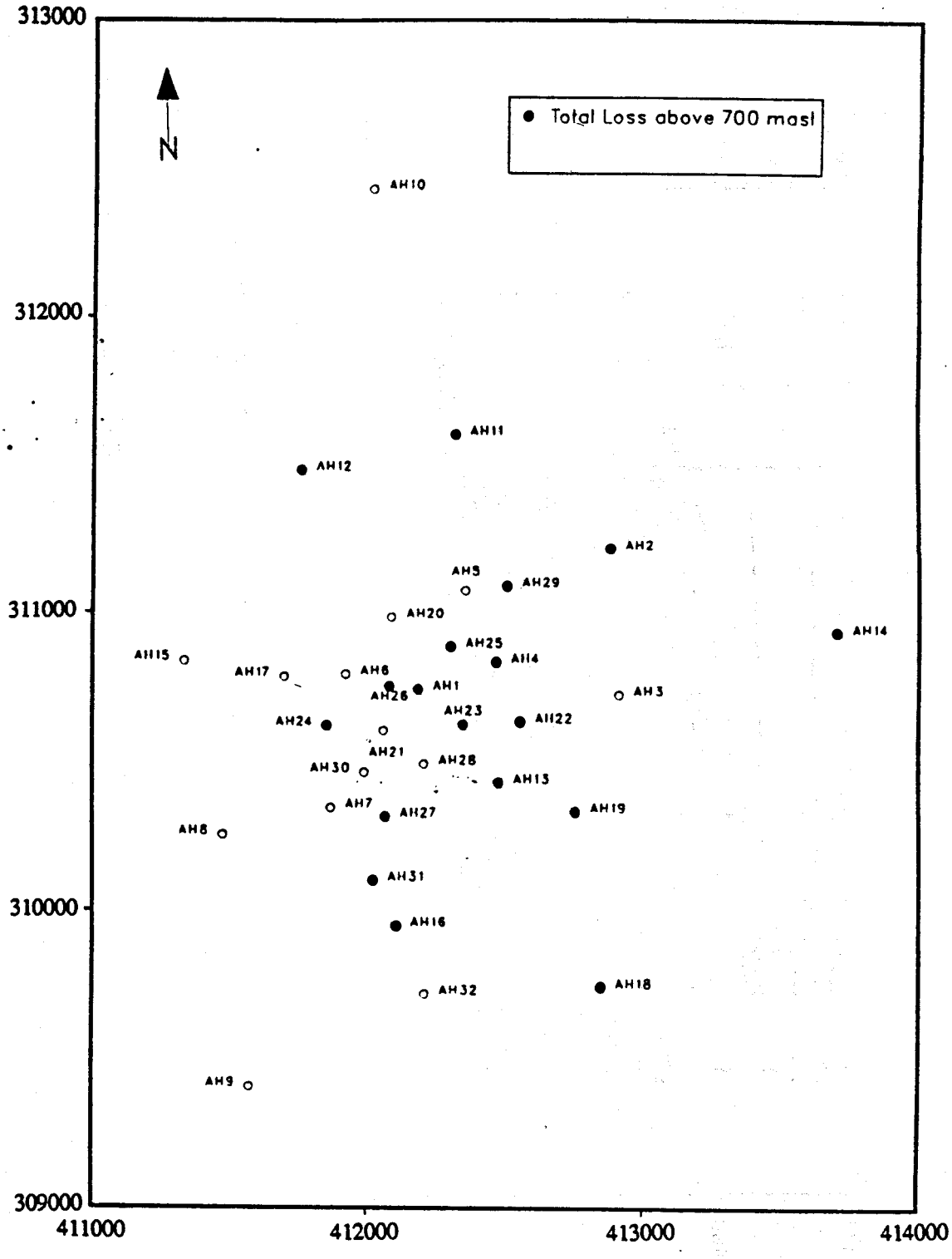

Figure 6.2. Wells having total loss above 700 masl (Shallow Aquifer).

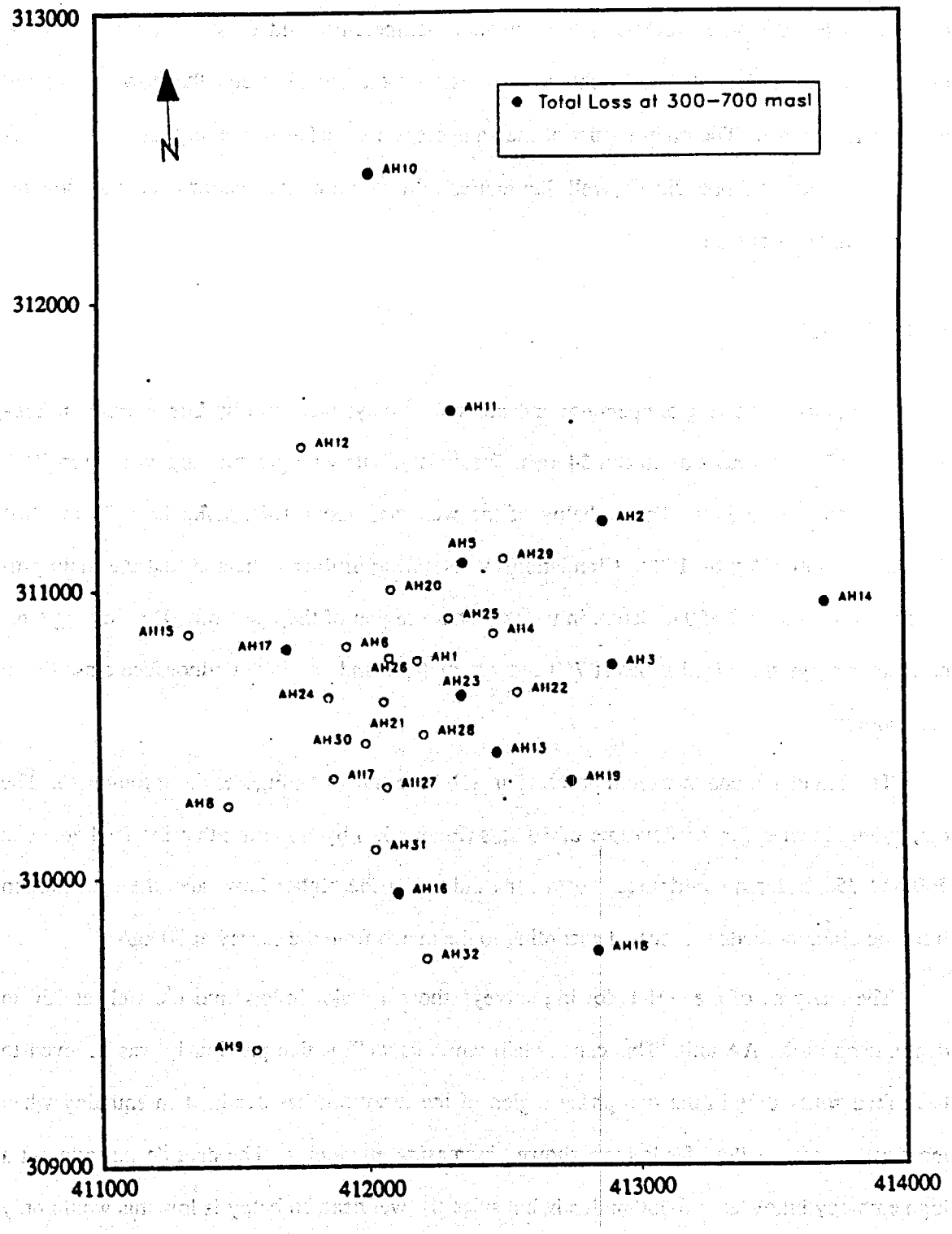

Figure 6.3. Wells having total circulation loss in the 300-700 masl interval (saturated zone).

feedzone simulator (Bjornsson, 1987; Bjornsson and Bodvarsson, 1987). The simulator calculates from wellhead data (wellhead pressure, total flowrate and enthalpy) and the well design (well diameter and pipe roughness) the downhole temperature and pressure distributions. A match with the measured data is obtained by varying the enthalpy and the flow rate of the different feed zones. The main results of the analyses are included in the discussion on individual wells given in Appendix C (Well Summaries). In the following sections selected flowing surveys will be discussed.

6.3.1. Well AH-1

Two pairs of flowing temperature and pressure surveys were run by Los Alamos in September 1987 at flow rates of 30 and 54 kg/s. Previously, a flowing pressure log was run in 1979 at a flow rate of 65 kg/s. The enthalpy of the well was about 1000 kJ/kg in 1979 but had declined to 950 kJ/kg by 1987. Circulation losses during drilling indicated that the main production zone is at 500-550 m depth, in the two-phase region of the reservoir. The flowing temperature surveys show feed zones at 750 and 775 m depth and possibly a minor feed close to the well bottom.

The calculated and measured profiles for AH-1 are shown on Figures 6.4 through 6.6. The data were matched for the flow rate of 30 kg/s (Figure 6.4) by assuming that the feed zones at 500 and 750 m depth contributed most of the fluid. For the higher flow rates the contribution from the different feeds was scaled according to the match from the survey at 30 kg/s.

The analyses of the AH-1 flowing surveys show a major inflow into the well at 750 m depth, deep in the AA unit. This can explain why this well, which previously was believed to have feed zones only in the two phase region of the reservoir, has declined in enthalpy when most wells with shallow feeds have showed increasing enthalpies. The data do not rule out a high enthalpy inflow at 500-550 m depth, but since the wellhead enthalpy is low this would only reduce further the contribution of shallower feed zones to the total flow in this well.

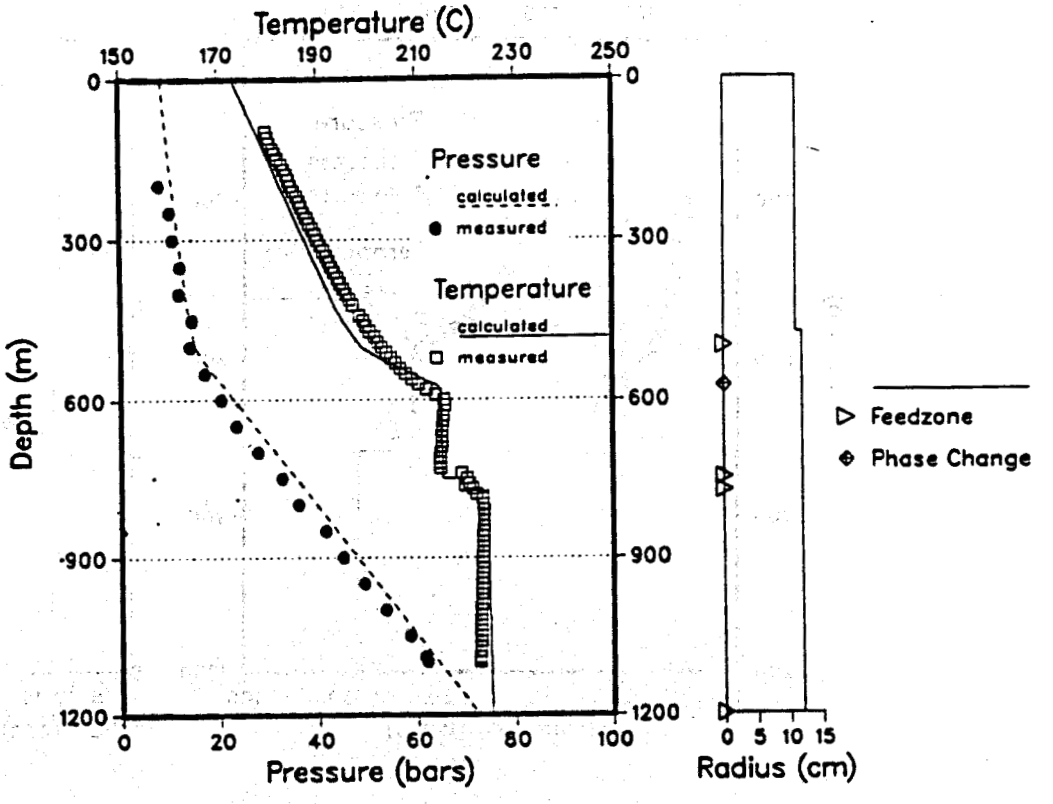

AHUACHAPAN WELL AH-1.
Calculated downhole pressure and temperature during production in 1987. Downhole data from Los Alamos.

Wellhead pressure (bar abs.)	:	8.50
Wellhead temperature (C)	:	172.94
Wellhead dryness	:	0.107
Wellhead enthalpy (kJ/kg)	:	950.00
Wellhead total flow (kg/s)	:	30.00

Feedzone no:	Depth (m)	Flow (kg/s)	Enthalpy (kJ/kg)
1	500.0	15.0000	990.0
2	750.0	10.0000	915.0
3	775.0	3.0000	920.0
4	1200.0	2.0000	968.8

Figure 6.4. Well AH-1 flowing temperature and pressure match at a discharge flowrate of 30 kg/s.

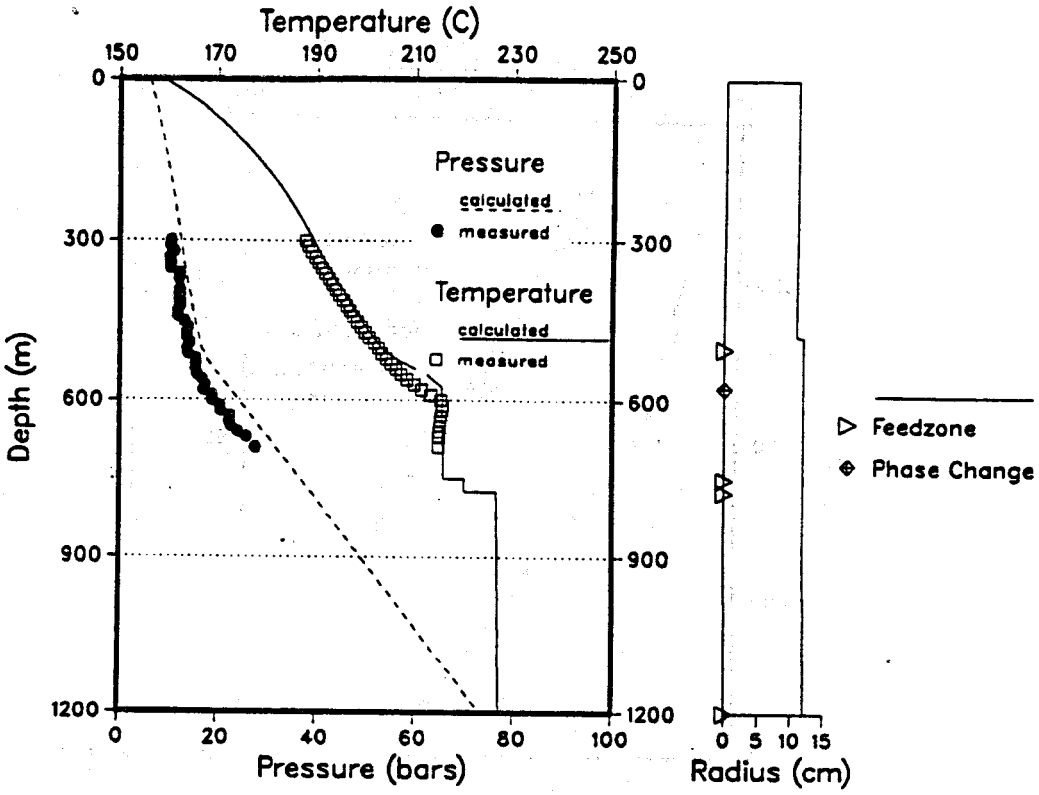

AHUACHAPAN WELL AH-1.
Calculated downhole pressure and temperature during production in 1987. Downhole data from Los Alamos.

Wellhead pressure (bar abs.)	:	6.00
Wellhead temperature (C)	:	158.84
Wellhead dryness	:	0.134
Wellhead enthalpy (kJ/kg)	:	950.00
Wellhead total flow (kg/s)	:	54.00

Feedzone no:	Depth (m)	Flow (kg/s)	Enthalpy (kJ/kg)
1	500.0	27.0000	990.0
2	750.0	18.0000	915.0
3	775.0	5.0000	920.0
4	1200.0	4.0000	978.4

Figure 6.5. Well AH-1 flowing temperature and pressure match at a discharge flowrate of 54 kg/s.

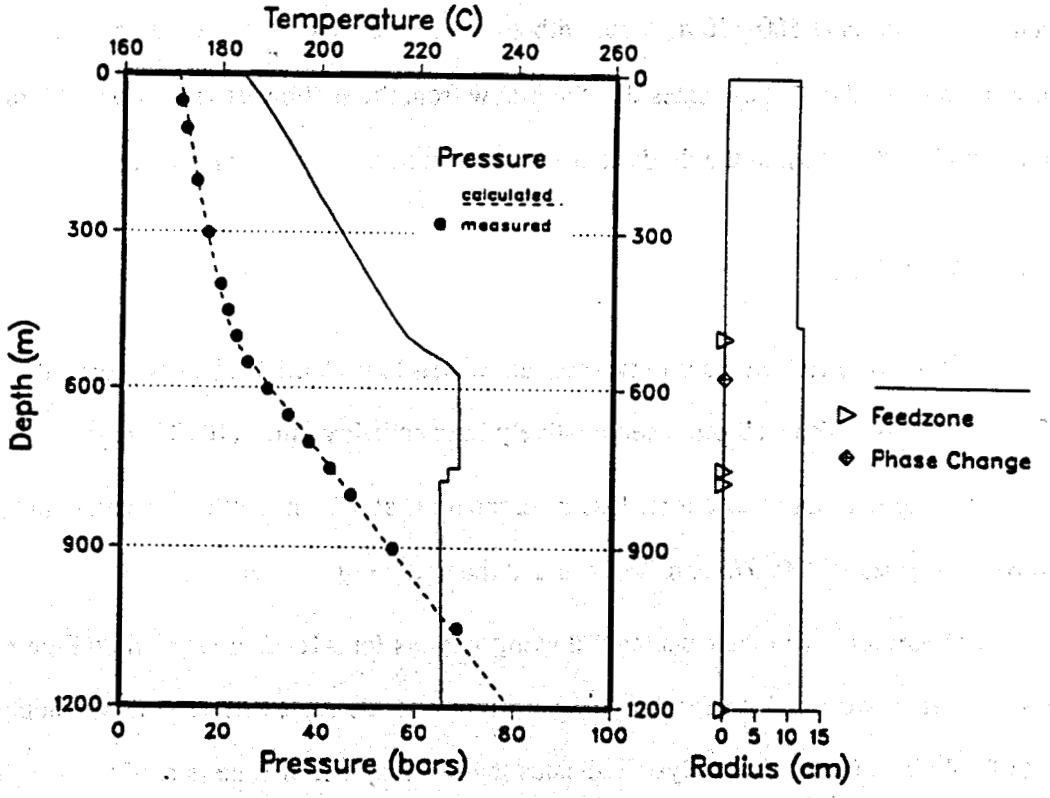

AHUACHAPAN WELL AH-1.
Pressure log during discharge. Measured 21-august-1979.
Downhole pressures calculated for the following conditions.

Wellhead pressure (bar abs.)	:	11.00
Wellhead temperature (C)	:	184.07
Wellhead dryness	:	0.110
Wellhead enthalpy (kJ/kg)	:	1000.00
Wellhead total flow (kg/s)	:	65.00

Feedzone no:	Depth (m)	Flow (kg/s)	Enthalpy (kJ/kg)
1	500.0	35.0000	1025.0
2	750.0	25.0000	987.0
3	775.0	3.0000	980.0
4	1200.0	2.0000	970.8

Figure 6.6. Well AH-1 flowing temperature and pressure match at a discharge flowrate of 65 kg/s.

6.3.2 Well AH-21

Temperature and pressure logs were run in 1983 while the well was producing 76 kg/s of a 990 kJ/kg enthalpy fluid. The measured and calculated values are shown in Figure 6.7. The main feed zone is at 500-600 m depth with a minor inflow close to the bottom of the well. The low enthalpy of the well indicates that the inflow from the shallowest feed zone (500 m) is probably small so that most of the fluids come from the feed zone at 600 m depth.

6.3.3 Well AH-32

Temperature and pressure logs were run in AH-32 in April 1988 at two different flowrates (20 and 45 kg/s). The well produced relatively high enthalpy fluids (1090 kJ/kg).

Drilling data indicate a total loss of circulation at 775 m depth and temperature surveys show feed zones at 800, 975 and 100 m and at the bottom of the well.

The measured and the calculated flowing surveys for AH-32 are shown on Figures 6.8 and 6.9. A match was obtained for the 20 kg/s survey and the scaled flowrates were applied to the data for 45 kg/s flow. The analysis indicates that the major feed zone is at 975 m depth and that the high enthalpy fluids come from 775-800 m feed zones. The results show no major feed zones below 1000 m depth.

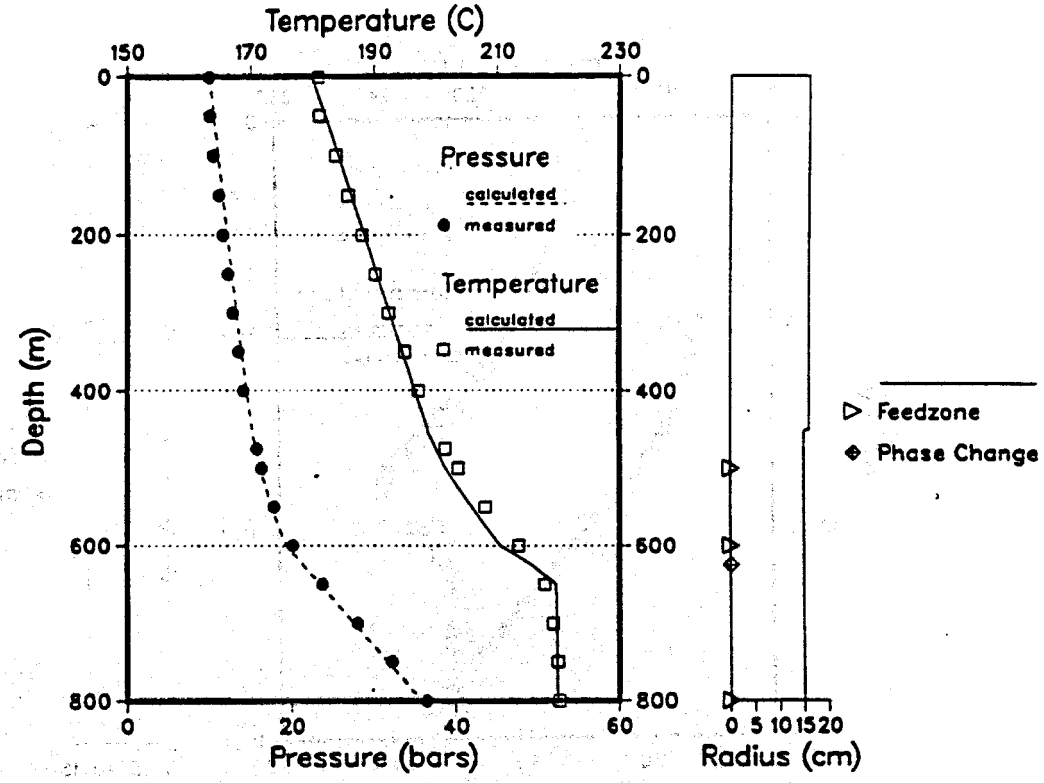

AHUACHAPAN WELL AH-21.
Temperature and pressure log during discharge. Measured april 16, 1983.
Downhole pressures calculated for the following conditions.

Wellhead pressure (bar abs.)	:	10.00
Wellhead temperature (C)	:	179.88
Wellhead dryness	:	0.113
Wellhead enthalpy (kJ/kg)	:	990.00
Wellhead total flow (kg/s)	:	76.00

Feedzone no:	Depth (m)	Flow (kg/s)	Enthalpy (kJ/kg)
1	500.0	40.0000	1008.0
2	600.0	30.0000	990.0
3	800.0	6.0000	943.9

Figure 6.7. Well AH-21 flowing temperature and pressure match at a discharge flowrate of 76 kg/s.

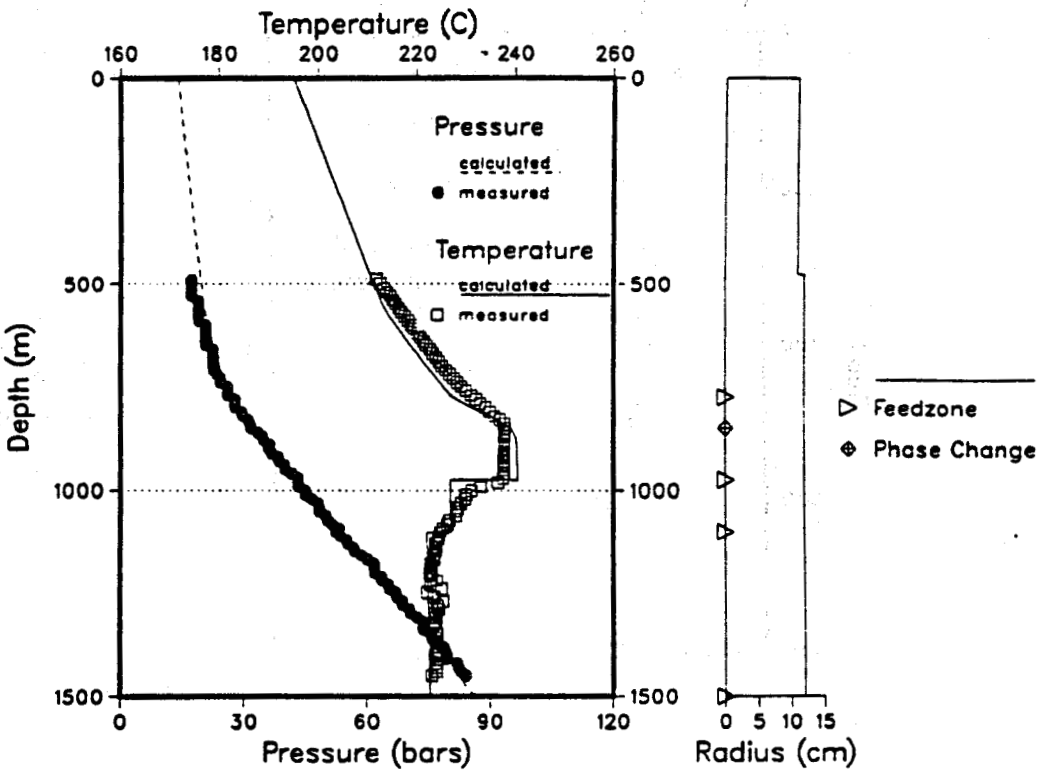

AHUACHAPAN WELL AH-32.
Calculated downhole pressure and temperature during production in 1988. Downhole data from Los Alamos.

Wellhead pressure (bar abs.)	:	14.00
Wellhead temperature (C)	:	195.04
Wellhead dryness	:	0.133
Wellhead enthalpy (kJ/kg)	:	1090.00
Wellhead total flow (kg/s)	:	20.00

Feedzone no:	Depth (m)	Flow (kg/s)	Enthalpy (kJ/kg)
1	775.0	4.5000	1300.0
2	975.0	13.5000	1050.0
3	1100.0	1.0000	1000.0
4	1500.0	1.0000	958.4

Figure 6.8. Well AH-32 flowing temperature and pressure match at a discharge flowrate of 20 kg/s.

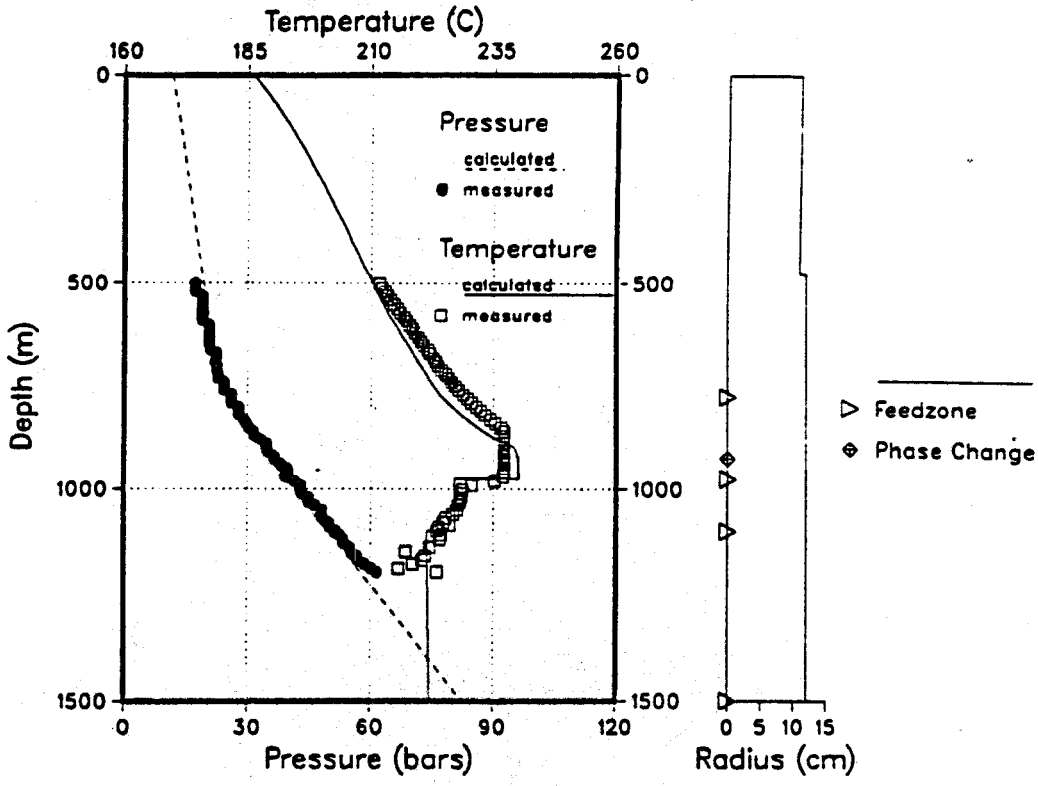

AHUACHAPAN WELL AH-32.
Calculated downhole pressure and temperature during production in 1988. Downhole data from Los Alamos.

Wellhead pressure (bar abs.)	:	11.50
Wellhead temperature (C)	:	186.05
Wellhead dryness	:	0.151
Wellhead enthalpy (kJ/kg)	:	1090.00
Wellhead total flow (kg/s)	:	45.00

Feedzone no:	Depth (m)	Flow (kg/s)	Enthalpy (kJ/kg)
1	775.0	10.5000	1300.0
2	975.0	29.0000	1050.0
3	1100.0	3.0000	1000.0
4	1500.0	2.5000	955.0

Figure 6.9. Well AH-32 flowing temperature and pressure match at a discharge flowrate of 45 kg/s.

7.0 INITIAL THERMODYNAMIC CONDITIONS

Temperature and pressure logs from the Ahuachapán wells obtained during 1968-1975 have been examined in order to determine the initial conditions in the field. A significant amount of fluid was withdrawn from the reservoir during this period, causing changes in temperature and especially in reservoir pressures. The flow testing of wells culminated in 1972-73 and relatively little fluid was produced before exploitation began in 1975. When production was stepped down, the reservoir showed rapid recovery, indicating that data from 1974 and early 1975 closely reflect the initial reservoir conditions. In general, the reservoir pressures were only about 1-2 bars lower in 1975 than in 1968.

7.1 Initial Pressure Distribution

Plots of pressure logs from all wells are given in Appendix E. The data have been analyzed in order to determine initial pressures, pressure differences between aquifers and changes due to mass extraction from the field. Most of the wells reflect pressure conditions in the geothermal reservoir (the saline aquifer), but some of the peripheral wells are only connected to the saturated aquifer (wells AH-9, 10, 12 and 15). These wells show higher pressures (higher water level) than wells communicating with the geothermal reservoir, indicating a pressure difference of more than 5 bars between the saturated and the saline aquifers. All of the geothermal wells are cased through the shallow aquifer. Shallow water table data measured in early exploration wells indicate, however, that the ground water aquifer has a considerably higher pressure potential than the saturated aquifer.

Figure 7.1 shows a simplified pressure profile for the field and demonstrates the different pressure potentials of the three aquifers. The estimated pressures for the shallow aquifer are not accurate because of limited data; the pressure will vary with topography. As the elevation of the wellfield averages 800-850 masl, the water level of the shallow pressure aquifer should be

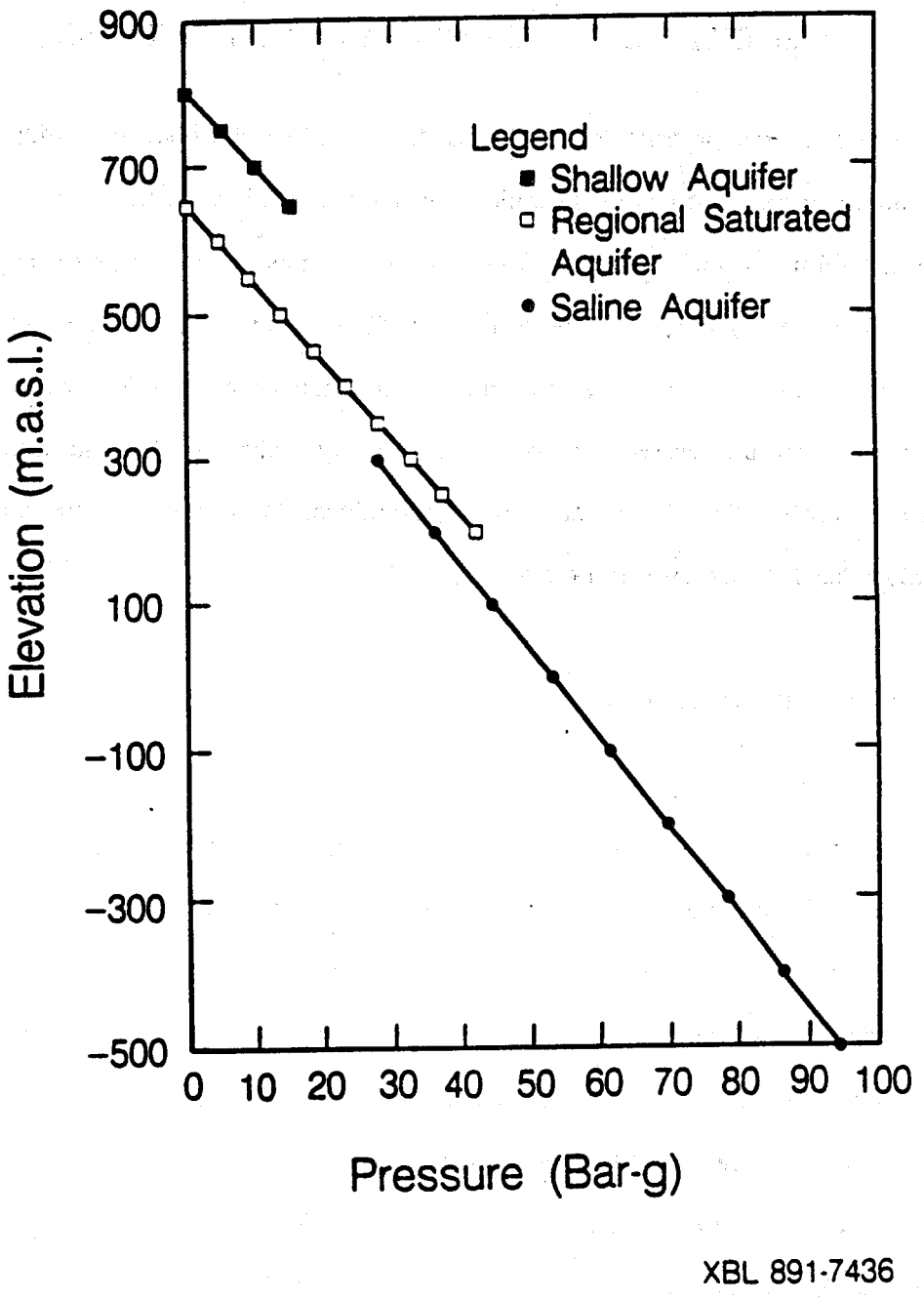

Figure 7.1. Pressure profiles of the different aquifers.

close to 800 masl. The pressure potential difference between the shallow and the saturated zone is in the order of 10-20 bars. The wells connected to the saturated aquifer have water levels at 620-660 masl, corresponding to a pressure of 40-44 bars at 200 masl, the reference depth for monitoring geothermal reservoir pressure. The pressure distribution in the reservoir (the saline aquifer) in the wellfield was uniform prior to exploitation. The reported pressure at 200 masl in well AH-1 was close to 36 bars in 1968, indicating a pressure potential 4 to 8 bar lower than in the saturated zone.

Figure 7.2 shows measured or estimated 1974-75 pressure at 200 masl. High values are found in the wells connected to the saturated zone (above 40 bars), but most pressures in the wellfield lie in the range of 34-36 bars. Compared with a 36-bar initial (1968) pressure in well AH-1, this indicates a drawdown of 1-2 bars caused by flow testing of wells during the exploration years. As the scattering of the data on Figure 7.2 is smaller than the measurement error, no fieldwide variation can be determined from this pressure distribution map.

7.2 Initial Temperature Distribution

Plots of temperature surveys from all the geothermal wells are given in Appendix D. The logs mainly reflect the reservoir temperatures and cannot be used to determine the temperature in the shallow aquifer. Only few of the logs show temperatures within the saturated aquifer.

The only information available on near-surface temperatures are logs from shallow temperature gradient wells in the area. The data has been analyzed for temperatures at 100 m depth (Figure 7.3). The temperature values within the well field were found to range between 40 and 100°C, but higher temperatures should be expected in areas near surface manifestations (Figure 7.3).

The information available on saturated aquifer temperatures is summarized in Figure 7.4. The data suggest temperatures of 110-130°C at 450 masl on the periphery of the production area and decreasing temperatures towards wells AH-10 and M-1 in the north. No information is available on temperatures at this level within the well field. Production wells develop wellhead

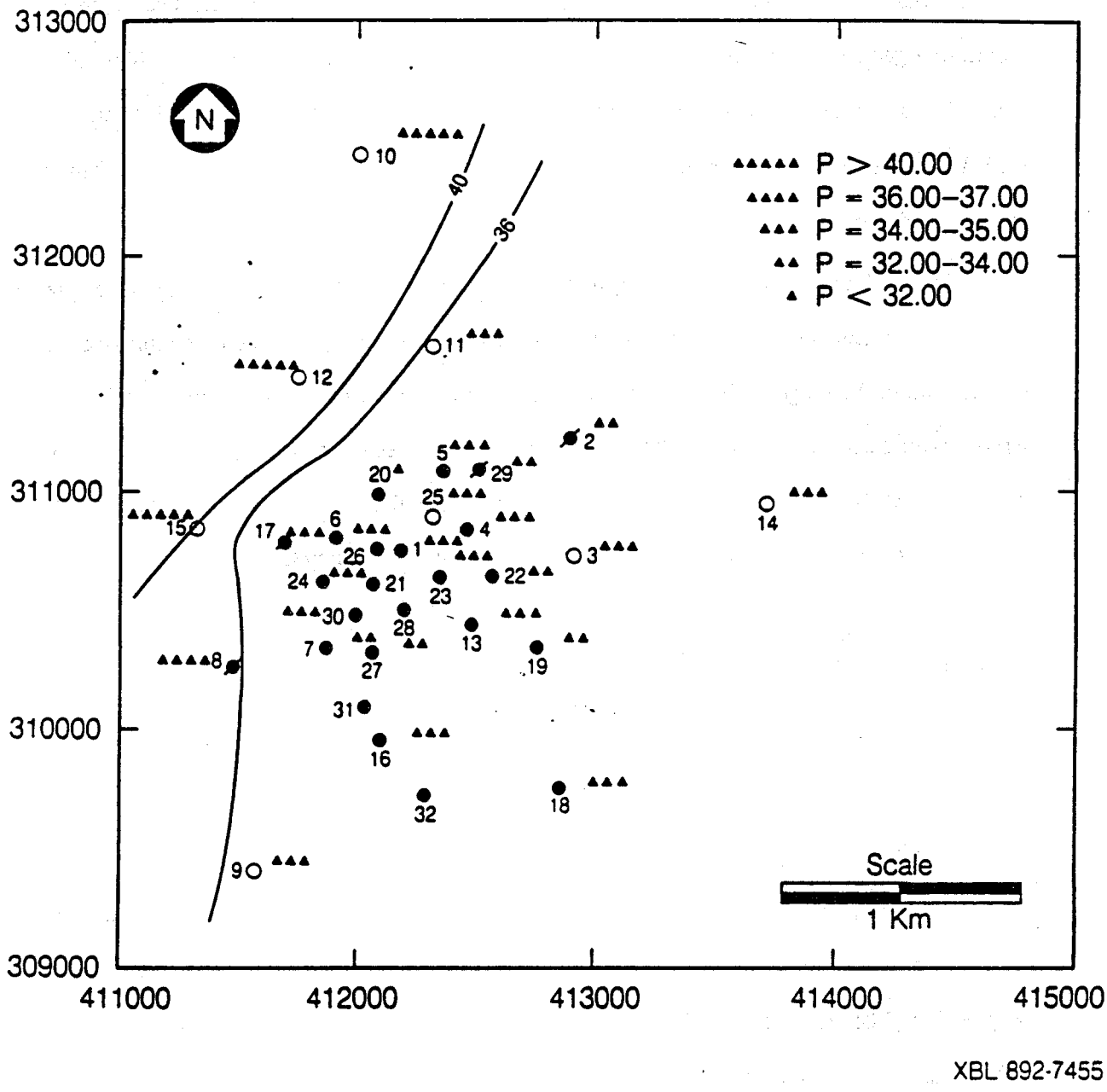

Figure 7.2. 1974-75 pressure distribution at 200 masl (in bar-g).

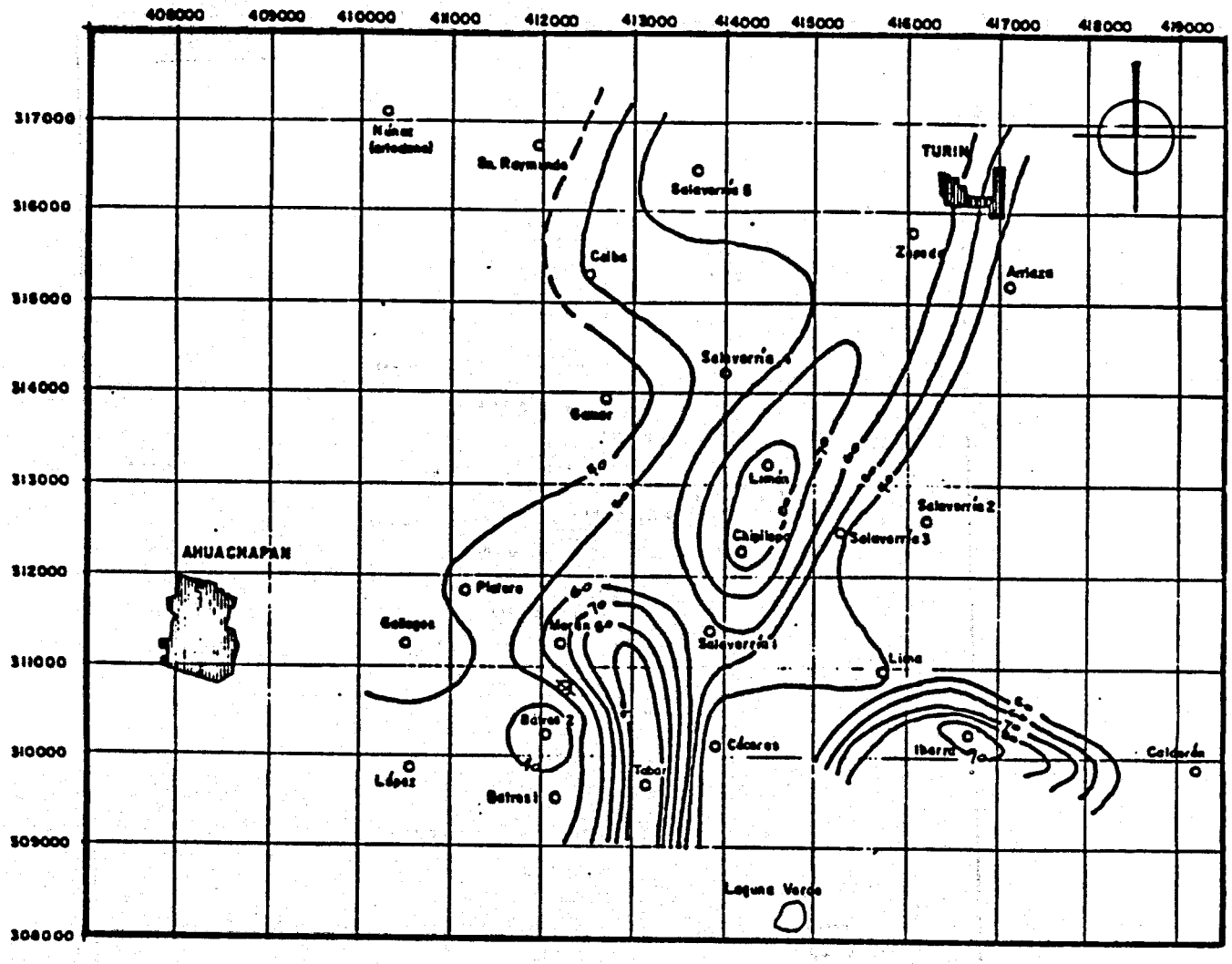

Figure 7.3. Temperature contours (in °C) at 100 meters depth (shallow aquifer, from Jiménez and Campos, 1976).

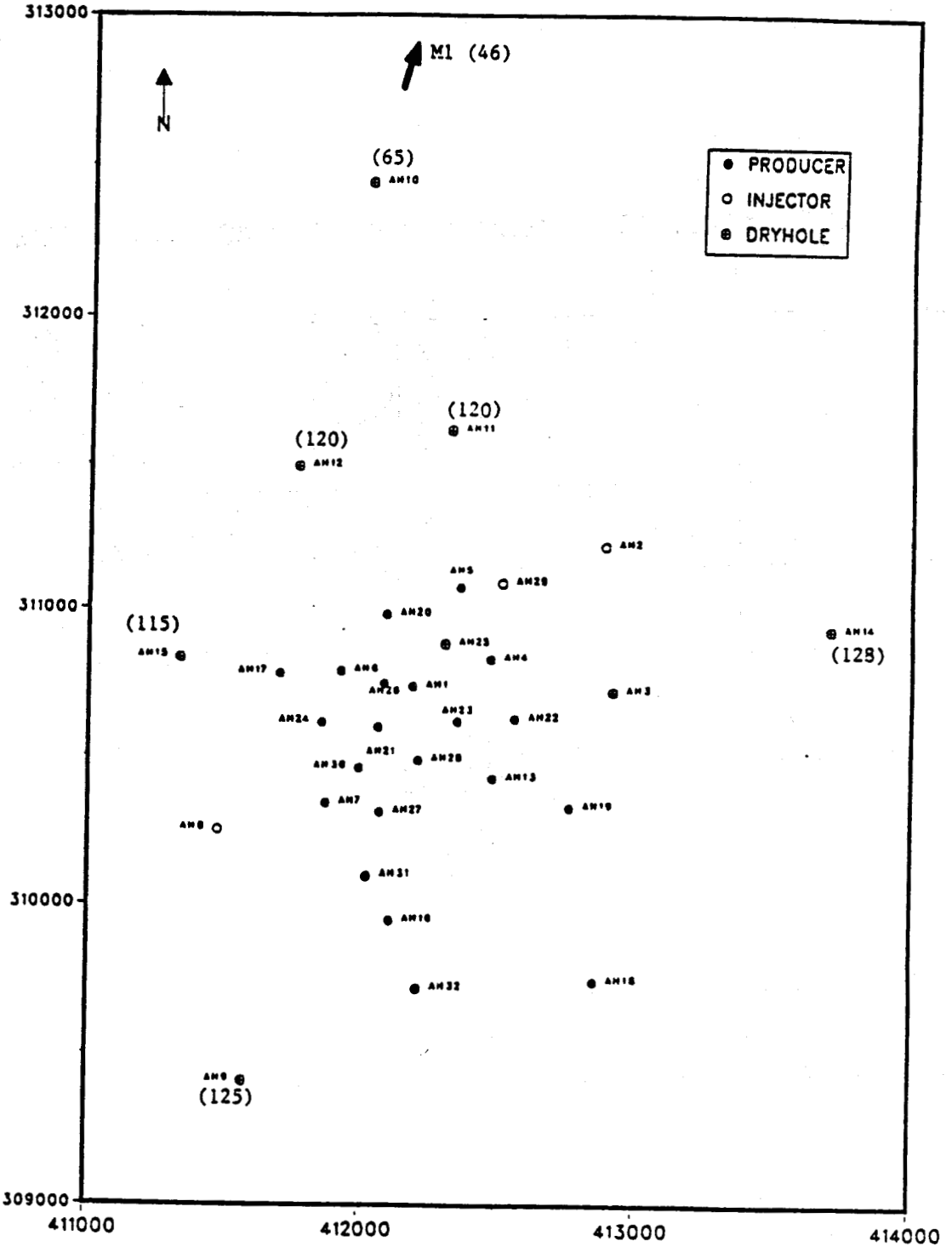

Figure 7.4. Temperatures (in °C) in the saturated aquifer at 450 masl.

pressures and have a deep boiling level. Shallow temperature readings in these wells reflect, therefore, only wellhead conditions and steam migration from the boiling level to the wellhead.

All temperature logs obtained before 1975 have been examined in order to determine the initial reservoir conditions. Several logs are available for each well, which made it possible to evaluate and eliminate calibration errors in some of the logs and temperature variations caused by drilling or flow testing, and determine the stable initial temperature profiles in the wells.

Temperature maps and cross sections of the field have been developed based on the stable initial temperature profiles. The cross sections include two N-S sections reaching from wells AH-10 to AH-18 (Figures 6.1b and 6.2c), and two W-E sections from wells AH-15 to AH-14 (Figures 6.1d and 6.1e). All of the cross sections show, in addition to isotherms, a simplified geological section and the location of main feed zones in the wells. The temperature cross sections show increasing temperatures with depth through the upper aquifers (the shallow and saturated aquifers). In the production area, the top of the geothermal reservoir is found near the contact between the YA and AA units. Maximum temperatures of more than 230°C are reached in the AA unit, and temperature inversions are observed in most wells when entering the OA unit. The cross sections show clearly that the geothermal anomaly does not extend as far north as well AH-10, and also suggest a thermal boundary to the west, close to well AH-15. The highest temperatures (over 240°C) are found deep in the eastern and the southern parts of the wellfield, indicating that the field extends further in these directions.

Initial temperatures at 300 masl are contoured in Figure 7.5. This contour map basically reflects the depth of the AA unit with highest temperatures in the structural high located in the production area, where the top of the unit reaches 350 masl. The area enclosed by the 230 °C isotherm, defines the part of the reservoir which was boiling prior to field exploitation (the estimated initial reservoir pressure at 300 masl is about 27.5 bars). The bottom of this boiling zone was initially just below 300 masl.

Figure 7.6 shows the temperatures contours at 200 masl. The isotherm pattern is similar to that in Figure 7.5, with the highest temperatures in the production area andesites. The initial

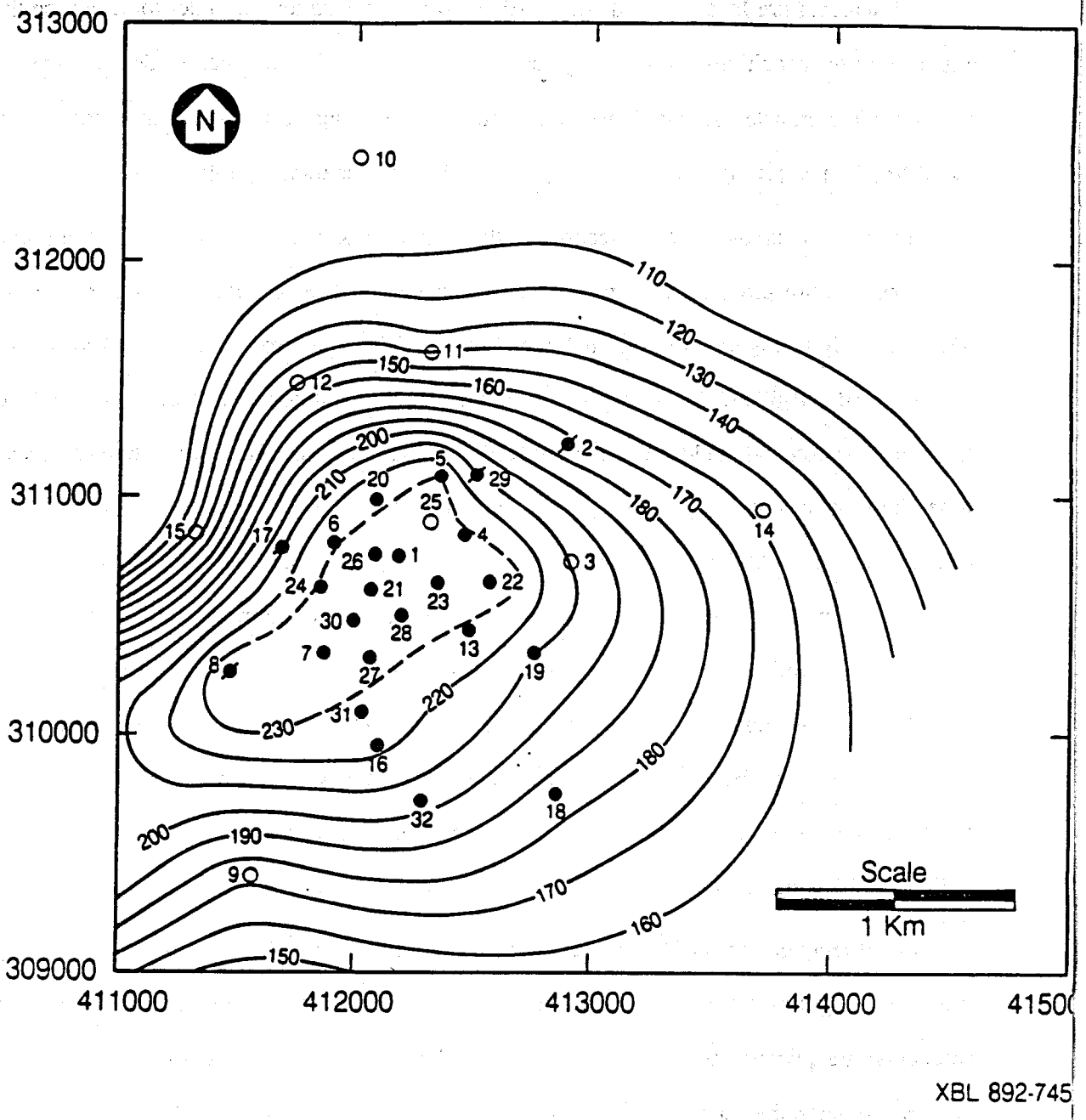

Figure 7.5. Initial temperature distribution (in °C) at 300 masl.

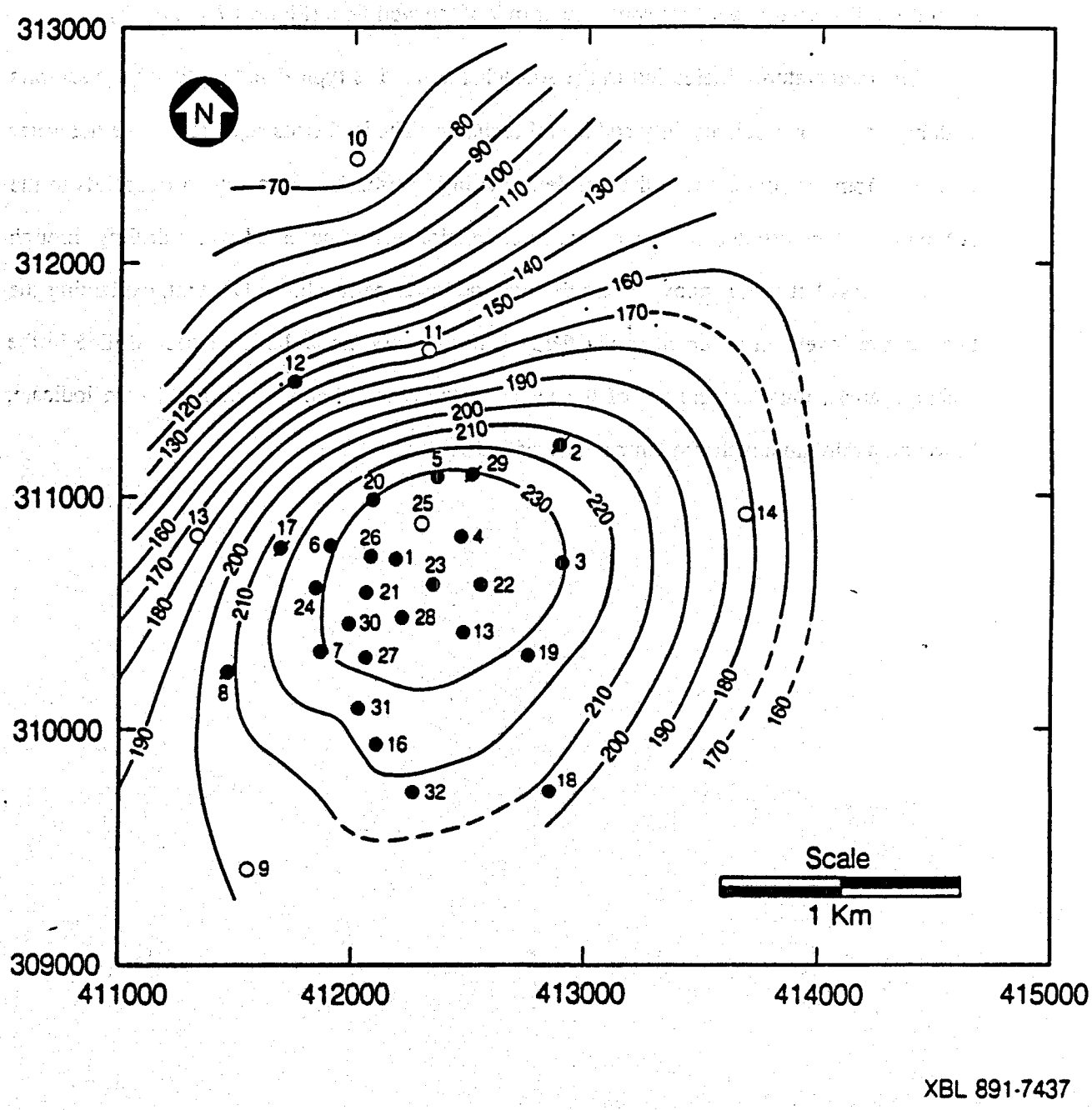

Figure 7.6. Initial temperature distribution (in °C) at 200 masl.

reservoir pressures at this elevation were about 36 bars, as discussed earlier. The saturation temperature at 36 bars is 245°C, about 10 degrees higher than maximum temperatures in the field. Deeper in the reservoir the isotherm distribution changes as the area of maximum temperature is displaced toward the southeast corner of the well field (Figures 7.7 and 7.8).

The temperature distribution in the Ahuachapán field is typical for geothermal reservoirs with high horizontal permeability and lateral recharge. The isotherms suggest that the hot water inflow is from the south/east of the wellfield; the high permeable formation corresponds to the AA unit, as demonstrated by several major circulation losses observed while drilling through this unit. Less hot water inflow occurs through the lower permeability OA unit, explaining the temperature inversion observed in the field. Unfortunately, no wells have been drilled in the recharge areas, thus temperature of the recharge fluids is unknown. Wellfield data indicate, however, a minimum recharge temperature of 245-250 °C.

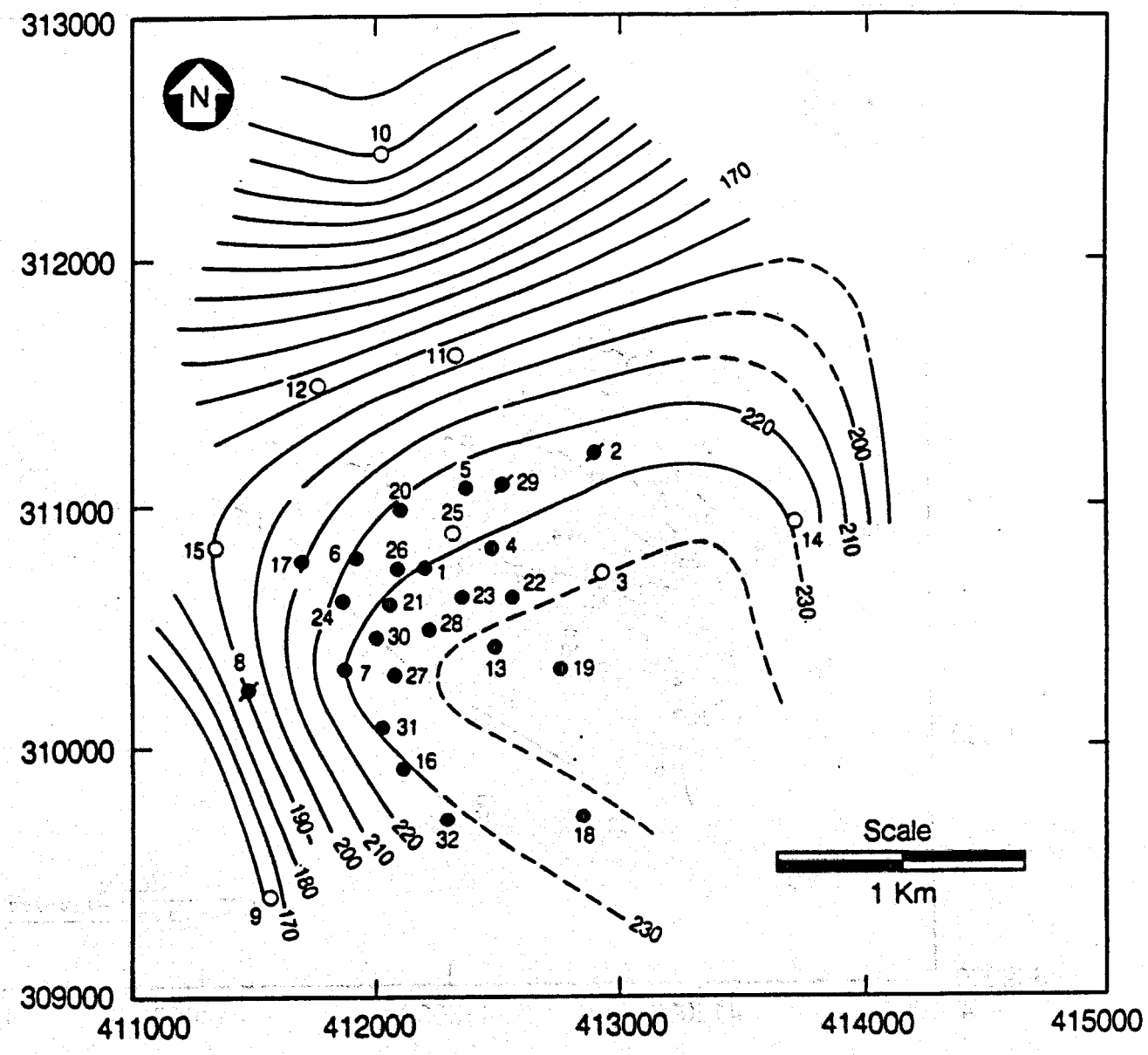

Figure 7.7. Initial temperature distribution (in°C) at mean sea level elevation.

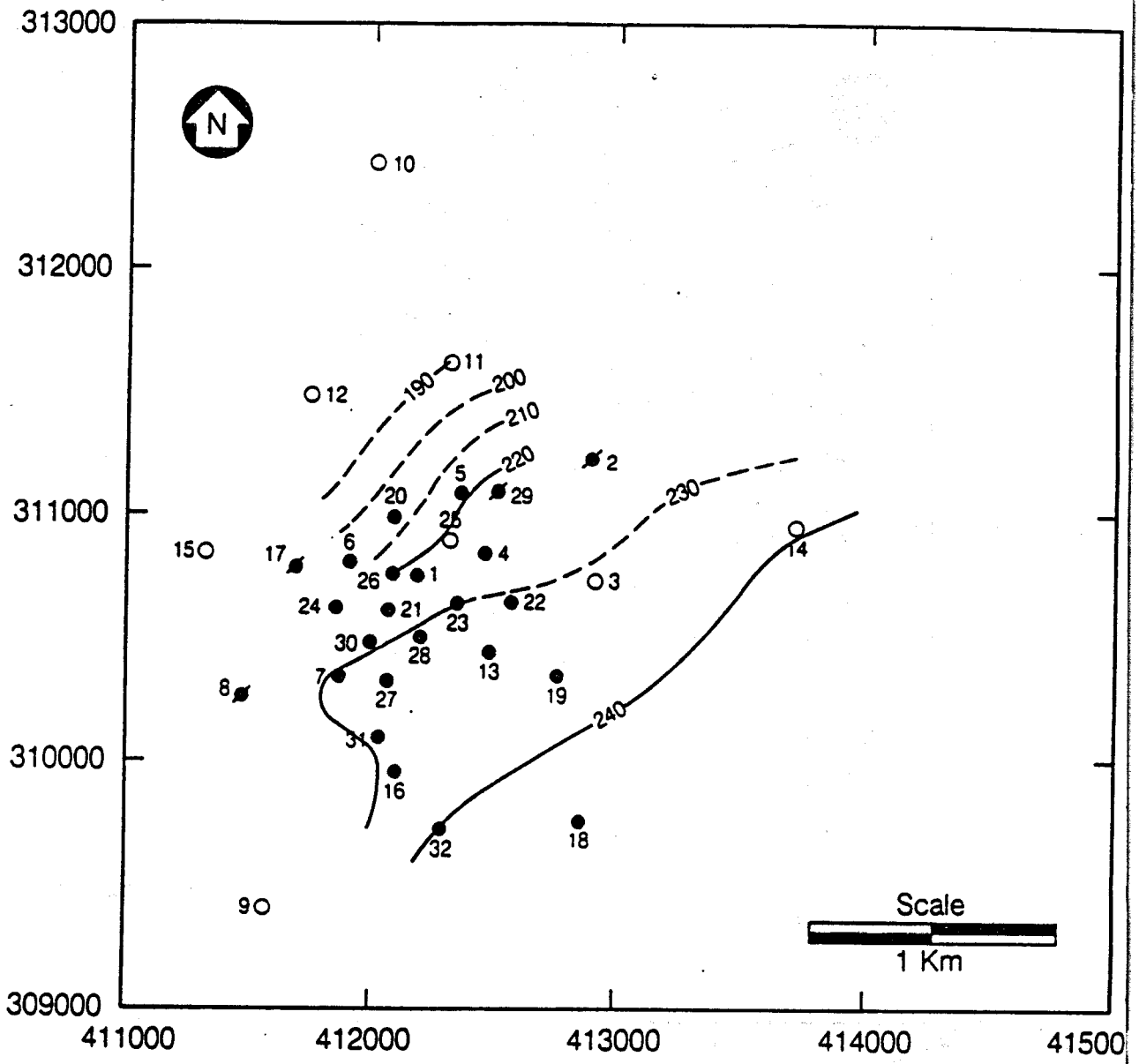

Figure 7.8. Initial temperature distribution (in °C) at -150 masl.

8.0 PRESSURE TRANSIENT TESTING

Pressure transient well tests are commonly used to investigate reservoir permeability and storativity. The various pressure transient tests that have been conducted in geothermal reservoirs include single-well drawdown, build-up, injection and fall-off tests, and interference tests that require two or more wells. The tests conducted at Ahuachapán include injection, drawdown, build-up, and interference tests. Data from some of these tests have been examined and those tests with interpretable data have been analyzed. Most of the tests are of short duration (e.g., injection and build-up tests), so that the reservoir pressure response is masked by wellbore storage. It was not considered worthwhile to reinterpret those tests because of their questionable validity, hence, analyses performed by CEL and Escobar (1985) were considered adequate. Instead, more emphasis was placed upon the analysis of available interference tests. In the following sections the available pressure transient test data and the results of the analyses are summarized.

8.1 Injection Tests

A series of injection tests were conducted in 15 Ahuachapán wells during 1975-1979. The data collected are published in the report "Indices de Inyectividad Ahuachapán" (Campos, 1980). All of the tests were conducted in a similar manner. A Kuster pressure gauge was lowered to a depth of several hundred meters into the wells and the pressure monitored for 5-30 minutes before injection started. The injection rate was increased in 10-15 l/s steps to a maximum of 40-50 l/s. Typically, each step lasted only 15 minutes. The pressure fall-off was monitored for 15 minutes after the final injection step. Only the pressure value at the end of each injection step is reported.

The injection data show that the wells did not reach "stable" conditions during the injection steps. First, the duration of each step is too short to expect a pressure stabilization in the wells and second the temperature conditions were not stable in the wells during the tests. This

can best be demonstrated by comparing the pressure during fall-off with the pressure prior to the tests.

The data have been analyzed for injectivity indices. As different injection steps give different injectivities, an average injectivity index was defined for each well and the transmissivity calculated using Thiem's solution. The results are given in Table 8.1. The tests indicate well injectivities of the order of 1 to 10 $\frac{1}{\text{s–bar}}$ and transmissivities of the order of 1×10^{-8} to 7×10^{-8} $\frac{\text{m}^3}{\text{Pa–s}}$. The results are generally consistent with the productivities of the wells. Good producers such as wells AH-21, AH-27 and AH-28 have relatively high transmissivity, while low transmissivities are found in the poor producers AH-14 and AH-18.

The transmissivity values obtained from the injection tests in Ahuachapán wells are much lower than values determined from interference tests (Section 8.3) and the production and drawdown history of the field (Chapter 9). This is probably due to inadequate well testing data caused by the short duration of the injection steps and non-isothermal conditions during the test. It should, however, be noted that only the near-well transmissivities determine the pressure response in the well during short duration injection tests, whereas interference tests measure global reservoir transmissivities. Experience from other geothermal fields shows that interference tests usually yield higher transmissivities than single-well tests.

8.2 Drawdown and Build-up Tests

Drawdown and build-up tests were carried out in few Ahuachapán wells during 1983-1984. In all of the tests the wells were flowed at a constant rate for a short period (generally about an hour) and then closed. The downhole pressure was monitored with a Kuster gauge showing the drawdown during the discharge period and the pressure build-up after closure. The data from the pressure transient test is published and analyzed in the report "Reservoir Engineering at Ahuachapán" (Escobar, 1985).

Table 8.1
Results of Injection Tests

Well no.	Injectivity $\left[\frac{l}{s\text{–}bar}\right]$	Transmissivity $\frac{kh}{\mu}\left[\frac{m^3}{Pa\text{–}s}\right]$
AH-2	3	$2.2 \cdot 10^{-8}$
AH-14	3	$2.2 \cdot 10^{-8}$
AH-16	8.5	$6.2 \cdot 10^{-8}$
AH-17	7.5	$5.5 \cdot 10^{-8}$
AH-18	1.5	$1.1 \cdot 10^{-8}$
AH-19	6	$4.4 \cdot 10^{-8}$
AH-21	9	$6.6 \cdot 10^{-8}$
AH-22	6	$4.4 \cdot 10^{-8}$
AH-23	5.5	$4.0 \cdot 10^{-8}$
AH-24	7	$5.1 \cdot 10^{-8}$
AH-25	3.5	$2.6 \cdot 10^{-8}$
AH-27	9	$6.6 \cdot 10^{-8}$
AH-28	7	$5.1 \cdot 10^{-8}$
AH-29	3	$2.2 \cdot 10^{-8}$
AH-30	3.5	$2.6 \cdot 10^{-8}$

Due to the short duration of the tests, the data were found to reflect merely wellbore storage effects and for some of the wells the monitoring depth was found to be above the boiling level in the well during discharge. The data can therefore not be used to determine the transmissivity of the wells.

8.3 Interference Testing

Several interference tests have been conducted at Ahuachapán. One such test was carried out during the period May 6 to August 19, 1982. The purpose of this test was to obtain data for determining reservoir transmissivity and storativity.

During the test period, wells AH-1, AH-4, AH-6, AH-7, AH-17, AH-20, AH-21, AH-22, AH-23, AH-24, AH-26, AH-27 and AH-28 were producing, and fluids were reinjected into wells AH-2, AH-8 and AH-29. Well AH-25 was used as an observation well. The pressure response observed at this well during the test period is shown in Figure 8.1. Because most of the Ahuachapán wells were flowing for a long period of time prior to the test, the wellfield pressures were in a state of quasi-equilibrium. Thus, the small pressure perturbations observed in well AH-25 were due to changes in flow conditions of the producers and injectors that were not operated at near-constant flow rates. Table 8.2 gives the flow rates of the producers and injectors having considerable changes in flow rate during the test period. The data shown in Table 8.2 were used in the analysis of the pressure response in well AH-25. Table 8.3 gives the flow rates of the producers and injectors that were considered "stable" during the test. These wells were not considered in the analysis.

In the analysis, the computer model VARFLOW (Benson, 1982; McEdwards and Benson, 1981; EG&G Idaho Inc. and LBL, 1982) was used. The model uses the basic Theis solution (Theis, 1935) for an arbitrary number of producers and injectors, employing principles of superposition. The Theis solution is a very simple model derived on the basis of the following assumptions:

(1) The reservoir is of infinite areal extent.

(2) The reservoir is completely saturated with a slightly compressible single-phase fluid.

(3) The reservoir is isothermal.

(4) The reservoir is horizontal and has a constant thickness.

(5) The flow of fluid in the reservoir is described by Darcy's law.

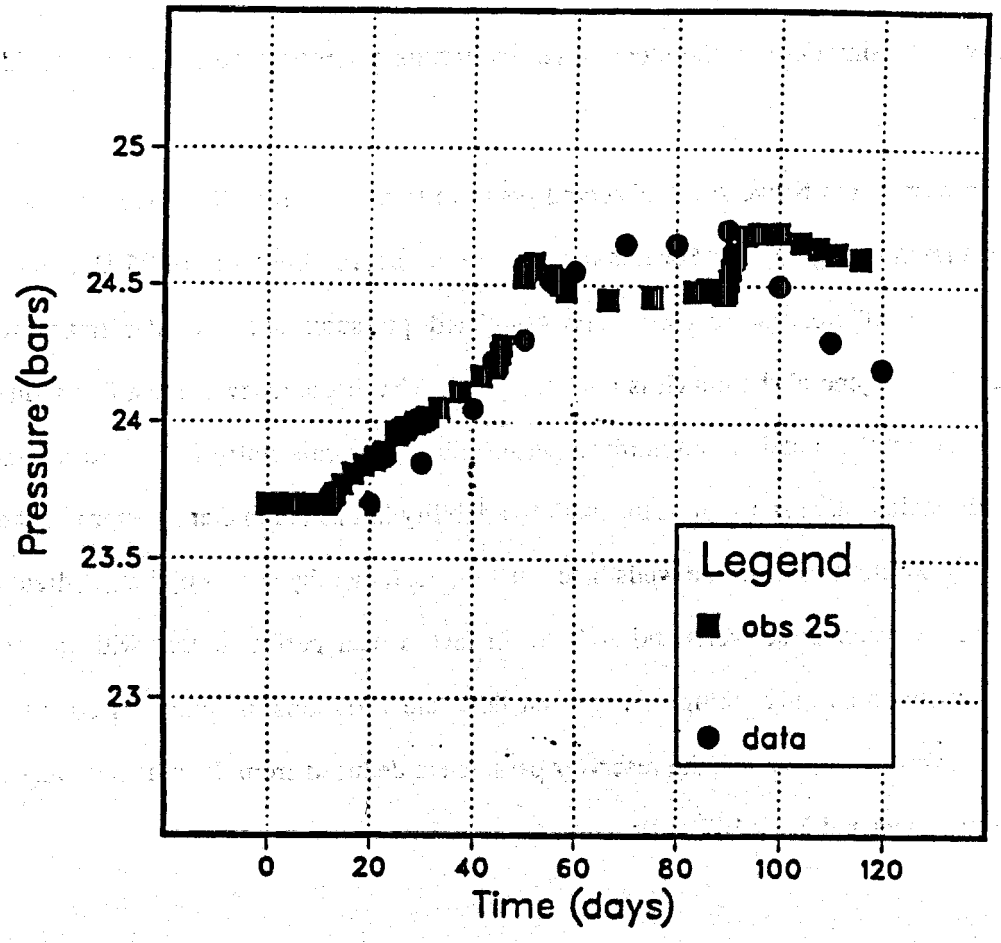

Figure 8.1. Match between observed and computed pressures for interference test, May-August 1982.

(6) The reservoir is homogeneous and bounded above and below by impermeable layers.

(7) The flow into (or from) a fully-penetrating well is uniformly distributed over the length of the well.

(8) The well is modeled as a line source.

Given the simplicity of the model used, the results obtained should only be considered as coarse estimates.

The best match between the observed pressure transients in well AH-25 and those computed is shown in Figure 8.1. For this match, a reservoir transmissivity of 25 Dm and a storativity of 2.5×10^{-6}m/Pa were used. The calculated pressures show similar trends to those observed, but in general the match is not very good. The discrepancy is most likely due to the fact that our simple model uses a uniform permeability (transmissivity) for the entire reservoir, whereas in reality there is a significant spatial variability in this parameter. Better matches were obtained by omitting some of the wells listed in Table 8.3, thereby assuming less hydraulic communication between these wells and AH-25. In fact, a near perfect match with the observed data was obtained by only taking into account flow rate variations of wells AH 20, AH-21 and AH-24. However, in all cases, the reservoir parameters deduced from the matches were similar, or close to 25 Dm and 2.5×10^{-6}m/Pa.

Table 8.2
Production/Reinjection (kg/sec) in Wells with Work Stoppage

Date	AH-2 R	AH-4 P	AH-8 R	AH-20 P	AH-21 P	AH-22 P	AH-23 P	AH-24 P	AH-26 P
May 6	-19.8	45.1	-33.9	37.8	72.9	56.6	31.3	37.5	23.1
May 15	-19.8	45.1	0.0	37.8	72.9	56.6	31.3	37.5	23.1
May 17	-19.8	45.1	0.0	0.0	72.9	56.6	31.3	37.5	23.1
May 26	-19.8	45.1	0.0	0.0	0.0	56.6	31.3	37.5	23.1
June 1	-28.3	50.8	0.0	0.0	0.0	57.7	49.0	35.9	22.5
June 3	-28.3	50.8	0.0	0.0	0.0	57.7	49.0	0.0	22.5
June 19	-28.3	50.8	0.0	0.0	0.0	0.0	0.0	0.0	0.0
June 25	-28.3	50.8	0.0	0.0	0.0	57.7	49.0	0.0	22.5
July 1	-42.2	63.2	0.0	0.0	0.0	58.5	49.8	0.0	21.5
Aug. 1	-53.4	74.2	0.0	0.0	0.0	57.7	50.1	0.0	40.0
Aug. 2	-53.4	74.2	0.0	0.0	82.5	57.7	50.1	40.0	40.0
Aug. 3	0.0	0.0	0.0	0.0	82.5	57.7	50.1	40.0	40.0
Aug. 29	0.0	0.0	0.0	0.0	82.5	57.7	50.1	40.0	40.0

Table 8.3
Production/Reinjection (kg/sec) in Wells without Work Stoppage

Date	AH-1 P	AH-6 P	AH-7 P	AH-17 P	AH-27 P	AH-28 P	AH-29 R
May 6	62.9	22.0	38.9	22.6	68.3	75.4	-55.5
June 1	63.3	23.2	32.5	21.8	68.8	73.0	-56.1
July 1	62.9	27.8	30.5	21.9	69.7	71.8	55.7
Aug. 1	63.9	26.5	31.6	21.7	69.9	70.1	56.4
Aug. 29	63.9	26.5	31.6	21.7	69.9	70.1	56.4

9.0 CHANGES DURING EXPLOITATION

The Ahuachapán field has been under development and exploitation for more than 20 years. The reservoir characteristics have changed drastically during this period due to heavy fluid production. Reservoir pressures have dropped some 15 bars and a cooling of 10-15°C has been observed. Consequently, the performance of the production wells has changed. All wells show a gradual flowrate decline as the reservoir drawdown increases; the two-phase region has expanded in the upper portion of the reservoir, resulting in increasing fluid enthalpies in wells with shallow feed zones.

CEL personnel have closely monitored the field during its development and exploitation phases. Considerable data on extraction/injection rates, reservoir response (pressure, temperature and fluid chemistry) and well performances have been obtained since 1968 (Campos, 1985). In the following section some of these data are shown and analyzed.

9.1 Mass Extraction History

Production of geothermal fluids from the Ahuachapán reservoir started on August 27, 1968, when well AH-1 was flowed for the first time. Fluid extraction increased significantly in the following years as new wells were completed and flow tested. Large scale exploitation started in June 1975, when the first 30 MW_e generator went on-line. A second 30 MW_e unit went on line in July 1976 and, a third unit (35 MW_e) in November 1980.

Presently, the existing production wells do not supply enough steam to operate the power plant at full capacity. The average mass extraction rate in the last few years has been approximately 500 kg/s, and the corresponding electrical production in the order of 45 MW_e.

Disposal of geothermal waste water has been of major concern in the development of Ahuachapán. One way of addressing this problem is to reinject the spent fluid into the reservoir. Ahuachapán was the first geothermal reservoir where large scale reinjection was used (Einarsson et al., 1975). The first experiments were conducted in 1971, when fluids from wells AH-1 and AH-6 were injected at a temperature of 150°C into well AH-5 for a period of one year. This

experiment showed that reinjection was a feasible solution to the disposal problem (Einarsson et al., 1975). Shortly after exploitation began, a reinjection program was initiated in August 1975. The rate of reinjection varied considerably. In early 1976 as much as 50% of the produced fluids were reinjected, but on the average about 25-30% of the produced fluids were injected back into the reservoir, until November 1982 when reinjection was stopped. Since that time the waste water has been gravity-flowed to the Pacific Ocean using a 75 km long concrete channel.

At present, 32 wells have been drilled in Ahuachapán. Sixteen wells have been used at one time or another to provide steam for the power plant. These are wells AH-1, AH-4, AH-5, AH-6, AH-7, AH-17, AH-19, AH-20, AH-21, AH-22, AH-23, AH-24, AH-26, AH-27, AH-28 and AH-31. During the reinjection period (1975-82) wells AH-2, AH-8, AH-17 and AH-29 were used as injectors.

Since August 1968, production and reinjection rates for all wells have been measured regularly and are available as monthly averages. As an example, the production data for well AH-1 is plotted in Figure 9.1. The plot shows flow rate fluctuations because the well was not discharged continuously, and indicates the gradual decline in production during the last decade.

The cumulative extraction history of Ahuachapán is shown in Figure 9.2. During the development phase, from August 1968 to May 1975, a total of 24 Mtons of fluids were produced from the reservoir with only 2 Mtons reinjected during the 1971 injection tests. Fluid production increased drastically when the first two generators went on-line and has averaged 17 Mtons/year since 1976. A considerable amount of the produced fluid was reinjected in the first years of exploitation, and at the time the reinjection program was stopped (November 1982), some 38 Mtons of fluid had been returned to the reservoir. By the end of September 1987, the total net fluid extraction from the field had reached 187 Mtons.

9.2 Pressure Drawdown

Although pressures in the Ahuachapán wellfield were fairly uniform prior to exploitation, as discussed in Chapter 7, exploitation has caused significant drawdown. This has been moni-

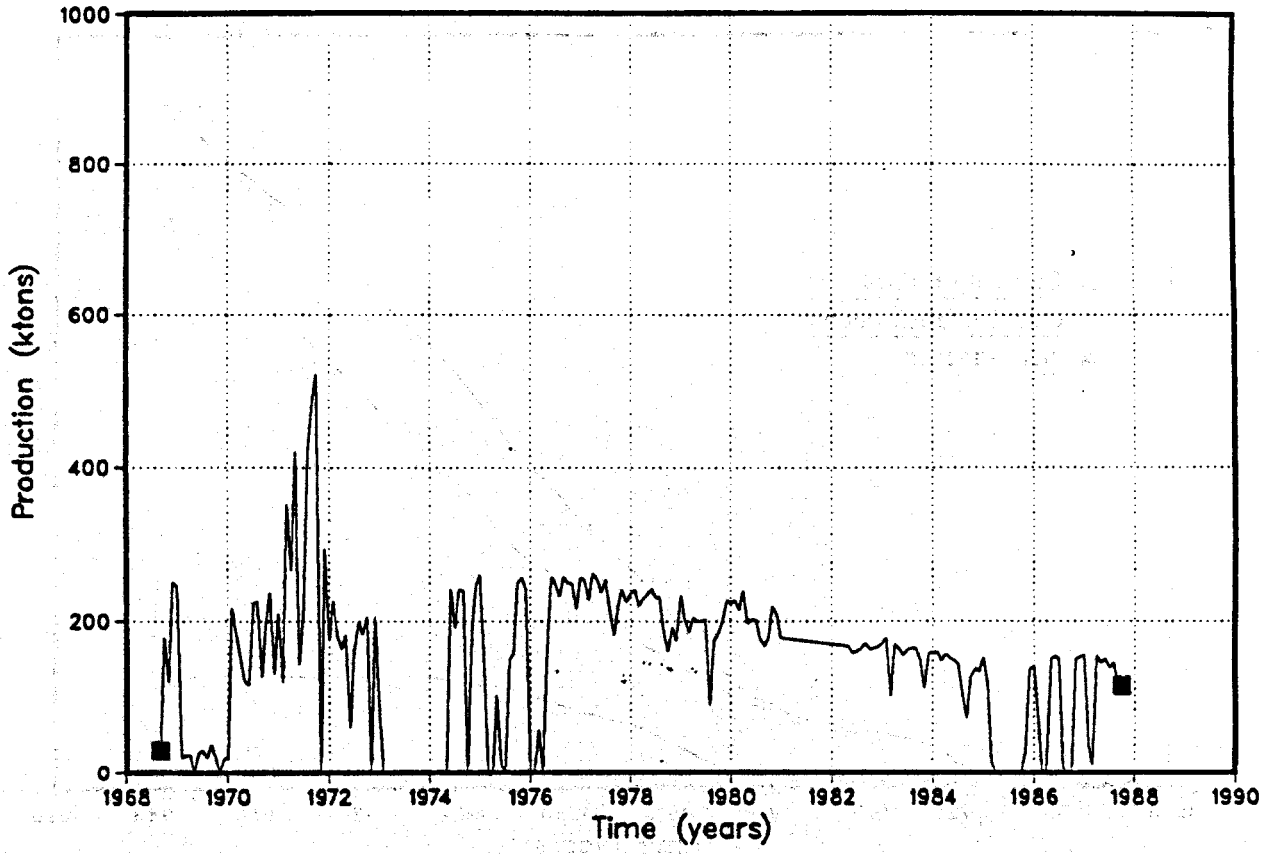

Figure 9.1. AH-1 monthly fluid production (1968-1988).

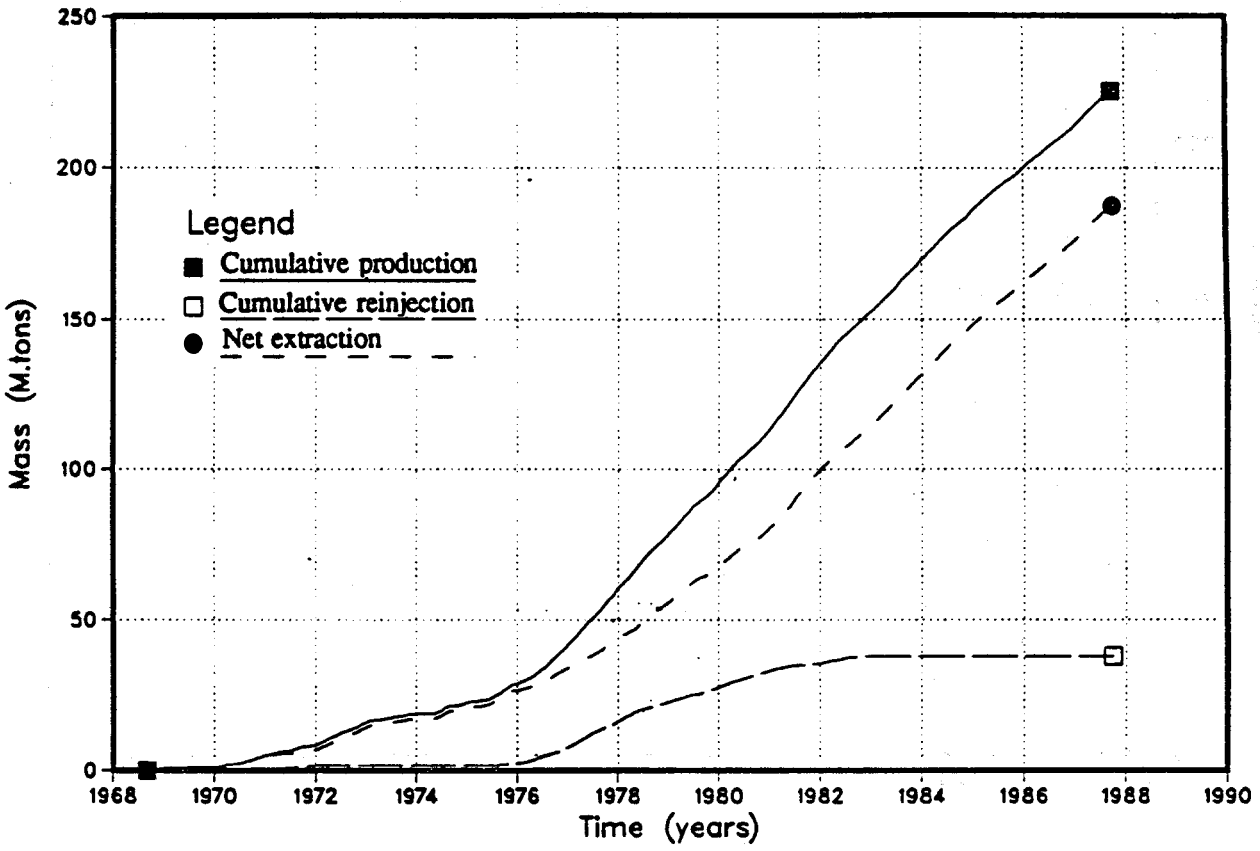

Figure 9.2. Cumulative fluid production (1968-1988).

tored by annual pressure surveys in all wells accessible to logging, and by daily pressure measurement at 200 masl in well AH-25. In most of the wells, the liquid portion of the geothermal reservoir is found at this elevation. The pressures are therefore not disturbed by boiling, making this elevation an excellent datum level. The initial (pre-exploitation) pressure at 200 masl was about 36 barg. During the period of development drilling flow testing of the wells resulted in an average reservoir drawdown of 1-2 bars in 1975, when field exploitation began (Chapter 7).

The 200 masl pressure data from the annual surveys have been analyzed and isobar maps have been developed for different years. Figures 9.3 and 9.4 show the maps for 1978 and 1986. Both figures show a reduced uniform pressure engulfing the entire production area. In 1978 the pressure values in that area were 28-30 barg and by 1986 the pressures had declined to 20-22 barg. Relatively high pressures in wells AH-8, AH-29, AH-17 and AH-2 in 1978 are the result of reinjection. The area of minimum pressure extends to the stand-by wells AH-16 and AH-32, in the southern part of the wellfield. Other peripheral wells showing substantially reduced pressures in 1986 are wells AH-14 (29.3 barg) in the east, AH-11 (23.6 barg) in the north and AH-8 (25.3 barg) in the western part of the well field. Wells AH-10, AH-12 and AH-15 are not in pressure communication with the geothermal reservoir, as mentioned earlier, and reflect pressures in the saturated zone. Initially, well AH-9 showed reservoir pressures, but the well is now plugged and its pressure corresponds to that of the saturated zone. No pressure drawdown has been dominated within the saturated aquifer.

The AH-25 pressure data has been supplemented with some 1968-1977 average well pressure values at 200 masl. Suspiciously high 1970-1971 pressures (40 bar) have not been included. They are judged to be incorrect as the calibration curves used were out of date (Bolton, 1979). The pressure values have been converted into drawdown by assuming an initial reservoir pressure of 36 barg, and are plotted on Figure 9.5 together with the monthly net extraction (production-reinjection) data. The plot demonstrates the close relation between net mass extraction rates and variations in drawdown, as should be expected. The few data points from the early years show that fluid production during well testing resulted in a significant drawdown

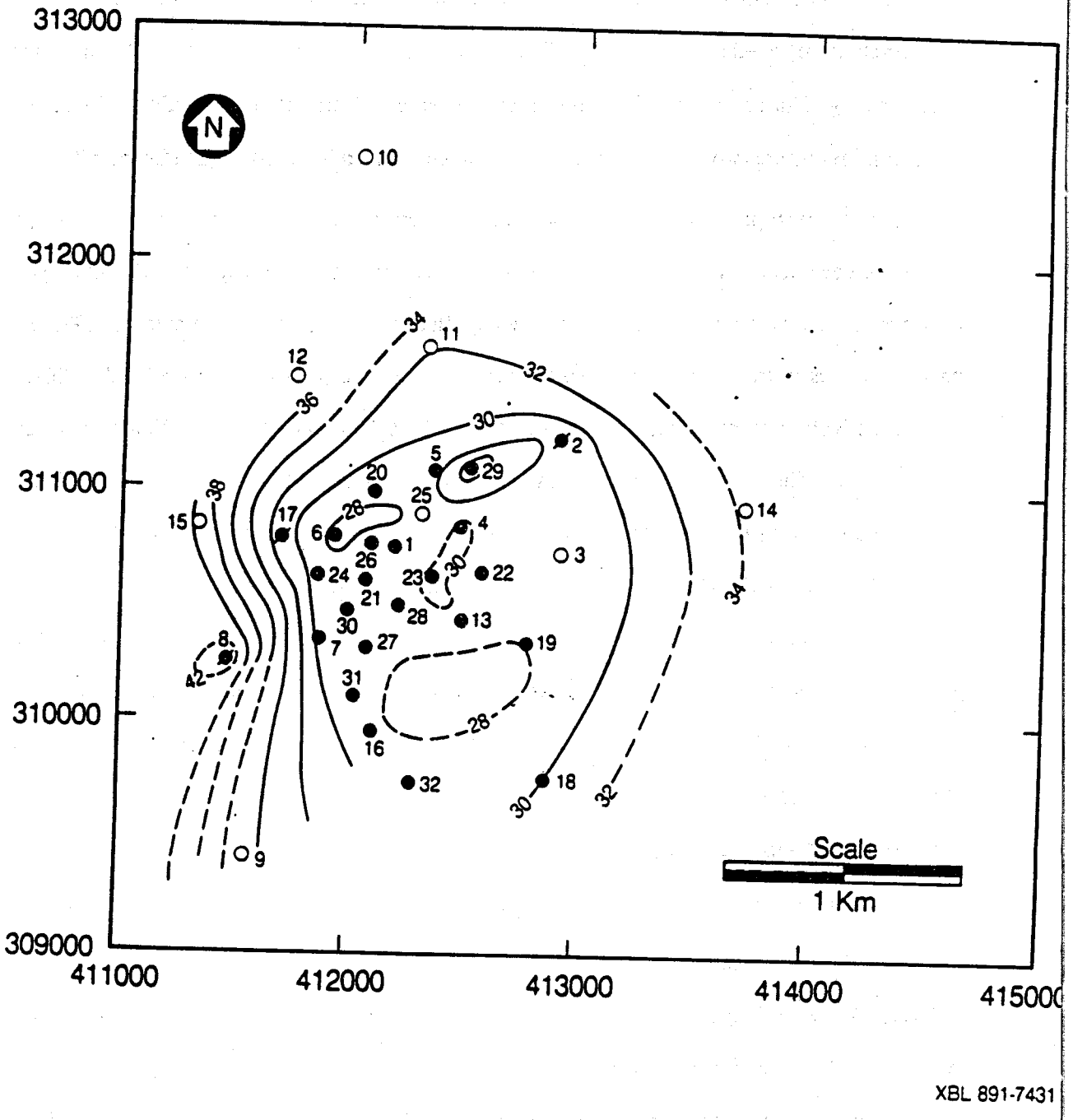

Figure 9.3. 1978 pressure contours in bar-g at 200 masl.

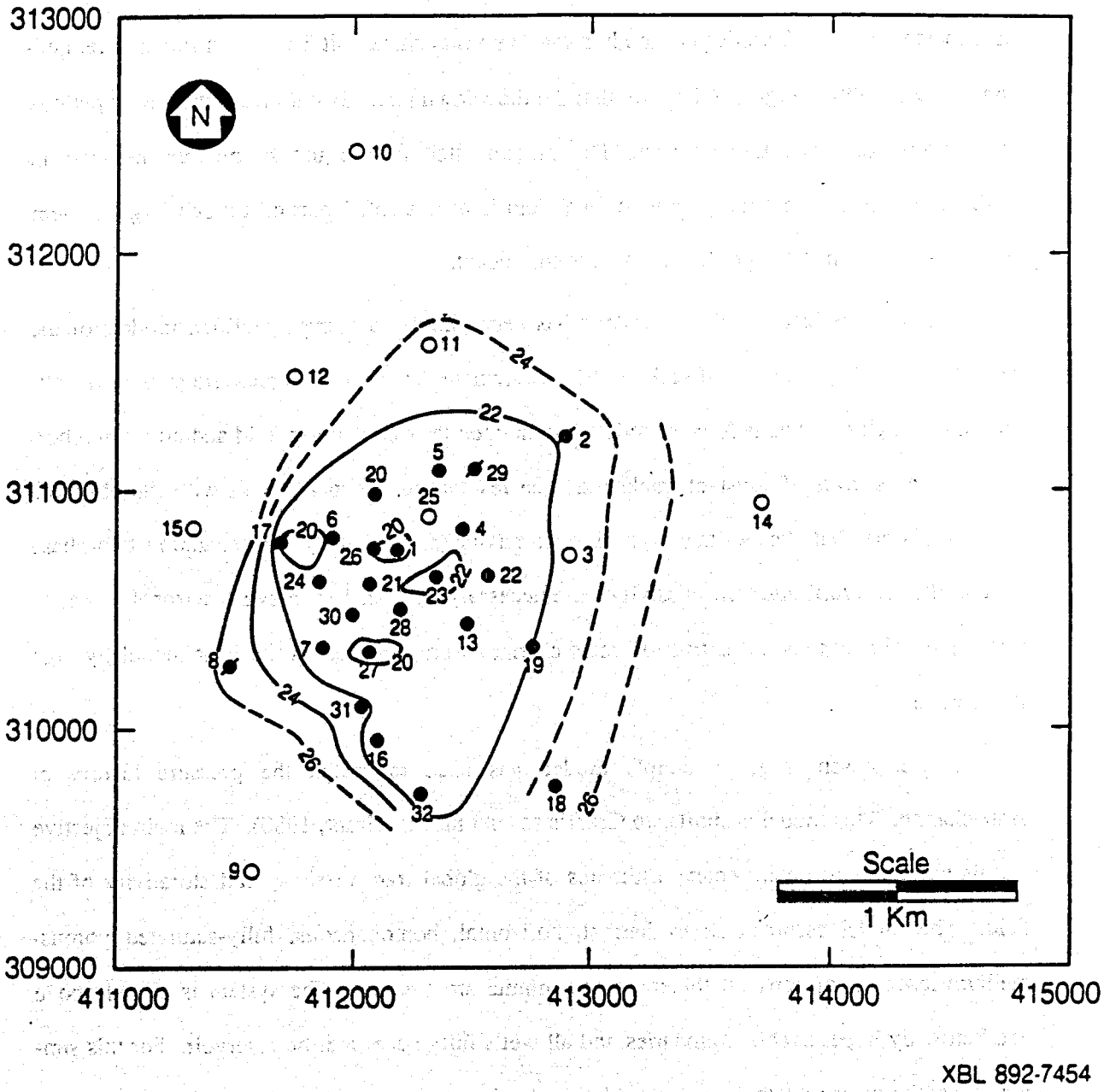

Figure 9.4. 1986 pressure contours in bar-g at 200 masl.

in 1972, but as the production testing was minimal during the next few years, the field had almost recovered to initial pressures when exploitation started in 1975.

Production from the Ahuachapán field was increased in steps during 1975-1980. With units 1 and 2 operating, the extraction rates were on the average 900-1000 ktons per month, but have increased to 1250 ktons per month in the five years since unit 3 came on-line and reinjection stopped (1982). Figure 9.5 shows that the drawdown tends to stabilize during long periods of relatively constant extraction rates. This pressure stabilization and the pressure recovery in 1973-1975 indicates that the production wellfield is only a small part of a much larger system and that recharge into the production field is significant. .

The pressure history of Ahuachapán has been simulated using simplified models of the field. Grant (1980) used two of such models to calculate the 1975-1978 pressure changes resulting from extraction. The field was modeled as an open tank containing fluid and an infinite horizontal porous layer of constant thickness. The results did not match well with the observed pressure history, but showed that both high storativity (explained by the expanding two-phase zone in the reservoir) and transmissivity were necessary in order to achieve a reasonable match. The rapid field response to extraction rates changes were matched in the tank model by high recharge rates.

In the present study a simple model was used to match the pressure history of Ahuachapán. This model is similar to Grant's second model (Grant, 1980). The main objective of this work was to obtain coarse estimates of the global transmissivity and storativity of the field. The model assumes an isothermal, horizontal, homogeneous, fully-saturated porous-medium reservoir of constant thickness and infinite areal extent. The system is closed above and below by impermeable boundaries and all wells fully penetrate the reservoir. For this simple model the pressure transients caused by production (or injection) can be calculated using the Theis solution (Theis, 1935). To analyze the Ahuachapán data we used the computer code VARFLOW (Benson 1982; McEdwards and Benson, 1981; EG&G and LBL, 1982). The program calculates at each observation point the pressure changes by superimposing the pressure

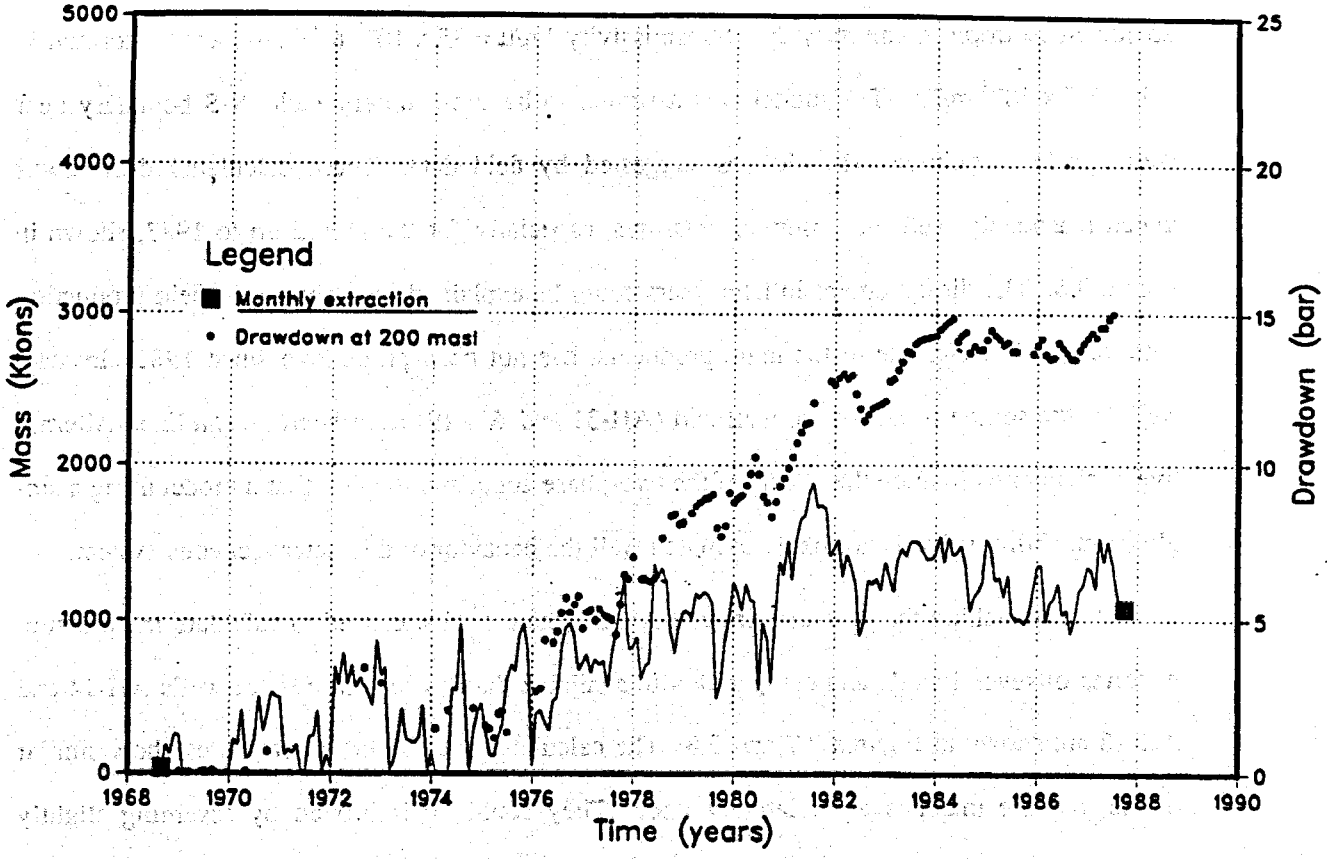

Figure 9.5. Monthly net extraction and reservoir drawdown (1968-1988).

transients (Theis solution) due to all producers/injectors. The program can handle variable flowrates and an anisotropic medium. A single linear hydrologic boundary can also be modeled. Input parameters are the coordinates and flow histories of all producers/injectors and coordinates of observations wells. In order to match the observed pressure transients, the reservoir transmissivity and storativity were varied, while the locations of the hydrologic boundaries were specified.

Figure 9.6 shows the best match obtained for the pressure history of observation well AH-25 for an isotropic medium with a transmissivity $kh/\mu = 35 \times 10^{-8}$ m^3/Pa–s, and a storativity, $\phi ch = 3.5 \times 10^{-6}$ m/Pa. The model was assumed to have an impermeable N-S boundary near well AH-15 (longitude: 411,450), as suggested by field data. These calculated drawdowns match reasonably well the observed pressures, especially for the period up to 1983, shown in Figure 9.6. The disagreement in later years could be explained by a change in field production pattern. Well AH-4, one of the main producers, has not been productive since 1982. Instead, wells in the southern part of the wellfield (AH-31 and AH-19) have been put on line. Alternative explanations include the effects of the two-phase zone, and the fact that a model using a single permeability value is not likely to match well the behavior of this heterogeneous system.

After matching the pressures in well AH-25, the model was used to calculate the pressure histories of several wells and compared with available data. The histories for wells AH-14 and AH-18 are shown in Figures 9.7 and 9.8. The calculated and observed pressures show similar trends, but the matches are relatively poor. They could be improved by assuming slightly different initial (1968) pressures for these wells instead of the uniform 36 bars over the field.

The transmissivity value obtained from matching the pressure data is high as one would expect given the well performance data. The storativity is about one order of magnitude higher than that corresponding to the compressibility of 230°C liquid water. This high storativity, can be explained by the existence of the two-phase region at the top of the reservoir, as indicated by temperature surveys and high enthalpies of some of the wells (Chapter 7).

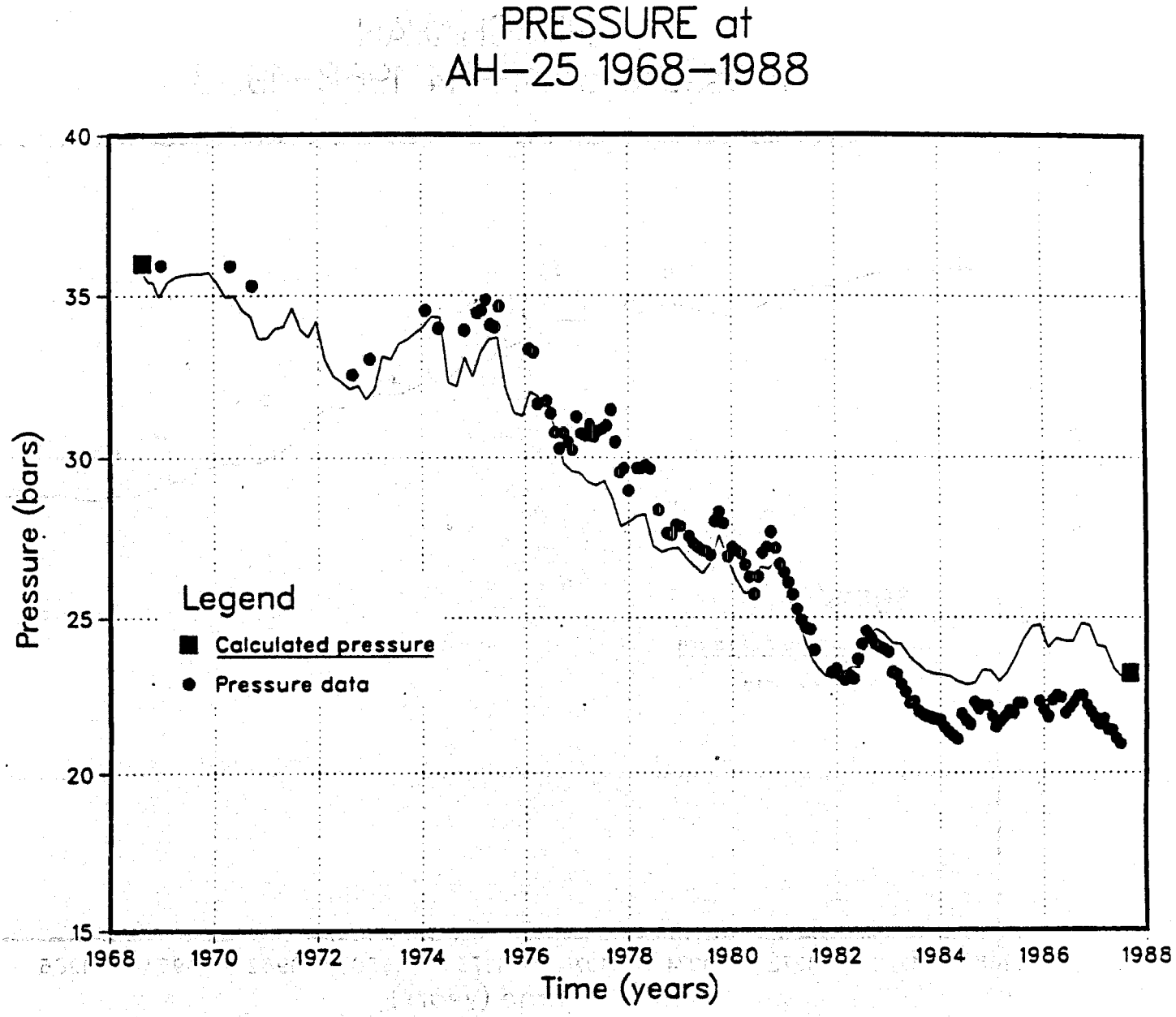

Figure 9.6. Pressure history match for well AH-25. Parameters used:
$kH/\mu = 35 \times 10^{-8}$ m^3/Pa–s, $\phi CH = 3.5 \times 10^{-6}$ m/Pa, isotropic medium with a N-S boundary.

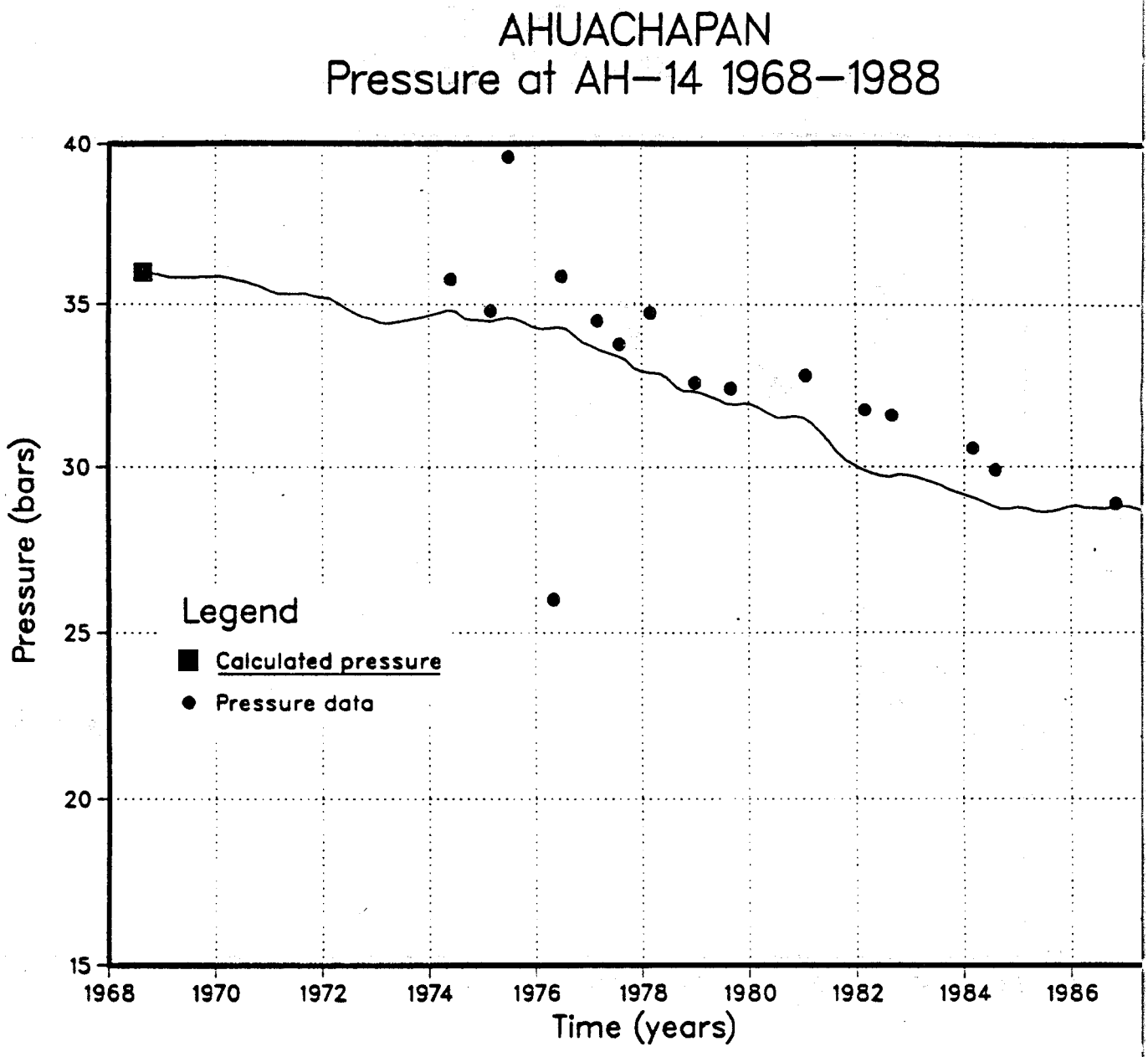

Figure 9.7. Pressure history match for well AH-14. Parameters used:
$kH/\mu = 35 \times 10^{-8}$ m^3/Pa–s, $\phi CH = 3.5 \times 10^{-6}$ m/Pa, isotropic medium with a N-S boundary.

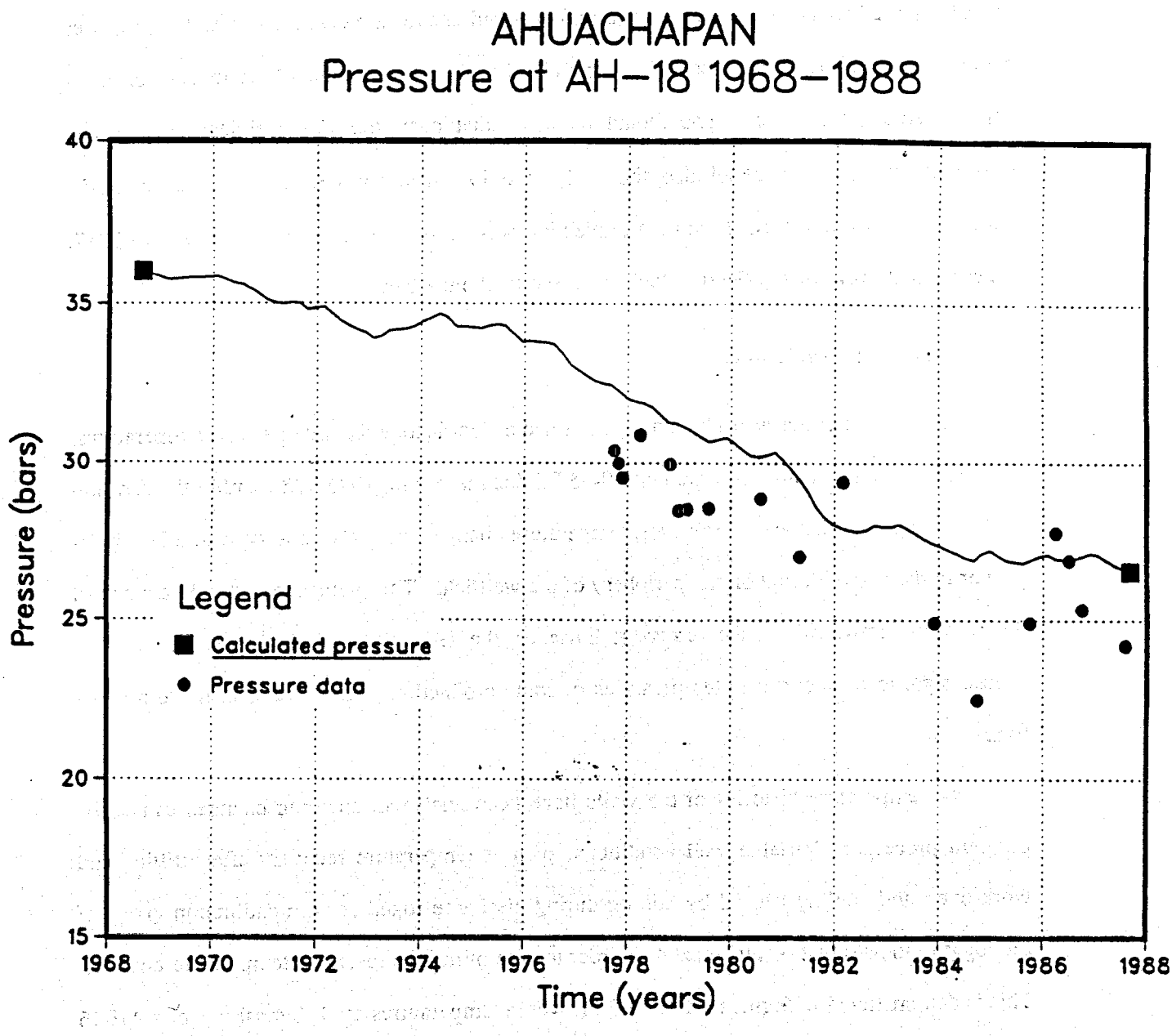

Figure 9.8. Pressure history match for well AH-18. Parameters used:
$kH/\mu = 35 \times 10^{-8}$ m^3/Pa–s, $\phi CH = 3.5 \times 10^{-6}$ m/Pa, isotropic medium with a N-S boundary.

The simple model described above can be used to estimate effects of the reinjection on Ahuachapán reservoir pressures. This is demonstrated in Figure 9.9, where the calculated values obtained from the pressure matching (described above) are compared with the pressures obtained assuming no reinjection. The figure clearly shows the benefits of reinjection for reservoir pressure maintenance. The model indicates that even the 1971 reinjection tests had significant effects. The model also shows that the 1977-1982 reinjection prevented an additional drawdown of 4 bars, at the time reinjection was halted in late 1982. By the end of 1987, the computed drawdown difference had decreased to about 1 bar.

9.3 Temperature Variations

Exploitation of the Ahuachapán field has had a significant effect on reservoir temperatures. The most dramatic change is a gradual 10-15 °C decline during 1975-1986 within the AA unit in the main production area. However, temperature changes were also observed in a few wells deeper in the reservoir and on the periphery of the wellfield. The changes are mainly a result of the pressure drawdown in the reservoir; however, the 1975-1982 reinjection seems to have caused significant declines in temperatures of some production wells located near the reinjectors.

The temperature histories of the wells have been analyzed, showing changes caused by different processes. Variable well conditions, such as temperature recovery after drilling and work-over, and cooling caused by boiling during discharge together with calibration errors of the logging tools, must be recognized in order to determine true reservoir temperature changes. This is demonstrated in Figures 9.10 and 9.11, where temperatures at -100 masl in wells AH-16 and AH-5 are plotted versus time. Neither of the temperature histories show any real changes in reservoir temperatures. Figure 9.10 shows recovery in AH-16 after work-over in 1977, and the relatively low temperature readings in 1983 and 1985 are due to flow testing of the well. The scattering of AH-5 data (Figure 9.11) is believed to be primarily due to measurement errors. For example, the abnormally high 1975-1976 temperatures measured are found in logs from all wells during this period and can only be explained as a calibration error of the Kuster gauges,

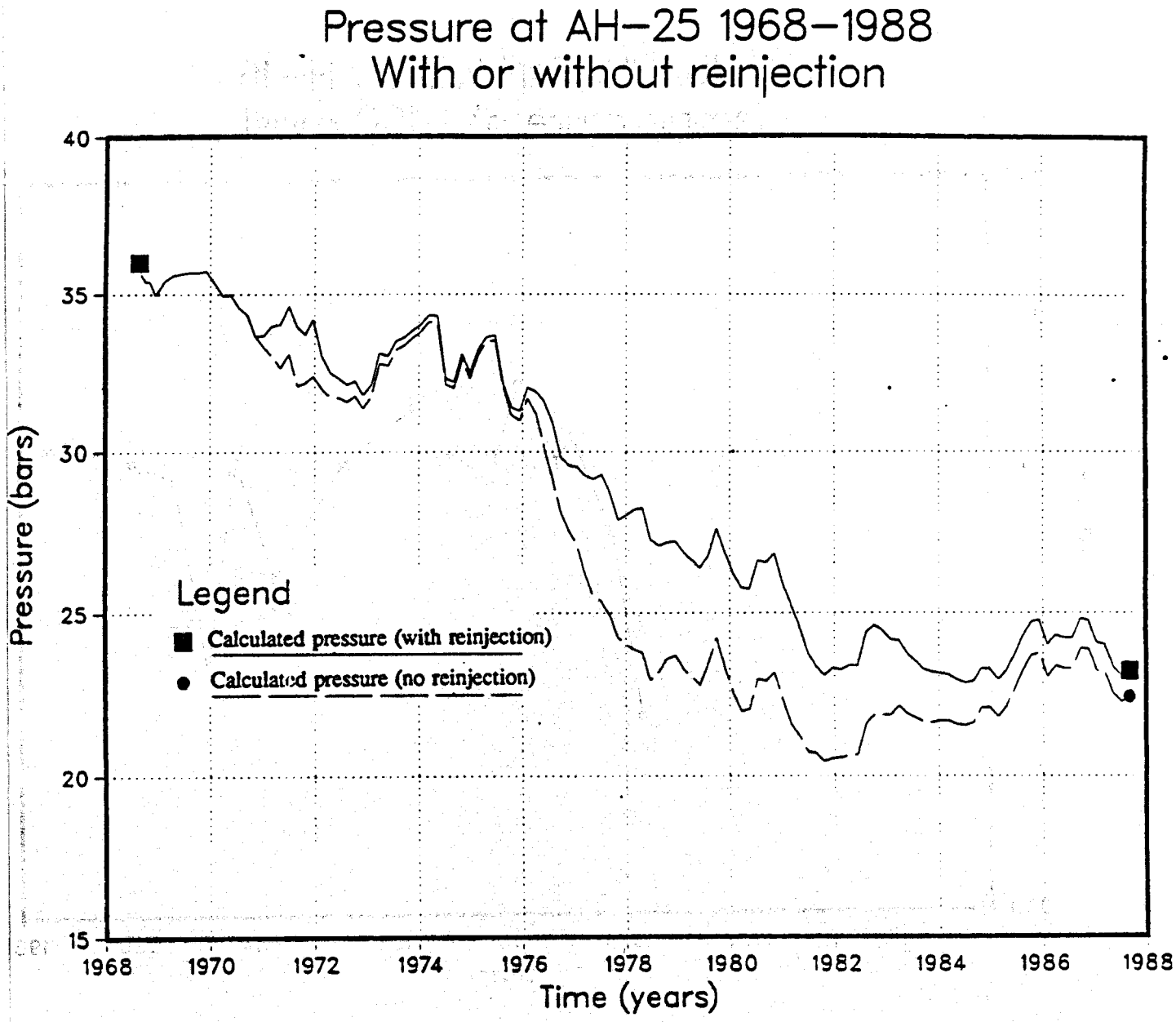

Figure 9.9. Comparison of computed pressure decline in well AH-25 with or without reinjection.

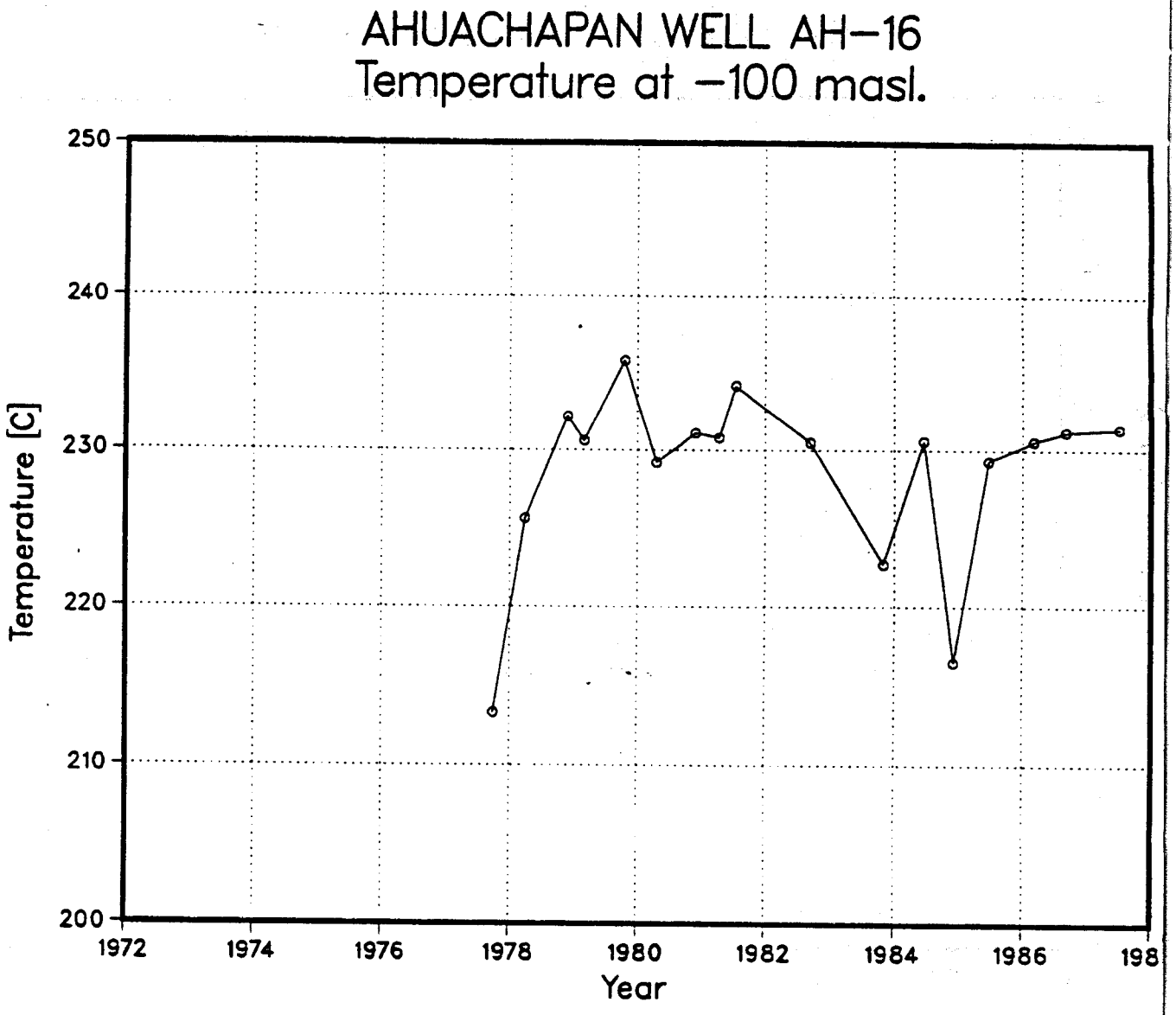

Figure 9.10. Temperature history for well AH-16 (at -100 masl).

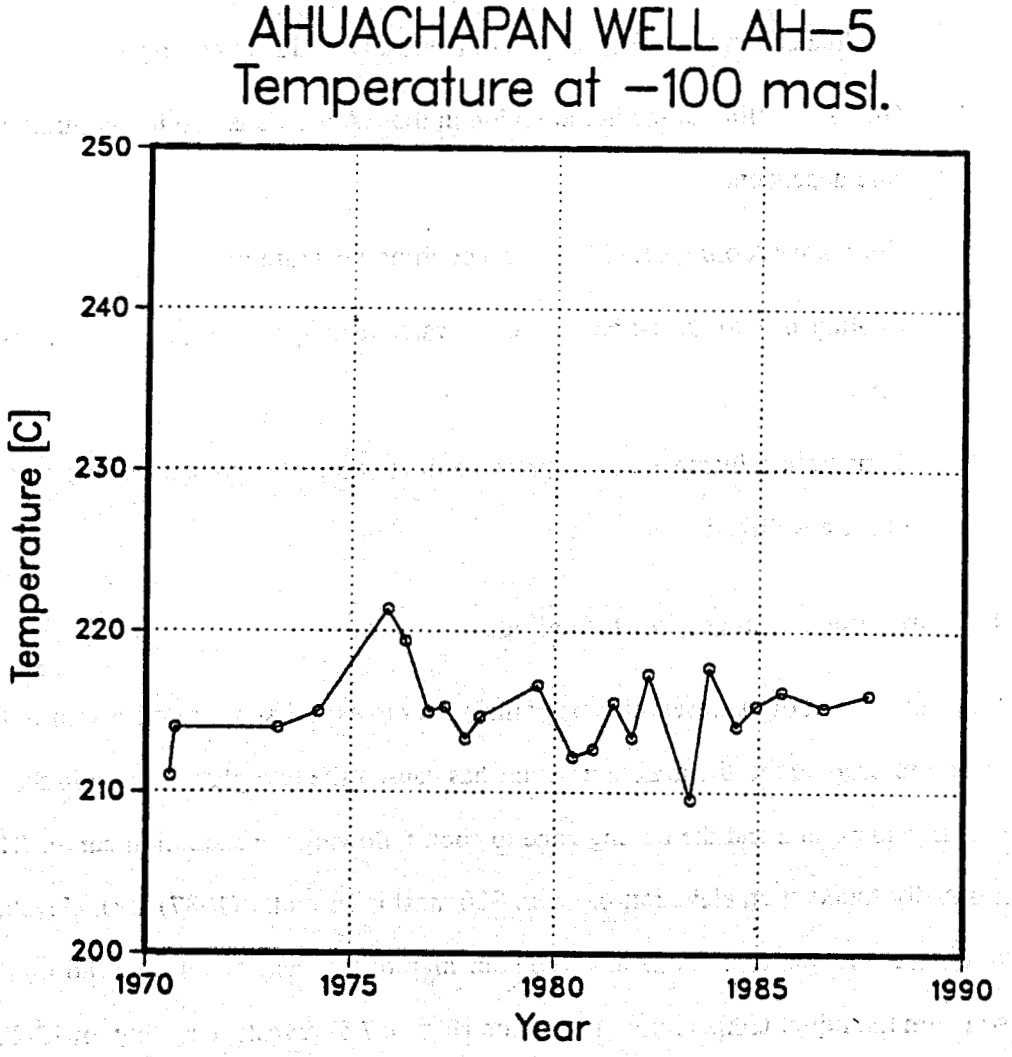

Figure 9.11. Temperature history for well AH-5 (at -100 masl).

causing about 5°C higher readings than in earlier and later logs. The inherent inaccuracy in the temperature readings are such that temperature changes on the order of a few degrees can not generally be determined from the data.

In the following discussion the observed temperature changes are discussed in terms of the different processes involved. These thermally related processes are:

1. Gradual cooling in the upper part of the reservoir due to boiling.
2. Gradual cooling of the liquid region in the AA unit; this cooling is surprisingly pressure dependent.
3. Temporary cooling caused by reinjection of the waste brine.
4. Cooling due to an increase in cold water recharge in response to reservoir drawdown.
5. Temperature increase as the pressure drop stimulates greater recharge of hot fluids into the wellfield.

9.3.1 Temperature Changes Due to Boiling

The upper part of the reservoir was boiling prior to exploitation, as discussed in Chapter 7. The pressure drop due to the mass extraction has caused the two-phase region in the main production area to expand and the boiling zone to cool, following the saturation curve. The boiling level initially found at an elevation of about 300 masl is currently (1987) at an elevation of 250 masl. Figure 9.12 shows a temperature contour map of the field based on 1986 logs. A comparison with the initial temperature distribution (Figure 7.6) reveals a cooling of 15-20°C in the production field during this period. It can be easily demonstrated that this cooling is because of boiling by either comparing the temperature and the pressure distributions at different times, or by plotting for each well the temperature and the pressure in the two-phase region at different times and comparing them with the saturation values. Examples of such plots are shown on Figures 9.13 and 9.14 (wells AH-1 and AH-5).

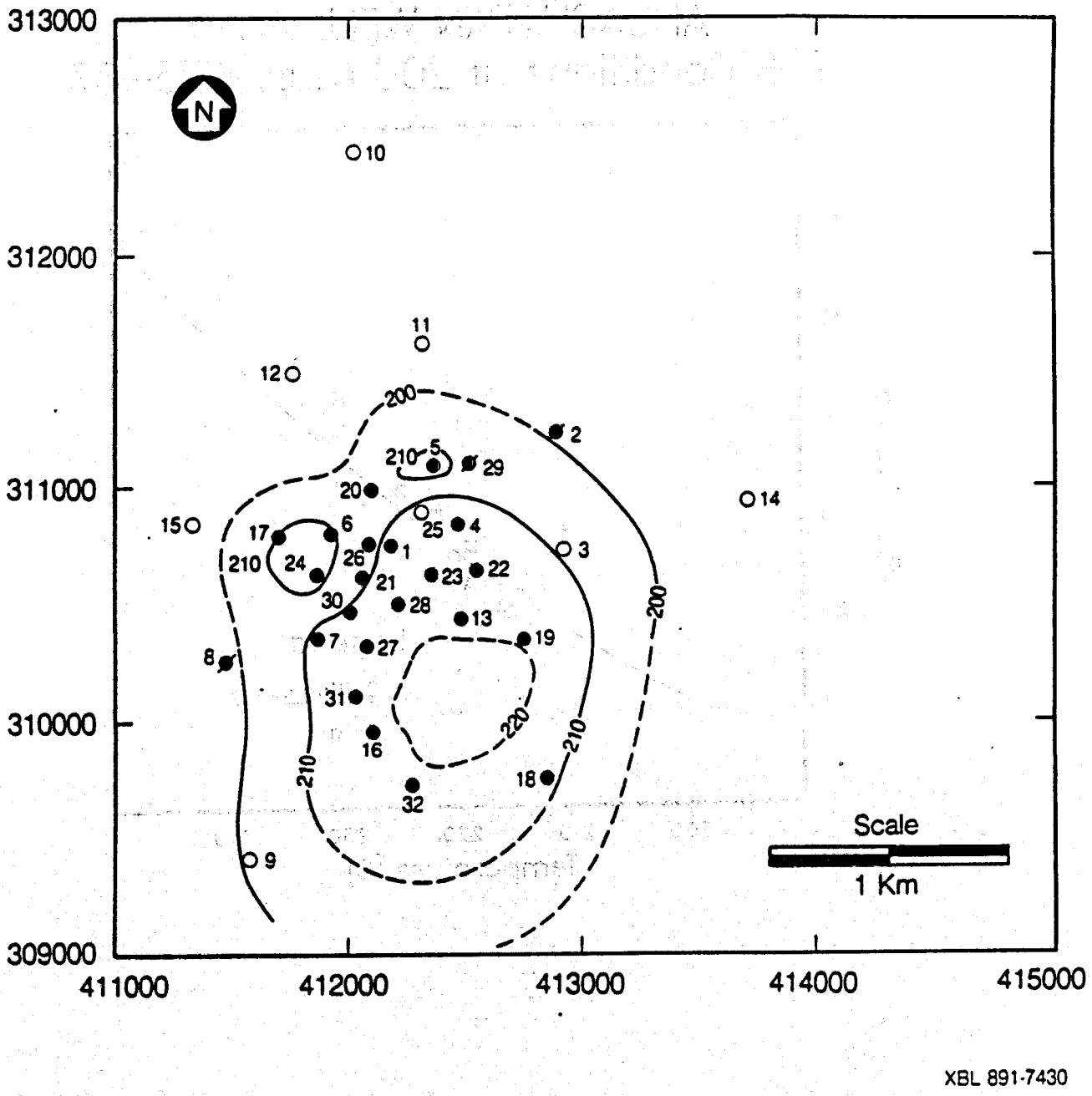

Figure 9.12. 1986 temperature contours (in °C) at 300 masl.

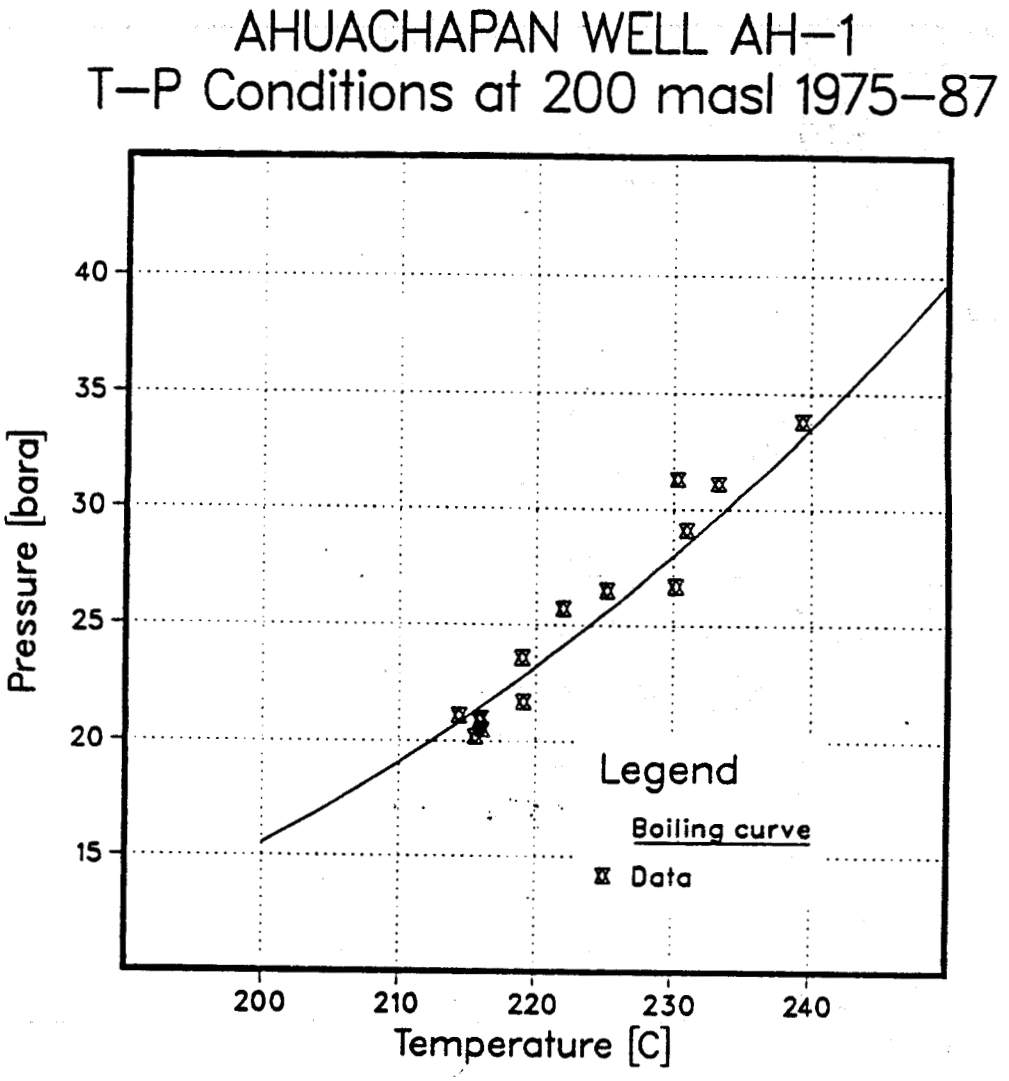

Figure 9.13. Plot of temperature vs. pressure for AH-1 (1975-1987).

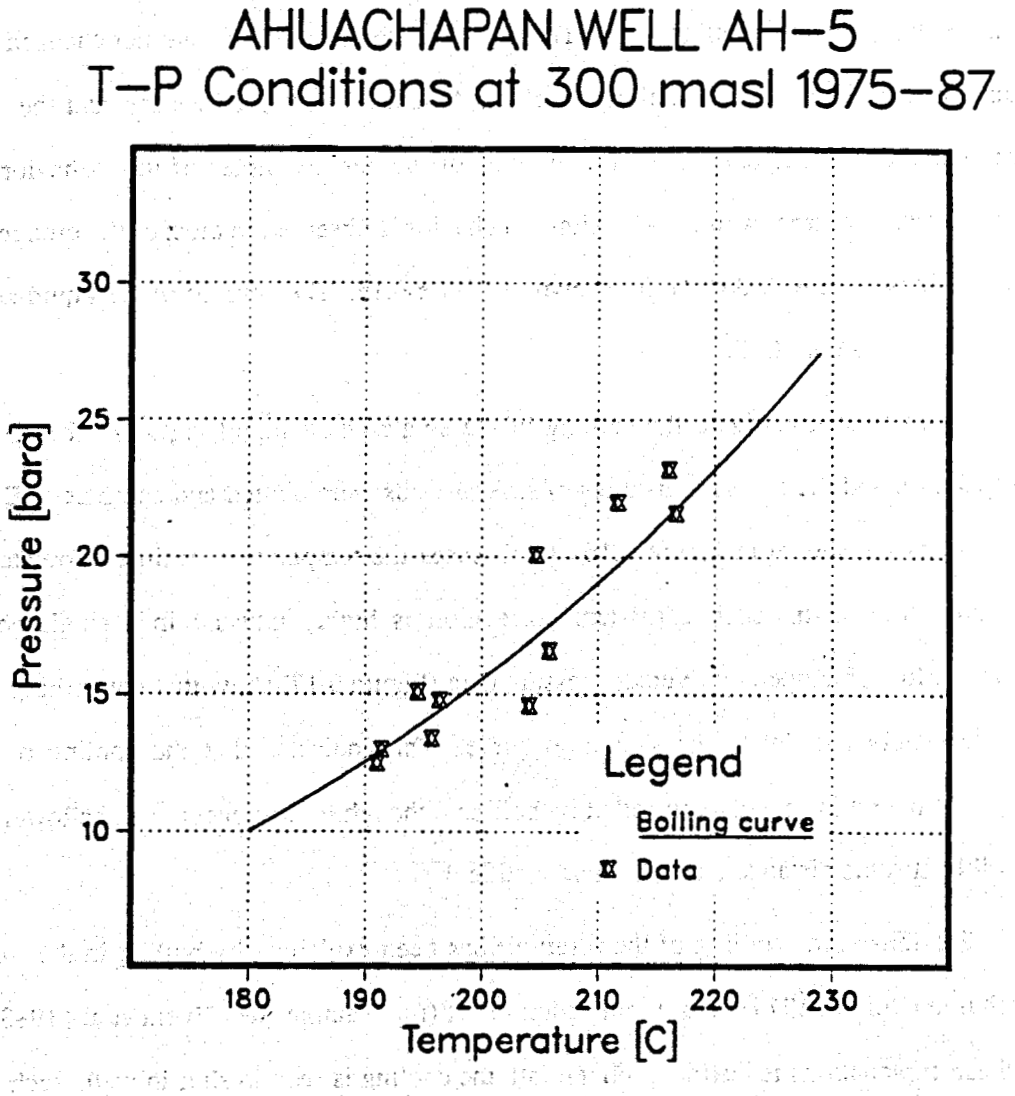

Figure 9.14. Plot of temperature vs. pressure for AH-5 (1975-1987).

9.3.2 Temperature Changes in Liquid Portion of the Geothermal Reservoir

The two-phase region resides in the upper portion of the AA unit. The underlying liquid-dominated zone in the andesites also shows a considerable cooling during the exploitation years, except in the southwest corner of the wellfield (around AH-7 and AH-31). Early temperature logs show boiling-point-to-depth curves through the two-phase region and a fairly isothermal interval below the boiling level. These general characteristics have not changed in the production field. However, the boiling level has fallen, as mentioned earlier, and the liquid zone has decreased in temperature with time. One of the best examples of this behavior is seen in temperature logs from well AH-21; similar behavior is observed in most of the production wells. Several logs from well AH-21 are shown in Figure 9.15. The cooling in the liquid zone during 1977-1986 is about 10°C.

In order to investigate the cooling of the single-phase liquid region of the reservoir, the temperature and the pressure histories of several wells were plotted and compared. Examples of these plots are shown in Figure 9.16. In all cases the temperature decline correlates with the pressure drawdown. Such consistent correlation is highly unusual in a single-phase liquid region. Plots of temperature versus pressure data (Figure 9.17) show that the cooling progresses approximately parallel to the saturation curve. This indicates that the cooling of the liquid reservoir region is actually controlled by boiling although it must occur at a shallower depth and possibly at some distance from the main wellfield.

Previously, the cooling of the reservoir has been explained by boiling in the wells during discharge (Bolton, 1979) or as a reinjection effect (for example, see Rivera et al., 1983). Neither of these explanations is justified. First of all, the cooling is seen in shut-in wells such as AH-25. In addition, in some of the producers where flowing surveys are available, the boiling level during discharge is found above the isothermal section in the well (e.g., AH-1). If, on the other hand, reinjection was responsible for the cooling, one would expect it to be most pronounced in wells located closest to the injectors, and thermal recovery would have been observed after reinjection was stopped in 1982.

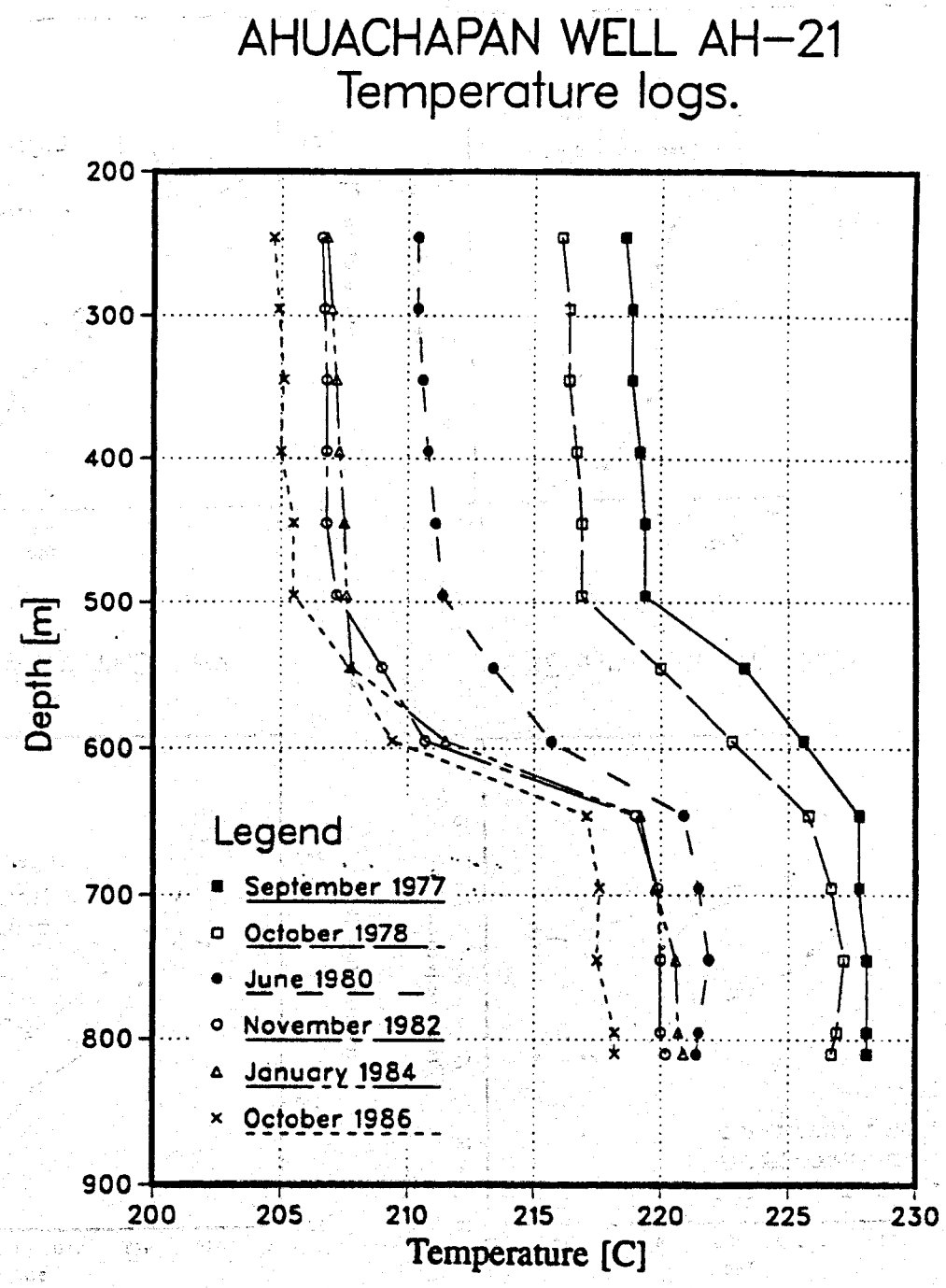

Figure 9.15. Selected temperature logs for well AH-21.

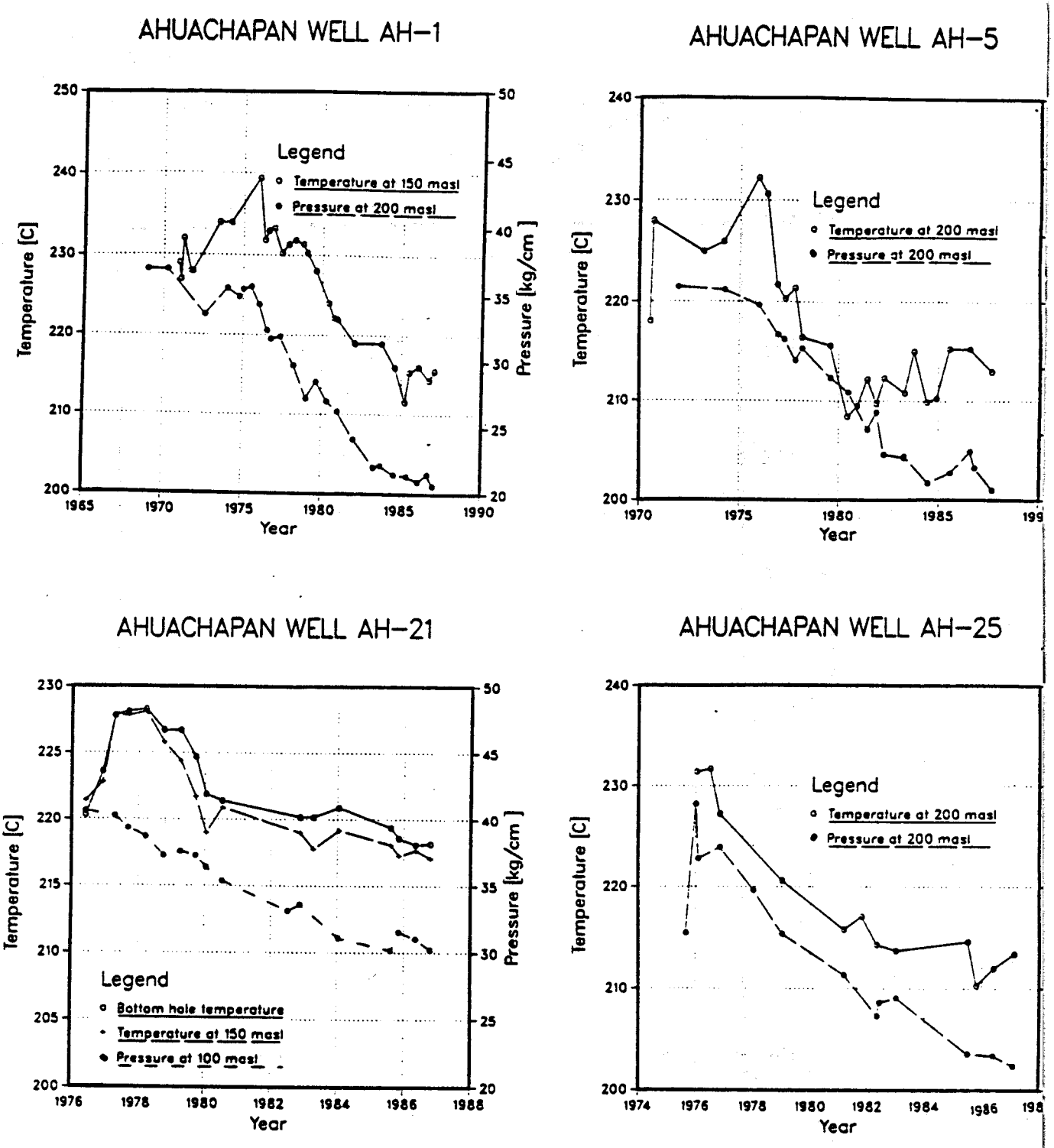

Figure 9.16. Temperature and pressure histories for several Ahuachapán wells.

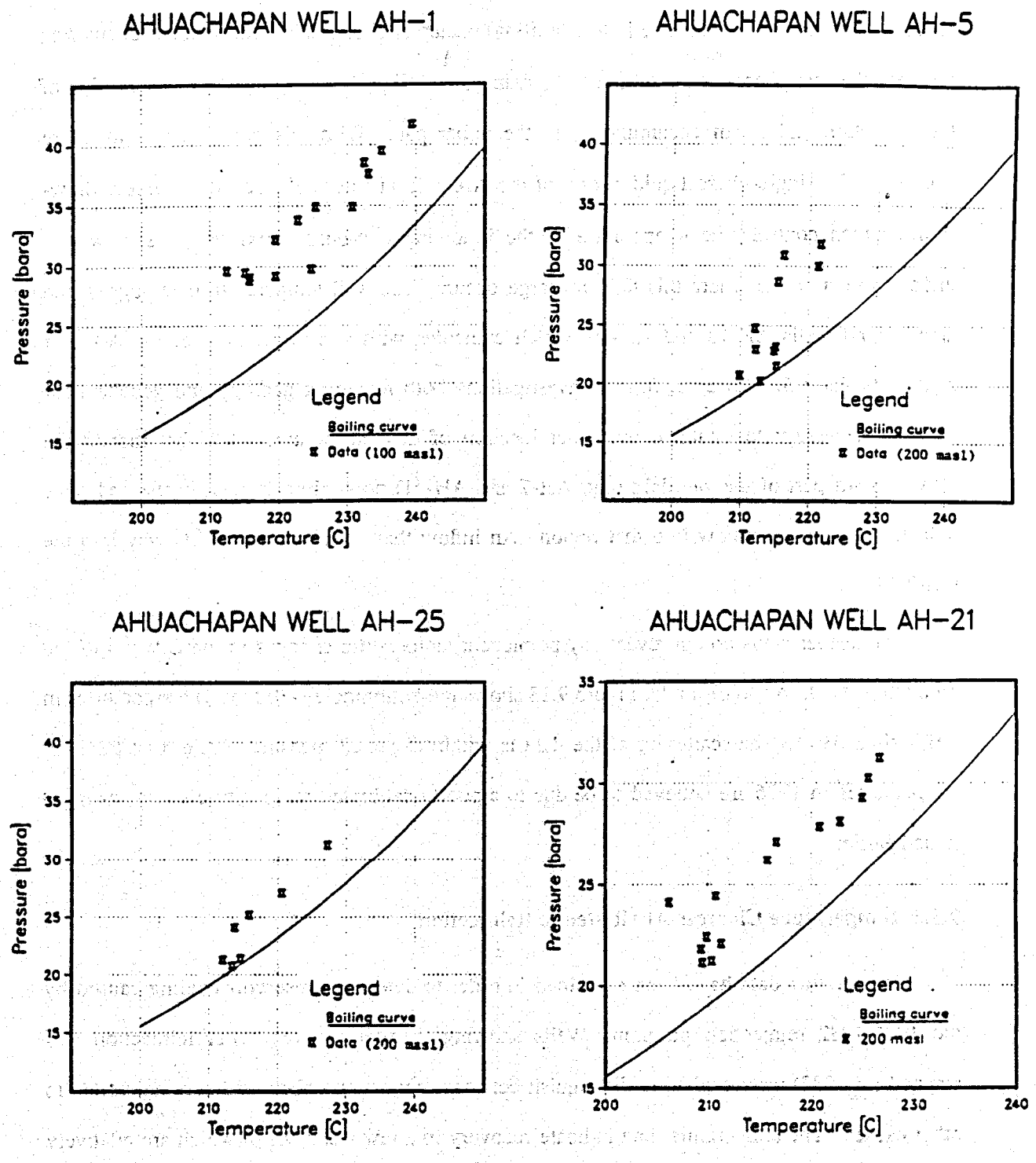

Figure 9.17. Temperature vs. pressure plots for several Ahuachapán wells.

The explanation offered here is that the geothermal reservoir is recharged by a two-phase mixture of water and steam. The inflow (boiling) occurs at or above 200 masl, but after entering the field the two phases separate due to bouyancy, with liquid occupying the lower portion of the formation and steam accumulating in the upper part. With this model the temperature decline in the single-phase liquid region of the AA unit will depend upon the pressure draw-down, which controls the temperature of the inflowing two-phase mixture. It is, however, difficult to determine where this fluid recharge occurs. The well temperature data suggest the area around wells AH-13 and AH-19, which coincides with a regional high of the AA unit caused by Fault 5. However, further investigations both regarding geology and geochemical data are necessary to establish the exact location of this inflow area. The fact that in the southwestern part of the wellfield (e.g. AH-7 and AH-31) no cooling is seen in the andesites indicates a separate inflow into that region. An inflow that does not boil on its way into the wellfield.

The deeper wells do not reveal any permanent temperature changes in the OA unit of the production field. As an example, Figure 9.18 shows the bottomhole (-300 masl) temperatures in AH-1 since 1971. The scattering of the data is within expected measurement errors; the high temperatures in 1976 are believed to be due to a poorly calibrated temperature gauge, as mentioned earlier.

9.3.3 Temperature Changes Attributed to Reinjection

Temperature data have been examined in order to determine reservoir cooling caused by the 1975-1982 reinjection program. Wells showing thermal recovery after reinjection was stopped (in 1982) were studied to distinguish between reinjection effects and cooling related to other causes. The temperature data indicate recovery in a few wells, all of which are relatively close to an injector. The cooling around injection well AH-8 is the most pronounced; some reinjection-related cooling was also observed in the vicinity of AH-29, another injector.

Figure 9.19 shows the temperature data at 100 masl for well AH-7, which is located near

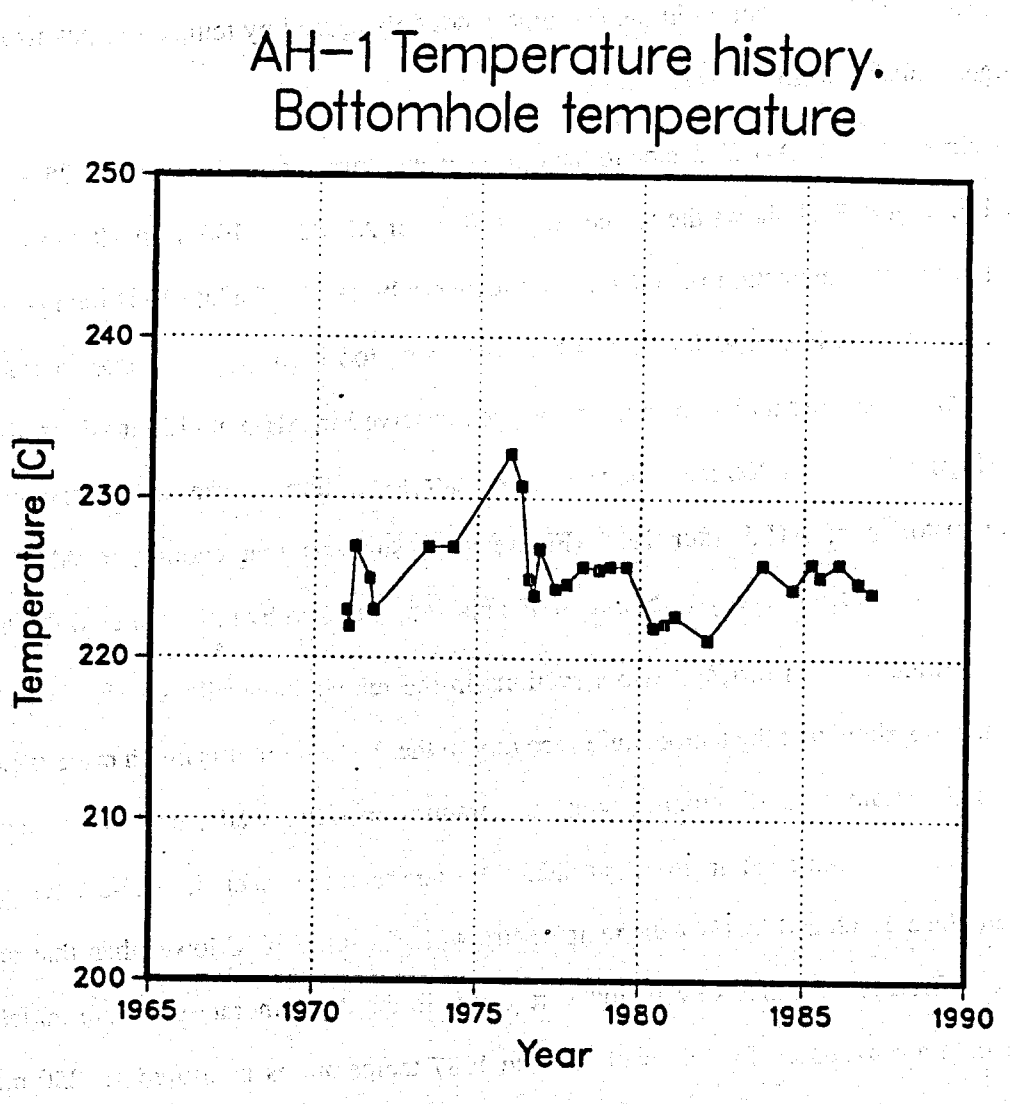

Figure 9.18. Bottomhole (-300 masl) masl temperature history for AH-1.

AH-8. It shows gradual cooling during the reinjection period (1975-1982) and a rapid recovery after 1982. The cooling which occurred up to 1982 was on the order of 15-20°C. By late 1987, the temperature had almost fully recovered. Similar cooling is seen deeper (-100 masl) in AH-7 (Figure 9.20), but the recovery is much slower and far from complete. This might indicate that around well AH-7, the cooling in the OA unit is not only caused by reinjection but also by cold recharge, probably from the west.

Reinjection into AH-29 seems to have influenced temperatures in well AH-25 and possibly AH-5. Figure 9.21 shows the temperature history of AH-25 at -100 masl. It shows 5-10°C cooling during the reinjection period and total recovery by 1987. The late 1981 data point is not consistent with this interpretation and is believed to be too high, probably due to calibration problems of the logging tool. No cooling has been observed in AH-5 at -100 masl, as discussed earlier (Figure 9.11). At 200 masl, however, the poor correlation between the temperature and pressure histories of AH-5 after 1982 (Figure 9.16) suggests that cooling in AH-5 during 1975-1982 was caused not only by boiling in the reservoir but also by inflow of cold fluids.

The temperature histories at two elevations in the reinjection wells are shown in Figure 9.22. The plots show that the temperature recovery in the Andesite unit is much more rapid than in the Agglomerate unit. Compared with temperatures in other wells, in 1987 a near total recovery had been achieved in the Andesite. The temperatures deep in AH-2 have slowly recovered since 1982, and in 1987 the temperature was still some 20°C lower than that prior to reinjection. Well AH-29 shows even slower recovery in the Agglomerate unit. No initial temperature data are available for this well, but the 1987 temperatures measured at -250 masl in AH-29 were more than 30°C lower than those at similar depth in other deep wells. The slow thermal recovery deep in wells AH-2 and AH-29 suggests that the agglomerates in northeast part of the the wellfield have been permanently cooled by cold recharge from the area north of the field and the low temperatures deep in AH-29 suggest that the recharge channel passes close to that well. Well AH-8 does not penetrate the agglomerates, but in the southwest part of the field a permanent cooling has been observed in that unit, as discussed earlier (Figure 9.20).

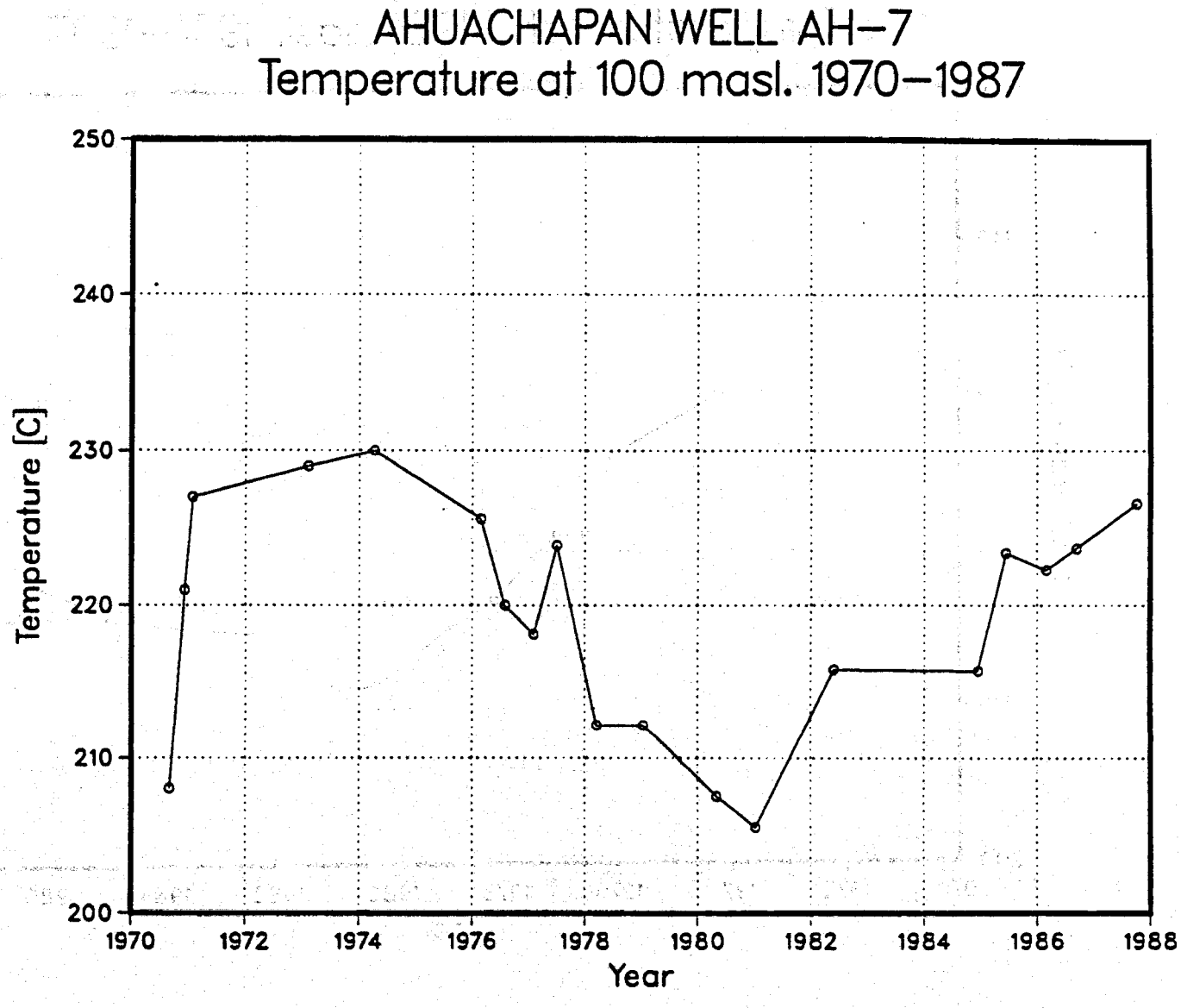

Figure 9.19. 1970-87 temperature history for AH-7 (100 masl).

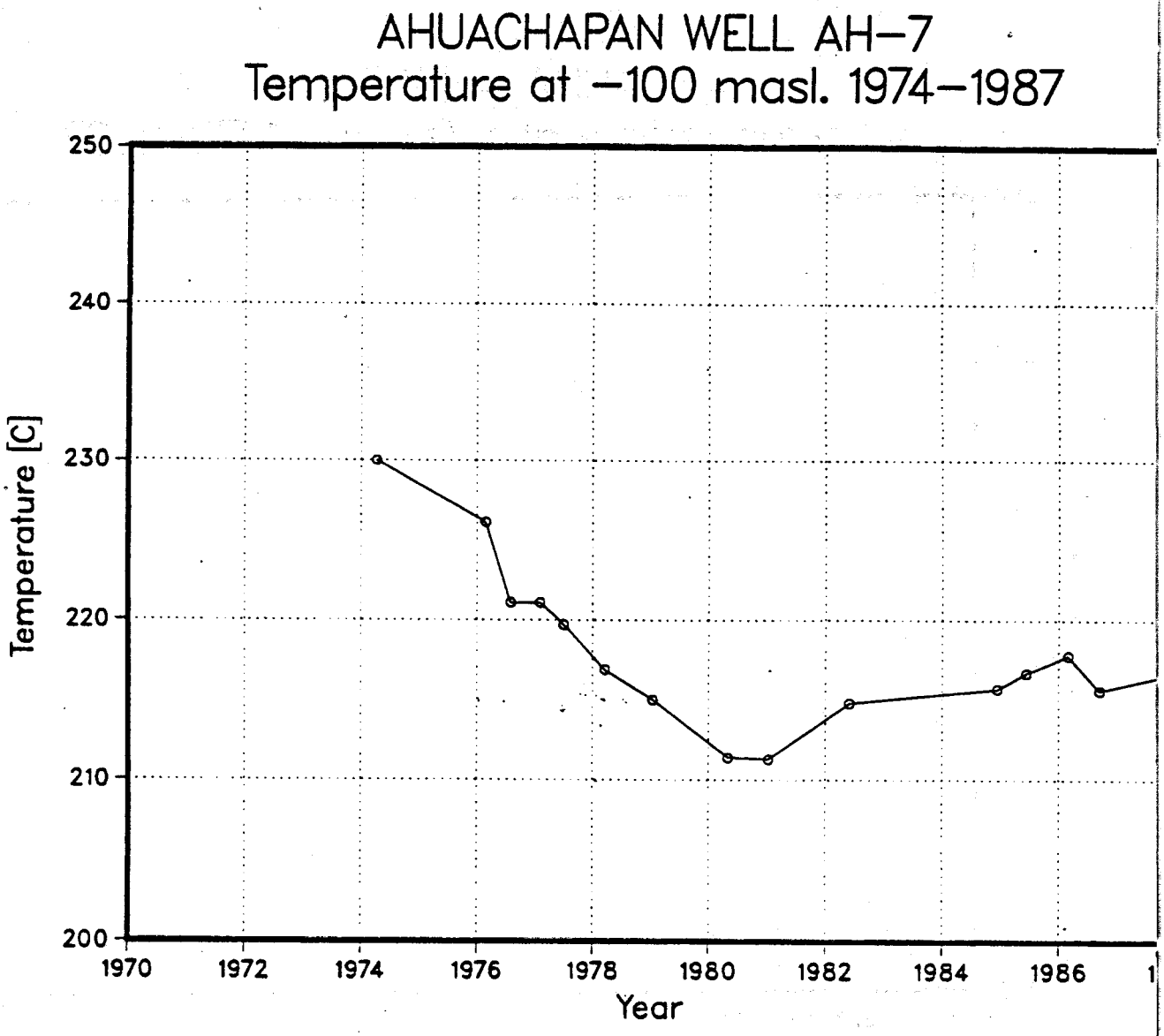

Figure 9.20. 1974-87 temperature history for AH-7 (-100 masl).

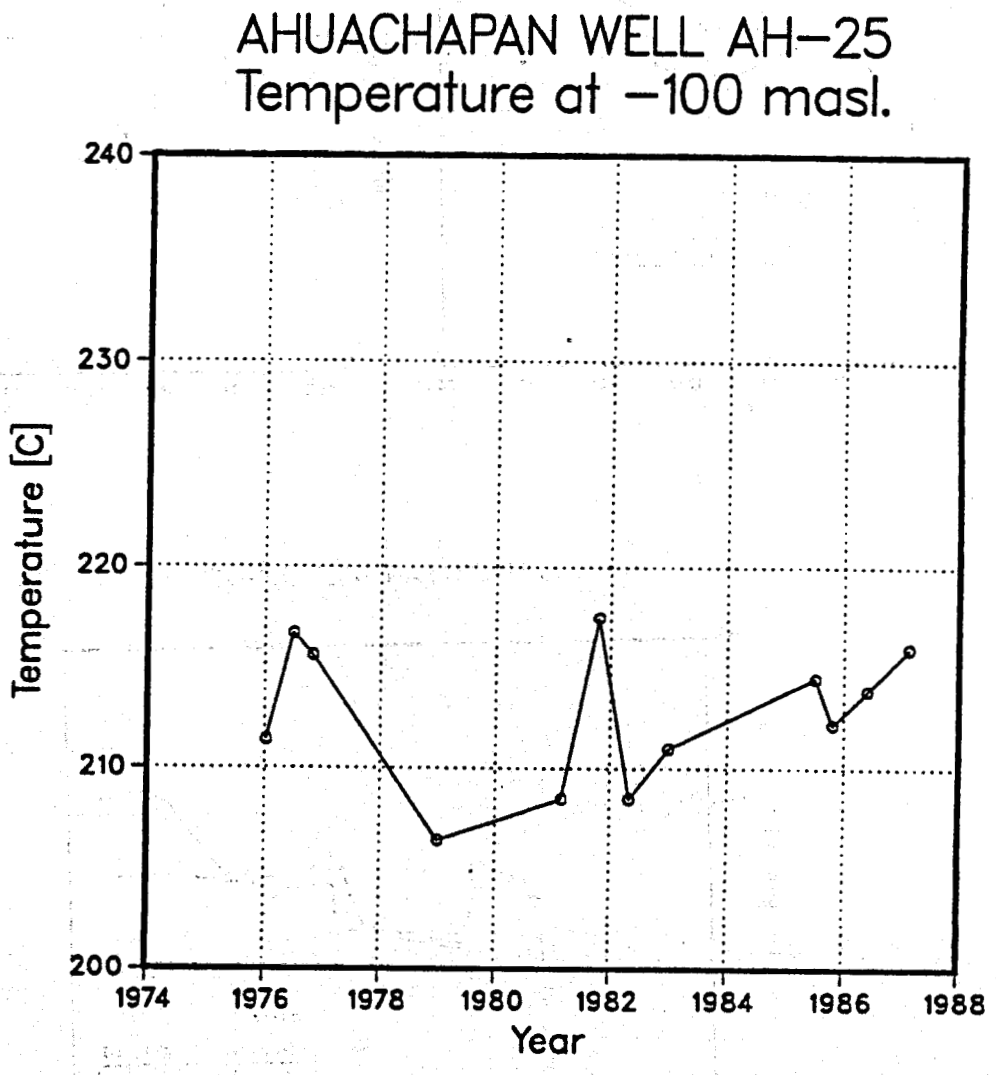

Figure 9.21. AH-25 temperature history (-100 masl).

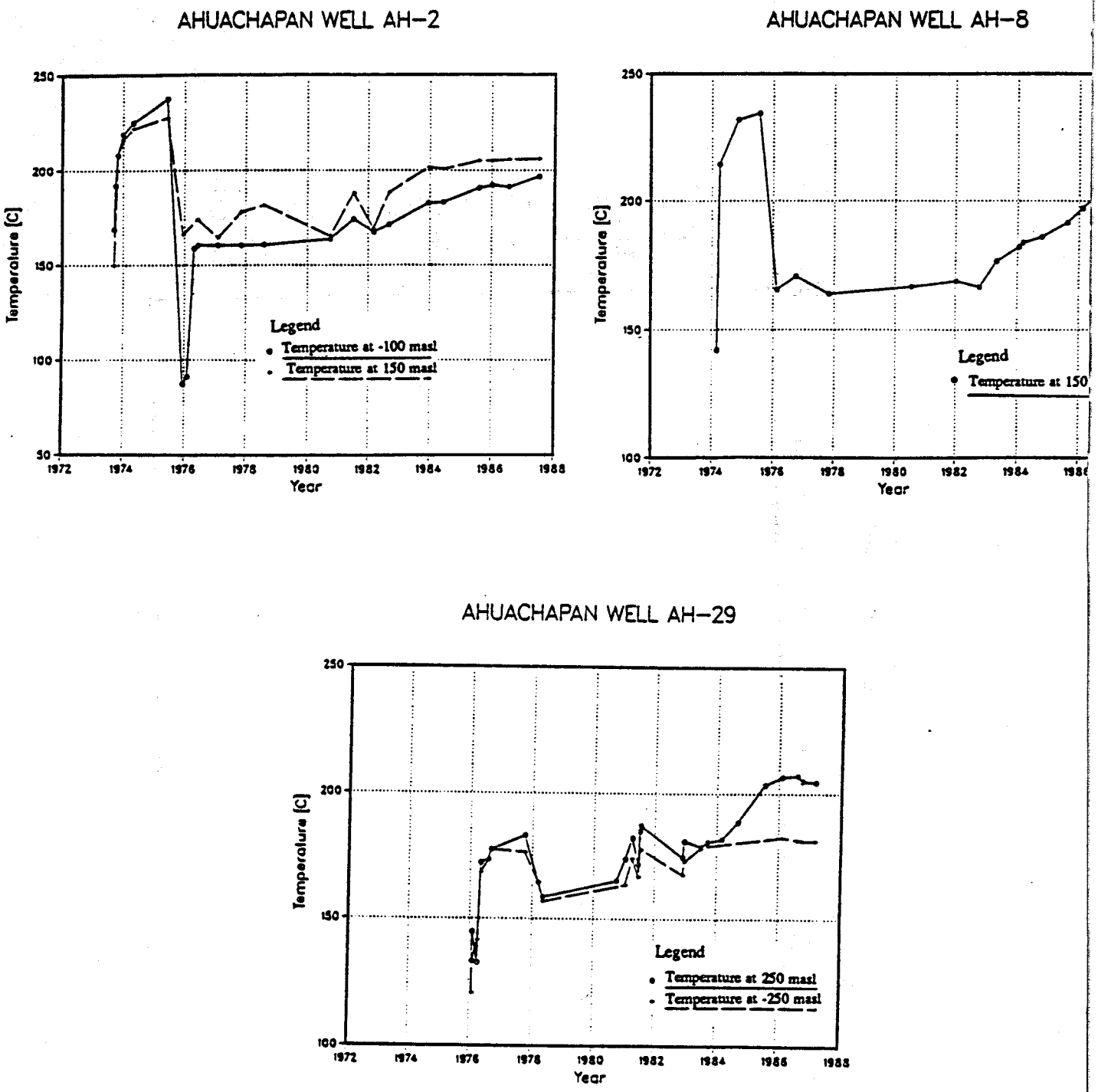

Figure 9.22. Temperature histories for different reinjection wells.

9.3.4 Temperature Changes Due to Natural Recharge

Cold water recharge into the Ahuachapán wellfield from the north and west can not be supported by temperature data from wells outside the production field. Temperature histories are not available for AH-10, AH-11, AH-12 and AH-15 because of obstructions in the wells at shallow depth shortly after drilling.

On the eastern margin of the wellfield no temperature changes have been observed, as shown by the AH-14 temperature logs (Figure 9.23). In the southern part most wells show constant reservoir temperatures since exploitation started (Figures 9.24-9.26), except for well AH-18 in the southeast corner of the wellfield. Figure 9.27 shows the temperature data at -75 masl in well AH-18. The early data show heating of the well after drilling in 1977 and the low readings in 1985 coincide with flow testing of the well (boiling). The interesting feature of the temperature history of well AH-18 is the gradual increase in temperature since 1978. The total temperature rise is about 10 °C, reaching 245°C in 1987, the highest reservoir temperature measured in Ahuachapán.

The temperature distribution in Ahuachapán indicates that the geothermal fluid recharges the wellfield from the southeast, close to well AH-18. The increasing temperatures in this well during exploitation support this interpretation and indicate that the recharge rate has increased due to the pressure decline in the production area.

9.3.5 Summary

The temperature history of Ahuachapán is complicated and has been influenced by several factors. The above discussion has focused mainly on the major temperature variations in the field during the last fifteen years. A more thorough analysis of the data should, however, be carried out and it is especially important to compare in detail the temperature history of the field and the changes seen in the chemistry of the produced fluids.

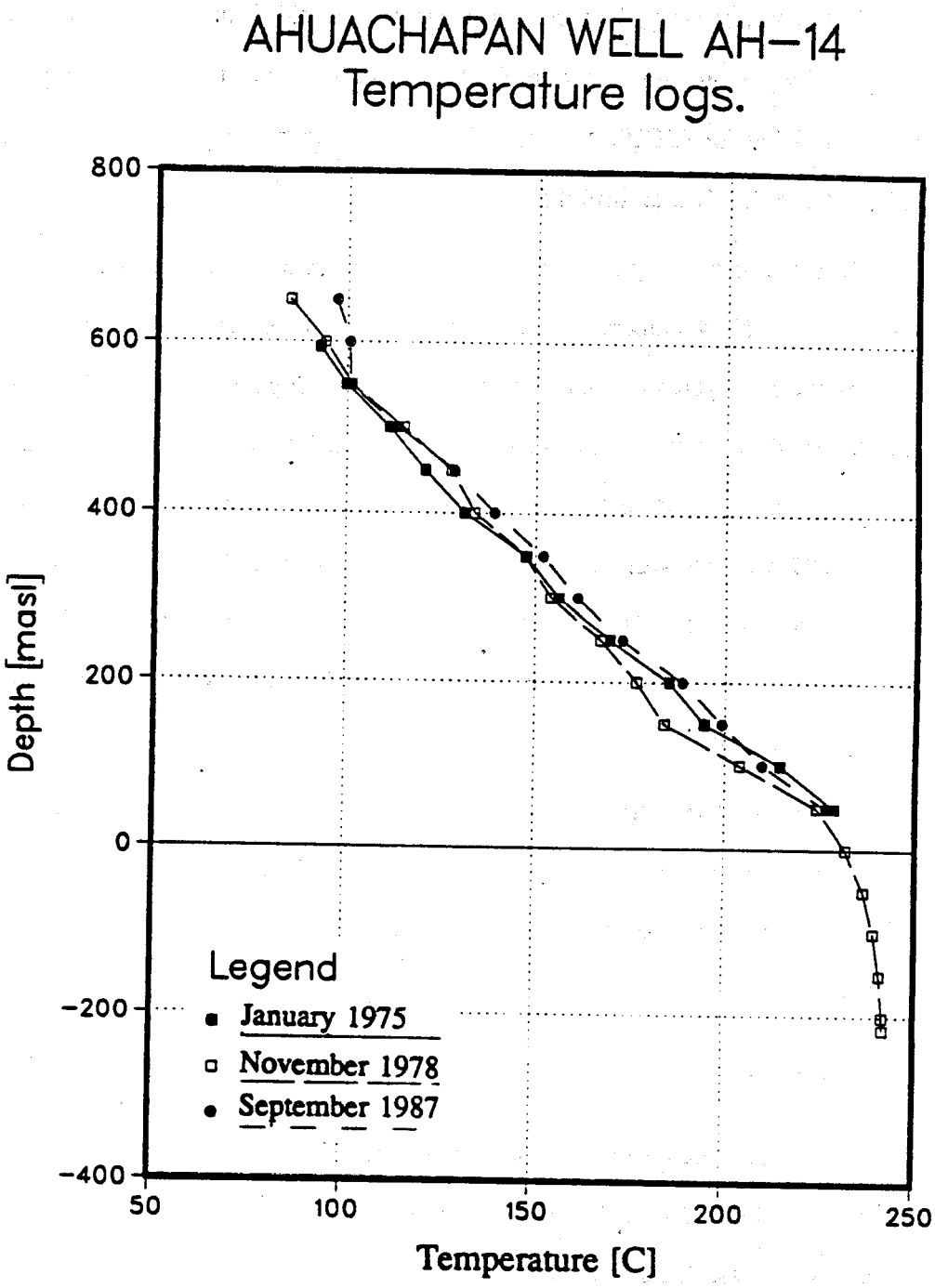

Figure 9.23. AH-14 temperature logs.

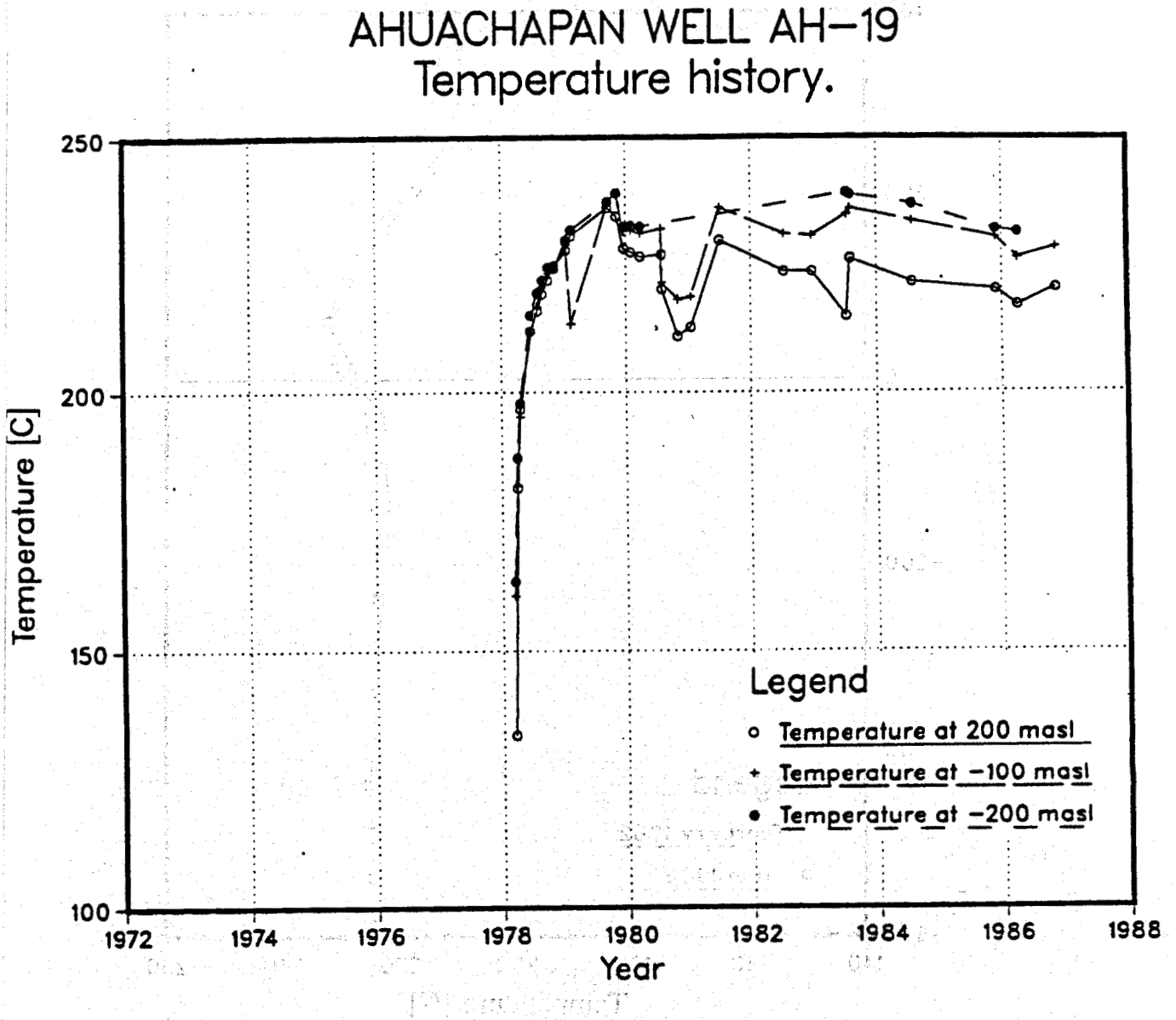

Figure 9.24. AH-19 temperature history.

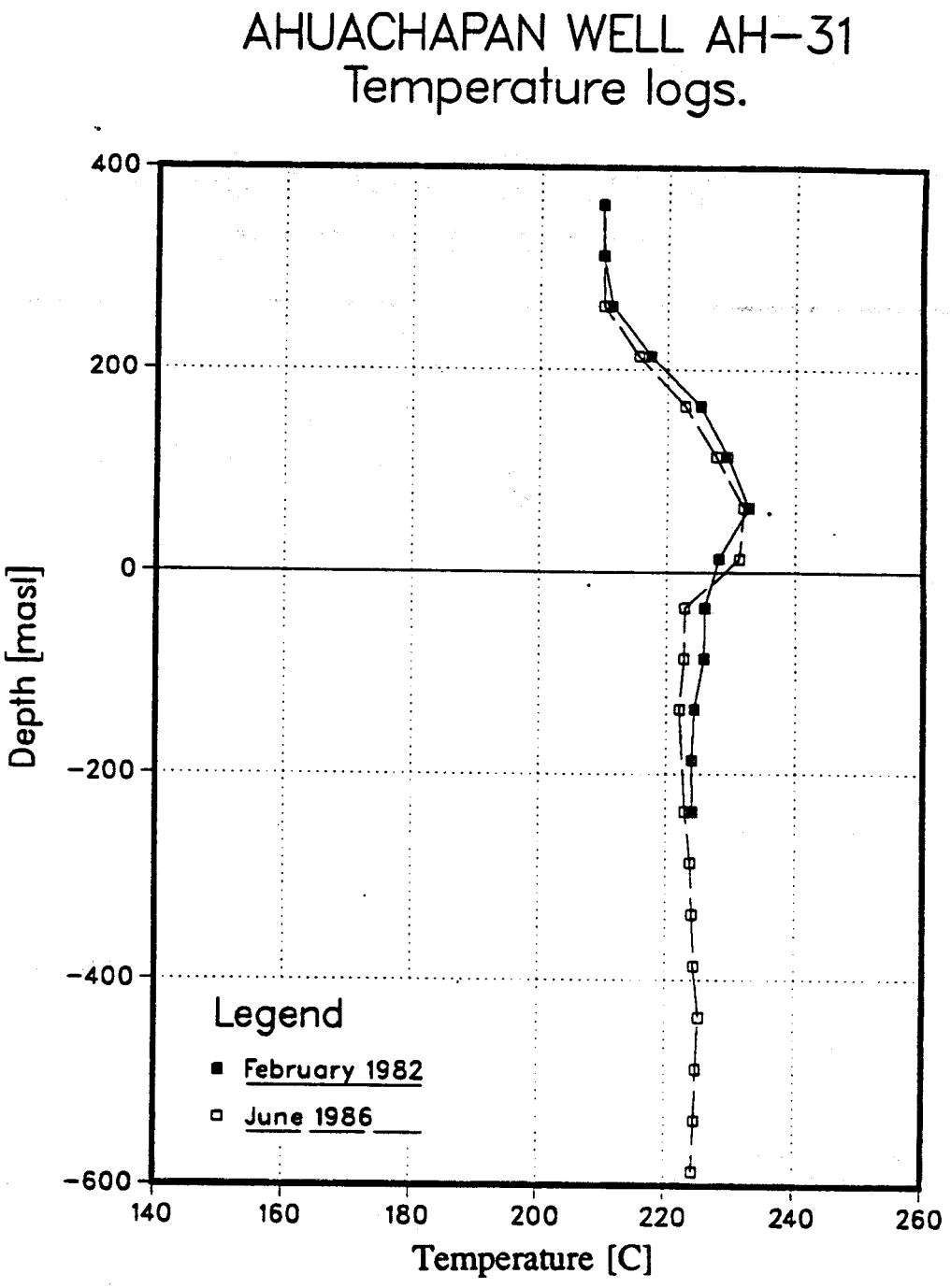

Figure 9.25. AH-31 temperature logs.

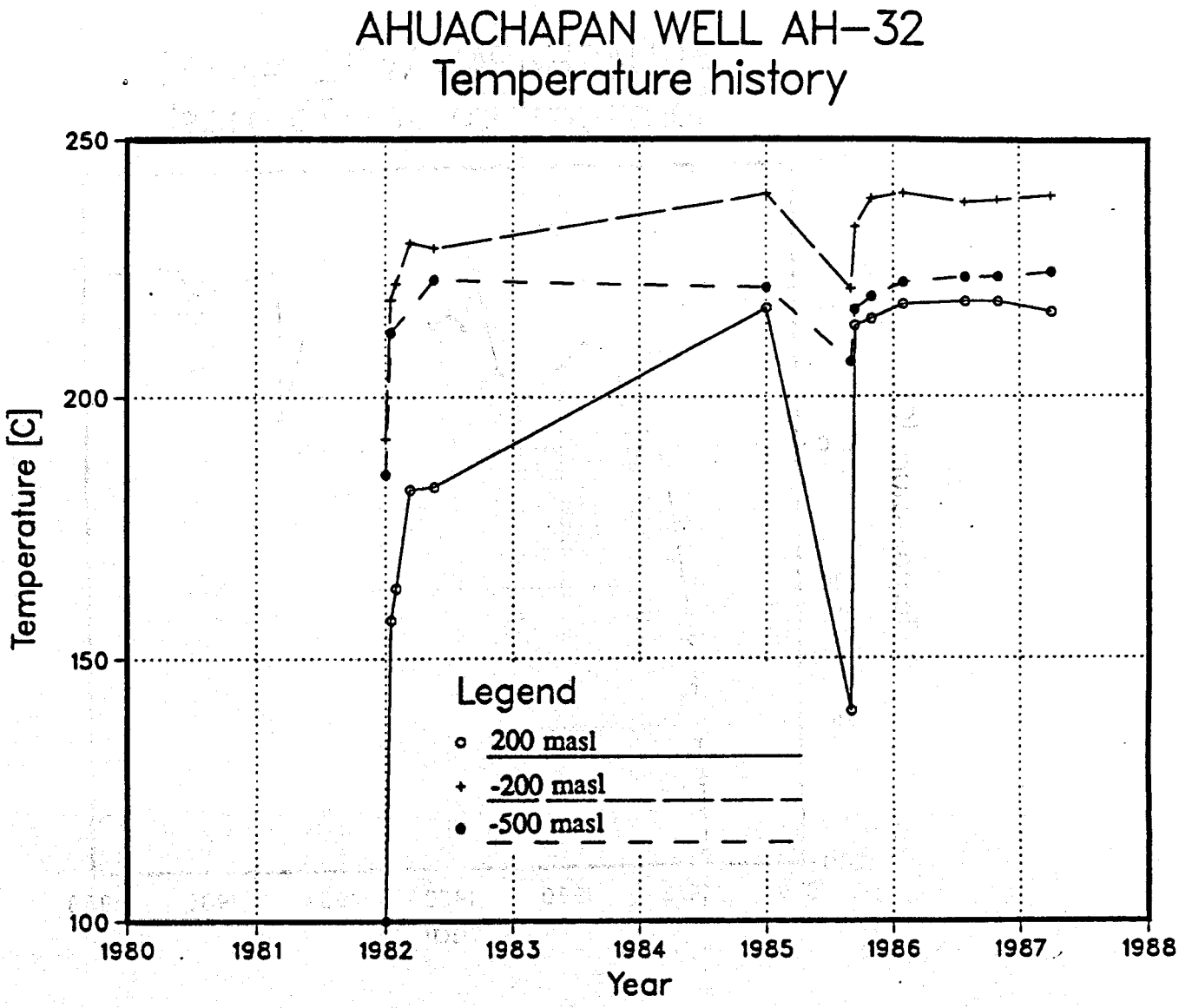

Figure 9.26. AH-32 temperature history.

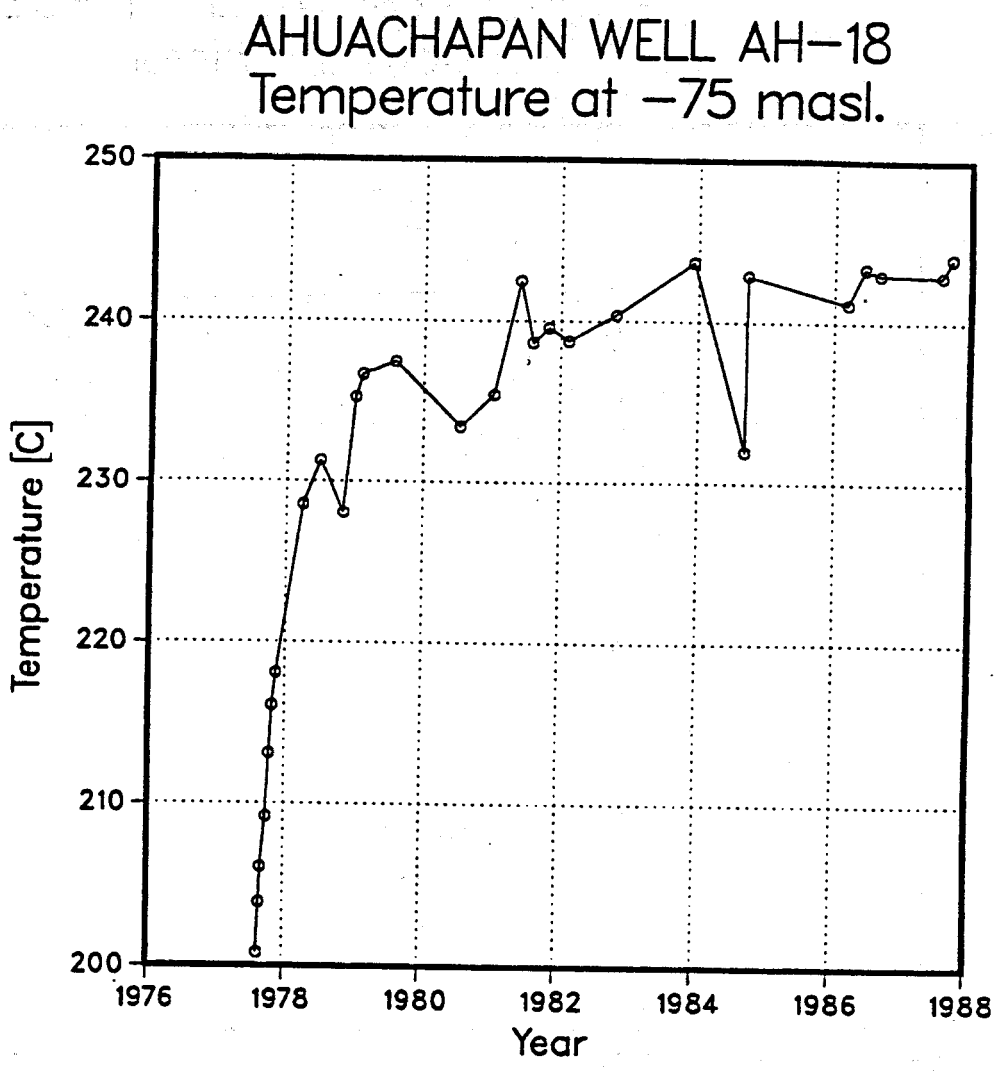

Figure 9.27. AH-18 temperature history at -75 masl.

9.4 Fluid Chemistry

Time series plots for individual wells have been plotted to determine the fluid chemistry changes in response to exploitation. Results of these analyses have been summarized for each well in Appendix C. The methods of analysis are described in detail in Chapter 5.

The reservoir response map (Figure 9.28) suggests that wells in the center of the field are affected by the inflow of cooler water caused by reservoir drawdown, while wells on the sides of the field show by boiling. These processes are in response to the gradual depletion of reservoir fluids. The shape of the central mixing zone suggests a fault or a zone of higher permeability that allows overlying colder water to leak into the reservoir. Comparing this figure with the fault map (Figure 4.13, Chapter 4) indicates that the zone of mixing is related to Faults 7 and 8, the youngest normal faults in the field.

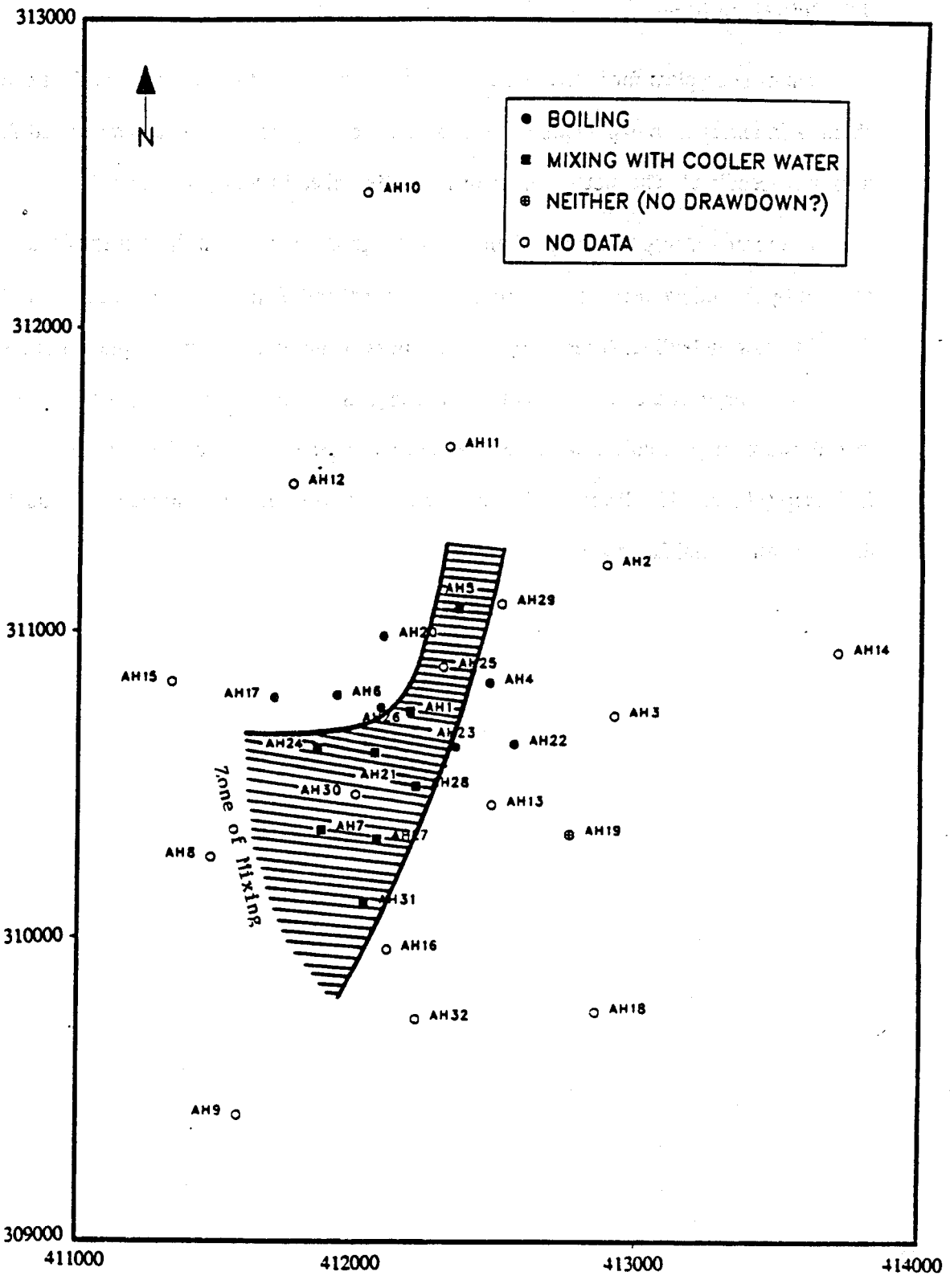

Figure 9.28. Reservoir response to drawdown.

10.0 CONCEPTUAL MODEL

A conceptual model of Ahuachapán has been developed based on all available data. Recent models of the field (Romagnoli, et al., 1975 and Aumento, et al., 1982) have been limited to the wellfield area, and have suggested that Ahuachapán and Chipilapa are separate geothermal systems. However, our study indicates that both fields are parts of a larger "regional" geothermal system. Similar ideas were expressed in the early exploration years (e.g. Sigvaldason and Cuellar, 1970).

10.1 Regional Geothermal System

Geothermal surface manifestations are spread over more than 100 km^2 in the vicinity of Ahuachapán. They can be divided into high-temperature fumaroles and steaming grounds on the northern slopes of the volcanoes and in the southern part of the area, and hot springs (40-100 °C) on the plain north of Ahuachapán.

The major fumaroles are: Cuyanausul on the northern slopes of Cerro Cuyanausul, east of Laguna Verde; El Sauce on the northern slopes of Laguna Verde; Agua Shuca and Playón de Ahuachapán near the Ahuachapán wellfield; and La Labor in Chipilapa. Chemical analyses of fumaroles gas samples show similar compositions indicating a common geothermal source fluid (Sigvaldason and Cuellar; 1970). A marked increase in hydrogen content in fumarole steam towards the volcanoes suggests the geothermal upflow zone is located probably near the Laguna Verde volcano. Data from Ahuachapán and Chipilapa wells show that the source fluid is highly saline (more than 8000 ppm Cl) and that the upflow temperatures are above 250 °C.

The relationship between Ahuachapán and Chipilapa has been disputed over the years. Early drilling showed identical fluid chemistry and similar reservoir temperatures (Sigvaldason and Cuellar, 1970). Later, a resistivity survey of the area suggested high-resistivity body (bar-

rier) separating the two fields. Recent resistivity studies, however, do not show this barrier. The previous interpretation is believed to be in error because of incorrect elevations being used in the data analyses. (James Fink, personal communication, 1988). All available data seem therefore to indicate that the two fields are connected and are fed by the same geothermal source. The ultimate proof of this connection would be to observe pressure interference between the fields. The simple reservoir model used to match the drawdown history of Ahuachapán (Chapter 9) predicts a drawdown in Chipilapa of a few bars due to production in Ahuachapán during the last twenty years. However, Chipilapa wells are plugged at shallow depth, this can not be measured. The planned drilling in Chipilapa will eventually determine the pressure communication between the fields.

The hot springs on the plain north of Ahuachapán are below 580 masl. They generally produce fluids from the saturated aquifer (Sigvaldason and Cuellar, 1970; Cuellar, et al., 1979). The maximum elevation of these springs matches with the pressure potential of the saturated zone in Ahuachapán where water levels of 600-660 masl are found. An exception to this is the main hot spring area, El Salitre, about 7 km north of Ahuachapán where more than 1000 l/s of 68-70 °C water used to be discharged. The fluid of these springs was, prior to exploitation at Ahuachapán, higher in dissolved solids (especially chloride) than that of the saturated aquifer. The original chemistry of El Salitre fluid has been explained to be the result of mixing saturated aquifer fluid with 10-20% of saline aquifer fluid, and considerable steam heating (Glover, 1970; Sigvaldason and Cuellar, 1970). There is pressure communication between the Ahuachapán field and El Salitre. The flow rates of the hot springs have decreased drastically during the last decade and the salinity of their fluid has been reduced to one fifth of its original value.

The hydrologic model discussed above is summarized in the simplified illustrations showed in Figures 10.1 and 10.2. We believe that saline, high-temperature (above 250 °C) fluid upflows underneath the volcanoes (probably Laguna Verde), southeast of Ahuachapán. From the upflow zone, fluid channels towards the north. A fraction of it flows toward the northwest and enters Ahuachapán near the southeast corner of the wellfield. Another fraction flows

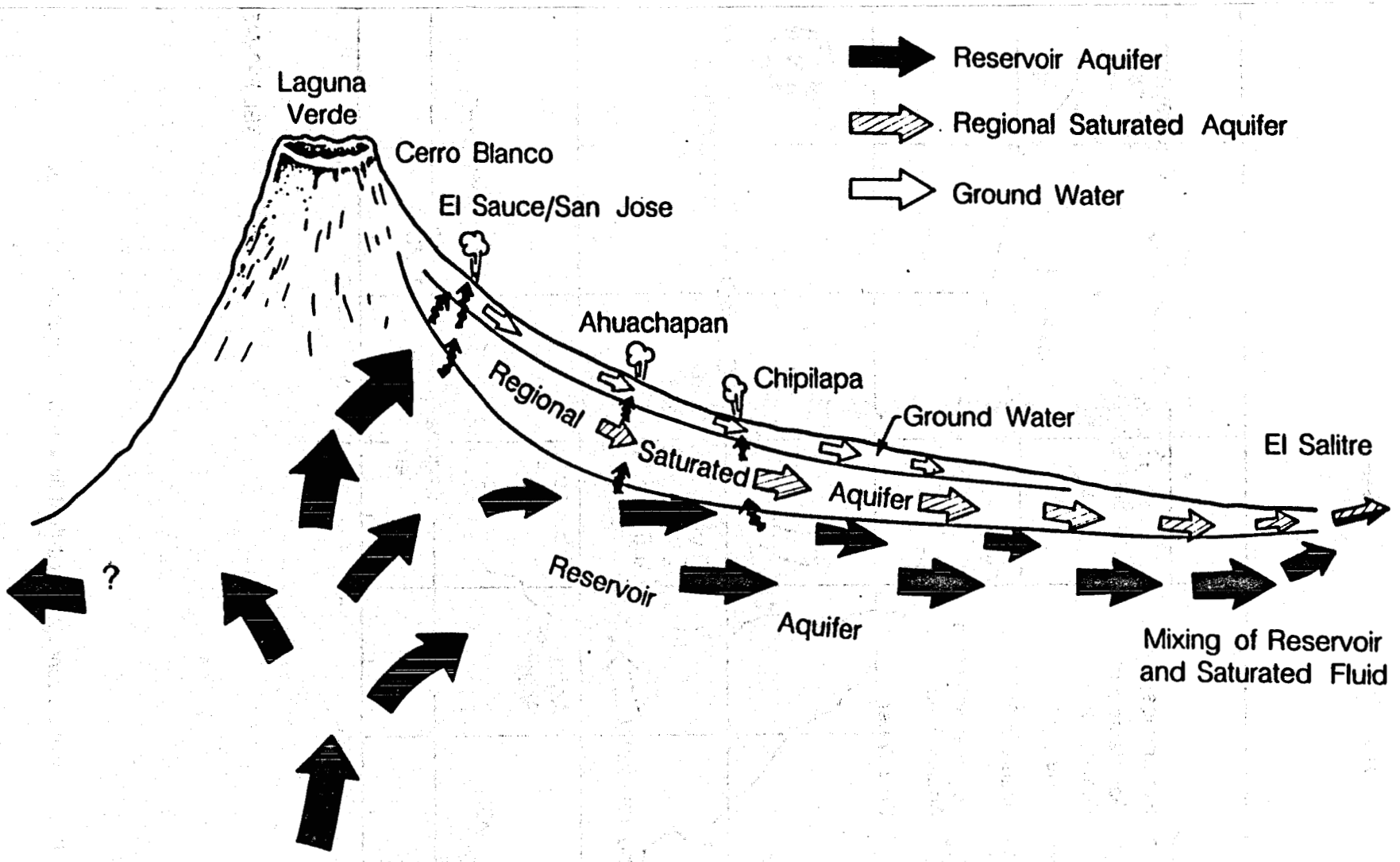

Figure 10.1. Schematic diagram of the conceptualized fluid flow in the Ahuachapán-Chipilapa field.

XBL 888-10368

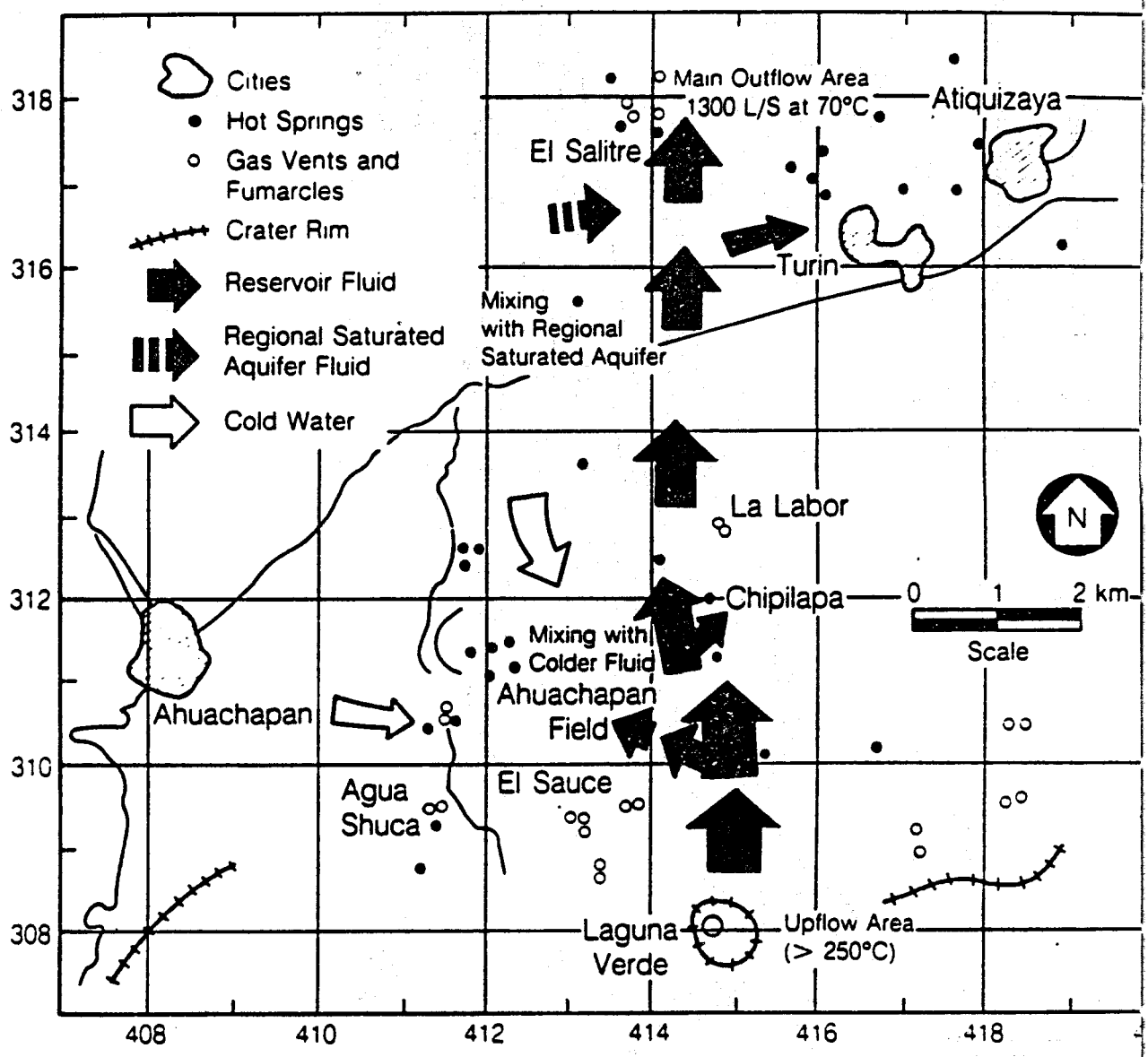

Figure 10.2. Plan view of the conceptualized fluid flow in the Ahuachapán-Chipilapa area.

toward the east to Chipilapa, however the main stream mixes with fluids from the saturated aquifer and is discharged to the surface at the El Salitre area.

10.2 Model Of Ahuachapán Wellfield

Detailed hydrogeological models of the field have been developed by Romagnoli et al. (1975) and Aumento et al. (1982); the latter model was based on mineralogy data. Although we agree with some of the features of their models, our fault system and lithology distribution in the field are quite different. Also, we have found no evidence to support fluid recharge from south of AH-9; the temperature reversal in AH-32 does not support this. Our present understanding of fluid flows in the Ahuachapán is shown in Figure 10.3 and is discussed below.

10.2.1 Aquifer Systems

Three different aquifer systems have been identified at Ahuachapán based on their depth, water chemistry and response to seasonal variations in precipitation (Chapter 9). These aquifers reside in different lithological units (Table 4.1).

10.2.1.1 Shallow Aquifer

The shallow aquifer is found in most wells associated with an elluvial layer referred to as the Surficial Materials (SM) unit (Chapter 4). Horizontal permeability is believed to dominate in this shallow groundwater system. The bottom of the aquifer is inferred to be at 700 masl. Fluid flow direction in this aquifer is toward the north, controlled by topography. This zone is of minor importance in terms of the geothermal reservoir.

10.2.1.2 Regional Saturated Aquifer

The saturated aquifer is associated with the Young Agglomerates (YA) unit. The pressure

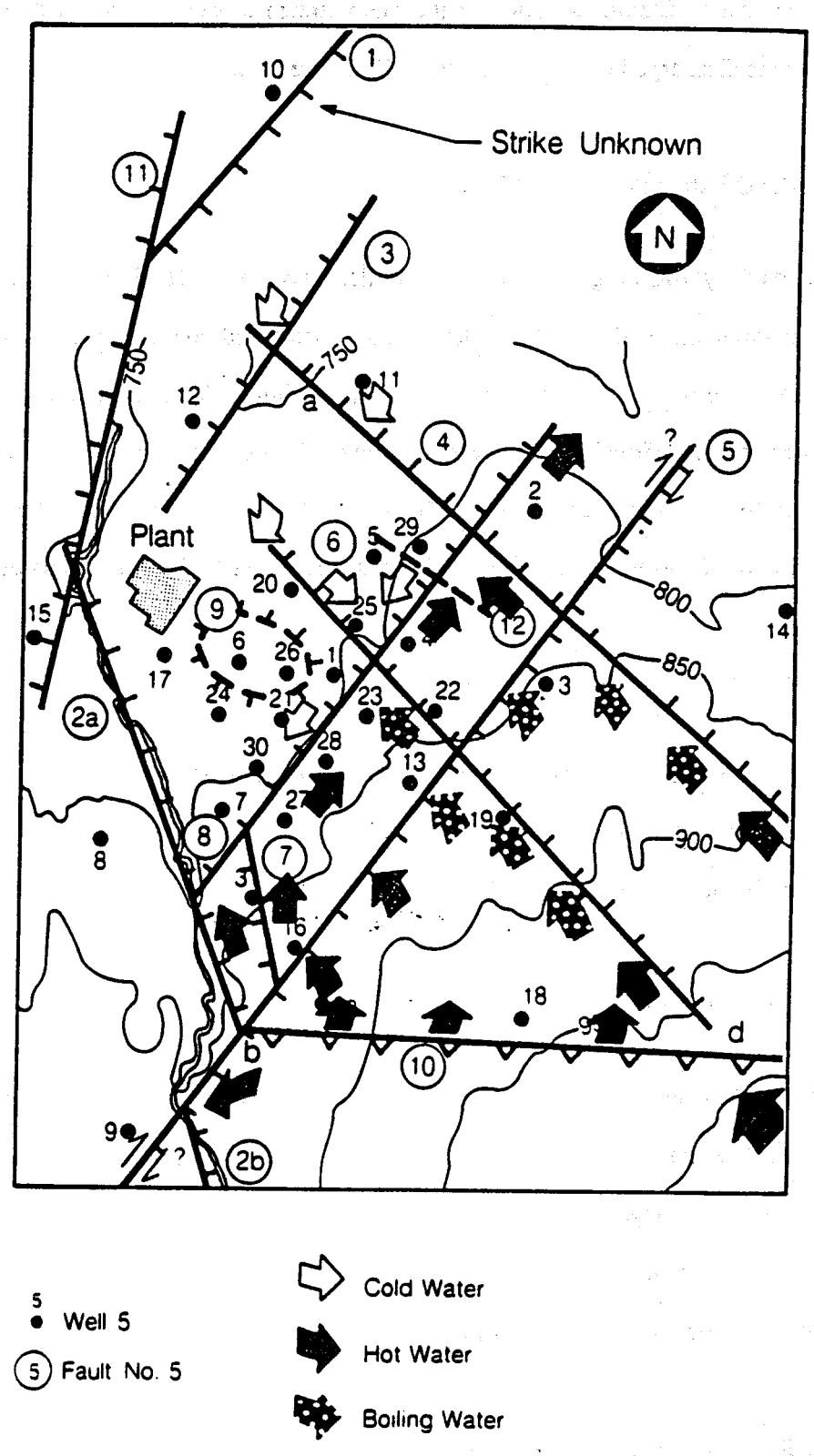

Figure 10.3. Inferred fluid flows and flow channels in the Ahuachapán field.

distribution in this zone also indicates fluid flow towards the north. This aquifer has a higher pressure potential than the underlying geothermal reservoir and is believed to be separated from the hot reservoir in most areas by a low permeability layer (caprock). However, in the eastern part of the field, there is hydrological communication between the saturated aquifer and the geothermal reservoir through faults/fractures allowing downward liquid flow into the reservoir. The chemistry of the geothermal fluid supports such mixing; there is generally lower chloride concentrations and geochemical temperatures in the eastern part of the field. Some steam may escape from the reservoir two-phase zone into the overlying saturated aquifer through permeable fractures.

10.2.2 Geothermal Reservoir

At Ahuachapán, the geothermal reservoir is found below 350 masl, associated with the Ahuachapán Andesites (AA) and Older Agglomerates (OA) units. The extent of the reservoir is limited to the north and to the west; both barriers may be associated with fault structures. The presence of a northern permeability barrier can be inferred from temperature data from wells AH-17, AH-2, AH-11 and AH-12 and, coincides with Fault 3 (Fig. 4.13). The western barrier may correspond to a fault west of Fault 2a.

The top of the geothermal reservoir, which corresponds to the top of the AA unit, is deeper both in the eastern and southern parts of the wellfield. The andesite controls to some extent the areal extent of the reservoir as it is not found in the colder wells in the north and west. The reservoir is believed to extend at depth into Chipilapa to the east and to the inferred upflow zone to the southeast. The OA unit also contributes fluids to producing wells, but is considerably less permeable than the AA unit.

10.2.3 Hot Fluid Recharge

The main hot fluid recharge enters the wellfield from the southeast, as indicated by the

temperature distribution of the field. The temperatures in the field increase in that direction. The hot recharge is channelled to the wellfield not only by faults but also horizontally through the highly permeable AA unit. As the geothermal recharge enters the wellfield it subdivides into two main streams feeding the main production well.

The main hot water inflow occurs through Fault 6, with boiling occurring where this fault intersects Fault 5. Evidence of this boiling include the cooling of the liquid portion of the Andesites (see Section 9.3.2) and the relatively low gas content of produced fluids. Cooler fluids recharge the eastern part of the wellfield from the north along Faults 4 and 6 and/or from the overlying Saturated Aquifer. This dilutes the geothermal fluids as is evident from the lower chloride concentrations in the eastern part of the wellfield (see Section 5.4).

Part of the hot recharge fluids flow along Faults 10 and 2a and recharge the western partition of the wellfield. No dilution in this part of the wellfield is evident so that the produced fluids should reflect the chemical composition of the hot water recharge. A small portion of this recharge fluids flows along Fault 5 towards the southwest, eventually feeding the mudpools in Agua Shuca and perhaps the other surface manifestations further to the south. As the AA unit resides relatively deep in this part of the wellfield, the recharging fluids do not boil. The Regional Saturated Aquifer seems to be less permeable or not present in the western part of the wellfield (see Section 6.1), hence, no dilution of cooler recharging fluids is observed.

10.2.4 Cold Water Recharge

Cooler fluids recharge the eastern part of the reservoir as indicated in the last section. This cooler fluid flows either horizontally from the north or vertically downward from the Regional Saturated Aquifer. In the eastern portion of the field, this cold water mixes with geothermal fluid, explaining the difference in fluid chemistry between the western and eastern area of the Ahuachapán. Slow temperature recovery of the northern reinjection wells in the OA unit (e.g. well AH-2 and AH-29), also supports this mixing.

Cold water recharge from the west is suggested from by the very slow recovery deep in AH-7 after reinjection had stopped. This cooler water flow is believed to occur underneath the AA unit and could explain the small temperature reversals observed in the OA unit. Although this recharge is not significant under natural state conditions, it became important during exploitation as pressure declined in the center of the field.

10.2.5 Boundaries

Two boundaries limiting the Ahuachapán geothermal reservoir have been inferred. The presence of a northern boundary is deduced from the rapid decline in temperature toward the north and the absence of the AA unit in well AH-10. This barrier to hot fluid flow is associated either with Fault 1 or 3. Rapid temperature decline toward the west also indicates a barrier in that direction. However, the controlling structure has not been identified. Both AH-8 and AH-9 showed high temperatures and pressure communication with the field, while AH-15 did not show any pressure decline with exploitation. The absence of the AA unit in this region and the low temperature in well AH-15, however, suggest that the boundary is close to this well and is west of AH-8.

11.0 NATURAL STATE MODEL

Geothermal systems are dynamic in nature, presenting a continuous flow of fluids, chemical species and heat. Hot fluids upwell from depth, circulate through the geothermal system, and discharge at the surface or mix with shallow groundwaters. The thermal energy supplied to the geothermal system by the rising hot fluids and by conductive heat gains is balanced by the energy losses at surface manifestations, conductive heat losses to the surface and lateral conductive cooling. The modeling of the natural conditions of a geothermal field yields valuable information regarding the mass and heat flow within the system and provides the necessary initial thermodynamic conditions for the subsequent exploitation modeling.

A number of simple mathematical models have been developed for the Ahuachapán geothermal field to simulate the production behavior and predict the reservoir's response to exploitation. Grant (1980) developed a simplified tank model of the field and matched the available field history. More detailed numerical studies of the field were carried out by Vides (1982) and ELC-Electroconsult (1984). However, none of this work involved natural state modeling of the field.

In modeling the natural state of the Ahuachapán field, the following objectives were considered:

(1) To verify the conceptual model of the system

(2) To quantify the natural mass and heat flow in the reservoir

(3) To better understand the hydrology of the field

(4) To obtain coarse estimates of the permeability structure of the field.

The simulation work was carried out using the numerical model MULKOM (Pruess, 1982).

11.1 Available Data

Considerable amounts of data have been collected from the field since the first well was tested in 1968. Many temperature and pressure profiles are available for each well, and geochemical data taken prior to and during exploitation have been useful in inferring fluid flow paths and reservoir boundaries. Lithology columns for each well were the basis for identifying the most significant structures controlling the hydrology of the field.

Pre-exploitation pressure distribution in the field showed no significant gradients. The pressures taken before 1975 were in the range of 32-36 barg at 200 masl. The nonproductive holes at the periphery of the production area show higher pressures than those within the main wellfield, suggesting that the saturated zone has a higher pressure potential than the geothermal reservoir (Section 9.0).

The temperature distribution in the field shows increasing temperature towards the southeast, where the highest reservoir temperature (245 °C) is found. This distribution suggests the inflow of hot fluids from the southeast. All productive wells show similar temperature profiles, with the top of the convective gradient coinciding with the top of the AA unit. Small inversions are often found in the OA unit. The largest inversion, of about 15°C, is found in well AH-32.

A number of fumaroles and hot springs are found in the Ahuachapán-Chipilapa area (Figure 11.1). However, no accurate flow measurements of these discharges have been made. Geochemistry data from the springs at El Salitre though suggest a strong connection with the Ahuachapán field.

11.2 Approach to Modeling

For the natural state modeling, one must attempt to represent all important features of the conceptual model of Ahuachapán:

1. Rising hot fluids recharge the system in an area southeast of well AH-18. The temperature

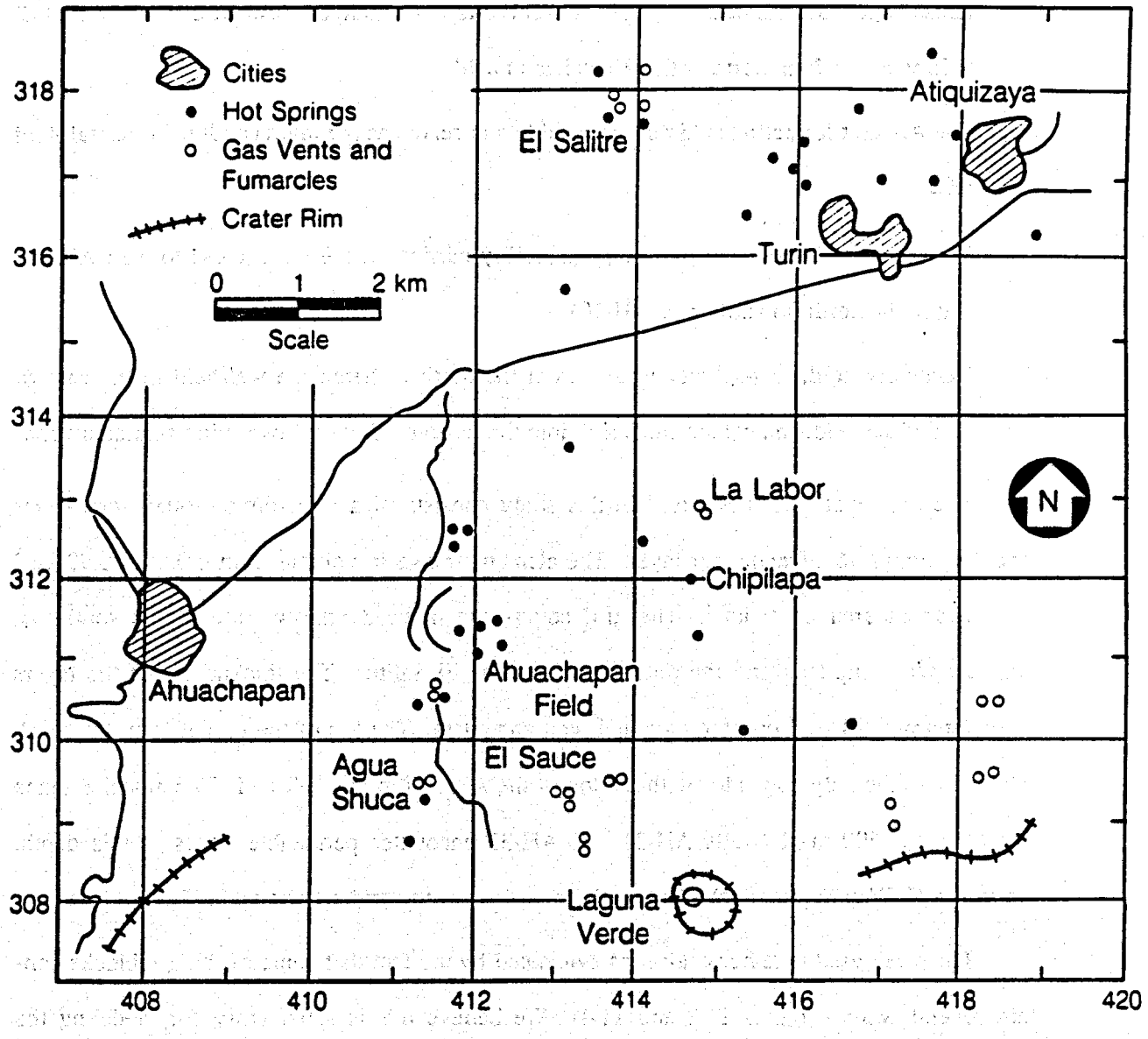

Figure 11.1. Map showing surface manifestations in the Ahuachapán and Chipilapa area.

of this fluid is estimated to be 250°C.

2. Most of the hot fluids flow towards the north, with smaller fractions recharging the Ahuachapán and the nearby Chipilapa reservoirs. The main outflow for the system is at El Salitre, about 7 km north of the Ahuachapán field.

3. The AA unit formation is highly permeable and serves as the main conduit for lateral fluid flow.

4. The reservoir is bounded by low permeability barriers in the west (close to well AH-15) and in the north (towards well AH-10).

5. Relatively cold, low-salinity waters from the north recharge the wellfield in the eastern part of the field, and colder fluids leak into the reservoir from the overlying saturated zone.

The computational mesh used in this study consists of a three-dimensional, three-layer grid containing 46 elements per layer. The elements range in volume from 0.027 to 0.99 km^3 and cover an area of 48 km^2. The grid covers the inferred upflow zone in the southeast, Ahuachapán, Chipilapa and the outflow area of the El Salitre. The thicknesses of the layers were determined based on lithologic and feed zone data. The top of the model is at 350 masl, which approximately coincides with the top of the AA unit in the wellfield. The model extends vertically to -600 masl (wells AH-31 and AH-32 encounter permeable zones at this depth, Appendix C, Well Summaries). The areal dimensions of the grid are shown in Figure 11.2.

The mesh used is rather coarse, as evidenced by the fact that some of the gridblocks contain several wells (Figures 11.3 and 11.4). We believe this is satisfactory for modeling the natural state since most of the wells near the center of the field have similar temperature profiles and because there is no observable variation in initial pressure across the field. In subsequent exploitation modeling, the grid will be appropriately refined so that each well will be represented by single gridblocks (Figure 11.5).

To date, no accurate flow measurements are available on the fumaroles and springs in the area. The natural spring discharge at El Salitre (the main outflow for this system) before exploi-

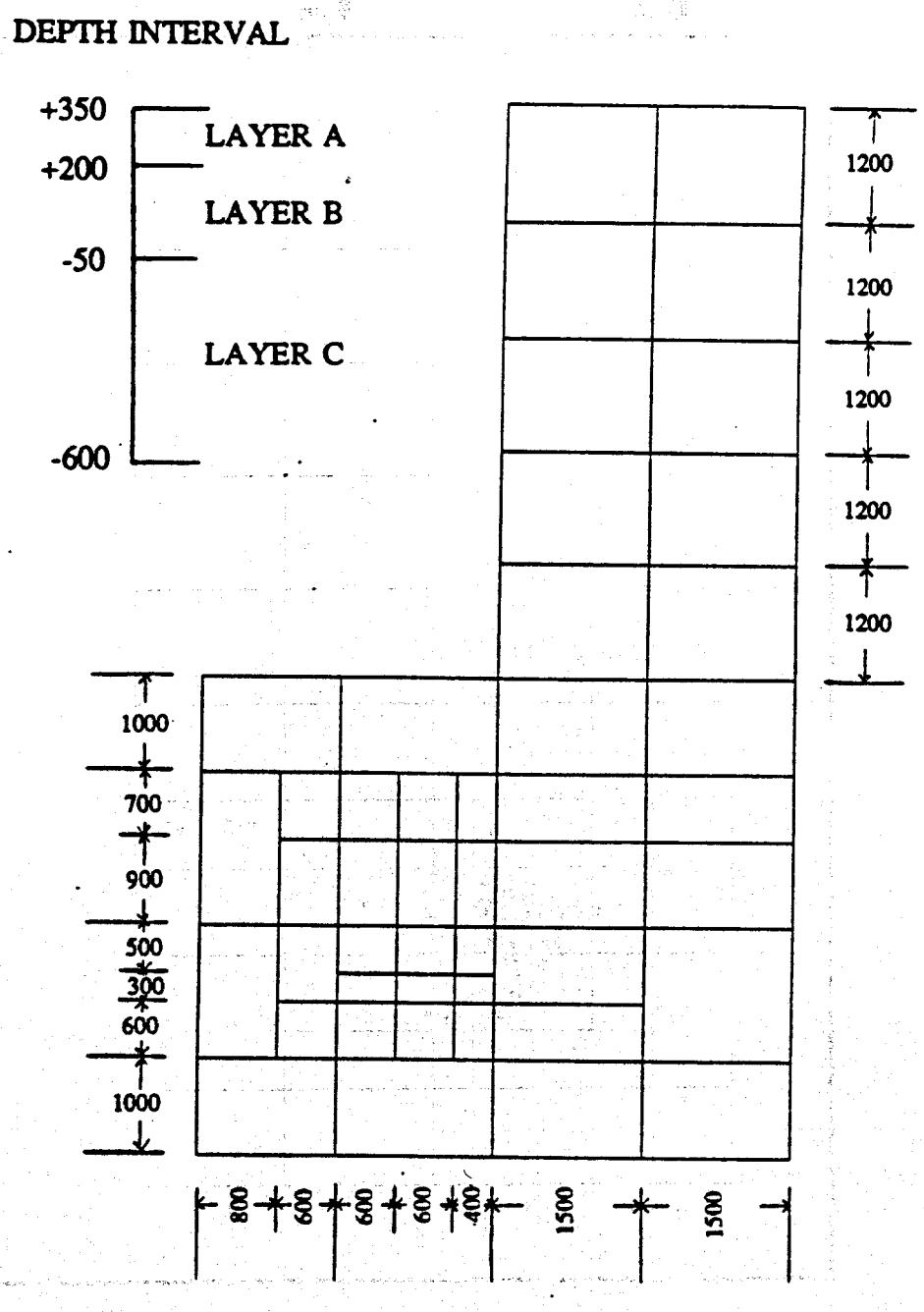

Figure 11.2. Grid block dimensions (in meters) used in modeling the natural state of the Ahuachapán geothermal field.

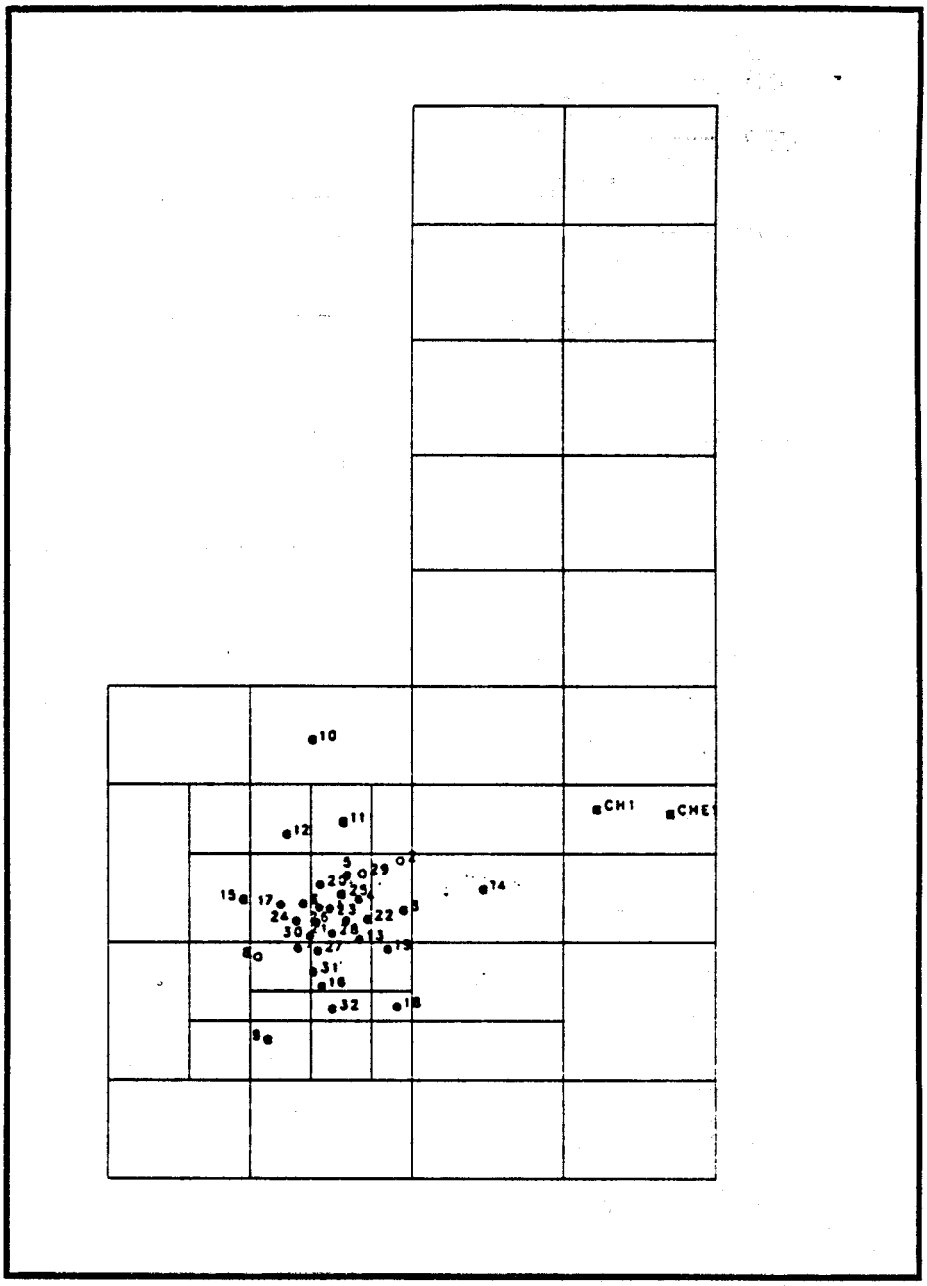

Figure 11.3. Grid blocks with well locations.

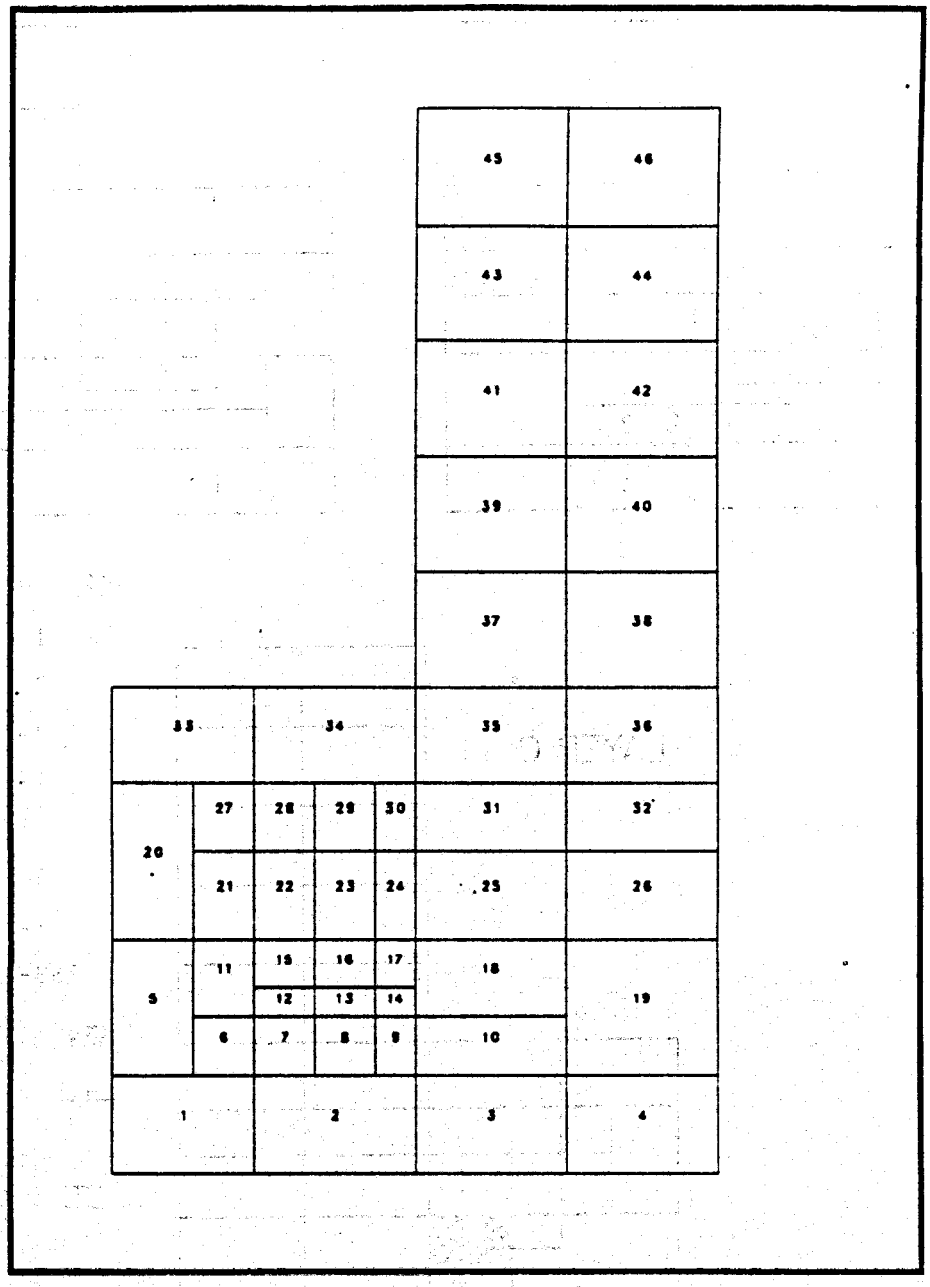

Figure 11.4. Node numbers assigned to the grid blocks of a given layer.

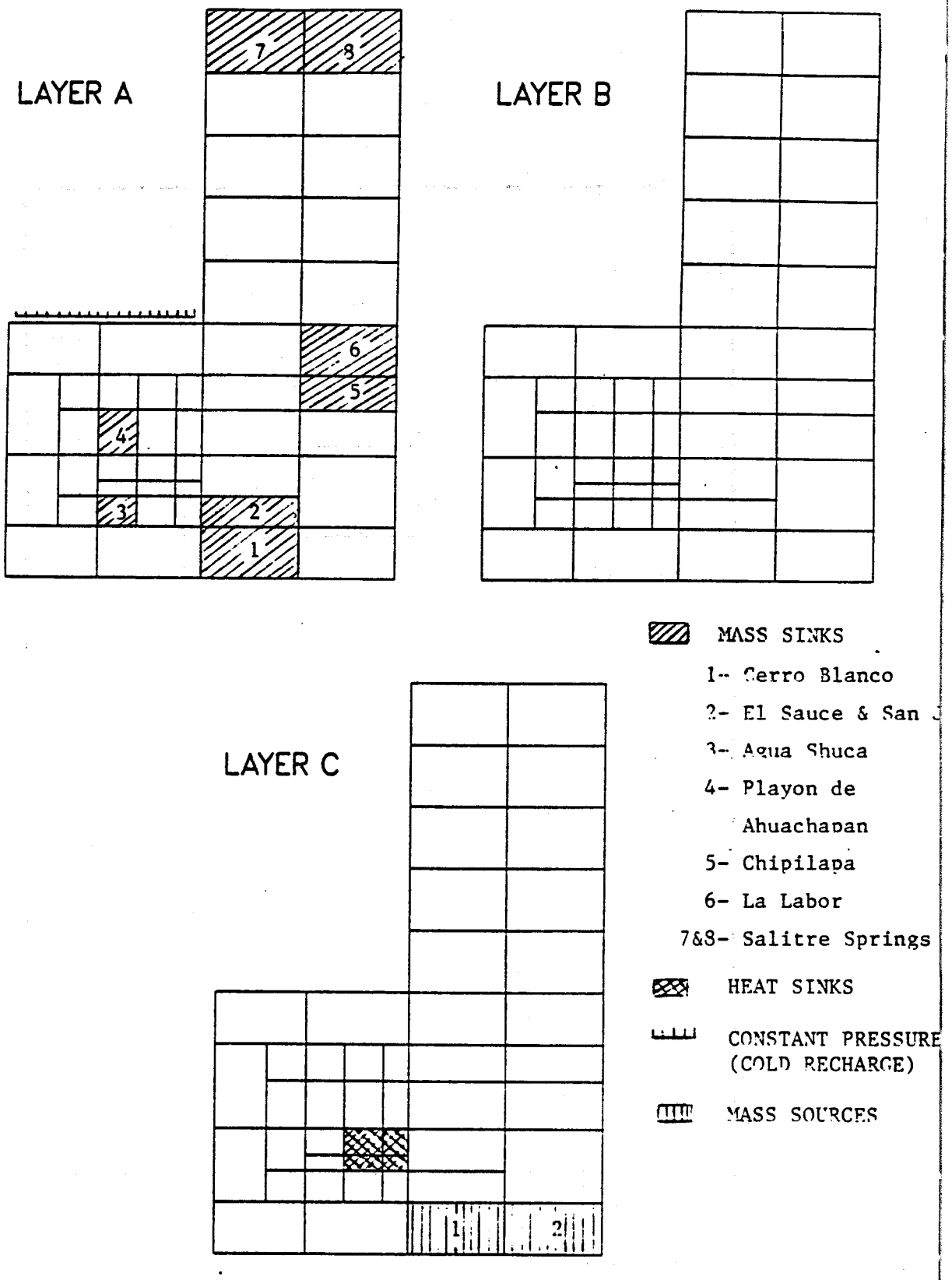

Figure 11.5. Ahuachapán Computational Mesh. Location of specified sources and sinks - Natural State.

tation is estimated to have been 1,300 l/s, with an unknown amount of mixing between geothermal and colder waters (about 70°C, Sigvaldson et al., 1970). Currently, the fluid outflow at El Salitre is estimated to be about 250 kg/s, with the decline attributed to pressure drawdown in the system caused by the exploitation of Ahuachapán. Using available temperature and chemistry data we estimated that before exploitation the geothermal component of the El Salitre outflow was about 170 kg/s.

Little data are available regarding other surface manifestations in the Ahuachapán area. For the modeling effort, we estimated the total energy output from these springs using course visual observations. In the model, the surface springs are represented by pressure dependent sinks that were designed so that proper spring outflows would occur when the correct pressure distribution was obtained. This feature of the model will be extremely useful in the exploitation simulations to evaluate the spring outputs as a function of reservoir pressure. The conductive heat losses to the surface are computed using an analytical algorithm developed by Vinsome and Westerfeld (1980).

In the simulations, we used a procedure similar to the one employed for the Krafla geothermal field in Iceland (Bodvarsson et al., 1984). The parameters that were adjusted during the modeling iterations were the flow rate and temperature of the upflow zone, spring flowrates and permeability distribution. The measured temperatures and pressures in the field were the main constraining parameters. A process of trial and error was carried out until a set of parameters was found that gave reasonable matches with well temperatures and pressures. The procedure employed is as follows,

1. Assign sources and sinks to the appropriate nodes.
2. Assign thermodynamic conditions to the source (recharge) fluid.
3. Adjust the permeability distribution.
4. Compute until steady-state thermodynamic conditions in the entire system are reached.
5. Evaluate the result and go back to Step 1 until the computed results reasonably match the

observed data.

11.3 Best Model

A natural state model was developed that reproduces reasonably well the temperature and pressure distributions in the field. The matches between observed and simulated temperatures and pressures are shown in Figures 11.6a-d and 11.7.

The model, however, does not match well the temperature observed in well CH-1, especially in the two lower layers. The temperature profile used for comparison with the simulated results was taken in 1969. This is the only log available that penetrates to this depth, and it may not show the stabilized temperature conditions of the well.

The simulated results show somewhat colder temperatures than those observed for well AH-15, which is due to the fact that the well is not in the center of node 21, but farther to the east. One expects lower temperatures west of the well, which is reflected in the simulated results. The slight difference between the simulated and observed pressures (simulated pressures are slightly higher) is thought to be due to the pressure drawdown caused by well testing during the field development phase. A considerable pressure decline was observed during that period. Although the pressure recovered during one and one half years prior to exploitation, data from 1977-1975 indicate pressures 1-2 bars lower than in 1968 (Chapter 7).

Results from the best model indicate that a total flow of 225 kg/s of 255 °C water upflows beneath the Laguna Verde volcanic complex. Only part of this fluid flows into the Ahuachapán (about 38 kg/s) and Chipilapa (about 30 kg/s) areas. The total thermal throughflow for the entire system is estimated to be 250 MW_t. About 60 MW_t are lost through the surface manifestations in the Ahuachapán and Chipilapa fields. Conductive heat losses to the surface are estimated to be at about 20 MW_t, with the remainder exiting the system by fluid discharge at the El Salitre area.

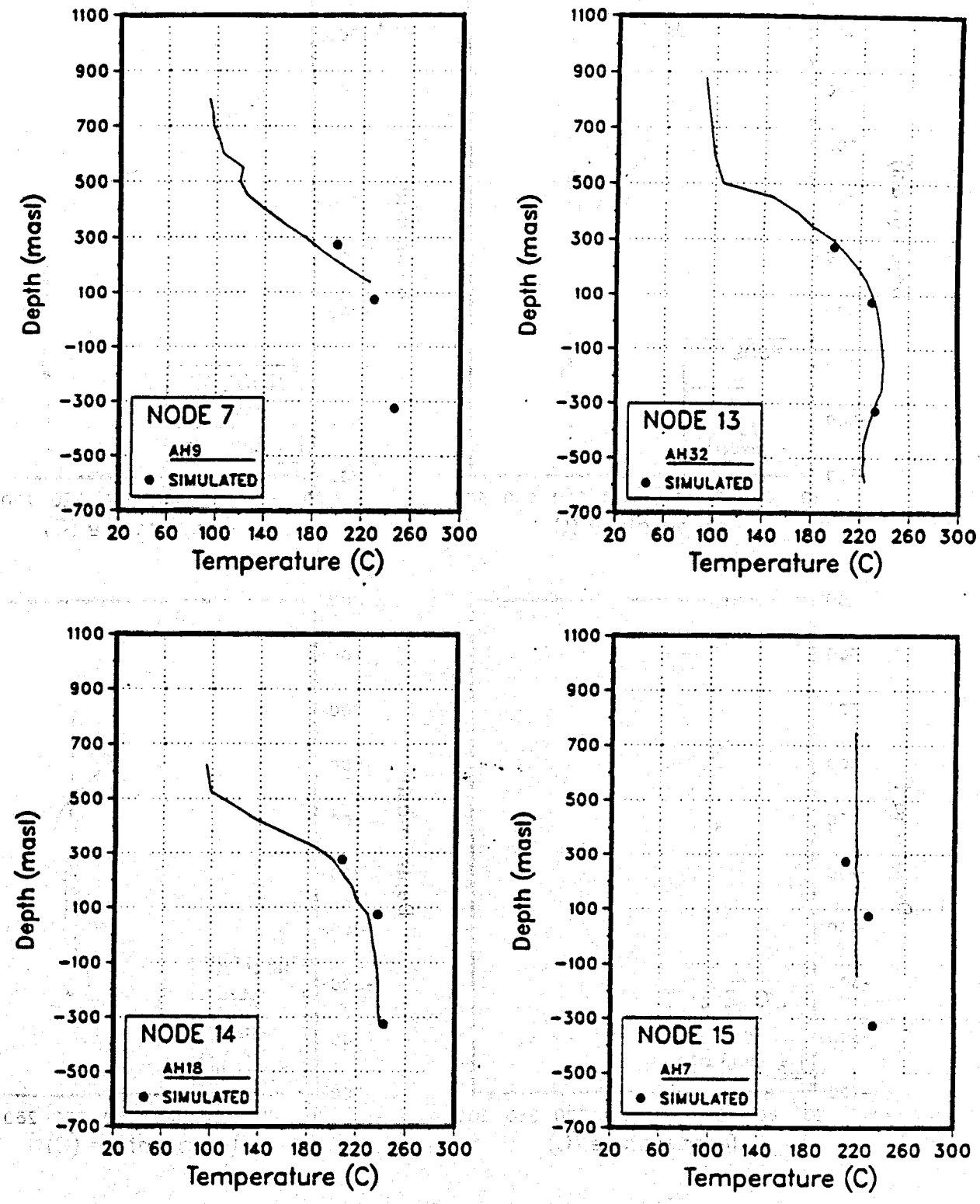

Figure 11.6a. Temperature match - Natural state.

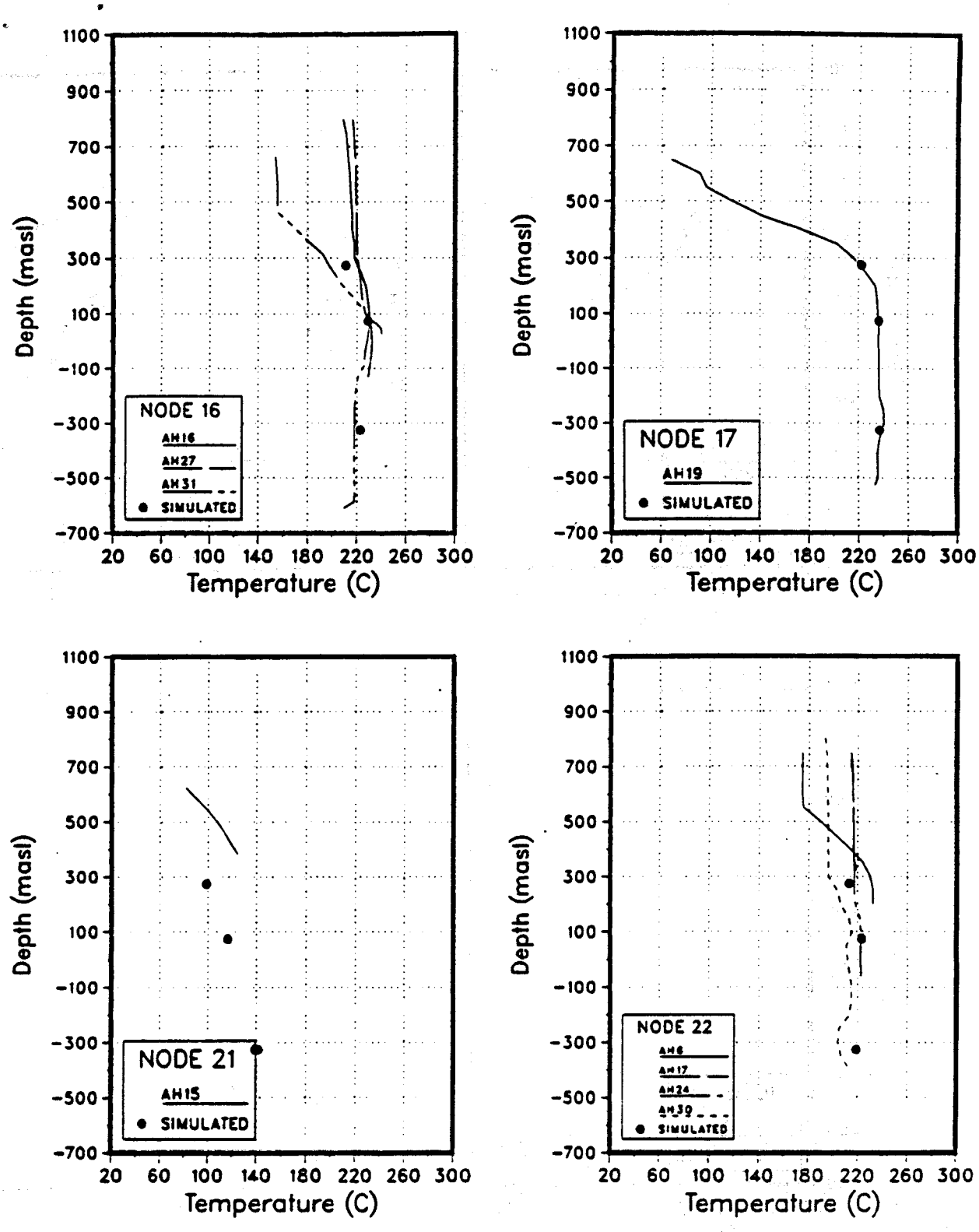

Figure 11.6b. Temperature match - Natural state.

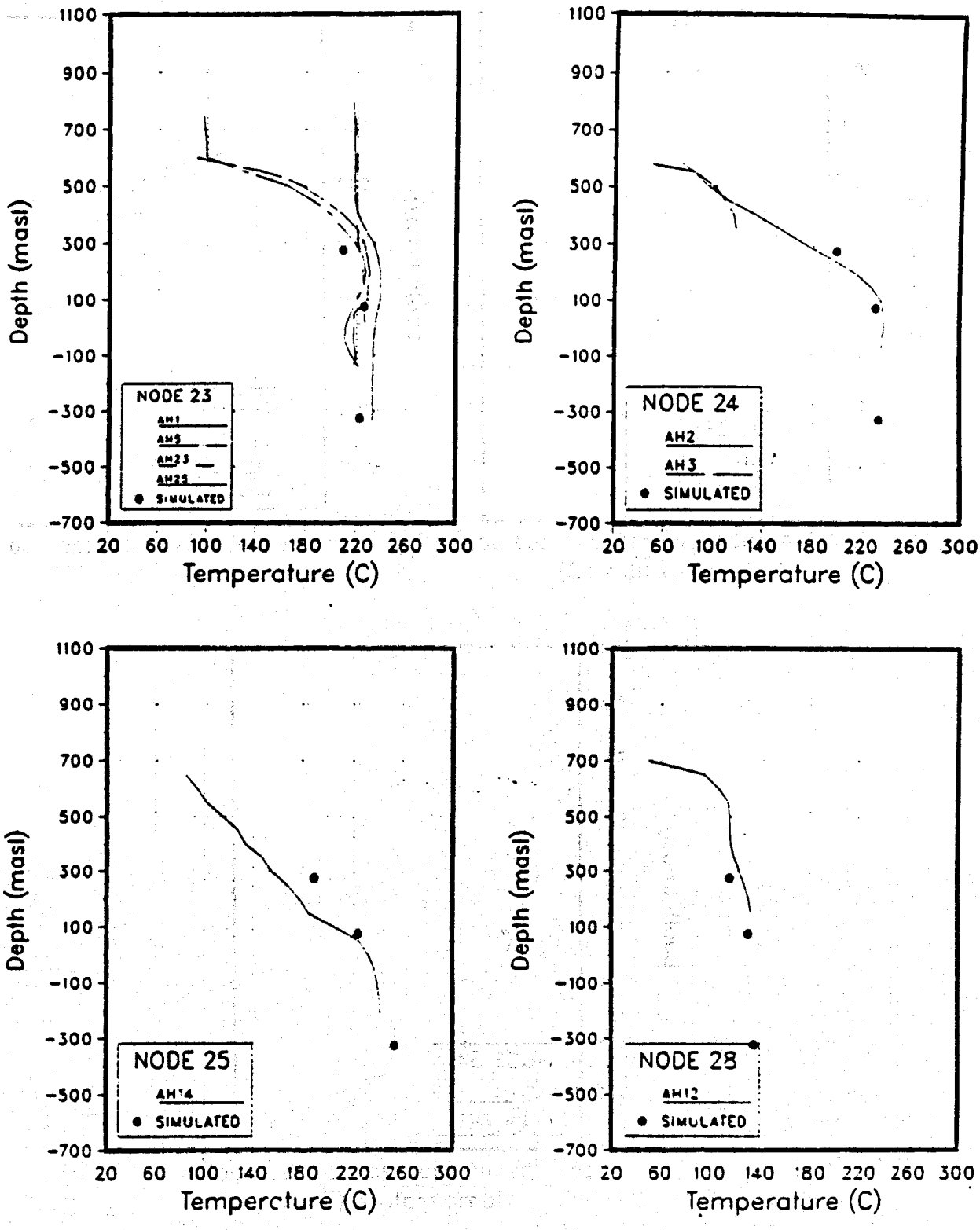

Figure 11.6c. Temperature match - Natural State.

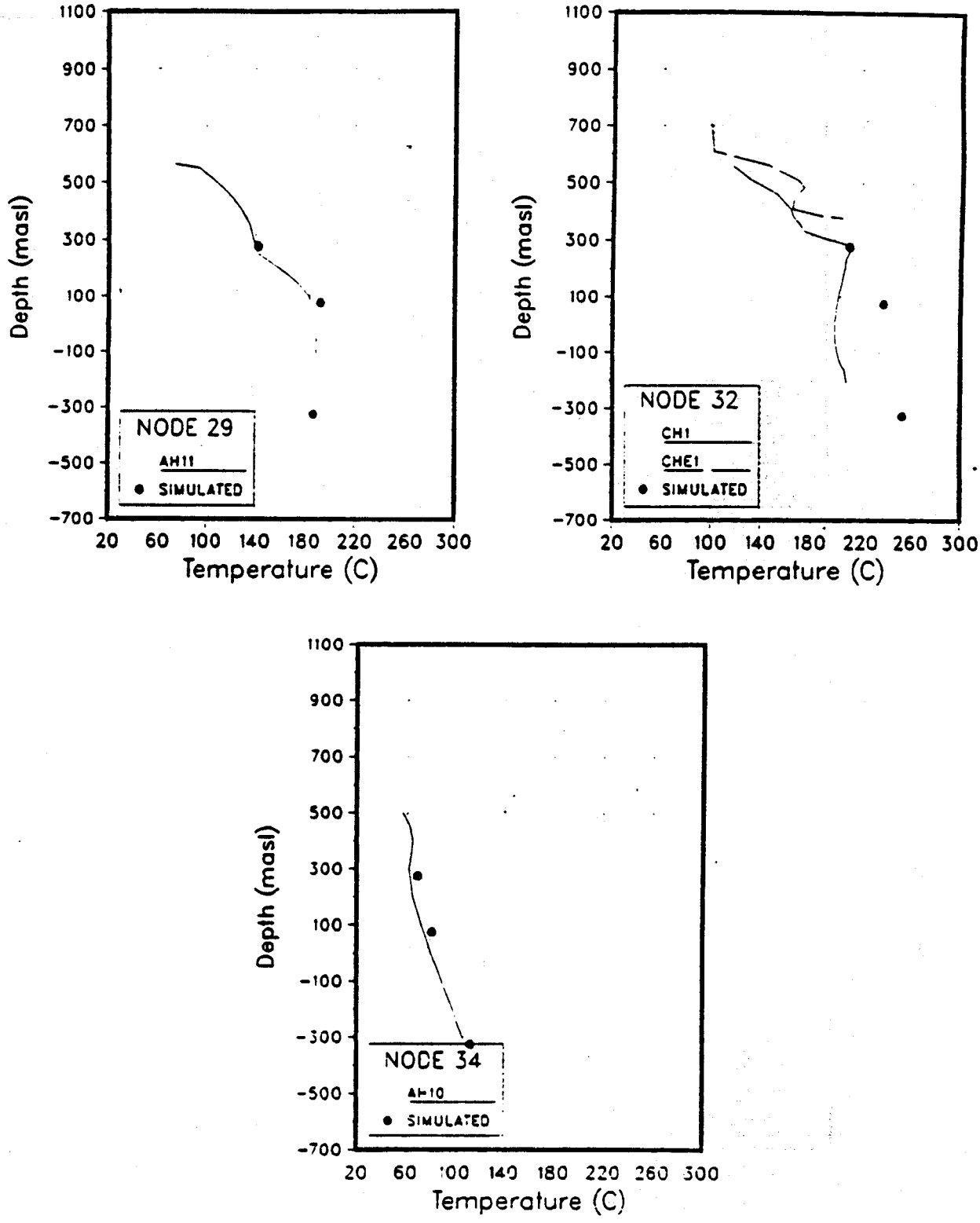

Figure 11.6d. Temperature match - Natural State.

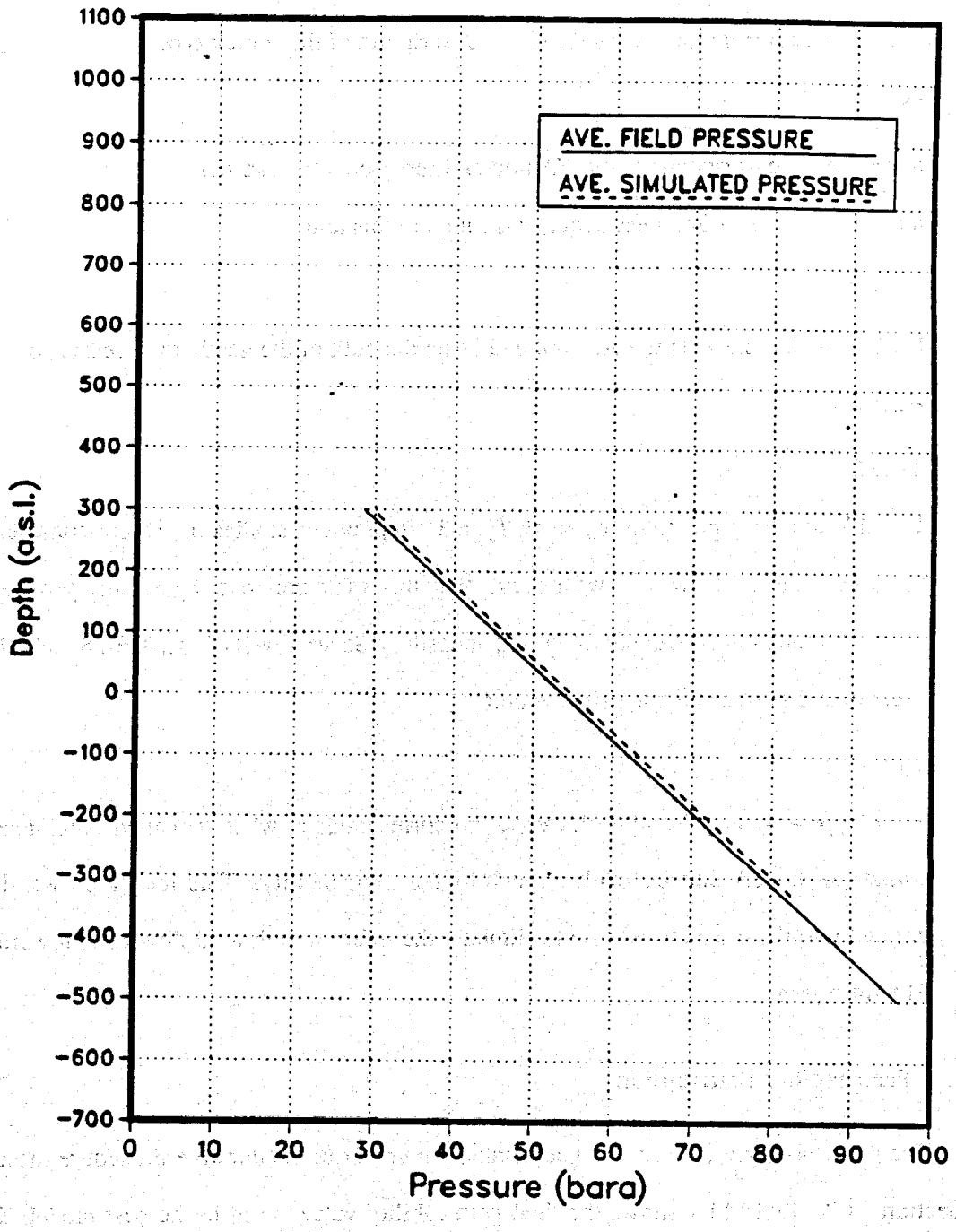

Figure 11.7. Pressure match - Natural State.

11.3.1 Lithology Distribution

Four rock types are used in the best model to represent the different units found in the Ahuachapán area (Figure 11.8). The material properties used are given in Table 11.1 and are partly based on data from Larios (1983, 1985) Description of these rock types are given below:

Rock Type 1

Rock Type 1 corresponds to the YA unit and represents the caprock of the geothermal system. The Regional Saturated Aquifer is found in this unit.

Rock Type 2

Rock Type 2 represents the AA unit and hosts the bulk of the geothermal reservoir (Saline Aquifer).

Rock Type 3

The OA unit are represented by Rock Type 3. In previous studies they were considered to be impermeable. However, we believe that this rock unit has significant permeability although much lower than the overlying andesites. Several wells (e.g., AH-28 and AH-29) encountered permeable zones in this unit.

Rock Type 4

Rock Type 4 was used only in Layer C and corresponds to what we called Agglomerates, similar to the YA unit but with a much higher permeability. This rock type was incorporated into the model to be able to simulate the inferred high fluid flow rates towards the El Salitre area.

11.3.2 Permeability Distribution

The permeability was used as an adjustable parameter in the iterative procedure discussed in Section 11.2. Table 11.1 shows the final permeability values used in the best model. Other assumed rock properties are also given in that table, including the rock density, heat capacity, porosity and thermal conductivity. Only the permeability, and the thermal conductivity affects the steady-state solution. The density, porosity and heat capacity are storage-type parameters

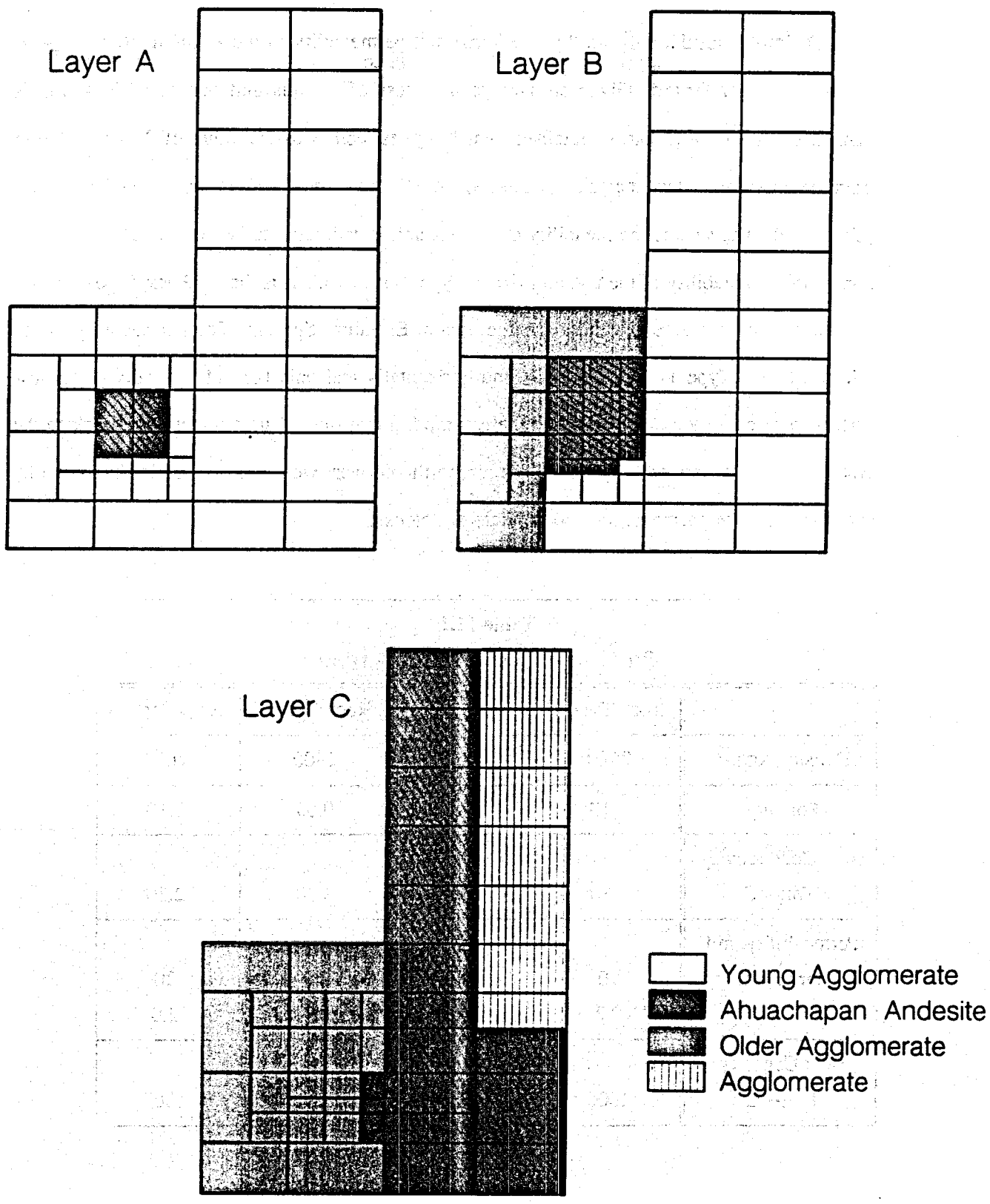

Figure 11.8. Lithology distribution assigned to each grid block

that do not affect steady-state results.

The model results indicate that the horizontal permeability of the AA unit (Rock Type 2) is rather high, or 80 md. Given an average thickness of the this unit between 300-400 m, a transmissivity of 24-32 Dm is obtained, which agrees well with the value of 25 Dm inferred from the interference test analysis (Chapter 8), and 35 Dm estimated from the production history (Chapter 9). The vertical permeability of the AA unit is estimated to be 20 md. The estimated horizontal permeability of the OA unit (Rock Type 3) is 20 md, as is that of Rock Type 4, which connect the upflow zone and the discharge area at El Salitre Springs. The permeability of the YA unit (Rock Type 1) is lower, or 10 md horizontally and only 0.2 md vertically. This low vertical permeability agrees well with the assumption that the YA unit acts as a caprock to the system. The low permeability barriers to the north and west were represented in the model by very low interface permeabilities appropriate gridblocks.

Table 11.1
Properties of the various rock types

	Rock Type 1	Rock Type 2	Rock Type 3	Rock Type 4
Density, kg/m^3	2680	2890	2800	2650
Porosity	0.10	0.10	0.05	0.10
Heat Conductivity W/m–°C	2.30	2.30	2.30	2.30
Permeability, md				
horizontal	10	80	20	20
vertical	0.2	16	4	2.0
Heat Capacity J/kg–°C	1000	1000	1000	1000

11.3.3 Sources and Sinks

Table 11.2 gives the characteristics of the sinks in the best model representing major surface manifestations.

Table 11.2
Characteristics of the sinks used in the model simulating major surface manifestations

	Flow (kg/s)	MW_t
Cerro Blanco	4.95	5.08
El Sauce & San José	3.35	3.37
Playón de Ahuachapán	20.51	18.72
Agua Shuca	2.18	1.85
Chipilapa	3.54	3.19
La Labor	29.16	27.76
El Salitre	170.47	169.36

The sink representing El Salitre only reflect the contribution of deeper aquifers (230 °C water). Assuming local mixing occurs with 40°C water at shallow depths, the total discharge rate of 70°C fluid would be approximately 1290 kg/s. This value agrees well with the estimate of 1300 kg/s. The temperature of the cold water used in this simple energy balance is based on a shallow temperature map of the field (Figure 7.3).

In addition to the sinks listed in Table 11.2, small heat sinks were specified in the bottom layers of nodes 13, 14, 16 and 17. These were necessary to match the temperature inversions, which we believed to be caused by a flow of a much colder fluid underlying the hot reservoir. Heats sinks of 3, 6, 1.5 and 3.75 W/m^2 were specified at nodes 13, 14, 16 and 17, respectively.

Recharge of colder fluids from the north was modeled in order to match the temperature profile of well AH-10. The cold recharge was simulated using a constant pressure boundary of 42 bars in the uppermost layers in nodes 33 and 34. The pressures in the boundaries were

specified such that nodes 33 and 34 would have a pressure about 5 bars higher than that in the wellfield, reflecting the high pressure of the saturated zone (Chapter 9).

11.4 Outputs from Surface Springs

Recently (15 June 1988), we received two reports authored by Durr (1960a, b) that give estimated values of thermal outputs of the surface manifestations in the Ahuachapán area. Table 11.3 compares our computed values for the thermal outputs with those of Durr. As the table shows the comparison is poor, especially for the Playón de Ahuachapán and La Labor, where our estimates are 4 to 6 times higher. Significant differences are also found for the other springs with the exception of Agua Shuca. When corrected for groundwater dilution our estimate for El Salitre (270 MW_t) agrees well with that made by Durr.

The estimates given by Durr were inputted into our numerical model and the calibration process repeated. The results obtained showed that using Durr's estimates it was possible to get reasonable matches with most of the well data (Figures 11.9 to 11.12), except for wells located close to Playón de Ahuachapán (Nodes 22 and 23) and in Chipilapa (close to La Labor). The shallow temperatures in these elements were too low, because of less throughflow of hot fluids (less flow to La Labor and Playón de Ahuachapán). From this we conclude that Durr's estimated thermal outputs for these springs are too low and that our estimates are closer to reality.

In order to get the best match with the observed thermodynamic data using thermal output estimates by Durr, the flowrate at the upflow zone had to be reduced to 190 kg/s (from 225 kg/s in our best model). Minor adjustments were also needed for the heat sinks at the bottom of the model in order to match the observed temperature inversions.

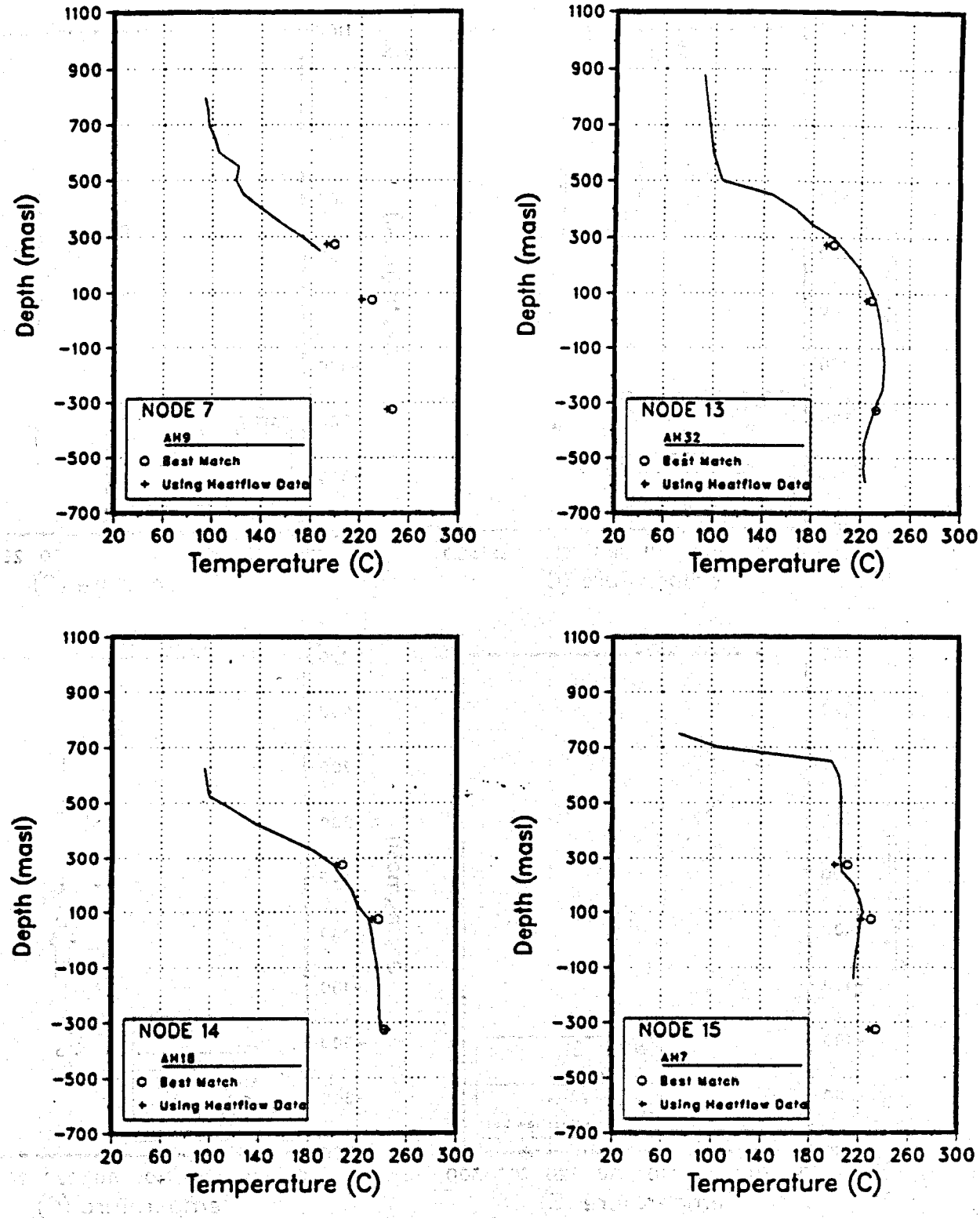

Figure 11.9. Comparison of temperature matches (in Nodes 7, 13, 14, and 15) between the best match and the simulation run using heat flow measurements by Fritz Durr.

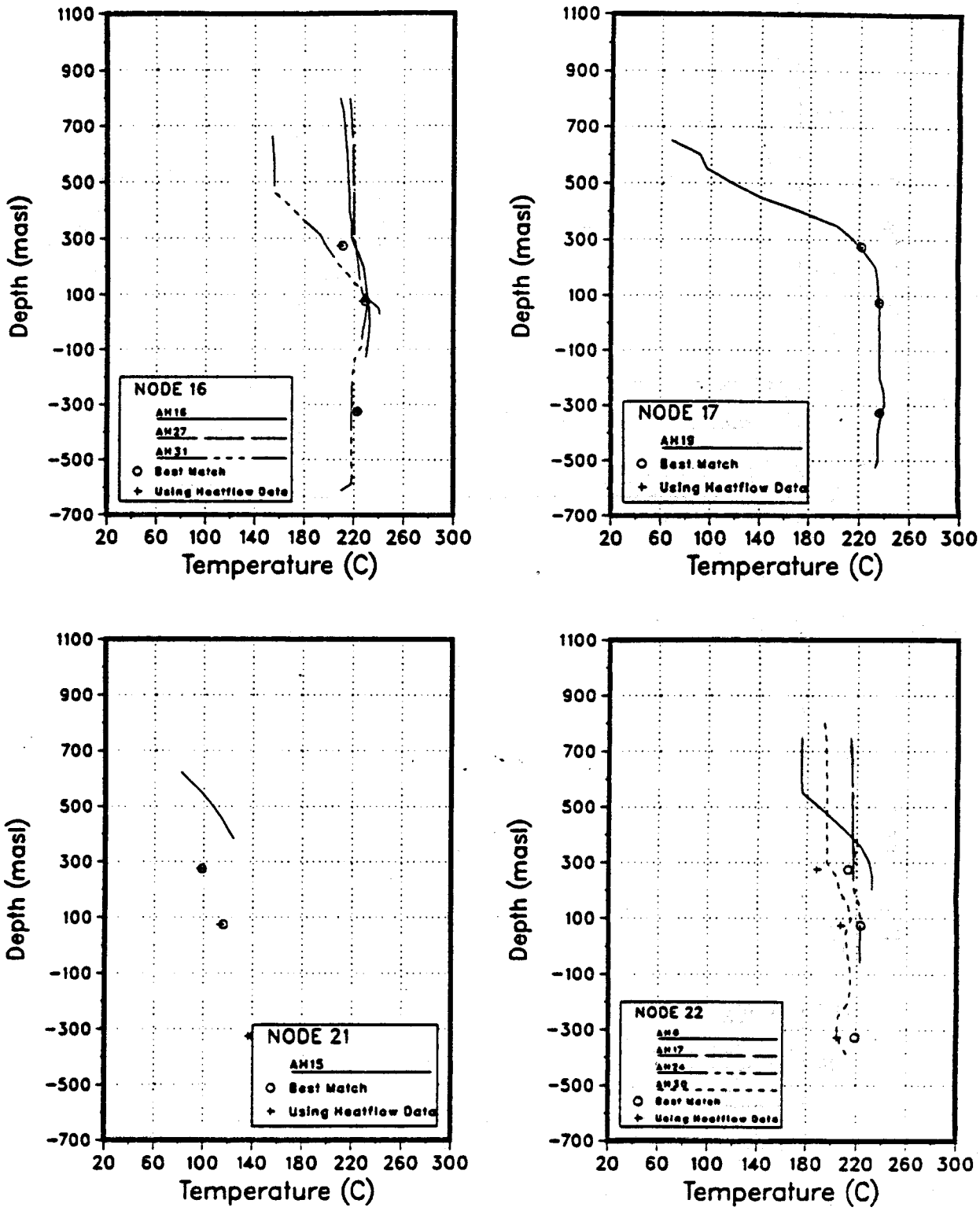

Figure 11.10. Comparison of temperature matches (in Nodes 16, 17, 21 and 22) between the best match and the simulation run using heat flow measurements by Fritz Durr.

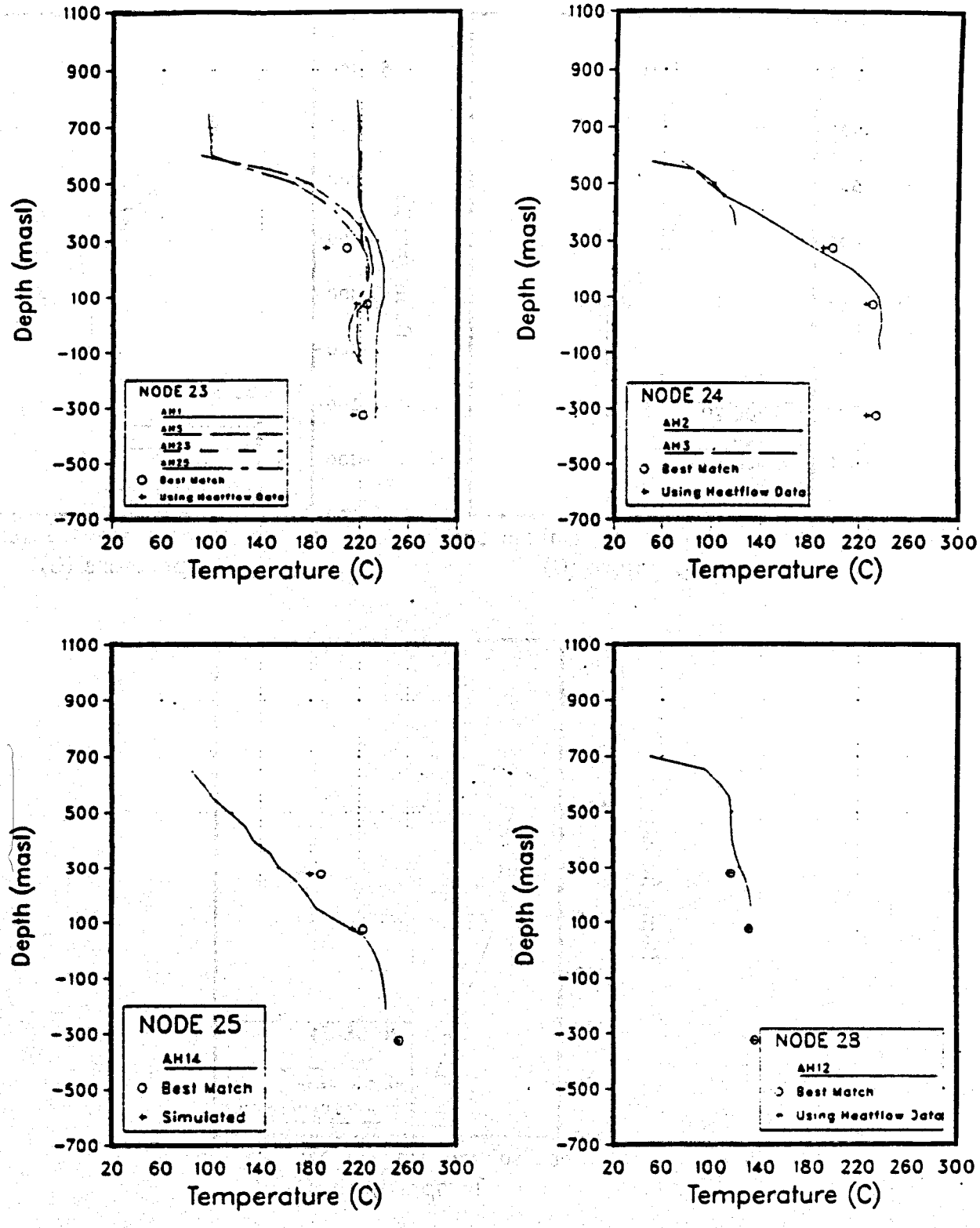

Figure 11.11. Comparison of temperature matches (in Nodes 23, 24, 25 and 28) between the best match and the simulation run using heat flow measurements by Fritz Durr.

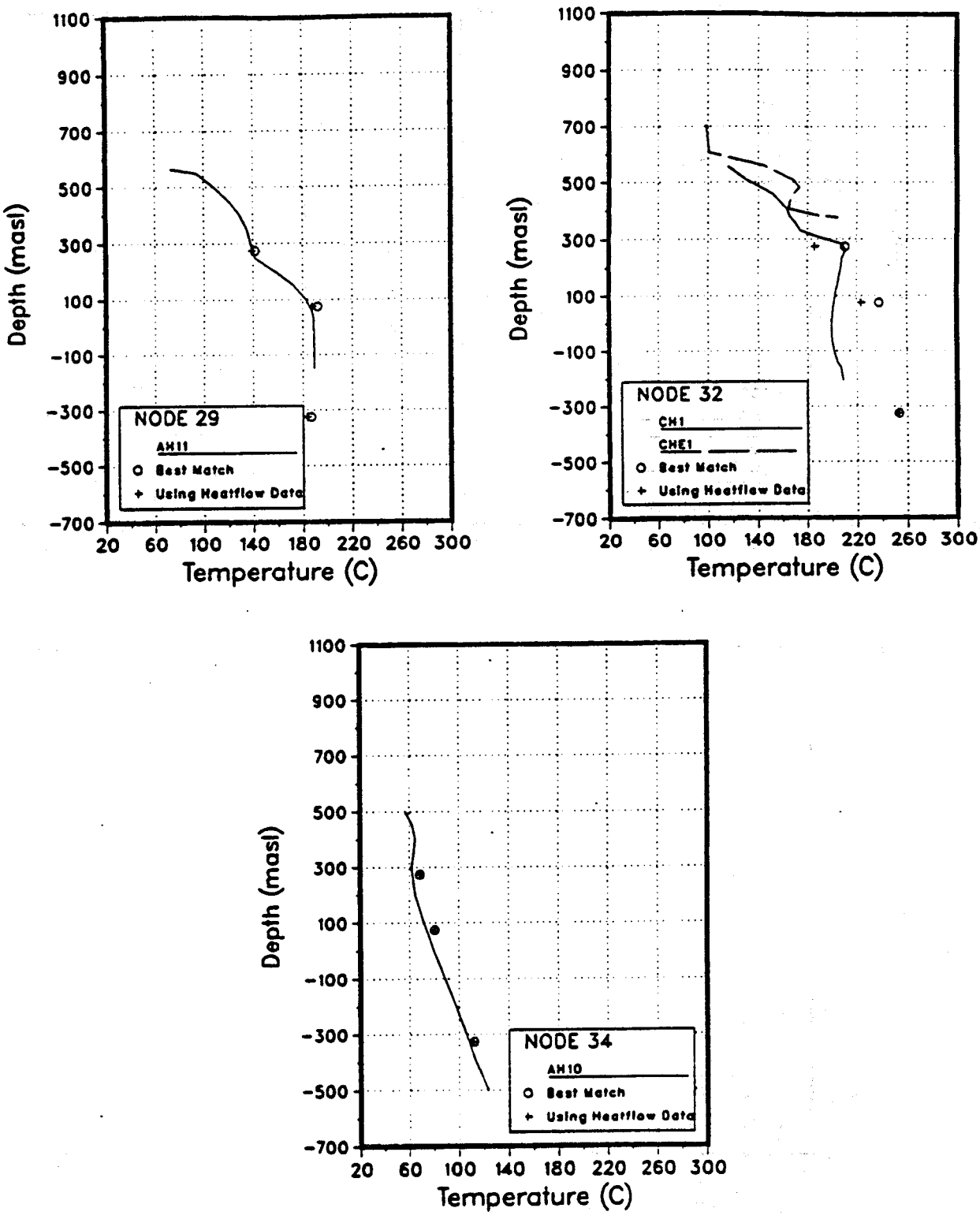

Figure 11.12. Comparison of temperature matches (in Nodes 29, 32 and 34) between the best match and the simulation run using heat flow measurements by Fritz Durr.

Table 11.3
Comparison between thermal outputs of the sinks used in the model and those estimated by Durr (1960a, b)

	Model sinks MW_t	Durr's estimates MW_t
Cerro Blanco	5.08	2.09
El Sauce & San Jose	3.37	0.84
Playon de Ahuachapán	18.72	4.18
Agua Shuca	1.82	2.09
Chipilapa	3.19	—
La Labor	27.76	4.18
El Salitre	169.36*	301.25

*does not include contributions from the shallow aquifer.

12.0 CONCLUSIONS

Various geological, geochemical and reservoir engineering studies have been conducted using data from the Ahuachapán geothermal field in El Salvador. The major tasks of this work included the development of a hydrogeological model, evaluation of pressure and temperature declines and the development of various reservoir models.

A hydrogeological model has been developed that considers the lithology and structural features of the area and discerns their impact on the movement of cold and hot fluids in the system. The main characteristics of the system are:

A1. Four major lithologic units have been defined. These are: Surficial Materials (SM), Young Agglomerates (YA), Ahuachapán Andesites (AA) and Older Agglomerates (OA).

A2. Three different aquifers have been identified based on the chemistry of the fluids and pressure response of the aquifers to seasonal variations. These aquifers coincides with the lithologic units. These are: the Shallow Aquifer (found in SM), the Regional Saturated Aquifer (found in YA) and the Saline Aquifer, the geothermal reservoir, (found in AA and OA).

A3. The structure of Ahuachapán fields appears to be dominated by seven major and five minor faults. These faults control the heat and fluid recharge and the flow within the reservoir.

A4. The Ahuachapán-Chipilapa system is recharged by an upflow zone southeast of the Ahuachapán wellfield, probably beneath the Laguna Verde volcanic complex. The temperature of this upwelling zone is believed to be 250 °C or higher, as suggested by geochemical temperatures of the discharged fluid.

A5. Most of the upwelling fluids flow to the north with the main outflow for this system being in the El Salitre springs area, located about 7 km north of the wellfield. The discharge is a mixture of geothermal and Regional Saturated Aquifers fluids, the mixing believed to

occur in the vicinity of the springs rather than close to the geothermal field.

A6. Colder fluids recharge the Ahuachapán reservoir as evidenced by observed gradients in chloride concentrations and geothermometer temperatures across the field. The cold water inflow is either laterally from the north or vertically downwards from the Regional Saturated Aquifer, which overlies the main reservoir and has a higher pressure potential.

A7. The main reservoir rocks are the Ahuachapán Andesites and the underlying Older Agglomerates. Most of the produced fluids come from the andesites, although the permeability of the Older Agglomerates is significant, as evidenced by several feed zones encountered in this unit.

A8. Faults limit the extent of the Ahuachapán reservoir towards the north and the west. The temperature reversal in well AH-32 also suggest that the extent of the field is limited toward the south.

A9. The Ahuachapán and Chipilapa fields seem to communicate at depth and to be outflow zones of a large geothermal system.

Large scale exploitation in Ahuachapán has greatly changed the pressure and temperature conditions in the reservoir. Drawdowns of up to 15 bars and cooling of up to 15 °C has been observed. In most cases temperatures have declined due to boiling in the reservoir stimulated by pressure drawdown. However, increasing temperatures in the southeast corner of the wellfield show that significant recharge of hot fluids to the wellfield comes from the southeast and also indicate that the recharge rate has increased with time as the pressure declines in the reservoir.

As expected the pressure drawdown correlates well with the net extraction rate, with quasi-steady pressure conditions reached after periods of near constant extraction rates. This suggests that natural recharge is very significant at Ahuachapán and that the system is much larger than the current wellfield.

The temperature changes in Ahuachapán have been influenced by several factors. These are:

B1. Gradual cooling of the upper part of the reservoir due to boiling resulting from pressure decline.

B2. Progressive cooling of the liquid region in the Ahuachapán Andesites of the main production area. This cooling is due to recharge of boiling (two-phase) fluid to the production area.

B3. Temporal cooling in the vicinity of injectors during the reinjection period. This cooling, however, did not cause significant detrimental temperature decline in producing wells.

B4. Cooling in the northern and the western part of the field due to increasing cold water recharge in response to reservoir drawdown.

B5. Heating-up in the southeastern part of the field due to increasing geothermal (hot) fluid recharge to the production area.

Modeling studies that include analyses of interference test, fieldwide pressure decline and development of a three-dimensional natural state model yields valuable information regarding the reservoir. The results from these works indicate that:

C1. Average transmissivity of the field ranges between 25 and 35 Dm and storativity between 2.5×10^{-6} and 3.5×10^{-6} m/Pa.

C2. Reinjection at Ahuachapán during the period 1976-1982 significantly helped maintain reservoir pressures.

C3. Horizontal permeability of the Ahuachapán Andesites is estimated to be about 80 md, yielding a transmissivity value of about 30 Dm for this unit. Vertical permeability is estimated to be about 16 md. The permeability of the Older Agglomerates is estimated to be 20 md horizontally and 4 md vertically.

C4. The total recharge to the Ahuachapán/Chipilapa geothermal systems is estimated to be

225 kg/s of 255 °C water, yielding a total thermal throughflow of 250 MW_t. Most of these fluids discharge in El Salitre Springs (170 kg/s), but significant energy is lost through surface springs in the Ahuachapán/Chipilapa areas (60 MW_t) and through conduction to the ground surface (20 MW_t).

13.0 REFERENCES AND RELATED PUBLICATIONS

Aerial Photos: L-3: 2-25, 2-26, 2-27; L-4: 0-16, 0-17, 0-18.

Alvarez, S.J., "Perdida Calorica del Campo Playon de Salitre".

Arevalo, M.J. and Campos, T., "Perforaciones Geotérmica en El Salvador", Simposio Internacional sobre la Energía Geotérmica en América Latina, Guatemala, October 1976.

Aumento, F. and Liguori, P.E., "Conceptual Reservoir Models through Geoscientific Investigations", *Geothermics, 15*, No. 5/6, 1986.

*Aumento, F., Viale, P., Choussy, M. and Santana, A., "Alteration Mineralogy of the Ahuachapán Geothermal Field", Geothermal Resource Council Trans., 6, 7-10, 1982.

*Benson, S.M., "Well Test Data Analysis from a Naturally Fractured Liquid-Dominated Hydrothermal System", Geothermal Resource Council Trans., 6, 237-240, 1982.

*Benson, S.M., "Interpretation of Non-isothermal Step Rate Injection Tests", Proc. 8th Workshop on Geothermal Reservoir Engineering, Stanford, Ca., Report SGP-TR-60, 103-109, 1982.

*Billings, M. P., *"Structural Geology"*, 3rd Edition, Prentice Hall Inc., Englewood Cliffs, NJ 1972.

*Bodvarsson, G. and Bolton, R.S., "A Study of the Ahuachapán Geothermal Field", UN report, May 1971.

Bodvarsson, G. S. and Cox, B. L., "Numerical Studies of Gravity Effects in Two-phase Reservoirs," GRC, Transactions, 10, September 1986, pp. 429-436.

*Bodvarsson, G., Pruess, K., Stefansson, V. and Eliasson, T., "The Krafla Geothermal Field, Iceland. 2. The Natural State of the System", *Water Resources Research, 20*, 11, 1531-1544, 1984.

*publications referred to in text

*Bolton, R.S., "Ahuachapán Geothermal Field, Report on Visit, May 7-18, 1979", June 1979.

*Burkart, B. and Self, S., "Extension and Rotation of Crustal Blocks in Northern Central America and Effect on the Volcanic Arc", *Geology, 13*, 22-26, January 1985.

Campos, A.R., "Reporte de Avance: Monitoreo Químico de las Aguas de la Zona Prospectiva de Chipilapa", CEL, July 1983.

*Campos, T., "Indices de Inyectividad en el Campo Geotérmico de Ahuachapán", CEL, 1980.

Campos, T., "Pruebas de Spinner, Pozos de Reinyeccion, Ahuachapán", CEL, 1986.

Campos, T., "Pruebas en Regimen Transitorio en el Pozo AH-26", CEL, July 1979.

Campos, T., "Pruebas en Regimen Transitorio de Presion, Temperatura y Distribución de Flujo en AH-6, AH-7, y AH-1", CEL, September 1979.

*Campos, T., "Ten Years of Commercial Exploitation of the Ahuachapán Geothermal Field", Proceedings 7th NZ-Workshop, pp. 15-20, 1985.

*Carr, M. J., Mayfield, D. G. and Walker, J. A., "Relation of Lava Compositions to Volcano Size and Structure in El Salvador", Journal of Volcanology and Geothermal Research, Vol. 10, pp. 35-48, 1981.

CEL Drilling and Workover Reports.

CEL, "Comportamiento del Campo Geotérmico de Ahuachapán, Estudios Geoquimicos, Durante 1984" CEL, 1984.

CEL, "Comportamiento del Campo Geotérmico de Ahuachapán, Estudios Geoquimicos Durante 1986", CEL, 1986.

*CEL, "Descripcion del Modelo Matematico del Campo Geotérmico de Ahuachapán Elaborado por Electroconsult," CEL, November 1982.

CEL, "Estudio de la Reinyeccion en el Campo Geotérmico de Ahuachapán (Reporte Interno)", CEL, August 1983.

CEL, "Isotopos en Estudios Geotérmico, Actividad: Estudios de los Isotopos Ambientales en el

*publications referred to in text

Area Geotérmico de Ahuachapán", CEL, May 1986.

CEL, "Resultado del Cierre de Pozos en el Campo Geotérmico de Ahuachapán, Junio-Septiembre 1982", CEL, October 1982.

Choussy, M. and Escobar, D., "Mediciones de Interferencia en el Campo Geotérmico de Ahuachapán", CEL, April 1979.

Cuellar, G., "Programa de Reinyeccion en el Campo Geotérmico de Ahuachapán", Simposio Internacional sobre la Energía Geotérmica en América Latina, Guatemala City, October 1976.

Cuellar, G., "Programas Quimicos en Desarollos Geotérmico", U.S. Environmental Protection Agency, 2nd Workshop on Sampling and Analysis of Geothermal Effluents, Las Vegas, Nevada, February 1977.

*Cuellar, G., Choussy, M. and Escobar, D., "Extraction-Reinjection at Ahuachapán Geothermal Field", CEL, 1979.

*DiPippo, R., "Geothermal Energy Developments in Central America", Geothermal Resources Council Bull., 3-14, November 1986.

*Durr, F., "Mediciones Calorimétricas", 1960a.

*Durr, F., "Perdida de Calor por Evaporacíon", 1960b.

Durr, F., "Perdidas Caloricas Superficiales de los Campos Geotermales de Ahuachapán", 1960.

*EG&G Idaho, Inc. and Lawrence Berkeley Laboratory, "Low-to-Moderate Temperature Hydrothermal Reservoir Engineering Handbook," Report IDO-10099, 1872,

*Einarsson, S., Vides, R.A. and Cuellar, G., "Disposal of Geothermal Waste Water by Reinjection", UN-Symposium, 1975.

ELC-Electroconsult, "Campo Geotérmico de Ahuachapán, Analisis del Comportamiento del Campo Hasta el Año 1980", CEL, June 1981.

ELC-Electroconsult, "Planta Geotérmico de Ahuachapán, Optimizacion de la Explotacion del Campo", CEL, November 1979.

*publications referred to in text

ELC-Electroconsult, "Campo Geotérmico de Ahuachapán, Asistencia a la Operacion del Campo y Estudio Geologico de Detalle", CEL, March 1982.

ELC-Electroconsult, "Campo Geotérmico de Ahuachapán, Optimizacion de la Explotacion del Campo", CEL, March, 1983.

*ELC-Electroconsult, "Campo Geotérmico de Ahuachapán, Asistencia a la Operacion del Campo y Estudio Geologico de Detalle", CEL, February 1984.

*Escobar, C. A., "Reservoir Engineering at Ahuachapán", Project for Diploma in Energy Technology (Geothermal), Project Report No. GEOTHERM. 85.07, Geothermal Institute, University of Auckland, New Zealand, October 1985.

Escobar, D., "El Campo Geotérmico de Ahuachapán Durante los Años 1979-1980", CEL, April 1981.

Escobar, D. and Martinez, J.A.M., "Respuesta del Campo Geotérmico de Ahuachapán a la Explotacion Durante 6 Años", CEL.

*Glover, R.B., "Geochemical Investigations of the Ahuachapán Geothermal Field", UN, October 1970.

*Grant, M., "Simple Modeling of Production and Reinjection at Ahuachapán", DSIR, February 1980.

*Hanold, R.J., Loose, V.W., Laughlin, A.W. and Wade, P.E., "Geothermal Initiatives in Central America", GRC Bulletin, Sept./Oct. 1986.

Jiménez, M., "Reporte Hidrogeológico del Area Geotermal de Ahuachapán", CEL, July 1971.

*Jiménez, M.A. and Campos, T.A.V., "Perforaciones Geotermales en El Salvador", Simposio Internacional sobre Energía Geotérmica en América Latina, Guatemala, 1976.

*Jonsson, J., "Report on Geological Investigation in Ahuachapán", UN, July 1970.

Kurman, M.J., "A Regional Blueprint for Geothermal Development in Central America", GRC Transactions, Vol. 9- Part 1, 1985.

*publications referred to in text

*Larios, D., "Estudio de la Permeabilidad, Porosidad y Densidad de las Rocas del Campo Geotérmico de Ahuachapán", CEL, April 1983.

*Larios, D., "Sintesis de las Propiedades Fisicas del Campo Geotérmico de Ahuachapán, Propiedades Texturales y Termicas", CEL, February 1985.

Larios, D., "Suceptibilidad Magnetica de las Rocas del Campo Geotérmico de Ahuachapán", CEL, February 1985.

Liguori, P., Jarach, F., Choussy, M., Campos, T. and Escobar, D. "Reservoir Engineering of the Ahuachapán Geothermal Field", GRC Trans., Vol. 6, pp. 289-292, 1982.

Mahon, W.A.J. "Preliminary Report on a Geochemical Assessment Study of the Ahuachapán Geothermal Field", UN, February 1970.

Martinez, J.A. "Consideraciones Geoquímicas sobre la Prueba de Máxima Extracción, Campo de Ahuachapán", CEL, July 1981.

*McEdwards, D.G. and Benson, S.M. "User's Manual for ANALYZE--A Variable-Rate, Multiple-Well, Least Squares Matching Routine for Well Test Analysis", Lawrence Berkeley Laboratory Report LBL-10907, 1981.

Mendoza, S.A. "Behavior of Ahuachapán Geothermal Field", Geothermal Institute, University of Auckland, Auckland, NZ, October 1985.

*Nielson, D. L. and Hulen, J.B. "Internal Geology and Evolution of the Redondo Dome, Valles Caldera, New Mexico", Journal of Geophysical Research, Vol. 89, No. B10, 1984.

Ondrej F., "A Hydrologic study of the Ahuachapán Geothermal Area", UN, February 1970.

*Pruess, K., "Development of the General Purpose Simulator MULKOM," 1982 Annual Report, Earth Sciences Division, Lawrence Berkeley Laboratory report LBL-15500, Berkeley, CA, 1982.

Rivera R.J., and Samaniego, V.F. "Reporte de la Misión sobre la Evaluación de las Condiciones Actuales del Yacimiento Geotérmico de Ahuachapán", CEL, July 1983.

*publications referred to in text

*Rivera, R.J., Vides, R.A., Cuellar, G., Samaniego, V.F. and Neri, I.G. "A Status Report on the Exploitation Conditions of the Ahuachapán Geothermal Field", Proceedings 9th Workshop on Geothermal Reservoir Engineering, Stanford, California, pp. 97-105, 1983.

Rodriguez, C.E. "Reporte Final de Interpretacion de las Resistividad Electrica del Area Geotérmica de Chipilapa", CEL, 1985.

*Romagnoli, P., Cuellar, G., Jiménez, M., and Ghessi, G. "Hydrogeological Characteristics of the Geothermal Field of Ahuachapán, El Salvador", Proceeding 2nd UN-Symposium, pp. 571-574, 1976.

Santana, A. "Analisis Microscopio de Muestra de Canal y Nucleos de 32 Pozos, Campo Geotérmico de Ahuachapán", CEL.

*Santana, A. "Distribución Vertical de Minerales de Alteración, Pozos Ahuachapán", CEL, March 1987a.

Santana, A. "Mapa Estructural, Correlaciones Litologicas y Patrones de Distribución de Minerales de Alteración, Campo Geotérmico de Ahuachapán", CEL, March 1987b.

*Sigvaldason, G.E. and Cuellar, G. "Geochemistry of the Ahuachapán Thermal Area, El Salvador", Proceedings UN Symposium on the Development and Utilization of Geothermal Resources, Pisa, 1392-1399, 1970.

*Theis, C.V., "The Relationship between the Lowering of Piezometric Surface and the Rate and Duration of Discharge Using Groundwater Storage," EOS, Trans., AGU, Vol. 2, 519-524, 1935.

Vega, D. "Avances de la Geotermia en El Salvador", Proc. International symposium on Development and Exploration of Geothermal Resource, Cuernavuca, Mexico, October 5-9, 1987, 36-41

Verduzco, R. "Reporte de la Misión sobre la Evaluación de las Condiciones Actuales del Yacimiento Geotérmico de Ahuachapán", 1983.

*publications referred to in text

*Vides, J.R. "Model Simulation of the Behavior of Ahuachapán Geothermal Field", Geothermal Institute, University of Auckland, Auckland, NZ, 1982.

Vides-Ramos, A., "Ahuachapán Field Management", Trans. Geothermal Resources Council, International volume, pp. 397-404, 1985.

*Vides-Ramos, A., "Desarrollo Acutal de la Geotermia en El Salvador," Seminario Latino Américano de Exploracion Geotérmica, Quito, Ecuador, September 5-6, 1983.

*Vides-Ramos, A. "The Current Development of Geothermal Energy in El Salvador", Latin American Seminar on Geothermal Exploration, Quito, Ecuador, September 1983.

*Vinsome, P. K. W. and Westerfield, V., "A Simple Method for Predicting Cap and Base Rock Heat Losses in Thermal Reservoir Simulations," *J. of Can. Petr. Tech.*, Vol. 19, No. 3, pp. 87-90, July-September, 1980.

*Ward, P. and Jacob, K., "Final Report on a Study of Microearthquakes and Ground Noise in the Ahuachapán Geothermal Field", U. N. Report, 1971.

*Weyl, R. "Geology of Central America", 2nd ed., Gebruder Borntraeger, Berlin, 1980.

*White, R. A., Harlow, D. H. and Alvarez, S. "The San Salvador Earthquake of October 10, 1986 - Seismological Aspects and Other Recent Local Seismicity", Earthquake Spectra, EERI, Vol. 3, No. 3, pp. 419-434, 1987.

*Wieseman, G. "Remarks on the Geologic Structure of the Republic of El Salvador, Central America", Mitt. Geol. Palaent., Inst. Univ. Hamburg, Vol. 44, 557-574, 1975.

Witherspoon, P.A. "Analysis of Reservoir Behavior at Ahuachapán Geothermal Field", CEL, March 1977.

Witherspoon, P.A. "Analysis of Reservoir Behavior at Ahuachapán Geothermal Field", CEL, May 1979.

14.0 ACKNOWLEDGEMENTS

The authors thank colleagues from CEL and LANL for their cooperation and help during this study, and Robert Hanold and Ed Van Eeckout of LANL for project management. Technical review of this work by M. A. Ripperda and S. Gaulke is most appreciated. This work was supported by USAID through a subcontract from LANL and through U.S. Department of Energy Contract No. DE-AC03-76SF00098.